

Hamdi A. Zurqani *Editor*

Environmental Applications of Remote Sensing and GIS in Libya

 Springer


Environmental Applications of Remote Sensing and GIS in Libya

Hamdi A. Zurqani
Editor

Environmental Applications of Remote Sensing and GIS in Libya

 Springer

Editor

Hamdi A. Zurqani 
University of Arkansas Agricultural
Experiment Station, Arkansas Forest
Resources Center, College of Forestry,
Agriculture and Natural Resources
University of Arkansas at Monticello
Monticello, AR, USA

ISBN 978-3-030-97809-9 ISBN 978-3-030-97810-5 (eBook)
<https://doi.org/10.1007/978-3-030-97810-5>

© The Editor(s) (if applicable) and The Author(s), under exclusive license to Springer Nature Switzerland AG 2022

This work is subject to copyright. All rights are solely and exclusively licensed by the Publisher, whether the whole or part of the material is concerned, specifically the rights of translation, reprinting, reuse of illustrations, recitation, broadcasting, reproduction on microfilms or in any other physical way, and transmission or information storage and retrieval, electronic adaptation, computer software, or by similar or dissimilar methodology now known or hereafter developed.

The use of general descriptive names, registered names, trademarks, service marks, etc. in this publication does not imply, even in the absence of a specific statement, that such names are exempt from the relevant protective laws and regulations and therefore free for general use.

The publisher, the authors and the editors are safe to assume that the advice and information in this book are believed to be true and accurate at the date of publication. Neither the publisher nor the authors or the editors give a warranty, expressed or implied, with respect to the material contained herein or for any errors or omissions that may have been made. The publisher remains neutral with regard to jurisdictional claims in published maps and institutional affiliations.

This Springer imprint is published by the registered company Springer Nature Switzerland AG
The registered company address is: Gewerbestrasse 11, 6330 Cham, Switzerland

Preface

Remote sensing and geographic information systems (GIS) technologies are well-established tools and have always generated informative data that have led to sustainable management. This book focuses on how remote sensing and GIS are used to generate data and how this information can be used in the decision-making process to achieve sustainable management of natural resources in Libya. The total land area of Libya is about 180 million hectares, with a population of about 6 million, and it is located in the arid and semi-arid regions of the world. Libya's climate is dominantly influenced by both the Mediterranean Sea in the northern regions and the desert in the southern regions. With the increasing pressure on natural resources due to the growing population, remote sensing and GIS can be very useful in the analysis and determination of factors that affect the utilization of these limited resources in an efficient and effective manner. Thus, by understanding these factors, sound decisions can be arrived at that will ensure the sustainable use of natural resources to meet the needs of both present and future generations. This book aims to provide adequate information about the use of remote sensing and GIS applications in the country. The book is comprised of 12 chapters written by distinguished scientists mainly from Libya and other countries who are interested in the Libyan environment. Chapter one “[Introduction to Environmental Applications of Remote Sensing and GIS in Libya](#)” introduces the book, *Environmental Applications of Remote Sensing and GIS in Libya*, and summarizes all the chapters presented in it. The second chapter “[Application of Remote Sensing and GIS in Land Cover/Land Use Mapping And Change Detection Using Google Earth Engine Platform: A Case Study in Northwestern Libya](#)” presents the use of Google Earth Engine and the public archive database in its platform for continuous monitoring of the spatial and temporal change of the land cover that occurs as a consequence of land use change in northwestern Libya. Chapter three “[Evaluation of Selected Vegetation Indices to Assess Rangeland Vegetation in Eastern Libya](#)” evaluates a range of vegetation indices derived from satellite imagery to identify those approaches best applicable for remotely assessing and monitoring vegetation cover in the semi-arid and arid rangelands in the country. Chapter four “[Spatiotemporal Analysis of Vegetation](#)

Health Index (VHI) and Drought Patterns in Libya Based on Remote Sensing Time Series” presents a spatiotemporal analysis of Vegetation Health Index (VHI) and drought patterns in Libya based on remote sensing time series. The fifth chapter (**Integration of Remotely Sensed Data and Machine Learning Technique for Spatial Prediction of Selected Soil Properties in Northwestern Libya**) discusses the integration of remotely sensed data and machine learning techniques for spatial prediction of selected soil properties in northwestern Libya. Additionally, Chapter six **“Field and Laboratory Estimation of Soil Erodibility, Erosion and Degradation of the Semi-Arid Aljabal Alkhdar Region, Libya”** discusses field and laboratory estimation of soil erodibility, erosion, and degradation of the semi-arid Al-Jabal Al-Akhdar region of the country. Moreover, Chapter seven **“DRAINMOD Applications to Design Drainage Systems in Libya Using Soil Salinity Data Predicted by GIS, Remote Sensing and Artificial Neural Networks”** employs artificial neural networks (ANNs) to develop soil salinity prediction maps to monitor the initial and simulated salinity under drained and undrained conditions. Chapter eight **“Surface Water Potential and Suitable Sites Identification for RWH in the Semi-Arid and Arid Watershed of Wadi Sammalus, Northeast Libya Using GIS and Remote Sensing Approach”** discusses the use of remote sensing and GIS approaches in assessing the potential surface water and identifying potential rainwater harvesting (RWH) sites, which are both critical tasks for effective water resource management. The ninth chapter (**Stepwise Approach for Morphometric Modeling of Wadi Zamzam Watershed in North-Western Libya Using GIS and Remote Sensing Techniques**) illustrates a step-by-step approach to delineate the spatial boundaries of the Wadi Zamzam watershed in Libya and establish a geographical database of its morphometric, geological, and climatic characteristics by using global information systems and remote sensing techniques based on the digital elevation model, the geological map of Libya, and climatic data. Chapter ten **“Geospatial Mapping and Analysis of the 2019 Flood Disaster Extent and Impact in the City of Ghat in Southwestern Libya Using Google Earth Engine and Deep Learning Technique”** demonstrates the development of a framework to identify flood-affected areas after storm impact and map the flooded areas caused by the heavy rainfall and thunderstorm in the southwestern region of the country. Chapter eleven **“Oil Pollution Monitoring and Detection Using GIS and Remote Sensing Techniques: A Case Study from Libya”** provides a high-level overview of the characteristics and extent of produced oil lakes, which can be utilized to perform further in-depth research in the future to enhance the extent and volume of even more oil damage assessment. The final chapter (Chapter twelve) **“Conclusions and Recommendations for Environmental Applications of Remote Sensing and GIS in Libya”** summarizes the key research findings in relation to the research aims, questions, and discussions for each chapter of the book, and also provides recommendations for future research in the area of environmental applications of remote sensing and GIS in Libya. This book has valuable contributions from many distinguished scientists from various universities and institutions in and outside of Libya.

Acknowledgments

I would like to acknowledge Margaret Deignan, senior series editor in chief of Springer Nature, and all the staff of Springer that kindly assisted us in our multiple queries during the elaboration of this book. Special thanks are also due to the many reviewers who shall remain anonymous, but who spent hours reading, reviewing, and providing valuable feedback to the authors. I would also like to thank all authors who contributed to this book and whose cooperation made my task as an editor a pleasure.

Monticello, AR, USA, May 2022

Hamdi A. Zurqani

University of Arkansas Agricultural
Experiment Station, Arkansas Forest
Resources Center, University of
Arkansas at Monticello, Monticello,
AR, USA

About This Book

This is the first book on the environmental applications of remote sensing (RS) and geographical information systems (GIS) in Libya published in English. The environmental applications include monitoring and mapping soil salinity and prediction of soil properties, monitoring and mapping of land degradation, spatiotemporal land cover/land cover, agricultural and meteorological drought monitoring, hydrological applications such as spatial rainfall distribution, surface runoff, geo-morphometric analysis, hydrologic and hydraulic modeling, flood hazard mapping and assessment, pollution hazard assessment, and climate-related geophysical processes. This book also assesses the impacts of climate change on natural resources using both RS and GIS, as well as other applications, covering different parts of Libya. The information presented in the chapters of the book includes a collection of maps extracted from remotely sensed imagery and other geospatial datasets, as well as tables and statistical relations derived from the findings of the studies conducted in different parts of the country. The book is written by distinguished scientists mainly from Libya and other countries who are interested in the Libyan environment. The book is therefore a useful source of information and knowledge on the Libyan environment for graduate students, researchers, policy planners, and stakeholders in Libya as well as similar regions.

Contents

Introduction to Environmental Applications of Remote Sensing and GIS in Libya	1
Hamdi A. Zurqani	
Application of Remote Sensing and GIS in Land Cover/Land Use Mapping and Change Detection Using Google Earth Engine Platform: A Case Study in Northwestern Libya	11
Hamdi A. Zurqani, Abdulsalam Al-Bukhari, and Mahmood B. Shanta	
Evaluation of Selected Vegetation Indices to Assess Rangeland Vegetation in Eastern Libya	33
Abdulsalam Al-Bukhari, Tim Brewer, and Stephen Hallett	
Spatiotemporal Analysis of Vegetation Health Index (VHI) and Drought Patterns in Libya Based on Remote Sensing Time Series	53
Khalid I. Elfadli and Hamdi A. Zurqani	
Integration of Remotely Sensed Data and Machine Learning Technique for Spatial Prediction of Selected Soil Properties in Northwestern Libya	81
Hamdi A. Zurqani	
Field and Laboratory Estimation of Soil Erodibility, Erosion and Degradation of the Semi-Arid Aljabal Alakhdar Region, Libya	97
Murad M. Aburas, Asama S. Alferjani, and Mohammed S. Yousef	
DRAINMOD Applications to Design Drainage Systems in Libya Using Soil Salinity Data Predicted by GIS, Remote Sensing and Artificial Neural Networks	119
Murad Ellafi, Hamdi A. Zurqani, Lynda K. Deeks, and Robert W. Simmons	

Surface Water Potential and Suitable Sites Identification for RWH in the Semi-Arid and Arid Watershed of Wadi Sammalus, Northeast Libya Using GIS and Remote Sensing Approach 145
Salah Hamad and Nilanchal Patel

Stepwise Approach for Morphometric Modeling of Wadi Zamzam Watershed in North-Western Libya Using GIS and Remote Sensing Techniques 175
Ali M. Salim, Ibtisam A. Albira, and Safa A. Ebsheer

Geospatial Mapping and Analysis of the 2019 Flood Disaster Extent and Impact in the City of Ghat in Southwestern Libya Using Google Earth Engine and Deep Learning Technique 205
Hamdi A. Zurqani, Abdulsalam Al-Bukhari, Alsaket O. Aldaikh, Khalid I. Elfadli, and Ali A. Bataw

Oil Pollution Monitoring and Detection Using GIS and Remote Sensing Techniques: A Case Study from Libya 227
Khalifa Abdunaser

Conclusions and Recommendations for Environmental Applications of Remote Sensing and GIS in Libya 245
Hamdi A. Zurqani

About the Editor



Hamdi A. Zurqani is an assistant professor of Geospatial Science in Natural Resource Management and Conservation at the University of Arkansas Agricultural Experiment Station, Arkansas Forest Resources Center, University of Arkansas at Monticello, Monticello, AR, USA. He is also an FAA (i.e., Pt107) Certified sUAS/Drones Pilot and has used this skill to enhance his knowledge of remote sensing and GIS. He is recognized for his work in remote sensing, geospatial analysis, and soil science. He is highly collaborative as evidenced by his publications. He is the author and coauthor of many peer-reviewed publications and technical publications (including teaching laboratory manuals). He has published widely in many peer-review journals (e.g., *International Journal of Applied Earth Observation and Geoinformation*, *Remote Sensing in Earth Systems Sciences*, *Frontiers in Environmental Science*, *Geoderma*, *Land*, *Frontiers in Environmental Science*, *Urban Forestry & Urban Greening*, and others). He is a member of the Editorial Board for Remote Sensing (MDPI) Journal, counseling outcome, and research evaluation. He also was appointed to serve as a guest editor for the Special Issue “Applications of Remote Sensing in Earth Observation and Geo-information Science.” In addition, he conducted peer-review for many journals including *Journal of Environmental Informatics*, *Applied Sciences*, *SN Applied Sciences*, *Remote Sensing*, *Heliyon*, *Geosciences*, *Land*, *Water*, *Agronomy*, *Agriculture*, *Sustainability*, *Arid Land Research and Management*,

International Journal of Environmental Research and Public Health, Natural Hazards, and Conference of the Arabian Journal of Geosciences. He conducts cutting-edge research in the field of environmental information science, remote sensing, land use management/planning, change detection of landscape degradation, and geographic information system (GIS) models. He has focused his research efforts on the development of novel applications for new technologies in analyzing spatial data, remote sensing, geostatistical modeling of environmental changes such as erosion, mapping and predicting soil salinity, and land use/ land cover changes. His new publications include: “Mapping and quantifying agricultural irrigation in heterogeneous landscapes using Google Earth engine” in the *Journal of Remote Sensing Applications: Society and Environment* (Elsevier); “Evaluating the integrity of forested riparian buffers over a large area using LiDAR data and Google Earth engine” in the *Journal of Scientific Reports* (Nature); “Mapping urbanization trends in a forested landscape using Google Earth engine” in the *Journal of Remote Sensing in Earth Systems Sciences* (Springer Nature); “Geospatial analysis of land use change in the Savannah River Basin using Google Earth engine” in the *International Journal of Applied Earth Observation and Geoinformation* (Elsevier); and “Application of non-hydraulic delineation method of flood hazard areas using LiDAR-based data” as well as “Assessing ecosystem services of atmospheric calcium and magnesium deposition for potential soil inorganic carbon sequestration” in the *Geosciences Journal* (MDPI).

Contributors

Khalifa Abdunaser Libyan Petroleum Institute, Tarabulus, Libya

Murad M. Aburas Department of Soil and Water, Faculty of Agriculture, University of Omar Al-Mukhtar, Al Bayda, Libya

Ibtisam A. Albira Department of Geography, Faculty of Education, University of Misurata, Misurata, Libya

Abdulsalam Al-bukhari Department of Forest and Rangeland, Faculty of Natural Resources and Environmental Sciences, Omar Al-Mukhtar University, Al-Bayda, Libya

Alsaket O. Aldaikh Department of Forest and Rangeland, Faculty of Natural Resources and Environmental Sciences, University of Omar Al-Mukhtar, Al-Bayda, Libya

Asama S. Alferjani Department of Soil and Water, Faculty of Agriculture, University of Omar Al-Mukhtar, Al Bayda, Libya

Ali A. Bataw Department of Zoology, Faculty of Sciences, University of Omar Al-Mukhtar, Al-Bayda, Libya

Tim Brewer School of Water, Energy and Environment, Cranfield University, Bedford, UK

Lynda K. Deeks Cranfield Soil and Agrifood Institute, Building 52a, Cranfield University, Bedfordshire, MK, UK

Safa A. Ebsheer Ministry of Education, Misurata, Libya

Khalid I. Elfadli Libyan National Meteorological Centre, Tripoli, Libya

Murad Ellafi Cranfield Soil and Agrifood Institute, Building 52a, Cranfield University, Bedfordshire, MK, UK

Stephen Hallett School of Water, Energy and Environment, Cranfield University, Bedford, UK

Salah Hamad Faculty of Natural Resources and Environmental Science, Omar Al Mukhtar University, Al Baydah, Libya

Nilanchal Patel Department of Remote Sensing, Birla Institute of Technology Mesra, Ranchi, India

Ali M. Salim Department of Geography, Faculty of Education, University of Misurata, Misurata, Libya

Mahmood B. Shanta Department of Range and Forestry, Faculty of Agriculture, University of Tripoli, Tripoli, Libya

Robert W. Simmons Cranfield Soil and Agrifood Institute, Building 52a, Cranfield University, Bedfordshire, MK, UK

Mohammed S. Yousef Department of Soil and Water, Faculty of Agriculture, University of Omar Al-Mukhtar, Al Bayda, Libya

Hamdi A. Zurqani University of Arkansas Agricultural Experiment Station, Arkansas Forest Resources Center, College of Forestry, Agriculture and Natural Resources, University of Arkansas at Monticello, Monticello, AR, USA

Introduction to Environmental Applications of Remote Sensing and GIS in Libya



Hamdi A. Zurqani 

Abstract This chapter introduces the book “Environmental Applications of Remote Sensing and GIS in Libya”, and summarizes all the chapters presented in this book. The chapters of this book focus on the use and the role of remote sensing (RS) and geographic information system (GIS) techniques in understanding, monitoring, and investigating the extent of environmental disturbance (e.g., desertification, salinization, deforestation, land use changes, etc.) on the surface of the Earth. A wide range of applications for environmental planning and management topics are discussed in the book’s chapters including monitoring and mapping soil salinity and prediction of soil properties, monitoring and mapping of land degradation, spatiotemporal land cover/land use, agricultural drought monitoring, and hydrological applications such as spatial rainfall distribution, surface runoff, geo-morphometric analysis, hydrologic and hydraulic modeling, and climate-related geophysical processes.

Keywords North Africa · Mediterranean · Environmental disturbance · Land degradation · Sustainability · Earth observation · Modeling · Geospatial analysis

1 Libya: A Brief Background

Libya is a country located in the Maghreb region of North Africa, situated along the southern coast of the Mediterranean Sea, approximately between longitude 9° and 25°E and latitude 18° and 33°N. It is the fourth largest country in Africa by geographic area, covering about 1,759,540 km² and a population of more than 6 million residents (Zurqani et al. 2019). Libya is surrounded by six other African countries, with one water-based border that lies on the coast of the Gulf of Sidra and the Mediterranean Sea. The countries of Tunisia and Algeria lie along the western edge of Libya. To the south, Libya shares borders with Niger and Chad. In the east, both Egypt and Sudan lie on the other side of Libya’s eastern border (Zurqani 2021).

H. A. Zurqani (✉)

University of Arkansas Agricultural Experiment Station, Arkansas Forest Resources Center,
University of Arkansas at Monticello, Monticello, AR, USA

e-mail: Zurqani@uamont.edu; Hzurqani@uark.edu

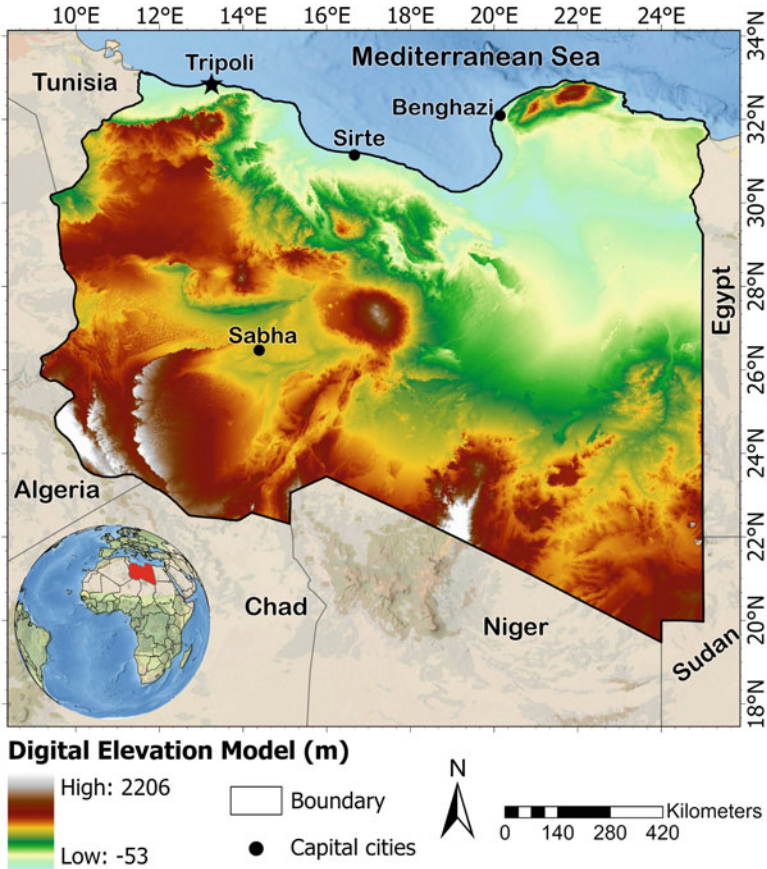


Fig. 1 Map of Libya with capital cities and the spatial distribution of Digital Elevation Model (m)

Generally, the terrain of Libya slopes gently to the north. The mountains, which are located in the northwest, northeast, south, and central parts of the country, are of low to medium latitudes (CEDARE 2014). The Tibesti Mountains in southern Libya, are the only hills that rise to more than 2200 meters (Fig. 1).

Libya's climate is dominated by the hot arid Sahara Desert in the southern regions, but it is moderated along the coastal littoral by the Mediterranean Sea in the northern regions. During winter, the weather is cool with some rain on the coastal areas, and in the desert, the temperature may drop to around freezing at night. There is almost no rain in the summer, as it is the major hot and drought period of the year. The average annual precipitation ranges from 0 mm in southern Libya to 600 mm at Al Jabal Al Akhdar in the northeast (Zurqani 2021).

The vegetation cover in Libya is divided into three main parts, grass or herbaceous, shrubs, and trees (Zurqani 2021). The most productive agricultural lands that are suitable for agricultural activities in Libya are limited to a strip along the Mediterranean Sea, which represents 2% of the surface area (Zurqani et al. 2019).

In the northwest region of the country, the triangular plain of Al Jafara which is dominated by the highlands of Jabal Nafusah, is known for being the main producer of agricultural products in the country. Another important plain is the Benghazi plain and the fertile upland and heavily forested area of the Al Jabal Al Akhdar in the northeastern tip. These areas of the country account for more than 80% of food production from agriculture, which mostly depends on rainfall and groundwater. The remaining area consists of sand or gravel dunes, mountains, or marshes (salt marshes) with some scattered oases (Zurqani 2021).

2 The Use of Remote Sensing and GIS Applications in Libya

The use of remote sensing and GIS Applications in Libya has grown by leaps and bounds during the past few years. Spatial problem-solving approaches are becoming more involved and extended for mapping, change detection, and monitoring for land use, vegetation, climate, crop growth and yield inventory, and many other aspects of environmental management and natural resources assessment. Examples of the areas in which satellite remote sensing and GIS technologies have been broadly applied in Libya include:

- Agriculture
- Disaster monitoring and mitigation
- Water resource management
- Environmental monitoring
- Survey and urban planning
- National spatial data infrastructure
- Infrastructure development planning and monitoring
- Mineral exploration
- Telecommunication

Some of the above projects like Agriculture have been a leader in the development and use of remote sensing data and tools and the evolution of GIS data and applications in Libya. In 2001, a natural resource mapping project for agricultural use and planning was established in Libya in collaboration with the Food and Agriculture Organization of the United Nations (FAO/UN) experts under the Ministry of Agriculture. The project has several goals, the most important being to contribute to a better understanding of the natural resources of Libya, and to provide useful information and recommendations through graphical representation to decision-makers for planning, management, business, and others. The FAO LIB/00/004 “Mapping of Natural Resources for Agriculture Use and Planning in Libya Project” was specialized for:

- Digitizing all topographic, soil and land maps and consolidating the date and information they contain.

- Building databases of natural resources (soil, water, and climate) and their management systems.
- Building a Land Resource Information Management System in Libya (LRIMS).
- Mapping land/vegetation cover in Libya.
- Monitoring and assessing land degradation, and then preparing maps and identifying areas affected by desertification that require rapid intervention.
- Preparing an appropriate national methodology for drought control and then reducing its effects.
- Developing different scenarios of early warning for food security risks under climate changes.
- Training some local experts in the areas of GIS, remote sensing, land/vegetation covers and preparing digital maps.

In 2009, the FAO LIB/00/004 project published the first land cover map of the country using remote sensing and GIS techniques (Fig. 2). This map was first created with a visual interpretation of satellite imagery covering the period (2001–2002), using the FAO Land Cover Classification System (LCCS) with affiliated software (GeoVIS, etc.), followed by an extensive field examination using a series of field surveys all over the country. At the end of December 2005, the land cover database was updated with additional information to improve the precision of the estimate within the framework of the LIB/00/004 project. Landsat satellite images in the 1980s, 1990s, and 2000s were compared using change detection analysis and coupled with a very active field investigation. The final map of the land cover was generated by grouping over one hundred of the original land cover classes into just ten generalized classes based on Libya's most sensitive land cover features (Fig. 2).

Until now, this map and its accompanying statistics are one of the most reliable sources of the land cover in Libya, where it is also used by the provincial agencies and public and private stakeholders for different purposes including development and conservation projects country-wide.

The use of remote sensing and GIS technologies have proven to be effective tools in mapping large areas, and thus have a wide range of applications for environmental planning and management including monitoring and mapping soil salinity and prediction of soil properties, monitoring and mapping of land degradation, spatio-temporal land use/cover, agricultural drought monitoring, hydrological applications including spatial rainfall distribution, surface runoff, geo-morphometric analysis, hydrologic and hydraulic modeling, and climate-related geophysical processes.

The chapters of this book provide information on the latest research studies that used remote sensing and GIS techniques for environmental applications in Libya. The information presented in these chapters includes a collection of maps extracted from remotely sensed imagery and other geospatial datasets, as well as tables and statistical relations derived from the findings of the studies conducted in different parts of the country.

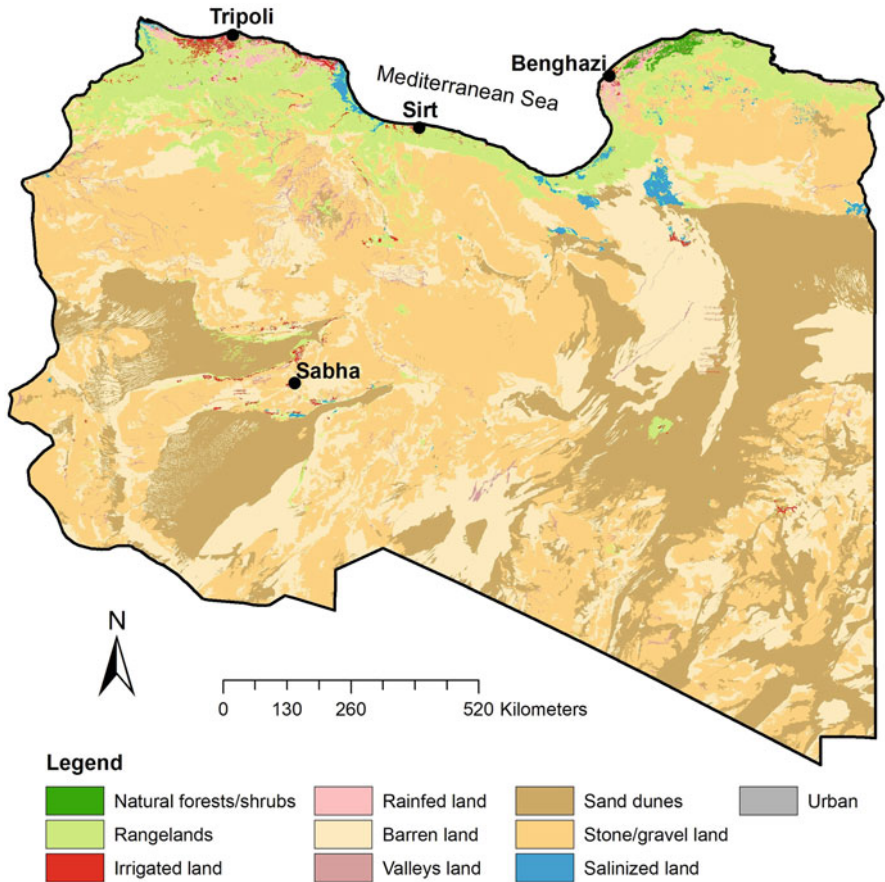


Fig. 2 The predominant land cover types in Libya. (Adapted from: Zurqani 2021)

3 Summaries of the Book’s Chapters

This chapter aims to introduce the book by providing a brief summary of each chapter of the book. Chapter 2 is titled “[Application of Remote Sensing and GIS in Land Cover/Land Use Mapping and Change Detection Using Google Earth Engine Platform: A Case Study in Northwestern Libya](#)”. The chapter presents the use of Google Earth Engine and the public archive database in its platform for continuous monitoring of the spatial and temporal change of the land cover that occurs as a consequence of land use change in northwestern Libya. A supervised machine learning classifier algorithm (i.e., random forest) was used in the GEE platform to obtain the land cover classification maps for each chosen year. Over the whole study period, the predominant land cover alteration at each time interval (i.e., 1990–2000, 2000–2010, 2010–2020, and 1990–2020) was generally caused by changes from

plantation forests and shrubs and rainfed agriculture areas to rangelands and built-up land areas.

Chapter 3 focuses on “[Evaluation of Selected Vegetation Indices to Assess Rangeland Vegetation in Eastern Libya](#)”. Vegetation cover in the eastern Libyan rangelands has changed both qualitatively and quantitatively due to natural factors and human activity. The aim of this research is to evaluate a range of vegetation indices derived from satellite imagery to identify those approaches best applicable for remotely assessing and monitoring vegetation cover in the semi-arid and arid rangelands. A number of vegetation indices applied in arid and semi-arid rangelands similar to the study area were assessed using ground-based color vertical photography (GBVP) methods to identify the most appropriate index for classifying the percentage vegetation cover. The results from five years of NDVI values across the study area showed that the peak of vegetation production was from February to April and was therefore the optimum time for a ground survey. This also in accord with the opinions of Libyan rangeland experts who were consulted during the research. Furthermore, in order to identify the most appropriate method for classifying the GBVP images, three methods of classification available in the ENVI Feature Extraction tool were tested. The K Nearest Neighbor (KNN) and Principal Components Analysis (PCA) did not perform well but the Support Vector Machine (SVM) was identified as the most appropriate method for classification with an overall accuracy of 85%, followed by K Nearest Neighbor (KNN) and Principal Components Analysis (PCA) with overall accuracies of 40% and 30%, respectively.

In chapter 4, the authors present a “[Spatiotemporal Analysis of Vegetation Health Index \(VHI\) and Drought Patterns in Libya Based on Remote Sensing Time Series](#)”. In this study, remote sensing-based Vegetation Health Index (VHI) was used to measure the drought conditions in vegetated areas of Libya. In order to ensure the high performance of this index, it was evaluated by a developed ground-based drought index called the Vegetation-Precipitation and Temperature Index (VPTI). The results showed a high level of confidence that VHI is scientifically reliable. Moreover, the assessment and analysis of drought risks in Libya using a drought hazard mapping model found that 82% of the areas were subjected to high and very high drought risk during 2000–2014. The country has also experienced three major spells of drought (2000–2002, 2009–2011, and 2012–2014), the most severe and prolonged of which was during the 2000/2001 and 2001/2002 seasons, reaching 18 months of moderate drought conditions.

On the other hand, chapter 5 discusses “[Integration of Remotely Sensed Data and Machine Learning Technique for Spatial Prediction of Selected Soil Properties in Northwestern Libya](#)”. This study investigated the use of satellite imagery data (i.e., Landsat), terrain, and laboratory analyzed soil samples to map the spatial distribution of soil properties in the most arable land in northwestern Libya. The main aim of this chapter is to conduct a spatial prediction of selected topsoil properties such as Soil pH, calcium carbonate (CaCO_3); exchangeable sodium percentage (ESP); Cation exchange capacity (CEC) by integrated remotely sensed data and machine learning approach in northwestern Libya. The results showed that soil pH and CEC had the

lowest variation, while ESP and CaCO_3 had the highest variation, respectively. In addition, the results indicated that the coefficient of determination (R^2) varies from 0.22 to 0.42, the Root Mean Square Error (RMSE) ranges between 0.35 and 6.96, and the Normalized Root Mean Square Error (NRMSE) ranges between 0.12 and 0.26 indicating less residual variance and thus a proper operation of the machine learning model used.

Furthermore, chapter 6 discusses “[Field and Laboratory Estimation of Soil Erodibility, Erosion, and Degradation of the Semi-arid Aljabal Alkhdar Region, Libya](#)”. The fragile ecosystems in this Mediterranean semi-arid region of eastern Libya are affected by soil degradation driven by soil erosion as a result of the introduction of intensive land use. In this chapter, field measurements were carried out using erosion plots and field observations in order to estimate soil loss and erodibility. The field erosion plots and the rainfall simulation experiments showed that the moderate aggregate stability of Typic and Calcic Rhodoxeralfs soils significantly improved their resistance to water erosion compared to the Lithic Rhodoxeralfs soils. This study also suggested that water stable aggregates can efficiently determine soil erodibility. Accordingly, well designed soil conservation measures need to be applied to enhance soil depth and its holding capacity, so that soil productivity can be recovered and consequently prevent land degradation.

In addition, chapter 7 “[DRAINMOD Applications to Design Drainage Systems in Libya Using Soil Salinity Data Predicted by GIS, Remote Sensing and Artificial Neural Networks](#)” develops soil salinity prediction maps to monitor the initial and simulated salinity under drained and undrained conditions and evaluates the performance of a drainage system based on measured and predicted electrical conductivity of the saturated paste extract (ECe). The expectation is that this will provide a low-cost alternative to drainage system design, making it more accessible to farmers, planners, and decision-makers in the least developed countries.

In chapter 8 with the title “[Surface Water Potential and Suitable Sites Identification For RWH in the Semi-arid and Arid Watershed of Wadi Sammalus, Northeast Libya Using GIS and Remote Sensing Approach](#)” the authors discuss the use of remote sensing and GIS approach in assessing the potential surface water and identifying potential Rainwater Harvesting (RWH) sites, which are both critical tasks for effective water resource management. The runoff was estimated using the Soil Conservation Service Curve Number (SCS-CN) method, where the CN is computed by the LULC map generated from Landsat 8 OLI imagery that was intersected with the HSG layer. The RWH suitability sites were delineated based on the Analytical Hierarchy Process (AHP) method, where the criteria selection was performed based on literature review, followed by weighted overlay analysis to determine the layer of suitable sites. The results showed that optimal and suitable sites cover 2.5% and 9% of the watershed, while the rest of the watershed is covered by moderate, marginal, and unsuitable sites covering 17.7%, 25%, and 45.7%, respectively.

Continuing on this line of research, chapter 9, which is entitled “[Stepwise Approach for Morphometric Modeling of Wadi Zamzam Watershed in North-Western Libya Using GIS and Remote Sensing Techniques](#)” illustrates a step-by-

step approach to delineate the spatial boundaries of the Wadi Zamzam watershed in Libya and establish a geographical database of its morphometric, geological and climatic characteristics by using global information systems and remote sensing techniques based on the digital elevation model, the geological map of Libya, and climatic data. Furthermore, the study also determined the characteristics of the water network, riverbeds, their numbers and lengths, and the bifurcation ratio. It also extracted shape properties such as the ratio of elongation, circularity, and form factor in the Wadi Zamzam watershed.

Additionally, chapter 10 is devoted to “[Geospatial Mapping and Analysis of the 2019 Flood Disaster Extent and Impact in the City of Ghat in Southwestern Libya Using Google Earth Engine and Deep Learning Technique](#)”. The main objectives of this study were to develop a framework to identify flood-affected areas after the storm impact, map the flooded areas caused by the heavy rainfall and thunderstorm in the region, and assess the major effect of the storm on the land cover during the flood period. The results of the flood extent extraction analysis indicated that approximately 2255.67 hectares of the study area were flooded during the wave of the heavy rainfall and thunderstorm event in June 2019, which caused flooding and damage in several locations around the city.

Moving to environmental pollution detection and monitoring, chapter 11 deals with “[Oil Pollution Monitoring and Detection Using GIS and Remote Sensing Techniques: A Case Study from Libya](#)”. This chapter provides a high-level overview of the characteristics and extent of produced water lakes, which can now be utilized to perform further in-depth research in the future to enhance the extent and volume of even more oil damage assessment. The main target of this project was to produce high maps of oil-contaminated surfaces as well as series time maps of events induced by oil pollution via multi-temporal satellite data and then to validate the accuracy of the produced maps.

The book ends with the conclusions and recommendations chapter 12 which is entitled “[Conclusions and Recommendations for Environmental Applications of Remote Sensing and GIS in Libya](#)”. This chapter summarizes the key research findings in relation to the research aims, questions, and discussions for each chapter of the book, and also provides recommendations for future research in the area of environmental applications of remote sensing and GIS in Libya.

Author Contributions **Hamdi A. Zurqani:** conceptualization, methodology, supervision, software, data curation, formal analysis, validation, investigation, writing—original draft, visualization, writing—review and editing, review of analysis. The author has read and agreed to the published version of the manuscript.

References

- CEDARE (2014) Libya water sector M & E rapid assessment report. Monitoring and evaluation for water in North Africa (MEWINA) project, Water Resources Management Program, CEDARE. Available online: https://www.humanitarianresponse.info/sites/www.humanitarianresponse.info/files/assessments/libya_water_sector_me_rapid_assessment_2014.pdf. Accessed on 6 Dec 2021
- Zurqani HA, ed. (2021) The soils of Libya. Springer. Available online: <https://link.springer.com/book/10.1007%2F978-3-030-66368-1>. Accessed on 6 Dec 2021
- Zurqani HA, Mikhailova EA, Post CJ, Schlautman MA, Elhawej AR (2019) A review of Libyan soil databases for use within an ecosystem services framework. *Land* 8(5):82

Dr. Hamdi A. Zurqani is an Assistant Professor of Geospatial Science in Natural Resource Management and Conservation at the University of Arkansas Agricultural Experiment Station, Arkansas Forest Resources Center, University of Arkansas at Monticello, Monticello, AR, USA. He is also an FAA (i.e., Pt107) Certified sUAS/Drones Pilot, and has used this skill to enhance his knowledge of remote sensing and GIS. Dr. Zurqani is a recognized expert as a result of his internationally acclaimed work in the areas of environmental information science, remote sensing, geospatial analysis, land evaluation, sustainability, pedology, and soil science education. He has conducted research across the world, including the United States of America, and Africa, and has served as PI, co-PI, or co-investigator on several grants-funded research projects. Dr. Zurqani is highly collaborative as evidenced by his publications. He is the author and co-author of many peer-reviewed publications, book chapters, and technical publications (including teaching laboratory manuals). He also edited two books with Springer Nature (i.e., “The Soils of Libya”, and “Environmental Applications of Remote Sensing and GIS in Libya”), and has published widely in many peer-review journals (e.g., *International Journal of Applied Earth Observation and Geoinformation* (Elsevier); *Remote Sensing in Earth Systems Sciences* (Springer Nature); *Scientific Reports* (Nature); *Frontiers in Environmental Science* (Frontiers); *Geoderma* (Elsevier); *Land* (MDPI); *Urban Forestry & Urban Greening* (Elsevier), and others). Dr. Zurqani is a member of the Editorial Board for *Remote Sensing* (MDPI) Journal, counseling outcome, and research evaluation. He also was appointed to serve as a Guest Editor for the Special Issue “Applications of Remote Sensing in Earth Observation and Geo-Information Science”. In addition, Dr. Zurqani conducted peer-review for many journals including *Journal of Environmental Informatics*, *Applied Sciences*, *SN Applied Sciences*, *Remote Sensing*, *Geo-spatial Information Science*, *AgriEngineering*, *Sensors*, *Heliyon*, *Geosciences*, *Land*, *Soil Systems*, *Water*, *Agronomy*, *Agriculture*, *Resources*, *Sustainability*, *Arid Land Research and Management*, *Quaestiones Geographicae*, *Geocarto International*, *International Journal of Environmental Research and Public Health*, *Natural Hazards*, and *Conference of the Arabian Journal of Geosciences*. Dr. Zurqani conducts cutting-edge research in the field of Environmental Information Science, Remote Sensing, Land use management/ planning, change detection of landscape degradation, and Geographic Information System (GIS) models. He has focused his research efforts on the development of novel applications for new technologies in analyzing spatial data, remote sensing, geostatistical modeling of environmental changes such as erosion, mapping and predicting soil salinity, and land use/ land cover changes. His new publications include: “Mapping and Quantifying Agricultural Irrigation in Heterogeneous Landscapes Using Google Earth Engine” in the *Journal of Remote Sensing Applications: Society and Environment*; “Evaluating the integrity of forested riparian buffers over a large area using LiDAR data and Google Earth Engine” in the *Journal of Scientific Reports*; “Mapping Urbanization Trends in a Forested Landscape Using Google Earth Engine” in the *Journal of Remote Sensing in Earth Systems Sciences*; “Geospatial analysis of land use change in the Savannah River Basin using Google Earth Engine” in the *International Journal of Applied Earth Observation and Geoinformation*; and “Application of Non-Hydraulic Delineation Method of Flood Hazard Areas Using LiDAR-Based Data” as well as “Assessing ecosystem services of atmospheric calcium and magnesium deposition for potential soil inorganic carbon sequestration” in the *Geosciences Journal*.

Application of Remote Sensing and GIS in Land Cover/Land Use Mapping and Change Detection Using Google Earth Engine Platform: A Case Study in Northwestern Libya



Hamdi A. Zurqani , Abdulsalam Al-Bukhari, and Mahmood B. Shanta

Abstract Rapid urbanization development in Libya increases decision-makers' concerns regarding issues related to natural resources, such as converting plantation forests, natural vegetation, and agricultural lands into urban development. Assessment of land cover is fundamental to understand and cope with these concerns. The objectives of this study are to: (1) determine the classes and the distribution of land cover in northwestern Libya (i.e., Tripoli); (2) identify the spatial and the temporal change of the land cover that occurs as a consequence of land use change in the area; and (3) discuss the potential effects of land use change in this region. The land cover maps were produced using random forest supervised classification at four time periods for seven common land cover classes with overall accuracy and Kappa coefficient values ranging from 83.49% to 84.71% and 0.81 to 0.82, respectively. The results of this study not only indicate land use change, but also demonstrate the advantage of utilizing Google Earth Engine and the public archive database in its platform for continuous monitoring of this change over time. Land cover and land-use change assessment at spatial and temporal scales provides the decision-maker adequate information for understanding, planning, and managing various phenomena associated with natural resources.

H. A. Zurqani (✉)

University of Arkansas Agricultural Experiment Station, Arkansas Forest Resources Center, College of Forestry, Agriculture and Natural Resources, University of Arkansas at Monticello, Monticello, AR, USA

e-mail: Zurqani@uamont.edu; Hzurqani@uark.edu

A. Al-Bukhari

Department of Forest and Rangeland, Faculty of Natural Resources and Environmental Sciences, Omar Al-Mukhtar University, Al-Bayda, Libya

M. B. Shanta

Department of Range and Forestry, Faculty of Agriculture, University of Tripoli, Tripoli, Libya

Keywords Geospatial analysis · Google Earth Engine (GEE) · Landsat · Supervised classification · Machine learning · Random Forest classifier · Land cover/land use change

1 Introduction

Worldwide many countries are suffering rapid changes in land cover and land use in an unprecedented way. The significant outcome of the increased rapid population globally is the speedy land-use change (Wu et al. 2006). The changes of land cover and land use as agriculture expansion, urbanization, and deforestation occur worldwide at a fast pace. The influence of these changes is not only on the environment but also on human welfare through food provision (Foley et al. 2005). Mapping these changes and knowing its fundamental mechanism has achieved notable concentration over two decades (Gutman et al. 2012; National Research Council 2005). Land use/Land cover is a map illustrating the Earth's surface vegetation, water, and natural attractions. Though the meanings of land cover and land use are pretty distinct, they are usually utilized interchangeably. Land cover is determined by the physical characteristics of the earth's surface, whereas land use is described as the purpose of utilizing people for the land cover (Lambin et al. 2006; Lu and Weng 2007).

Libya has experienced rapid urban growth like many other developing countries, which has been considerably fast since the start of the oil exploration and the initiation of planned development in the mid-50s. Rapid urban increase coinciding with socioeconomic change has encroached on limited and potentially fragile agricultural lands (Mahmood-Misrati 1983; Alawamy et al. 2020). Historically, the majority of the population was concentrated in narrow parts of the coastal strip (Mahmood-Misrati 1983), and the most considerable population is located in the northwestern part of the country (Zurqani et al. 2019a). The coastal strip also has an area where the most agricultural activities are carried out in the country. These areas represent less than 10% of the country's total land (Zurqani et al. 2019a); however, the urban expansion in the northwestern part of the country is overgrowing in the recent decade. This expansion has led to a tremendous continuous decrease in agricultural lands (Al-sharif and Pradhan 2014). Moreover, the climatic zone and soil types influence natural vegetation spreading, mainly scattering plantation forests and some other natural vegetation with predominant nonwoody shrubs (Zurqani 2021).

However, implementing efficient monitoring of land cover and land-use change required a significant amount of data at various scales relating to the study area. Over the years, remotely sensed data had been used in mapping land cover in a short time with cost-effective and sufficient accuracy (Lu and Weng 2007; Berberoglu and Akin 2009; Al-Bukhari et al. 2018). Monitoring land use and cover with remote sensing technologies has become more effective and comprehensive, precisely manipulating multispectral satellite imagery. Moreover, it is an efficient tool for assessing natural resources at a regional level (Lu and Weng 2007). In contrast to the traditional remote sensing processes, Google Earth Engine (GEE) has shown great potential for land cover classification (Gorelick et al. 2017). The GEE platform made

much of the freely available satellite imagery available online so that researchers can analyze changes to the Earth's surface in near real-time, and it can handle big data processing rapidly (Zurqani et al. 2019b).

Assessing the patterns in the land cover/land use change in Libya is the primary concern for a better understanding of the issues associated with it, especially in areas undergoing rapid extent of vegetation removal in the region. Consequently, Libya's first land cover map was published in 2009 (LIB/00/004 2009) that indicates only the main categories of land cover types without showing changes over time (Zurqani 2021). The present study utilizes the advantage of the geospatial technology of GEE and the historical record of Landsat satellite data to investigate the land use change in northwestern Libya.

The objectives of this study are to: (1) determine the classes and the distribution of land cover in northwestern Libya (i.e., Tripoli); (2) identify the spatial and the temporal change of the land cover that occurs as a consequence of land use change in the area; and (3) discuss the potential effects of land use and land cover change in this region.

2 Materials and Methods

2.1 Study Area

The study area is situated in northwestern Libya (i.e., Tripoli) (Fig. 1) and extends from longitudes of approximately $12^{\circ} 77' 3''$ to $13^{\circ} 56' 2''$ E and $32^{\circ} 92' 5''$ to $32^{\circ} 22' 2''$ N latitudes; it occupies an area of about 2280 km². Climatically, the study area follows the Mediterranean climate characterized by hot and dry summers and cold and wet winters. The average annual temperature is 20.3 °C, the average maximum temperature is 26.3 °C and the average minimum temperature is 13.3 °C. The average annual precipitation is 370 mm, with precipitation occurring mainly in November through February (Climate-Data.org, 2016). July and August are the hottest months of the year, with a complete drought and no rainfall (Zurqani 2021). The topography of the study area is generally undulating, lying at an altitude ranging between 0 and 301 m above sea level (Fig. 1). Vegetation in this area consists of plantation forests, arid shrubby steppe, and herbaceous plants. Among the major agricultural crops grown in the study area are barley, wheat, and maize (Zurqani and Ben Mahmoud 2021).

2.2 Data Processing

The approach of mapping the land cover and change detection used in this study requires image preprocessing and normalization, and reference dataset as shown in

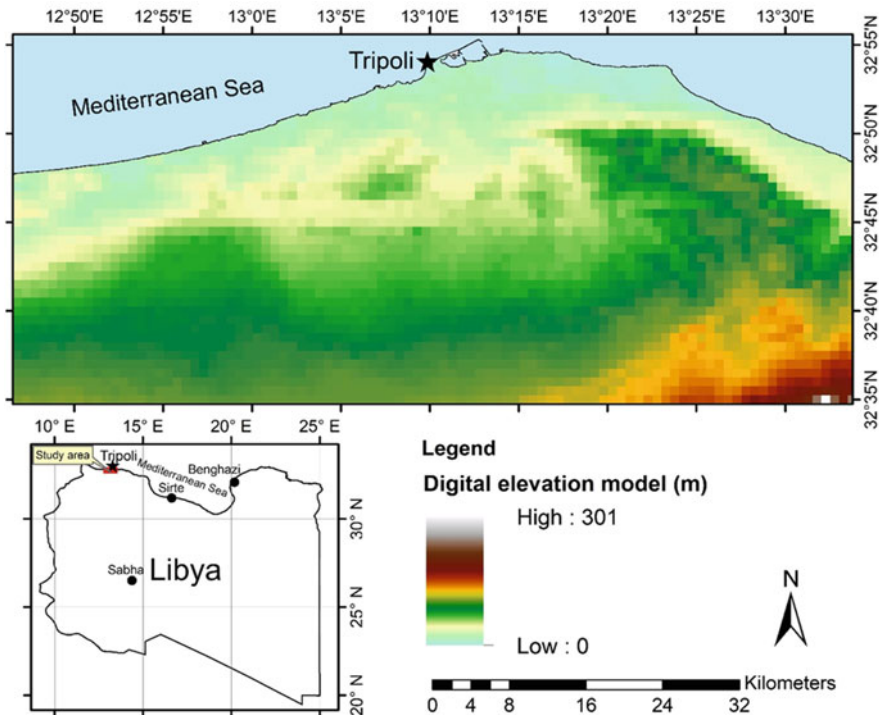


Fig. 1 Location of the study area

Fig. 2. First, the cloud-free composite Landsat images for 1990, 2000, 2010, and 2020 were analyzed by developing code in the GEE platform using a supervised classifier algorithm for each chosen year. Second, the type of land cover change detection was determined using a post-classification approach by overlying the land cover classification maps. The change detection was described and identified using NDVI Change Ratio to Previous Year (RPNDVI) approach.

2.2.1 Image Preprocessing

Google Earth Engine facilitates a fast analysis platform using Google’s computing infrastructure (Gorelick et al. 2017). Pre-processed Landsat 5 Surface Reflectance imagery (1990, 2000, and 2010) and Landsat 8 Surface Reflectance imagery (2020) were selected for the land cover classification and used to assess land use/land cover change across the study area in GEE (Table 1). In order to obtain cloud-free pixels over the entire study area, a cloud masking (i.e., median filtering) approach was performed to generate annual cloud-free Landsat composites (1990, 2000, 2010, and

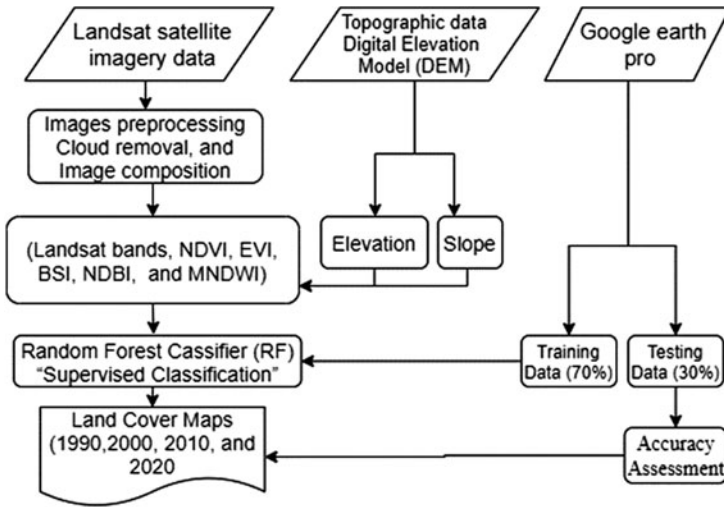


Fig. 2 Flow chart of data processing. NDVI Normalized Difference Vegetation Index, EVI Enhanced Vegetation Index, BSI Bare Soil Index, NDBI Normalized Difference Built-up Index, MNDWI Modified Normalized Difference Water Index

Table 1 Data sources and descriptions

Data layer	Source	Spatial resolution (m)	Date
Landsat 8 surface reflectance	Google earth engine (GEE) data provided by U.-S. Geological Survey (USGS)	30	2020
Landsat 5 surface reflectance	Google earth engine (GEE) data provided by U.-S. Geological Survey (USGS)	30	1990, 2000, and 2010
Digital elevation model (DEM)	Google earth engine (GEE) data provided by NASA/USGS/Jet Propulsion Laboratory-Caltech	30	2000

2020). Data normalization can reduce image noise and classification errors using multi-sensor and multi-scene images (Yang and Lo 2002). The Normalized Difference Vegetation Index (NDVI) (Tucker 1979), Enhanced Vegetation Index (EVI) (Huete et al. 2002), Bare Soil Index (BSI) (Polykretis et al. 2020), Normalized Difference Built Index (NDBI) (Xu 2007), and Modified Normalized Difference Water Index (MNDWI) (Xu 2007; Rokni et al. 2014) were performed for each image using the at-sensor reflectance values and stacked for later classification. The topographic data USGS digital elevation model (DEM) was used to distinguish the vegetation cover and other land cover classes in high-terrain areas (Zurqani et al., 2020).

2.2.2 Land Cover Categories

Land cover categories in this study were divided into seven classes (plantation forests and shrubs, rangeland, irrigated agriculture, rainfed agriculture, barren land, built-up land, and water) (Table 2) (Zurqani and Ben Mahmoud 2021). Next, the samples were selected from historical images in Google Earth Pro using a visual assessment. A total of 1900 sample points were collected in 2000, 2010, and 2020, respectively, considering no less than 200 reference points per land cover category (Zurqani et al. 2018). The collected samples were randomly divided into 70% training data and 30% validation data. Unfortunately, due to the unavailability of high-resolution imagery in Google Earth Pro for the year 1990, there were no available ground truth data for this year.

2.2.3 Image Classification and Accuracy Assessment

A variety of classification algorithms have been used to map land cover/land use changes from remotely sensed data (Lam 2008; Thanh Noi and Kappas 2018; Dabija et al. 2021). Supervised machine learning classifiers, such as Classification and Regression Trees (CART) and Random Forest (RF) are progressively used to classify remotely sensed data (Azeez et al. 2020). The RF is an ensemble learning algorithm, which uses bootstrap aggregating or “bagging” to generate an ensemble of classification (using multiple decision trees) with each tree training on a specific subset of the entire training data (Waske and Braun 2009). The prediction model of the RF classifier only requires two parameters to be identified: the number of

Table 2 The description of land cover classes (Zurqani and Ben Mahmoud 2021)

No.	Land cover classes	Description
1	Plantation forests (PF)	Planted forests consist of one or a few tree species (<i>eucalyptus</i> and <i>pinus</i> , <i>Acacia spp</i>). They were part of afforestation projects attempting to combat sand encroachment and soil erosion control.
2	Rangelands (RL)	These areas contain a significant proportion of natural vegetation, including native grasses, grass-like plants, and shrubs. Rangeland also consists of seeded areas to native or adapted introduced species that are managed like native vegetation.
3	Irrigated agriculture (IA)	RE-word. It is primarily used to replace missing rainfall in periods of drought and protect plants against frost.
4	Rainfed agriculture (RA)	This area includes the cultivation of crops under conditions of natural rainfall.
5	Barren land (BL)	This area consists of soil that is so poor that plants cannot grow in it, usually with sandy soils and few trees, and relatively infertile.
6	Built-up land (BUL)	This area is a nonlinear built-up area covered by impervious structures adjacent to or connected by streets. This land cover is related to centers of population.
7	Water (W)	Water bodies (i.e., Sea)

classification trees desired, and the number of prediction variables used in each node to make the tree grow (Rodríguez-Galiano et al. 2012). Each tree has several nodes, and the majority vote determines the final result. Random Forest methods are not sensitive to noise or over classifying (Zurqani et al. 2018). Thus, the RF classifier algorithm using ensemble size (i.e., 500 trees) was used in the GEE platform to obtain the land cover classification maps for each chosen year.

Accuracy assessments are valuable and practical techniques to determine how well the classification process accomplished the task of studies (Lucas et al. 1994; Tsutsumida and Comber 2015; Zurqani et al. 2020). In this study, accuracy assessment was an intricate task as there was no high-resolution imagery available for the study area in Google Earth Pro for the year 1990. Thus, there were no available ground truth data for this year. However, it was possible to perform the accuracy assessment using ground truth data for the 2000 classification output. The accuracy assessment of 2000 confidently confirmed the accuracy of the 1990 image, as the same signature and training information was used for classifying these two images. The produced land cover classification maps were validated using the validation dataset obtained from 1/3 of the reference locations. Following the previous studies (Foody 2002; Lyons et al. 2018; Zurqani et al. 2019b), a confusion matrix of land cover maps was calculated to evaluate the accuracy of the results using producer's accuracy, user's accuracy, F1 score (Deus 2016), and Kappa statistics (Congalton and Green 2009). Kappa statistics reflect the difference between actual agreement and the agreement expected by chance, as shown in Eq. (1), and F1 scores show how good the classifier is in the context of both producer's and user's by weighting the average of producer's and user's (Zurqani et al. 2020) as shown in Eq. (2):

$$Kappa\ statistics = \frac{observed\ accuracy - agreement\ chance}{1 - agreement\ chance} \quad (1)$$

$$F1\ score = \frac{2}{\frac{1}{producer's} + \frac{1}{user's}} = 2 * \frac{user's * producer's}{user's + producer's} \quad (2)$$

2.2.4 Change Detection Analysis

Change detection analysis is conducted to monitor the rate and spatial distribution of the land cover change that occurs as a consequence of land-use change over time in the area (Zurqani et al. 2018). In this study, the post-classification comparison approach was conducted by using the land cover classified images to calculate each land cover class area and observe the changes that are taking place at that time. This analysis identifies the various changes that occur in land cover for each category. The multi-date differencing NDVI bands were also used to determine the change in each pixel by using NDVI Change Ratio to Previous Year (RPNDVI) (Zurqani et al. 2019b) as shown in the following equation (Eq. 3):

$$RPNDVI = \frac{NDVI_i(x,y) - NDVI_{i-1}(x,y)}{NDVI_{i-1}(x,y)} * 100\% \quad (3)$$

where $NDVI_i(x, y)$ is the NDVI value to the current year at location (x, y) and $NDVI_{i-1}(x, y)$ is the NDVI value to the previous year. The change detection approach was applied with a threshold value of negative (0.1) to the $RPNDVI$ layer to detect the change between the years 1990 to 2000, 2000 to 2010, 2010 to 2020, and over the whole study period (30 years) between the years 1990 to 2020. The noise of NDVI change ratio was filtered by grouping the pixels based on size and eliminating the small patches. This approach provides information that illustrates “from-to” change that has occurred which can be easily calculated and mapped (Zurqani et al. 2019b). The pixels with change in this approach will be flagged as “probable change.”

3 Results and Discussion

3.1 Spectral Behavior of Land Cover Classes

Spectral resolution refers to the ability of a sensor to define fine wavelength intervals in the electromagnetic spectrum (bands). The spectral signature values of the seven land cover classes are presented in (Fig. 3a, b). The spectral signature values of the actual Landsat imagery bands reflectance (Blue, Green, Red, Near-Infrared, Shortwave-infrared 1, and Shortwave-infrared 2) are shown in (Fig. 3a). Generally, the red and near-Infrared parts of the spectrum are most important for vegetation classification (Zurqani et al. 2020). The red band was instrumental in distinguishing between the vegetation classes except for the rainfed agriculture, where it was confused with the built-up land spectra. The Shortwave-infrared 1 band was also useful in distinguishing between the vegetation classes except for the plantation forests and shrubs, where it was confused with the built-up land spectra as well. The water presented a typical behavior with all the band’s reflectance, where it was easily distinguished from the other land cover classes. The reflectance of barren land was visible in both the red and the near-Infrared bands. The urban areas were well separated in the blue and near-Infrared spectra.

The spectral indices results include NDVI, Normalized Difference Vegetation Index; EVI, Enhanced Vegetation Index; BSI, Bare Soil Index; NDBI, Normalized Difference Built Index; and MNDWI, Modified Normalized Difference Water Index, which are shown in (Fig. 3b). The vegetation classes were easy to distinguish in the EVI, while water was much easier to identify in the MNDWI.

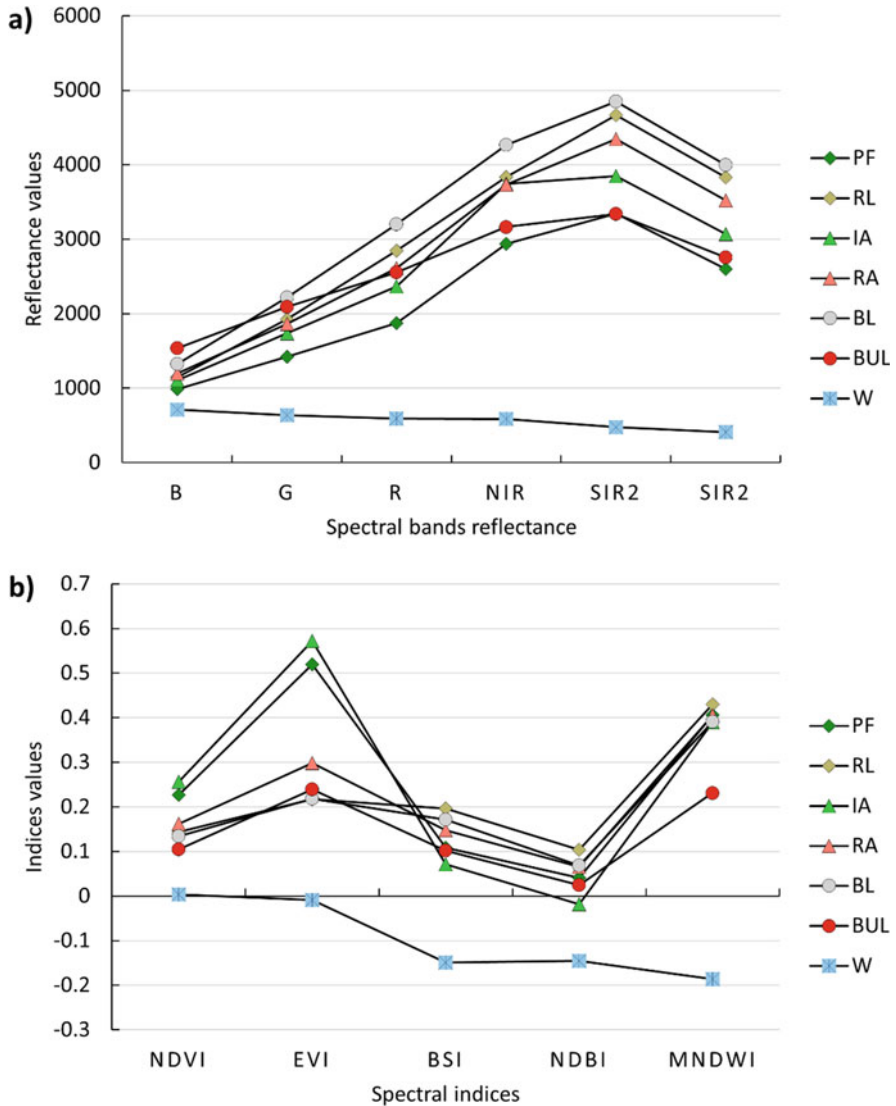


Fig. 3 The spectral values of each land cover type in the study area: (a) spectral bands reflectance (B Blue, G Green, R Red, NIR Near-Infrared, SIR1 Shortwave-infrared 1, SIR2 Shortwave-infrared 2), and (b) indices spectral (NDVI Normalized Difference Vegetation Index, EVI Enhanced Vegetation Index, BSI Bare Soil Index, NDBI Normalized Difference Built Index, MNDWI Modified Normalized Difference Water Index)

3.2 Land Cover Classification and Accuracy Assessments

As described in Sect. 2.2.3, the land cover classification maps were produced using supervised classification for the years 1990, 2000, 2010, and 2020 with a total of seven land cover categories identified and classified in the study area: plantation forests, rangelands, irrigated agriculture, rainfed agriculture, barren land, built-up land, and water as shown in (Fig. 4a-d). The RF classifier produced satisfactory accuracies, with overall accuracy assessments of (83.49%) 2000, (83.68%) 2010, and (84.71%) 2020, respectively, and the Kappa accuracies were (0.81) 2000, (0.81) 2010, and (0.82) 2020 (Table 3). The particular land cover class areas for the four selected years are summarized in (Table 4).

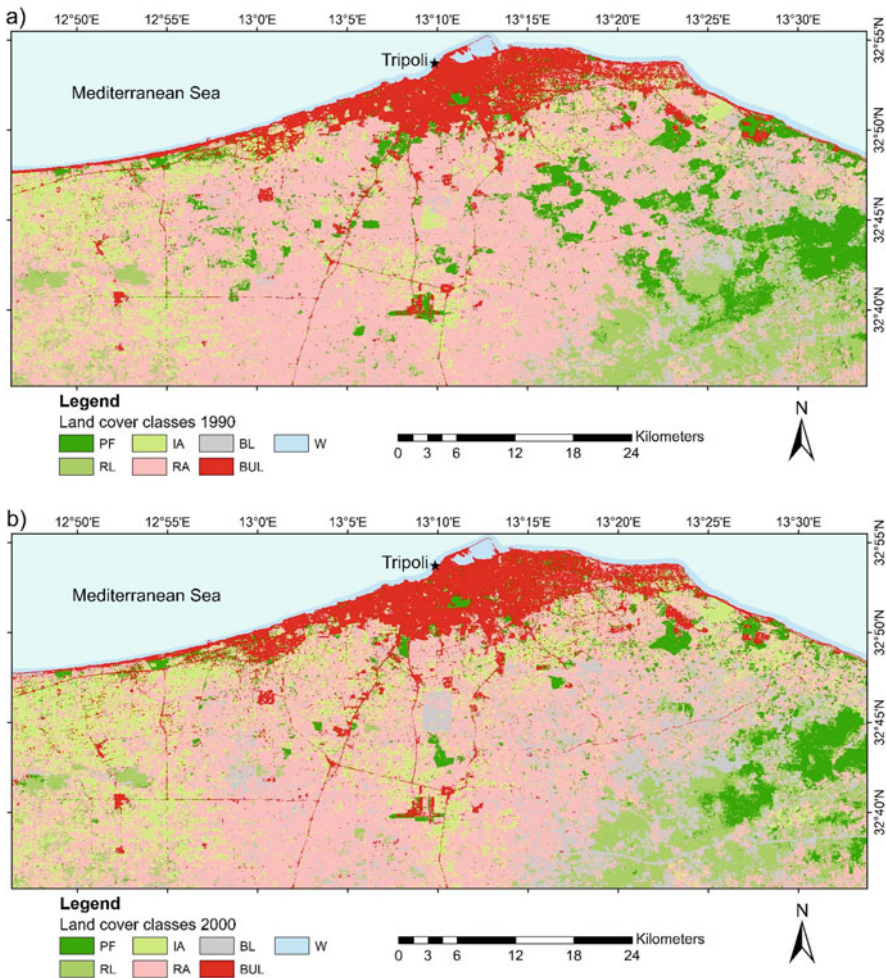


Fig. 4 Land cover classification at 30 m resolution for the years: (a) 1990, (b) 2000, (c) 2010, and (d) 2020

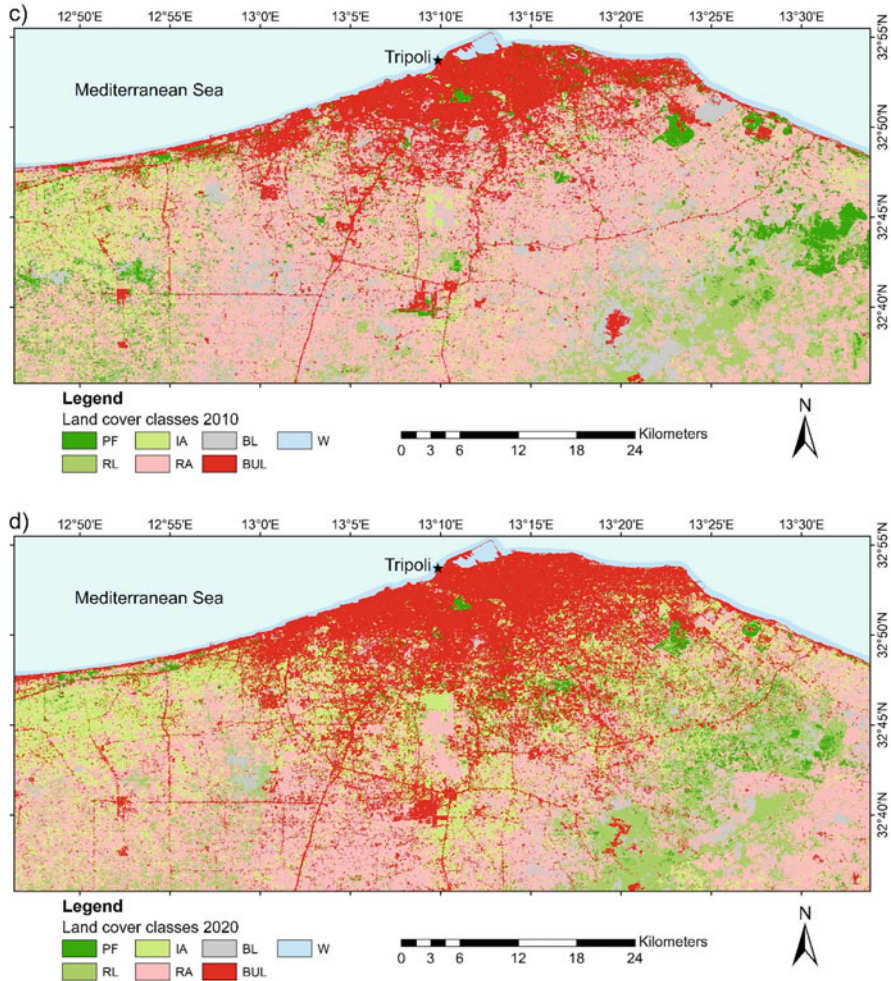


Fig. 4 (continued)

Over the whole study period 1990–2020, approximately 50.31% of the total study area remained unchanged, while 49.68% changed. The built-up areas and infrastructure expansion were continuously increasing over time.

Plantation forests and shrubs areas experienced the highest decline in vegetation cover, while rangelands areas inherently tended to be stable (Table 4). In the first study year 1990, the plantation forests and shrubs areas were 230.20 km² (9.93%), while the rangelands areas were 284.38 km² (12.26%); in the second year 2000, plantation forests and shrubs areas declined to 157.02 km² (6.77%), while the rangelands areas decreased to 265.51 km² (11.45%); in the third year 2010, plantation forests and shrubs areas decreased to 149.63 km² (6.45%), while the rangelands areas decreased to 263.93 km² (11.38%). In the last year of the study period 2020,

Table 3 User's accuracy, producer's accuracy, F1 score, overall accuracy, and kappa coefficient by land cover classes

Accuracy assessment	Land cover classes						
	PF	RL	IA	RA	BL	BUL	W
	Year: 2000						
User's accuracy	82.97%	73.03%	98.07%	60.00%	100.00%	97.43%	100.00%
Producer's accuracy	65.00%	84.41%	76.11%	100.00%	81.03%	79.16%	100.00%
F1 score	0.73	0.78	0.86	0.75	0.90	0.87	1.00
Overall accuracy	83.49%						
Kappa coefficient	0.81						
	Year: 2010						
User's accuracy	80.95%	90.14%	86.36%	56.62%	81.81%	100.00%	100.00%
Producer's accuracy	75.55%	76.19%	67.85%	83.92%	93.44%	94.44%	100.00%
F1 score	0.78	0.82	0.76	0.67	0.87	0.97	1.00
Overall accuracy	83.68%						
Kappa coefficient	0.81						
	Year: 2020						
User's accuracy	97.29%	79.16%	93.93%	56.81%	80.95%	97.77%	100.00%
Producer's accuracy	94.73%	32.20%	88.57%	87.71%	100.00%	100.00%	100.00%
F1 score	0.95	0.45	0.91	0.68	0.89	0.98	1.00
Overall accuracy	84.71%						
Kappa coefficient	0.82						

Table 4 The distribution of land cover classification for each year

Land cover classes	The coverage area for each year							
	1990		2000		2010		2020	
	Km ²	(%)	Km ²	(%)	Km ²	(%)	Km ²	(%)
Plantation forests(PF)	230.20	9.93	157.02	6.77	149.63	6.45	81.25	3.51
Rangelands (RL)	284.38	12.26	265.51	11.45	263.93	11.38	278.52	12.01
Irrigated agriculture (IA)	206.99	8.88	287.11	12.35	178.37	7.69	413.4	17.83
Rainfed agriculture (RA)	1229.28	53.00	1107.01	47.72	1134.97	48.90	893.42	38.52
Barren land (BL)	148.73	6.42	251.12	10.83	245.45	10.59	101.69	4.34
Built-up land (BUL)	176.39	7.61	208.63	9.00	303.76	13.10	508.28	21.92
Water (W)	43.87	1.90	43.44	1.88	43.73	1.89	43.28	1.87
Total	2319.84	100.00	2319.84	100.00	2319.84	100.00	2319.84	100.00

the plantation forests and shrubs areas decreased to 81.25 km² (3.51%), while the rangelands increased to 278.52 km² (12.01%), respectively.

In the agricultural areas, irrigated agriculture was 206.99 km² (8.88% of the study area) in 1990 and increased to 287.11 km² (12.35%) in 2000. The area of the irrigated agriculture category declined to 178.37 km² (7.69%) in 2010, and this area witnessed a substantial increase to 413.40 km² (17.83%) in the last year of the study period 2020. The rainfed agriculture area was 1229.28 km² (53.00% of the study area) in 1990 and decreased to 1107.01 km² (47.72%) in 2000. The rainfed agriculture category area increased to 1134.97 km² (48.90%) in 2010, and this area substantially decreased to 893.42 km² (38.52%) in the last year of the study period 2020 (Table 4).

The barren land area was 148.73 km² (6.42% of the study area) in 1990 and increased to 251.12 km² (10.83%) in 2000, and this area also decreased to 245.45 km² (10.59%) in 2010. The barren land category area experienced a substantial decrease to 101.69 km² (4.34%) in the last year of the study period 2020 (Table 4).

The built-up land area experienced a remarkable change over time, where it was 176.39 km² (7.61%) in the first year 1990, and 208.63 km² (9.00%), in the second year 2000, respectively. In the third year 2010, this area increased to 303.76 km² (13.10%) and showed a remarkable increase to 508.28 km² (21.92%) in the last year of the study period 2020 (Table 4). Water bodies area showed no distinct changes, where it was ranged between about 43.87 km² (1.90%) and 43.28 km² (1.87%) over the whole study period 1990–2020.

3.3 Land Use Change Detection Using Post-classification Comparison Approach

Over the whole study period, the predominant land cover alteration at each time interval was generally caused by changes from plantation forests and shrubs and rainfed agriculture areas to rangelands and built-up land areas. The mosaic plot in (Fig. 5) represents a statistical summary of losses and gains for four-time intervals: 1990–2000, 2000–2010, 2010–2020, and 1990–2020. The plot indicates that the loss of plantation forests and shrubs is substantially more significant than expected in the first interval between the years 1990–2000. That resulted in less than an expected loss to rangelands, irrigated agriculture, and barren land in this interval. The mosaic plot (Fig. 5) also shows substantial changes in the third and fourth intervals between the years 2010–2020, and 1990–2020. For example, in the third interval, the loss of rainfed agriculture area is substantially greater than would be expected, while substantial and unexpected loss is observed in irrigated agriculture in this interval. In addition, the gains of built-up land area are substantially greater than would be expected in the third and fourth intervals between the years 2010–2020, and 1990–2020, respectively.

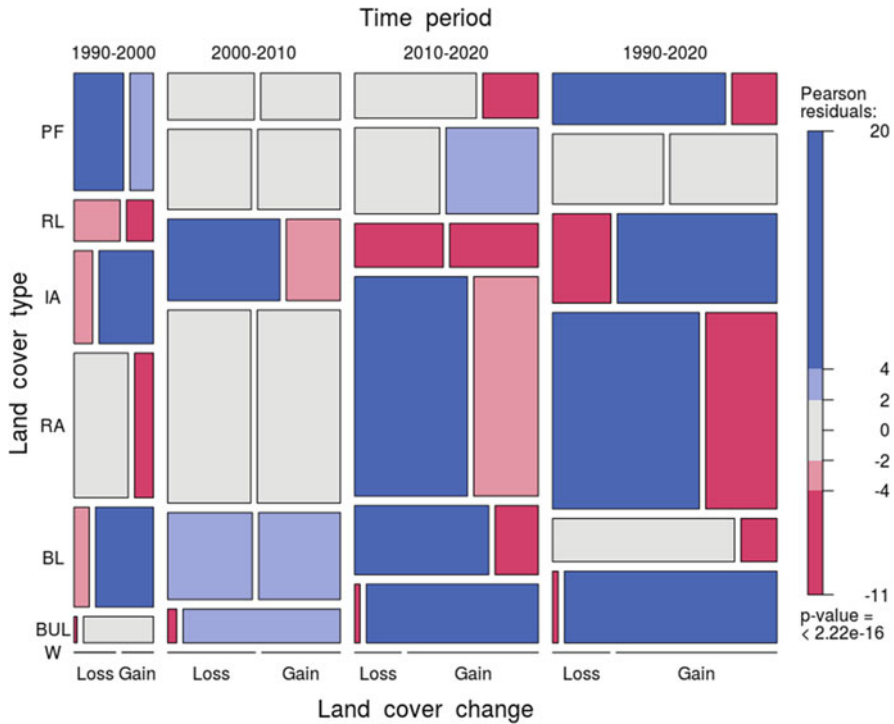


Fig. 5 Mosaic plot of the land cover type (i.e., loss and gain) in each time interval (NFS plantation forests and shrubs, RL rangelands, IA irrigated agriculture, RA rainfed agriculture, BL barren land, BUL, built-up land, W water)

3.4 Land Use Change Detection Using NDVI Change Ratio

NDVI change detection is a robust alternative to more traditional approaches used in land cover classification (Zurqani et al. 2019b). In this study, NDVI Change Ratio to Previous Year (RPNDVI) change detection approach helped clarify and provide a better understanding of the land cover change dynamics analysis. However, the effect of the different bandwidths between the Landsat 5 and Landsat 8 images influenced the result of the NDVI change ratio approach, as this approach worked better in the first interval 1990–2000 and the second interval 2000–2010 (Fig. 6a–d).

The NDVI change detection analysis revealed that the most vegetation loss during the study period occurred in the first 1990–2000, and the second 2000–2010 intervals, where the areas of land use change were 785.93 km² (34.47%), and 843.17 km² (36.98%), respectively. In the third interval between 2010 and 2020, the land use change areas were approximately 366.19 km² (16.06%). Over the whole study period between 1990 and 2020, the land use change areas were about 464.96 km² (20.39%) (Table 5; Fig. 6a–d).

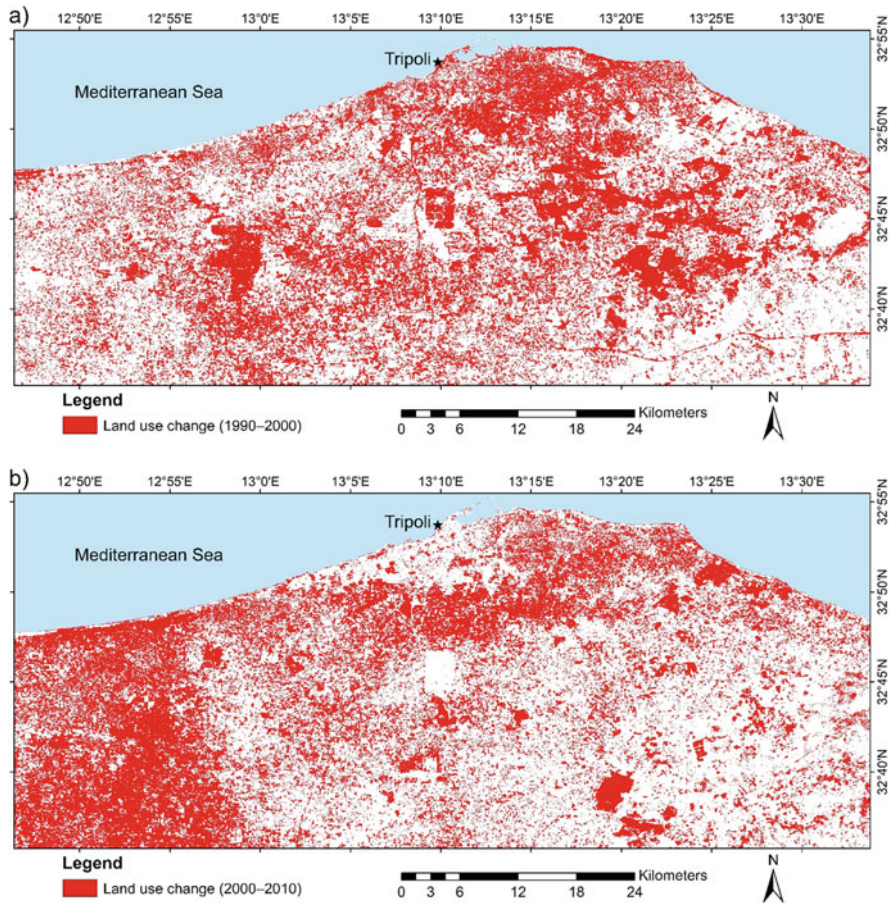


Fig. 6 The areas of land use change using NDVI change ratio: (a) First interval 1990–2000, (b) Second interval 2000–2010, (c) Third interval 2010–2020, and (d) Overall change 1990–2020

3.5 Potential Impacts of Land Cover and Land Use Change

Understanding the land cover trends that have occurred over time is key to the future success of increasing environmental awareness and monitoring. It is concluded that agricultural expansion, deforestation, and increase in built-up land (urbanization) are the main drivers of land cover and land use changes in the studied area. These changes may have several environmental consequences in the region. The expansion of the agricultural regions may boost food production to meet the rising food demand of a growing population, but it also decreases biodiversity (Chaplin-Kramer et al. 2015). Furthermore, converting the plantation forest and natural vegetation to agricultural land is likely to impact soil properties. For instance, agricultural machinery and heavy equipment lead to soil compaction (Ungureanu et al. 2015) which

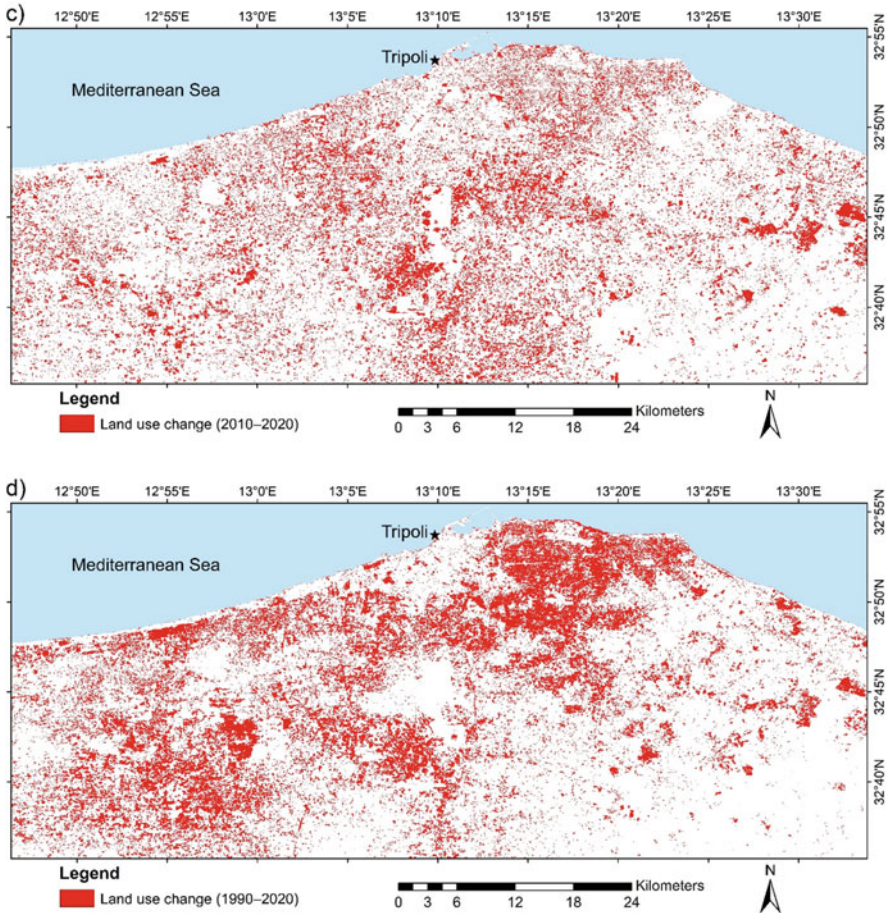


Fig. 6 (continued)

causes a reduction in soil porosity and a decrease in infiltration rates. Consequently, this leads to increased water runoff and increases soil erosion risks (Gill and Vandenberg 1968; Pimentel and Burgess 2013). This soil loss may significantly impact agriculture and local economies (Alcantara-Ayala et al. 2006).

Deforestation or forest clearance is another driving factor of land cover and land use changes (Lambin et al. 2001; Zurqani and Ben Mahmoud 2021). Deforestation can have local and large-scale impacts on the environment. Local impacts include degradation of soil and water resources, wood fuel supplies for household energy, and the overall quality of life, especially in rural areas (Allen and Barnes 1985; Zurqani 2021). On a larger-scale, deforestation is associated with climate change (Malhi et al. 2008), biodiversity loss (Alroy 2017), flooding (Bradshaw et al. 2007) and affecting the ability of ecosystems to provide essential services to humankind

Table 5 Land use change areas from 1990 to 2000, 2000 to 2010, 2010 to 2020, and the overall change from 1990 to 2020

Time interval	Main land use change	Coverage area km ² (%)
First interval (1990–2000)	1. Plantation forests and shrubs to rangelands, irrigated agriculture, and rainfed agriculture. 2. Rangelands to rainfed agriculture. 3. Rainfed agriculture to rangelands, irrigated agriculture, and barren land.	785.93 (34.47%)
Second interval (2000–2010)	1. Rangelands to rainfed agriculture, and barren land. 2. Rainfed agriculture to plantation forests and shrubs, rangelands, and barren land.	843.17 (36.98%)
Third interval (2010–2020)	1. Plantation forests and shrubs to irrigated agriculture, and rainfed agriculture. 2. Rangelands to rainfed agriculture. 3. Barren land to built-up land. 4) Rainfed agriculture to irrigated agriculture, and built-up land.	366.19 (16.06%)
Overall change (1990–2020)	1. Plantation forests and shrubs to irrigated agriculture. 2. Rangelands to rainfed agriculture. 3. Irrigated agriculture to rainfed agriculture. 4. Rainfed agriculture to rangelands, irrigated agriculture, and built-up land. 5. Barren land to rangelands, rainfed agriculture, and built-up land.	464.96 (20.39%)

(Foley et al. 2005). Deforestation is also related to CO₂ emissions, as crops and marginal lands that usually replace trees after land clearing tend to hold less carbon per unit area than forests (Betts 2000; Bala et al. 2007).

The increase of built-up land (also called urbanization and industrialization) is another major driver of land cover and land use change (Allington et al. 2017; Zurqani et al. 2019b). Urban expansion due to the construction of buildings and other artificial surfaces may lead to serious ecological implications, such as a decrease in ecological carrying capacity, desertification, soil erosion, vegetation degradation, biodiversity losses, invasion of alien species, and environmental pollution (Li and Liu 2011; Zhao and Huang 2014). Acceleration of urbanization and industrialization may also contribute to the fragmentation of natural habitats and the loss of important ecosystems that provide essential goods and services (Yi et al. 2017). In addition, these land use and land cover changes and their consequent effects have direct impacts on the livelihoods of local societies (Soltani et al. 2014).

4 Conclusion

Mapping and identifying land cover/land use and its change is the most important and widely researched topic in remote sensing. This study provides an efficient methodology for temporal land cover mapping and change detection analysis utilizing GEE and the public archive database in its platform. Using this approach in GEE allows comparing multiple indices used in the classification process by showing the classification accuracy while performing the image classification. This study indicated that the northwestern region of Libya experienced a dramatic land cover change from 1990 to 2020. The overall accuracy and Kappa coefficient values ranged from 83.49% to 84.71% and 0.81 to 0.82, over the past 30 years. The northwestern region of Libya experienced an increase in built-up land and irrigated agriculture and a decrease in plantation forests and shrubs and barren land in the study area. In general, land cover patterns have undergone a rapid change due to accelerated expansion over the years. In future research, continuous monitoring of this change over time is needed to better understand its impact in the region and return more effective management strategies.

Author Contributions **Hamdi A. Zurqani**: conceptualization, methodology, supervision, software, data curation, formal analysis, validation, investigation, writing—original draft, visualization, writing—review and editing, review of analysis. **Abdulsalam Al-Bukhari**: data curation, writing—original draft, writing—review and editing. **Mahmood B. Shanta**: writing—review and editing. All authors have read and agreed to the published version of the manuscript.

Data Availability The datasets analyzed in this study are publicly available at this GEE App (<https://hzurqan.users.earthengine.app/view/land-cover-mapping-and-change-detection-in-north-western-libya>). The data that support the findings of this study are available from the corresponding author upon reasonable request. Source data are provided with this chapter.

References

- Alawamy JS, Balasundram SK, Hanif AHM, Sung CTB (2020) Detecting and analyzing land use and land cover changes in the region of Al-Jabal Al-Akhdar, Libya using time-series Landsat data from 1985 to 2017. *Sustainability* 12(11):4490
- Alcántara-Ayala I, Esteban-Chávez O, Parrot JF (2006) Landsliding related to land-cover change: A diachronic analysis of hillslope instability distribution in the Sierra Norte, Puebla, Mexico. *Catena* 65(2):152–165
- Al-Bukhari A, Hallett S, Brewer T (2018) A review of potential methods for monitoring rangeland degradation in Libya. *Pastoralism* 8(1):1–14
- Allen JC, Barnes DF (1985) The causes of deforestation in developing countries. *Ann Assoc Amer Geog*, 75(2):163–184
- Allington GRH, Li W, Brown DG (2017) Urbanization and environmental policy effects on the future availability of grazing resources on the Mongolian Plateau: modeling socio-environmental system dynamics. *Environ Sci Pol* 68:35–46
- Alroy J (2017) Effects of habitat disturbance on tropical forest biodiversity. *Proc Natl Acad Sci* 114(23):6056–6061

- Al-sharif AA, Pradhan B (2014) Monitoring and predicting land use change in Tripoli Metropolitan City using an integrated Markov chain and cellular automata models in GIS. *Arab J Geosci* 7(10):4291–4301
- Azeez N, Yahya W, Al-Taie I, Basbrain A, Clark A (2020) Regional agricultural land classification based on random forest (RF), decision tree, and SVMs techniques. In: Fourth international congress on information and communication technology. Springer, Singapore, pp 73–81
- Bala G, Caldeira K, Wickett M, Phillips TJ, Lobell DB, Delire C et al (2007) Combined climate and carbon cycle effects of large-scale deforestation. *Proc Natl Acad Sci U S A* 104(16):6550–6555
- Berberoglu S, Akin A (2009) Assessing different remote sensing techniques to detect land use/cover changes in the eastern Mediterranean. *Int J Appl Earth Obs Geoinf* 11(1):46–53
- Betts R (2000) Offset of the potential carbon sink from boreal forestation by decreases in surface albedo. *Nature* 408(6809):187–190
- Bradshaw CJA, Sodi NS, Peh KSH, Brook BW (2007) Global evidence that deforestation amplifies flood risk and severity in the developing world. *Glob Chang Biol* 13:2379–2395
- Chaplin-Kramer R, Sharp RP, Mandle L, Sim S, Johnson J, Butnar I, i Canals, L.M., Eichelberger, B.A., Ramler, I., Mueller, C. and McLachlan, N. (2015) Spatial patterns of agricultural expansion determine impacts on biodiversity and carbon storage. *Proc Natl Acad Sci* 112(24): 7402–7407
- Congalton RG, Green K (2009) Assessing the accuracy of remotely sensed data: principles and practices, 2nd edn. CRC Press, Boca Raton
- Dabija A, Kluczek M, Zagajewski B, Raczko E, Kycko M, Al-Sulttani AH, Tardà A, Pineda L, Corbera J (2021) Comparison of support vector machines and random forests for Corine land cover mapping. *Remote Sens* 13(4):777
- Deus D (2016) Integration of ALOS PALSAR and Landsat data for land cover and forest mapping in northern Tanzania. *Land* 5(4):43
- Foley J, de Fries R, Asner GP, Barford C, Bonan G, Carpenter SR, Chapin FS, Coe MT, Daily GC, Gibbs HK, Helkowski JH, Hollaway T, Howard EA, Kucharik CJ, Monfreda C, Patz JA, Prentice IC, Ramankutty N, Snyder PK (2005) Global consequences of land use. *Science* 309(5734):570–574
- Foody GM (2002) Status of land cover classification accuracy assessment. *Remote Sens Environ* 80(1):185–201
- Gill WR, Vandenberg GE (1968) Soil dynamics in tillage and traction, U.S.A. Department of Agriculture, Handbook No. 316
- Gorelick N, Hancher M, Dixon M, Ilyushchenko S, Thau D, Moore R (2017) Google Earth Engine: planetary-scale geospatial analysis for everyone. *Remote Sens Environ* 202:18–27
- Gutman G, Janetos AC, Justice CO, Moran EF, Mustard JF, Rindfuss RR, Skole D (2012) In: Cochrane MA, Turner BL II (eds) *Land change science: observing, monitoring and understanding trajectories of change on the earth's surface*. Springer Science & Business Media, Dordrecht
- Huete A, Didan K, Miura T, Rodriguez P, Gao X, Ferreira G (2002) Overview of the radiometric and biophysical performance of the MODIS vegetation indices. *ISPRS J Photogramm Remote Sens* 83(1–2):195–213
- Lam NSN (2008) Methodologies for mapping land cover/land use and its change. In: *Advances in land remote sensing*. Springer, Dordrecht, pp 341–367
- Lambin EF et al (2001) The causes of land-use and land-cover change: moving beyond the myths. *Glob Environ Chang* 11:261–269
- Lambin EF, Geist H, Rindfuss RR (2006) Introduction: local processes with global impacts. In: Lambin EF, Geist H (eds) *Land-use and land-cover change, Global change - the IGBP series*. Springer, Berlin/Heidelberg. https://doi.org/10.1007/3-540-32202-7_1
- Li Y, Liu Y (2011) The ecological analysis of a new round land use planning based on ecological footprint in Guangxi. In: 2011 second international conference on mechanic automation and control engineering, pp 6981–6984

- LIB/00/004 (2009) Mapping of natural resources for agriculture use and planning in Libya Project, Atlas of natural resources for agricultural use in Libya. <http://www.fao.org/geospatial/resources/detail/en/c/1024739/>. Accessed 01 Aug 2021
- Lu D, Weng Q (2007) A survey of image classification methods and techniques for improving classification performance. *Int J Remote Sens* 28(5):823–870
- Lucas IFJ, Janssen F, van der Wel FJ (1994) Accuracy assessment of satellite derived landcover data: A review. *Photogramm Eng Remote Sens* 60(4):479–426
- Lyons MB, Keith DA, Phinn SR, Mason TJ, Elith J (2018) A comparison of resampling methods for remote sensing classification and accuracy assessment. *Remote Sens Environ* 208:145–153
- Mahmood-Misrati AA (1983) Land conversion to urban use: its impact and character in Libya. *Ekistics*:183–194
- Malhi Y et al (2008) Climate change, deforestation, and the fate of the Amazon. *Science* 319:169–172
- National Research Council (2005) Population, land use, and environment: research directions. The National Academies Press, Washington, DC
- Pimentel D, Burgess M (2013) Soil erosion threatens food production. *Agriculture* 3:443–463
- Polykretis C, Grillakis MG, Alexakis DD (2020) Exploring the impact of various spectral indices on land cover change detection using change vector analysis: a case study of Crete Island. *Greece Remote Sens* 12(2):319
- Rodriguez-Galiano VF, Ghimire B, Rogan J, Chica-Olmo M, Rigol-Sanchez JP (2012) An assessment of the effectiveness of a random forest classifier for land-cover classification. *ISPRS J Photogramm Remote Sens* 67:93–104
- Rokni K, Ahmad A, Selamat A, Hazini S (2014) Water feature extraction and change detection using multitemporal Landsat imagery. *Remote Sens* 6(5):4173–4189
- Soltani A, Angelsen A, Eid T (2014) Poverty, forest dependence and forest degradation links: evidence from Zagros. *Iran Environ Dev Econ* 19:607–630
- Thanh Noi P, Kappas M (2018) Comparison of random forest, k-nearest neighbor, and support vector machine classifiers for land cover classification using Sentinel-2 imagery. *Sensors* 18(1): 18
- Tsutsumida N, Comber A (2015) Measures of Spatio-temporal accuracy for time series land cover data. *Int J Appl Earth Obs* 41:46–55
- Tucker CJ (1979) Red and photographic infrared linear combinations for monitoring vegetation. *Remote Sens Environ* 8(2):127–150
- Ungureanu N, Croitoru Ș, Biris S-S, Voicu G, Vladut V, Selvi KÇ, Boruz S, Marin EM, Mihai G, Manea D, Ionescu M, Constantin GA (2015) Agricultural soil compaction under the action of agricultural machinery. In: Kovacev I (ed) *Aktualni Zadaci Mehanizacije Poljoprivrede: Actual tasks on agricultural engineering*, vol 43. *Agronomski Fakultet Sveucilista U Zagrebu, Zagreb*, pp 31–42
- Waske B, Braun M (2009) Classifier ensembles for land cover mapping using multitemporal SAR imagery. *ISPRS J Photogramm Remote Sens* 64(5):450–457
- Wu Q, Li H-q, Wang R-s, Paulussen J, He Y, Wang M, Wang B-h, Wang Z (2006) Monitoring and predicting land use change in Beijing using remote sensing and GIS. *Landsc Urban Plan* 78: 322–333. <https://doi.org/10.1016/j.landurbplan.2005.10.002>
- Xu H (2007) Extraction of urban built-up land features from Landsat imagery using a thematic-oriented index combination technique. *Photogramm Eng Remote Sens* 73(12): 1381–1391
- Yang X, Lo CP (2002) Using a time series of satellite imagery to detect land use and land cover changes in the Atlanta, Georgia metropolitan area. *Int J Remote Sens* 23(9):1775–1798
- Yi H, Güneralp B, Filippi AM, Kreuter UP, Güneralp İ (2017) Impacts of land change on ecosystem services in the San Antonio River basin, Texas, from 1984 to 2010. *Ecol Econ* 135:125–135
- Zhao QG, Huang GQ (2014) Study of ecological security in Guangxi Province (in Chinese). *Acta Ecol Sin* 34:5125–5141

- Zurqani HA (2021) Introduction. In: Zurqani HA (ed) The soils of Libya. World soils book series. Springer, Cham. https://doi.org/10.1007/978-3-030-66368-1_1
- Zurqani HA, Ben Mahmoud KR (2021) Land cover, land use, and vegetation distribution. In: Zurqani HA (ed) The soils of Libya, World soils book series. Springer, Cham. https://doi.org/10.1007/978-3-030-66368-1_6
- Zurqani HA, Post CJ, Mikhailova EA, Schlautman MA, Sharp JL (2018) Geospatial analysis of land use change in the Savannah River basin using Google earth engine. *Int J Appl Earth Obs Geoinf* 69:175–185
- Zurqani HA, Mikhailova EA, Post CJ, Schlautman MA, Elhawej AR (2019a) A review of Libyan soil databases for use within an ecosystem services framework. *Land* 8(5):82
- Zurqani HA, Post CJ, Mikhailova EA, Allen JS (2019b) Mapping urbanization trends in a forested landscape using google earth engine. *Remote Sens Earth Syst Sci* 2(4):173–182
- Zurqani HA, Post CJ, Mikhailova EA, Cope MP, Allen JS, Lytle B (2020) Evaluating the integrity of forested riparian buffers over a large area using LiDAR data and Google Earth Engine. *Nature “Scientific Reports”* 10(1):1–16

Hamdi A. Zurqani is an Assistant Professor of Geospatial Science in Natural Resource Management and Conservation at the University of Arkansas Agricultural Experiment Station, Arkansas Forest Resources Center, University of Arkansas at Monticello, Monticello, AR, USA. He is also an FAA (i.e., Pt107) Certified sUAS/Drones Pilot, and has used this skill to enhance his knowledge of remote sensing and GIS. Dr. Zurqani is a recognized expert as a result of his internationally acclaimed work in the areas of environmental information science, remote sensing, geospatial analysis, land evaluation, sustainability, pedology, and soil science education. He has conducted research across the world, including the United States of America, and Africa, and has served as PI, co-PI, or co-investigator on several grants-funded research projects. Dr. Zurqani is highly collaborative as evidenced by his publications. He is the author and coauthor of many peer-reviewed publications, book chapters, and technical publications (including teaching laboratory manuals). He also edited two books with Springer Nature (i.e., “The Soils of Libya”, and “Environmental Applications of Remote Sensing and GIS in Libya”), and has published widely in many peer-review journals (e.g., *International Journal of Applied Earth Observation and Geoinformation* (Elsevier); *Remote Sensing in Earth Systems Sciences* (Springer Nature); *Scientific Reports* (Nature); *Frontiers in Environmental Science* (Frontiers); *Geoderma* (Elsevier); *Land* (MDPI); *Urban Forestry & Urban Greening* (Elsevier), and others). Dr. Zurqani is a member of the Editorial Board for *Remote Sensing* (MDPI) Journal, counseling outcome, and research evaluation. He also was appointed to serve as a Guest Editor for the Special Issue “Applications of Remote Sensing in Earth Observation and Geo-Information Science”. In addition, Dr. Zurqani conducted peer-review for many journals including *Journal of Environmental Informatics*, *Applied Sciences*, *SN Applied Sciences*, *Remote Sensing*, *Geo-spatial Information Science*, *AgriEngineering*, *Sensors*, *Heliyon*, *Geosciences*, *Land*, *Soil Systems*, *Water*, *Agronomy*, *Agriculture*, *Resources*, *Sustainability*, *Arid Land Research and Management*, *Quaestiones Geographicae*, *Geocarto International*, *International Journal of Environmental Research and Public Health*, *Natural Hazards*, and *Conference of the Arabian Journal of Geosciences*. Dr. Zurqani conducts cutting-edge research in the field of Environmental Information Science, Remote Sensing, Land use management/ planning, change detection of landscape degradation, and Geographic Information System (GIS) models. He has focused his research efforts on the development of novel applications for new technologies in analyzing spatial data, remote sensing, geostatistical modeling of environmental changes such as erosion, mapping and predicting soil salinity, and land use/ land cover changes. His new publications include: “Mapping and Quantifying Agricultural Irrigation in Heterogeneous Landscapes Using Google Earth Engine” in the *Journal of Remote Sensing Applications: Society and Environment*; “Evaluating the integrity of forested riparian buffers over a large area using LiDAR data and Google Earth Engine” in the *Journal of Scientific Reports*; “Mapping Urbanization Trends in a Forested Landscape Using Google Earth Engine” in the *Journal of Remote Sensing in Earth*

Systems Sciences; “Geospatial analysis of land use change in the Savannah River Basin using Google Earth Engine” in the International Journal of Applied Earth Observation and Geoinformation; and “Application of Non-Hydraulic Delineation Method of Flood Hazard Areas Using LiDAR-Based Data” as well as “Assessing ecosystem services of atmospheric calcium and magnesium deposition for potential soil inorganic carbon sequestration” in the Geosciences Journal.

Abdulsalam Al-Bukhari is Lecture of rangeland science at the Department of Forestry and rangeland, Faculty of Natural Resources and Environmental Sciences, Omar Al-Mukhtar University, Al-Bayda, Libya. He received his M.Sc. in Environmental Sciences (rangeland ecology and management) in 2010 from Omar Al-Mukhtar University, Al-Bayda, Libya. Dr. Albukhari achieved his Ph.D. in (Natural resource management) from Cranefield University, Cranefield, UK, in 2019. He specialized in rangeland ecology and management. His main research interests focused on monitoring and assessment of rangeland degradation, the environmental information sciences (Remote Sensing and GIS). Dr. Albukhari is a member of the Editorial Board for Al-Mukhtar Journal of Sciences.

Mahmood B. Shanta is an associate professor of Plant Ecology at the Department of Range and Forestry, Faculty of Agriculture, University of Tripoli, Tripoli – Libya. Dr. Shanta obtained his M. Sc. degree in Plant Eco-physiology, from Faculty of Science, University of Malaya, Kuala Lumpur – Malaysia in 1999. He also completed his Ph.D. in Plant Ecology from University of Sheffield, Sheffield – United Kingdom, in 2008. He attended many workshops, training programs, conferences on plant ecology and field & experimental ecology. His major research and teaching activity focused mainly on plant ecology, effects of climate manipulation on diversity & vegetation composition and environmental degradation.

Evaluation of Selected Vegetation Indices to Assess Rangeland Vegetation in Eastern Libya



Abdulsalam Al-Bukhari, Tim Brewer, and Stephen Hallett

Abstract Observation methods used at ground-based sites are widely used in studies assessing rangeland degradation. However, observations through time are often not integrated nor repeatable, making it difficult for rangeland managers to detect degradation consistently. Vegetation cover in the eastern Libyan rangelands has changed both qualitatively and quantitatively due to natural factors and human activity. This raises concerns about the sustainability of these resources, which play an important role in providing part of the food needs of large numbers of grazing animals, in turn providing food for human consumption. The aim of this research is to evaluate a range of vegetation indices derived from satellite imagery to identify those approaches best applicable for remotely assessing and monitoring vegetation cover in the semi-arid and arid rangelands. This approach was achieved through the utilization of medium resolution satellite imagery to classify vegetation cover. A number of vegetation indices applied in arid and semi-arid rangelands similar to the study area were assessed using ground-based colour vertical photography (GBVP) methods to identify the most appropriate index for classifying percentage vegetation cover. The Modified Soil Adjusted Vegetation Index (MSAVI2) was identified as the most appropriate as this had good correlation with ground data due to the mixture of soil background and vegetation reflectance in low-density vegetation cover areas. Even though the Normalized Difference Vegetation Index (NDVI) remains the most widely-used index, it has limitations as it does not adequately address the influence of the soil background. In arid and semi-arid areas, reducing the soil background noise offers a significant quantitative and qualitative enhancement. These results allow the application of these indices to images from different dates to detect changes in vegetation, allowing monitoring of change in this fragile environment in response to natural and anthropogenic processes.

A. Al-Bukhari

Department of Forest and Rangeland, Faculty of Natural Resources and Environmental Sciences, Omar Al-Mukhtar University, Al-Bayda, Libya

T. Brewer (✉) · S. Hallett

School of Water, Energy and Environment, Cranfield University, Bedford, UK

e-mail: t.brewer@cranfield.ac.uk

Keywords Libyan rangeland · Rangeland degradation · Vegetation index · MSAVI2 · Remote sensing

1 Introduction

Rangeland in Libya provides a significant pillar of support for the national economy, where it represents some 70% of the national landmass. Approximately half of the Libyan rangelands, estimated to be some five million ha in extent, are located in the east of Libya and they play an important role in providing part of the food needs of large numbers of grazing animals (Bayoumi et al. 1998), protecting the environment and conserving the soil from erosion by water and wind.

The eastern Libyan rangeland vegetation cover has changed both qualitatively and quantitatively over the past four decades in response to: decline in rainfall, frequent droughts, wind and water erosion, and human activities such as overgrazing, seasonal fire outbreaks and mismanagement by both pastoralists and rangeland managers (Omar Al Mukhtar University 2005). Managers of Libyan rangelands need effective monitoring systems to help them detect potential problems and to provide data to enable better decisions to be made for the future, to ensure sustainable rangeland management (Al-Bukhari et al. 2018). The accurate monitoring of vegetation condition in rangeland is important for demonstrating rangeland condition, characterizing land cover type and quantifying its extent (Meyer and Turner 1994).

Vegetation cover is frequently used as an indicator when utilising remote sensing data for land condition assessment. Vegetation indices are one of the most widely implemented applications of remotely sensed data for observing and evaluating vegetation by integrating reflectance measurements from two or more wavebands (Pickup et al. 1993; Bannari et al. 1995). Vegetation indices derived from remote sensing data have been widely applied in studies of arid and semi-arid areas at different scales to estimate vegetation cover (Pickup et al. 1994; Gilibert et al. 2002; Jiang et al. 2008). By using these indices, several vegetation parameters such as leaf area, biomass and physiological activities can be assessed (Baret and Guyot 1991; Verrelst et al. 2008), as these parameters are highly correlated to vegetation indices in the red and near infrared wavebands (Broge and Leblanc 2001). The implementation of these indices is generally straightforward and can be used to calculate surface properties when the vegetation canopy is not too dense (less than 50%) or too sparse as the density variation causes significant alteration to the indices as the amount of soil background signal varies (Huete 1988; Liang 2005).

The most widely implemented vegetation index is the Normalized Difference Vegetation Index (NDVI) (Tucker 1979) which has been applied successfully in many studies of arid and semi-arid rangelands (Al-Bakri and Taylor 2003; Jafari et al. 2007; Homer et al. 2012; Sant et al. 2014). However, the NDVI has limitations in areas affected by the soil background in sparsely vegetated areas (Huete 1988). The reflection of soil and sand are much greater than the reflection of vegetation in the red waveband and hence estimating vegetation cover is challenging. Therefore,

soil reflectance adjusted indices such as the Soil Adjusted Vegetation Index (SAVI) (Huete 1988), the Optimized Soil Adjusted Vegetation Index (OSAVI) and the Modified Soil Adjusted Vegetation Index (MSAVI2) (Qi et al. 1994), have been proposed to overcome this limitation (Gilabert et al. 2002; Shupe and Marsh 2004). The Soil and Atmospherically Resistant Vegetation Index (SARVI) (Kaufman and Tanre 1992) has also been developed to reduce the effect of the atmosphere in these regions. Overall, these indices tend to improve the differentiation between soil and vegetation while reducing the effects of illumination conditions (Baret and Guyot 1991). However, they have been identified as being sensitive to soil brightness effects (Huete 1988; Roujean and Breon 1995), particularly where the vegetation cover is low (Broge and Leblanc 2001).

Pickup et al. (1993) proposed the perpendicular distance vegetation index (PD54) to overcome this problem using visible green and red reflectance to separate vegetation cover from soil instead of red and NIR reflectance. They found that this index was less sensitive than red and NIR indices to differences in plant greenness. Although the PD54 index has been widely assessed with success in several Australian rangelands (Bastin et al. 1993; Pickup et al. 1994; McGregor and Lewis 1996), it was not the strongest predictor of perennial or total plant cover in the studied area. Also, it requires the subjective delineation of a soil line and vegetation dominated pixels in the spectral plot. This process needs considerable knowledge in image analysis, is subjective, and can result in a lack of consistency in the application of the index (Jafari et al. 2007).

Jafari et al. (2007) tested the stress related indices 1 and 4 (STVI-1, 4) to solve this problem in the southern arid rangeland in Australia in combination with 12 vegetation indices, comparing the results with measured vegetation cover at land system and landscape scale. They found that STVI-1 and 4 were highly to very highly correlated with vegetation cover at both scales. O'Neill (1996) in western New South Wales found similar results in a community dominated by chenopod shrublands. Barati et al. (2011) have analysed the vegetation cover fraction in sparsely vegetated areas near Esfahan, Iran, evaluating the relationships between 20 vegetation indices and vegetation cover fractions. Their results indicated that the Difference Vegetation Index (DVI) and Ratio Difference Vegetation Index (RDVI) were the most sensitive indices for assessing vegetation cover.

Although many vegetation indices have been proposed, it is obvious that much remains to be done to understand how these indices are implemented in various environments (Silleos et al. 2006) because the results from the studies are often at variance with each other. In addition, these indices cannot be applied to all arid and semi-arid areas as they do not have a standard universal value for the vegetation types found (Bannari et al. 1995).

Some studies have been conducted in Libyan rangeland that include remote sensing data resources for mapping vegetation cover. Mnsur and Rotherham (2010) mapped the change of land cover/land in selected areas of Al Jabal Alakhder from 1984 to 2005 using Landsat TM and Landsat ETM+ data applying a supervised classification method. Elaalem et al. (2013) applied supervised classification using SPOT 5 imagery for evaluating land cover/land use in the north-west region of the

Jeffara Plain. They found this approach led to the production of inaccurate land cover classes due to the limitations of the supervised classification adopted when classifying heterogeneous land cover/use classes. White et al. (2003) mapped changes in vegetation cover in the Wadi Al-Hayat in the south of Libya using NDVI derived from Landsat data. However, the techniques applied in these Libyan studies have limitations in arid and semi-arid areas where sparse vegetation causes increased reflectance response effects from the soil background.

However, a remotely sensed method still requires ground truth data to validate the results. The field-based digital photography method is gaining popularity for the purpose of cover estimation, as it can reduce field time and enable additional analysis in the future (Ko et al. 2017). High resolution, nadir photography can serve as a realistic ground plot. It is information rich, understandable to a broad base of people, and the unanalysed information can be archived for future use. High resolution imagery, of less than 1 cm, is being used by a number of researchers (Breckenridge et al. 2011; Cagney et al. 2011; Karl et al. 2012; Mirik and Ansley 2012). Using high resolution imagery, Pilliod and Arkle (2013) found that the photography-based grid point intercept (GPI) method in Great Basin plant communities was strongly correlated to the line intercept (LI) method but it was 20–25 times more efficient, identified 23% more plant species, and was more precise in determining percent cover. Furthermore, they found that GPI could precisely estimate cover of basic vegetation components when they exceeded 5–13% while LI cover estimates had to exceed 10–30% cover for equal precision. Detecting change when percent cover is low is very important in arid lands where land cover is typically sparse.

Richardson et al. (2001) indicated digital photography analysis was able to generate accurate results in much less time compared to the LI method. Another study which compared digital photo analysis and the point intercept (PI) method also suggested that the results between the two methods were similar when a sufficient number of plots were combined together (Booth and Tueller 2003). Analyzing digital images acquired from the field can be advantageous since the production of permanent images enables the researcher to reanalyze the data later on with more advanced methods and software (Boyd and Svejcar 2005). This method can be particularly helpful since it can drastically reduce time spent in the field and control surveyor-bias (Booth and Tueller 2003). The Sant et al. (2014) methodology has been demonstrated as being an appropriate method in the USA where ground-based photography has been used to assess the vegetation cover.

The aim of this study is not to review in general the use of vegetation indices, as intensive reviews have already been published (Bannari et al. 1995; Jensen 2000; Silleos et al. 2006; Jones and Vaughan 2010; Ren and Feng 2015) rather to evaluate the indices where the purpose is to solve the problem of assessing low vegetation cover in sparsely vegetated rangeland. The specific aim of this paper is to evaluate a range of vegetation indices derived from remote sensing data that have been implemented in other arid and semi-arid rangelands similar to the study area to identify those that are applicable for Libyan rangelands by comparing the performance of the selected spectral indices, using ground-based colour vertical photography (GBVP) to provide comparative ground based measurements of vegetation cover.

2 Materials and Methods

2.1 Study Area

The study area was located in the eastern Libyan rangeland (Fig. 1). This area, including Al Jabal Al Akhdar (the Green Mountain), contains more than 50% of the total number of Libyan floral species and represents one of the most important rangeland areas in Libya, especially during the winter months where the rainy season extends between October and March. The annual rates of rainfall lie between 50–200 mm, while the annual mean temperature is approximately 20 ° C (SWECO 1986).

The study area was selected to best represent the diversity of eastern Libyan rangeland conditions. The boundary was the 300 mm rainfall line to the north, 23° longitude to the east, 21° longitude to the west, and the 50 mm isohyet to the south, as officially in Libya rangeland is located within land receiving annual precipitation between 50 mm to less than 300 mm.

2.2 Field Survey

The field data collection area (Fig. 1) was selected to include representative rainfall, soil and land management variation within the study area and was located between the 50–200 mm isohyet zones from south to north, comprising an area of

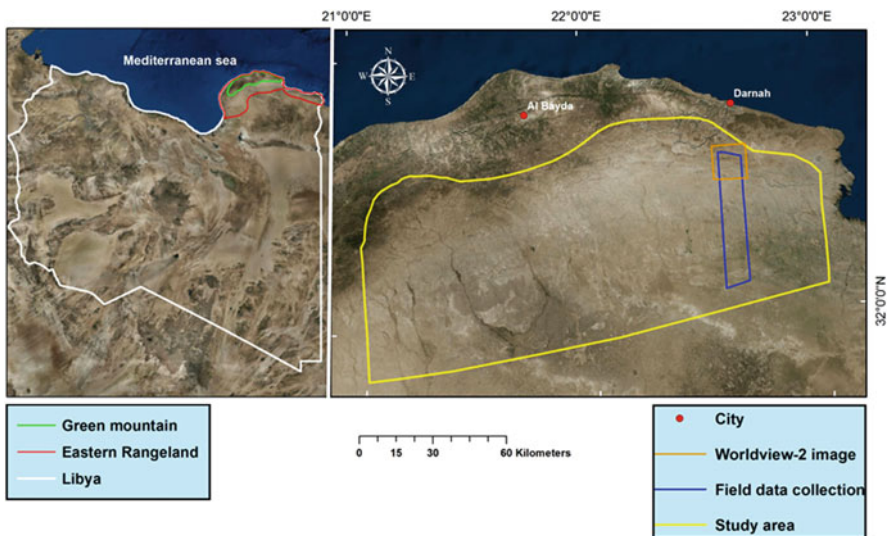


Fig. 1 The study area

approximately 500 km². A total of 100 sample sites were visited to allow for redundancy, with 50 samples used for training data and 50 as validation data. The sample locations were determined using the fishnet tool in ArcGIS (ESRI 2017) to give an even distribution of sites throughout the study area. The sites were greater than 650 m from each other to ensure independence based on semi-variance measurement of the spatial dependence among the observations as a function of distance (Karnieli et al. 2008). The optimum time for field and satellite data collection was based on advice from Libyan rangeland experts and analysis of MODIS NDVI data for the period 2012–2016 to establish the peak extent of vegetation cover.

Ground based vertical photography (GBVP) images (Sant et al. 2014) were taken at each sample site with a 24-megapixel, 10 mm focal length, Canon Digital D750 camera mounted on a portal boom (Fig. 2). Site location was recorded with a Garmin GPSMAP 64S GPS.

The GBVP image ground cover was calculated as follows (Avery and Berlin 1992) (Eq. 3.1):

$$\text{Image ground cover} = \frac{\text{SAW} \times \text{LH}}{\text{FL}} \quad (3.1)$$

Where SAW = sensor array width, LH = lens height and FL = focal length:



Fig. 2 GBVP image acquisition

The average lens height for each nadir image was 3.2 m at all sample locations with a standard deviation of ± 0.05 m, and the area of the image footprint was 34.5 m^2 with a standard deviation of $\pm 1 \text{ m}^2$. Additional high oblique images were taken from the centre point of the nadir image aligned to the four cardinal compass directions to provide additional vegetation cover context.

Adobe Lightroom and Photoshop software packages were used to manage the raw image data collected. The highest quality image at each sample location from the five replicates in each orientation was selected for the classification based on its histogram profile. Masking of the shadow from the portable boom was required for some images.

2.3 GBVP Image Classification

The GBVP nadir images were processed using a combination of the object based ENVI Feature Extraction tool (ENVI 2017) and ArcGIS to calculate the percentage vegetation cover. The objects were classified into three basic ground cover types: bare ground, shrub, and annual vegetation, as well as two additional categories: litter and shadow (Sant et al. 2014).

For each of the 100 GBVP images, a minimum of 15 samples for each ground cover type were digitised as polygons by visual interpretation. These polygons acted as training samples to classify the remaining image pixels. The ENVI Feature Extraction tool offers three methods of classification: K Nearest Neighbour (KNN), Support Vector Machine (SVM), and Principal Components Analysis (PCA). Each of these methods were applied and tested on 10 georeferenced GBVP nadir images, to determine the accuracy of each classification method by using 100 randomly located points in each GBVP image, created using the fishnet tool in ArcGIS. The 100 random points were visually interpreted and compared to each of the classified values from each of the three classification methods from which the most accurate classification method was determined (Congalton 1991).

The Support Vector Machine (SVM) method was identified as the most accurate classification method and was used to produce the percentage cover of shrub, annual vegetation, litter, shadow, and bare ground for each GBVP nadir image. These images were individually classified to overcome variances between images in terms of soil colour, degree of stone cover, and presence of a cryptobiotic cover (Sant et al. 2014). Shadow was classified for each image and was included as part of the % cover of the originating category of that shadow. Therefore, the percentage cover of shrub and annual vegetation (green cover) and any associated shadow were used to calculate the vegetation cover percentage from the satellite derived remotely sensed data.

3 Remote Sensing Data

Landsat 8 OLI images (C1 Level-1) were acquired in March 2017 (paths/ rows: 183/037, 183/038 and 182/038). This imagery was used to derive the vegetation map for the whole study area, represented by the yellow polygon outline in Fig. 1. A Worldview-2 image was also obtained from April 2017 (provided by Digital Globe Inc.) which covered part of the selected field data collection study area (Fig. 1). This image was used in an alternative processing method to evaluate the accuracy of the percentage vegetation cover classification for the selected vegetation index.

3.1 Landsat Image Classification

The ENVI software was used for pre-processing the Landsat 8 images to radiometrically correct, mosaic the three images and subset the study area. A comprehensive range of vegetation indices were selected for evaluation (Table 1). These indices were identified as being appropriate for measuring sparsely vegetated areas of arid and semi-arid rangelands as they have shown good performance in the literature.

Table 1 Vegetation indices selected for evaluation

Vegetation index	Equation	Reference
Normalized Difference Vegetation Index (NDVI)	$(NIR - RED)/NIR + RED)$	Tucker (1979)
Difference Vegetation Index (DVI)	NIR/RED	Tucker (1980)
Ratio Difference Vegetation Index (RDVI)	$NIR - RED/\sqrt{NIR + RED}$	Roujean and Breon (1995)
Soil Adjusted Vegetation Index (SAVI)	$[(NIR - RED)/NIR + RED + L] \times (1 + L)$	Huete (1988)
Optimized Soil Adjusted Vegetation Index (OSAVI)	$(NIR - RED)/NIR + RED + 0.16$	Rondeaux et al. (1996)
Modified Soil Adjusted Vegetation Index 2 (MSAVI2)	$\frac{2NIR+1-\sqrt{(2NIR+1)^2-8(NIR-RED)}}{2}$	Qi et al. (1994)
Soil and Atmospherically Resistant Vegetation Index (SARVI)	$(1 + L)(NIR - RB)/NIR + RB + L$	Kaufman and Tanre (1992)
Stress Related Vegetation index -1 (STVI-1)	$(MIR \times RED)/NIR$	Thenkabail et al. (1994)
Stress Related Vegetation index -3 (STVI-3)	$NIR/(RED + MIR)$	Thenkabail et al. (1994)
Stress Related Vegetation Index -4 (STVI-4)	$NIR - (RED \times MIR)/(NIR + MIR)$	Jafari et al. (2007)
Mid-infrared-3 Vegetation Index (MSVI-3)	$NIR/(MIR + SWIR)$	Thenkabail et al. (1994)
Modified Triangulation Vegetation Index-1 (MTVI1)	$1.2 [1.2(NIR - GREEN) - 2.5(RED - GREEN)]$	Haboudane et al. (2004)

The results from each index tested were compared to the GBVP nadir images to identify the most appropriate vegetation index to estimate vegetation cover data at the sample sites. The selected vegetation index from the GBVP image analysis was used to train the Landsat 8 image classification for the whole study area. Vegetation index threshold values were defined for the percentage vegetation cover classification to take into account the sensitivity of remote sensing data to vegetation cover and the minimum vegetation cover that could provide protection to the soil from erosion. The percentage vegetation cover classification boundaries were selected based on a previous study conducted in part of the study area (SWECO 1986): <10%, 10–35%, >35%. To calculate the accuracy of the percentage cover map, an error matrix was produced using the validation data generated from the GBVP images, to determine the overall accuracy, commission, and omission errors for each class. Kappa analysis was used to determine the agreement within the classification.

The accuracy assessment of the classified Landsat 8 image versus the nadir GBVP data gave a low classification accuracy, due to the very different resolutions and spatial extent of the two sets of imagery, ranging from 2 m resolution for the GBVP nadir data to 30 m for the Landsat 8 imagery. The ground extent of each GBVP nadir image was approximately 4% of a single Landsat pixel and therefore the ground cover percentage of the GBVP image may not be representative of the averaged pixel response on the Landsat image. The four cardinal direction GBVP images were therefore used to obtain a wide area training dataset equivalent to a 30 × 30 m Landsat pixel. The wider area was classified based on visual assessment of what could be seen on the four cardinal images to estimate a vegetation cover value for the 30 × 30 m area. The wide area training dataset was applied to the Landsat 8 imagery and a new vegetation cover classification derived that was assessed for accuracy.

3.2 Worldview 2 Image Classification

An alternative method was tested to enhance the accuracy of the classification, using a multi-resolution approach applied by Simms et al. (2017) in Afghanistan where the core mapping was undertaken within a 1 km² segment at 1 m resolution and statistically expanded to enable classification of 32 m DMC imagery to enable regional classification of imagery. The selected vegetation index that had the highest correlation using the GBVP data was applied to the Worldview 2 imagery to create a vegetation index classification image at 2 m resolution and an accuracy assessment was undertaken. The threshold values from the vegetation index were identified to classify the Worldview 2 image into the three vegetation cover classes. A training dataset from the Worldview 2 vegetation cover classification was selected to train the 2017 Landsat 8 image. This produced a new vegetation cover classification to

investigate whether this enhanced the accuracy of the medium resolution data classification compared to classifying the medium resolution data directly using the GBVP images. An accuracy assessment was conducted on the new classification using the GBVP images to enable this comparison to be made.

4 Results and Discussion

4.1 Ground Based Vertical Photography (GBVP) Method

The results from five years of NDVI values across the study area showed that the peak of vegetation production was from February to April (Fig. 3) and was therefore the optimum time for ground survey. This also agreed with the views of Libyan rangeland experts consulted during the research and other authors (Tehrany et al. 2017). The field data collection for the GBVP therefore took place in March 2017 to correspond with the peak of vegetation greenness.

In the field, shadow was minimized by taking GBVP images between 9:00 a.m. and 4:00 p.m. At each sample location, GBVP nadir and cardinal azimuth (north, east, south, and west) images were captured five times. The total number of images captured were 500 GBVP nadir images and 2000 images for the four cardinal directions. The 100 ‘highest quality’ GBVP nadir images (one for each sample location) and the 400 ‘highest quality’ images for the four cardinal directions (one from each cardinal direction at each sample location) were selected for analysis to extract the vegetation cover.

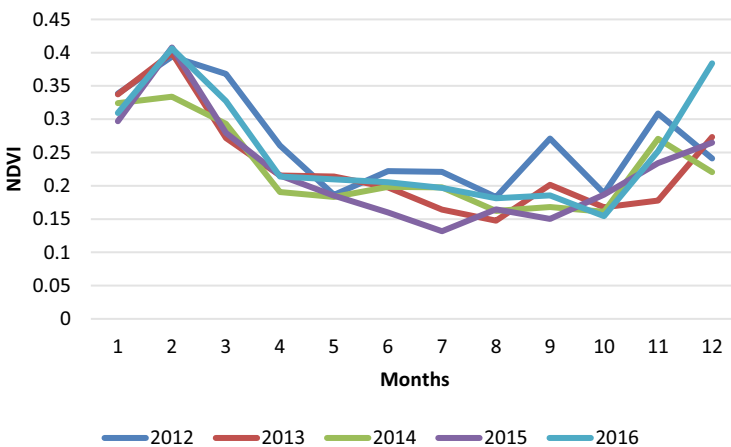


Fig. 3 Five-year trend of MODIS NDVI

4.2 GBVP Image Classification

In order to identify the most appropriate method for classifying the GBVP images, three methods of classification available in the ENVI Feature Extraction tool were tested. The K Nearest Neighbour (KNN) and Principal Components Analysis (PCA) did not perform well but the Support Vector Machine (SVM) was identified as the most appropriate method for classification with an overall accuracy of 85%, followed by K Nearest Neighbour (KNN) and Principal Components Analysis (PCA) with overall accuracies of 40% and 30%, respectively. The results of the classifications from the three methods can be seen in Fig. 4.

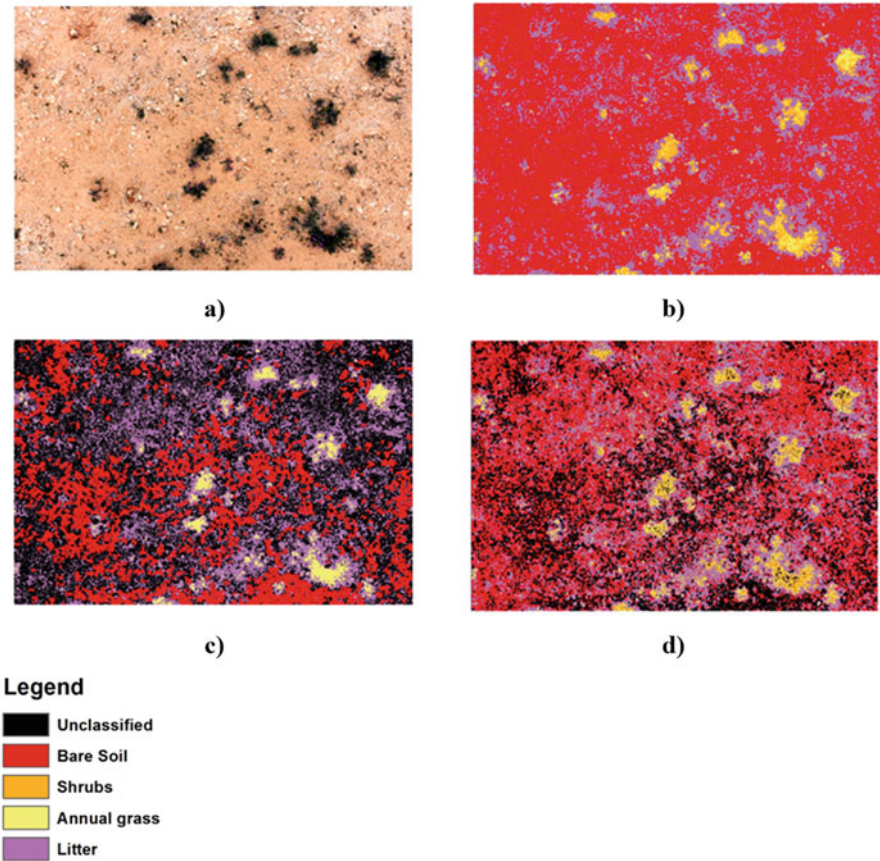


Fig. 4 Classification methods tested for GBVP images; (a) ground-based colour vertical, (b) support vector machine (SVM), (c) principal components analysis, and (d) k nearest neighbour (KNN)

4.3 Vegetation Indices Analysis Using GBVP Imagery

Twelve vegetation indices derived from the Landsat 8 imagery and the total vegetation cover extracted from the GBVP were analysed using simple linear regression. The results showed that all vegetation indices tested in this study were significantly and strongly correlated with the ground data (nadir image GBVP) with r values ranging from 0.653 to -0.821 (Table 2). STVI_1 was the most correlated index with ground measured vegetation cover extracted from the non-adjusted GBVP with $r = -0.821$ where a decreasing index value corresponds with increasing vegetation cover. This finding agrees with Jafari et al. (2007). The lowest correlation index was MSVI_3 with $r = 0.653$. This shows that the shortwave infrared index is less effective for predicting vegetation cover.

With the inclusion of visual interpretation from the four cardinal images, the results indicated that the correlation of all vegetation indices was enhanced. The correlations ranged from 0.697 to -0.894 (Table 3). STVI_1 remained the most correlated index to ground vegetation cover, and the correlation of STVI_1 increased from -0.821 to -0.894 . Even though the most highly correlated index was STVI_1, it has a negative relation with vegetation cover as the index decreases with increasing vegetation influence making it harder to interpret compared to the indexes that have a positive correlation (Jafari et al. 2007). The MSVI_3 correlation was also enhanced, reaching 0.697 compared to 0.653.

The results demonstrated that the use of the shortwave infrared MSVI_3 index instead of the near infrared in the STVI_3 index reduced the accuracies of prediction as it had the lowest correlation. This finding agreed with Barati et al. (2011). Also, indices that integrate the green band, such as MTVI1, are among the well correlated indices. This result is similar to Baret and Guyot (1991) and Haboudane et al. (2004) but is inconsistent with other results using the green band conducted in similar

Table 2 The relationship between the vegetation indices and nadir GBVP image

Vegetation indices	Mean	Std.Dv.	r (X,Y)	r^2
NDVI	0.141794	0.04578	0.792676	0.628336
DVI	0.121312	0.02173	0.743858	0.553325
RDVI	0.130861	0.03171	0.788842	0.622272
SAVI	0.133665	0.03435	0.794053	0.630520
OSAVI	0.119144	0.03482	0.795596	0.632972
MSAVI2	0.131119	0.03187	0.788526	0.621774
SARVI	-0.046473	0.04785	0.710057	0.504181
STVI_1	0.425994	0.07041	-0.820685	0.673523
STVI_3	0.537347	0.04395	0.755061	0.570117
STVI_4	0.272397	0.04356	0.809562	0.655391
MSVI_3	0.507744	0.04024	0.653112	0.426555
MTVI1	-0.001471	0.06045	0.807264	0.651674

p-value is 0.0000 with all indices

Table 3 The relationship between the vegetation indices and the GBVP images using visual interpretation of the four cardinal direction GDVP images

Vegetation indices	Mean	Std.Dev.	r(X,Y)	r ²
NDVI	0.141794	0.04578	0.870957	0.758566
DVI	0.121312	0.02173	0.835211	0.697577
RDVI	0.130861	0.03171	0.874532	0.764806
SAVI	0.133665	0.03435	0.879232	0.773050
OSAVI	0.119144	0.03482	0.877093	0.769292
MSAVI2	0.131119	0.03187	0.874669	0.765046
SARVI	-0.046473	0.04785	0.721251	0.520204
STVI_1	0.425994	0.07041	-0.894678	0.800449
STVI_3	0.537347	0.04395	0.814367	0.663194
STVI_4	0.272397	0.04356	0.877200	0.769480
MSVI_3	0.507744	0.04024	0.697431	0.486411
MTVI1	-0.001471	0.06045	0.887711	0.788032

p-value is 0.0000 with all indices

sparsely vegetated areas where a decrease in the sensitivity of the index gave a lower correlation with variations in vegetation cover fraction (Barati et al. 2011).

Moreover, the study indicates that SAVI, OSAVI, and MSAVI2 (soil adjusted indices) give similar correlations to NDVI; this result is similar to Ren and Feng (2015) but is not consistent with the findings of other work where soil-adjusted indices perform better than NDVI (Rondeaux et al. 1996; Huete 1988). However, NDVI does not cancel the noise caused by the soil background. In arid and semi-arid areas, reducing the soil background noise is a significant quantitative and qualitative enhancement (Silleos et al. 2006).

The optimised soil-adjusted vegetation index (OSAVI) is the same as SAVI with a soil adjustment factor of 0.16 rather than 0.5 that is based on vegetation cover density. However, since the vegetation cover was of relatively low density in the study area, the SAVI should result in better performance in a low-density vegetated area as it has a higher adjustment factor compared to OSAVI (Lawrence and Ripple 1998). For optimal adjustment of the soil effect, however, the L factor (a function of vegetation cover density) should vary inversely with the amount of vegetation present and ranges from 0 to 1. MSAVI2 replaces the constant L in the SAVI equation (Table 1) with a variable L function that is self-adjustable. This enhancement of the MSAVI2 minimises the soil background influences, resulting in greater vegetation sensitivity (Qi et al. 1994). The SAVI needs antecedent knowledge regarding densities of vegetation in terms of adopting an optimal L value while MSAVI2 does not require knowledge of vegetation cover to determine the L factor (Qi et al. 1994). The MSAVI2 was therefore selected and tested to map the vegetation cover within the eastern Libyan rangeland taking into account the soil background effect and also its designed correction with respect to how the non-modified SAVI index responds to vegetation.

4.4 Accuracy Assessment of Vegetation Cover

The accuracy assessment of the MSAVI2 derived percentage vegetation cover using the nadir only GBVP imagery indicated that the overall accuracy was 84% and the user’s accuracy for the three vegetation cover classes were 92.5%, 33.33% and 57.14%, respectively (Table 4).

Whereas when the cardinal GBVP imagery was included, the accuracy assessment of the MSAVI2 derived percentage vegetation cover showed an overall accuracy enhancement. The overall accuracy was 94.7% and the user’s accuracy for the three vegetation cover classes were 97.8%, 60% and 100%, respectively (Table 5 and Fig. 5).

4.5 Worldview 2 Image Classification

The result of using the Worldview 2 high-resolution image with GBVP to train the 2017 Landsat 8 image illustrated that the overall accuracy of the MSAVI2 derived percentage vegetation cover map decreased, but there was some enhancement in the

Table 4 Accuracy assessment of the percentage vegetation cover derived from Landsat 8 MSAVI2 using non-adjusted GBVP imagery

Reference data (ground data)						
Classified data (percentage vegetation cover)	Vegetation cover class	<10%	10–35%	>35	Total	User’s accuracy
	<10%	37	2	1	40	92.5%
	10–35%	2	1	0	3	33.33%
	>35%	1	2	4	7	57.14%
	Total	41	4	5	50	
	Producer’s accuracy	90.24%	25%	80%	Overall accuracy	84%

Table 5 Accuracy assessment of the percentage vegetation cover derived from Landsat 8 MSAVI2 using cardinal GBVP imagery

Reference data (ground data)						
Classified data (percentage vegetation cover)	Vegetation cover class	<10%	10–35%	>35%	Total	User’s accuracy
	<10%	38	1	0	39	97.82%
	10–35%	1	3	1	5	60%
	>35%	0	0	6	6	100%
	Total	39	4	7	50	
	Producer’s accuracy	97.82%	75%	85.71%	Overall accuracy	94.73%

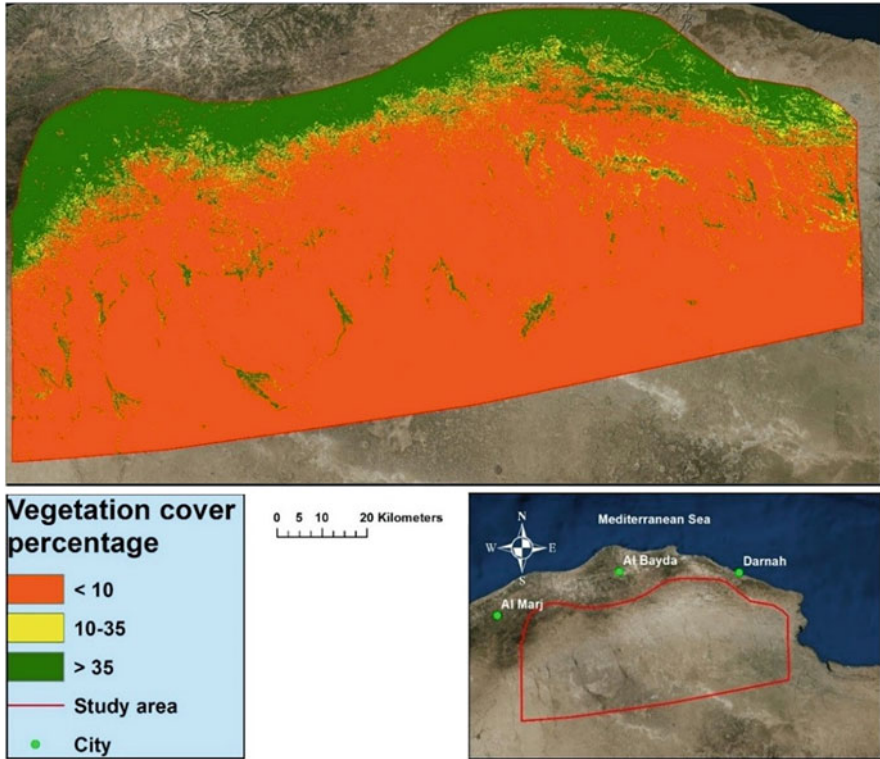


Fig. 5 Vegetation cover percentage derived from the MSAVI2 index using cardinal GBVP imagery

Table 6 Accuracy assessment of the percentage vegetation cover derived from Landsat 8 MSAVI2 using the Worldview 2 image

Reference data (ground data)						
Classified data (percentage vegetation cover)	Vegetation cover class	<10%	10–35%	>35%	Total	User’s accuracy
	<10%	127	46	7	180	70.5%
	10–35%	38	372	108	518	71.8%
	>35%	5	90	480	575	83%
	Total	170	508	595	1273	
	Producer’s accuracy	74.7%	70%	80.6%	Overall accuracy	76.9%

user and producer accuracies as indicated in Table 6. The overall accuracy was 76.9% and the user’s accuracy for the three vegetation cover classes was 70.5%, 71.8% and 83%, respectively.

In addition, the kappa value indicated good agreement ($K = 0.719$) according to the rating criteria of kappa statistics described by Landis and Koch (1977) and Rwanga and Ndambuki (2017) when compared with $K = 0.5079$ when the

classification of vegetation cover from the Landsat 8 image was implemented using the nadir GBVP imagery. Whereas when the cardinal GDVP imagery was used the agreement in the classification increased to $K = 0.8403$.

Overall, using the very high-resolution Worldview 2 imagery with the GBVP images did not enhance the accuracy of the Landsat 8 image classification compared to classifying the data directly using the GBVP images. The reason could be that the ground survey design was established for the greater spatial extent of the Landsat 8 imagery whereas the Worldview image only covered a small part of the study area that led to a low number of sample points located within the Worldview image area. More investigation is needed but using high-resolution satellite imagery is not recommended at this time due to the extra cost involved in obtaining the imagery.

The advantages of the GBVP method are that the vegetation indices assessment is based on much more detailed ground data producing a training and verification dataset that is more closely allied to the data produced by the satellite sensor. It gives a better assessment of the amount of soil versus vegetation taking into consideration the soil background effect. The GBVP can also be reanalysed and classified in the future with more advanced techniques and software applications.

5 Conclusions

The vegetation index approach, supported by the use of ground data, allowed the measurement of the low vegetation cover density in the arid and semi-arid Libyan rangeland taking into account the influence of the soil background. Twelve vegetation indices were tested with the ground-based colour vertical photography (GBVP) and Landsat 8 imagery.

The MSAVI2 index was identified as the most appropriate to use due to the mixture of soil background reflectance with vegetation reflectance in low-density vegetation cover areas. Also, the resolution of the imagery (30 m resolution) did not match the resolution of the information collected on the ground. A further consideration is that successful remote sensing vegetation analysis assessments require a statistically designed survey in terms of the number of points, the distance between the points and the strata used to ensure a fully representative ground survey for all classification categories that are going to be generated from the image.

Even though the NDVI remains the most widely used index, it has limitations as it does not address the influence of the soil background. In arid and semi-arid areas, reducing the soil background noise offers a significant quantitative and qualitative enhancement. Other indices such as STVI_1 were also highly correlated. However, the correlations were either too complex, as in the case of the STVI_1 index where it has a negative relation with vegetation cover making it harder to interpret compared to other indexes that have a positive correlation, or they required more specific parameterisation which would be more difficult to apply by non-experts.

Acknowledgements The authors acknowledge the Libyan Ministry of Higher Education and Scientific Research, for supporting this work. This research was supported by affiliation to the UK Natural Environment Research Council (NERC) (NE/M009009/1). We acknowledge the use of the “Ecosystem Services Databank and Visualisation for Terrestrial Informatics” facility, supported by NERC (NE/L012774/1).

Funding The research was supported by the Libyan Government through the scholarship programme of the Ministry of Higher Education and Scientific Research.

Availability of Data and Materials The vegetation indices presented in this paper derive from open source remote sensing information, specifically Landsat and MODIS from: <https://earthexplorer.usgs.gov>. A Worldview-2 image was provided by Digital Globe Inc.

Author Contributions **Abdulsalam Al-Bukhari:** conceptualization, methodology, supervision, software, data curation, formal analysis, validation, investigation, writing—original draft, visualization, writing—review and editing. **Stephen Hallett:** supervision, review of analysis, writing—review and editing. **Tim Brewer:** supervision, review of analysis, writing—review and editing. All authors have read and agreed to the published version of the manuscript.

Competing Interests The authors declare that they have no competing interests.

References

- Al-Bakri J, Taylor J (2003) Application of NOAA AVHRR for monitoring vegetation conditions and biomass in Jordan. *J Arid Environ* 54:579–593
- Al-Bukhari A, Hallett S, Brewer T (2018) A review of potential methods for monitoring rangeland degradation in Libya. *Pastoralism* 8(1):1–14
- Avery TE, Berlin G (1992) *Fundamentals of remote sensing and airphoto interpretation*, 5th edn. Prentice Hall, London
- Bannari A, Morin D, Bonn F, Huete A (1995) A review of vegetation indices. *Remote Sens Rev* 13: 95–120
- Barati S, Rayegani B, Saati M, Sharifi A, Nasri M (2011) Comparison the accuracies of different spectral indices for estimation of vegetation cover fraction in sparse vegetated areas. *Egypt J Remote Sens Space Sci* 14:49–56
- Baret F, Guyot G (1991) Potentials and limits of vegetation indices for LAI and APAR assessment. *Remote Sens Environ* 35:161–173
- Bastin G, Sparrow A, Pearce G (1993) Grazing gradients in central Australian rangelands: ground verification of remote sensing-based approaches. *Rangel J* 15:217–233
- Bayoumi MA, Al-Saadi OR, Awad JA (1998) The economic importance of rangeland. *J Arts Sci Garyounis Univ Al Marj Libya*:165–169. (in Arabic)
- Boyd CS, Svejcar TJ (2005) A visual obstruction technique for photo monitoring of willow clumps. *Rangel Ecol Manag* 58:434–438
- Booth DT, Tueller PT (2003) Rangeland monitoring using remote sensing. *Arid Land Res Manag* 17:455–467
- Breckenridge RP, Dakins M, Bunting S, Harbour JL, White S (2011) Comparison of unmanned aerial vehicle platforms for assessing vegetation cover in sagebrush steppe ecosystems. *Rangel Ecol Manag* 64(5):521–532

- Broge NH, Leblanc E (2001) Comparing prediction power and stability of broadband and hyperspectral vegetation indices for estimation of green leaf area index and canopy chlorophyll density. *Remote Sens Environ* 76:156–172
- Cagney J, Cox SE, Booth DT (2011) Comparison of point intercept and image analysis for monitoring rangeland transects. *Rangel Ecol Manag* 64(3):309–315
- Congalton RG (1991) A review of assessing the accuracy of classifications of remotely sensed data. *Remote Sens Environ* 37:35–46
- Elaallem MM, Ezlit YD, Elfghi A, Abushnaf F (2013) Performance of supervised classification for mapping land cover and land use in Jeffara Plain of Libya. In: *International proceedings of chemical, biological & environmental engineering*, vol 55
- ENVI (2017) Feature extraction with example based classification tutorial ENVI 5.4.1. Exelis Visual Information Solutions, Broomfield
- ESRI (2017) ArcGIS help, toolbox, ArcGIS desktop10.5. ESRI
- Gilabert M, González-Piqueras J, García-Haro F, Meliá J (2002) A generalized soil-adjusted vegetation index. *Remote Sens Environ* 82:303–310
- Haboudane D, Miller JR, Pattey E, Zarco-Tejada PJ, Strachan IB (2004) Hyperspectral vegetation indices and novel algorithms for predicting green LAI of crop canopies: modeling and validation in the context of precision agriculture. *Remote Sens Environ* 90:337–352
- Homer CG, Aldridge CL, Meyer DK, Schell SJ (2012) Multi-scale remote sensing sagebrush characterization with regression trees over Wyoming, USA: laying a foundation for monitoring. *Int J Appl Earth Obs Geoinf* 14:233–244
- Huete AR (1988) A soil-adjusted vegetation index (SAVI). *Remote Sens Environ* 25:295–309
- Jafari R, Lewis M, Ostendorf B (2007) Evaluation of vegetation indices for assessing vegetation cover in southern arid lands in South Australia. *Rangel J* 29:39–49
- Jensen J (2000) *Remote sensing of environment: an earth resource*. Prentice-Hall, Saddle River, p 526
- Jiang Z, Huete AR, Didan K, Miura T (2008) Development of a two-band enhanced vegetation index without a blue band. *Remote Sens Environ* 112:3833–3845
- Jones HG, Vaughan RA (2010) *Remote sensing of vegetation: principles, techniques, and applications*. Oxford University Press, Oxford
- Karl JW, Duniway MC, Schrader TS (2012) A technique for estimating rangeland canopy-gap size distributions from high-resolution digital imagery. *Rangel Ecol Manag* 65(2):196–207
- Karnieli A, Gilad U, Ponzet M, Svoray T, Mirzadinov R, Fedorina O (2008) Assessing land-cover change and degradation in the Central Asian deserts using satellite image processing and geostatistical methods. *J Arid Environ* 72:2093–2105
- Kaufman YJ, Tanre D (1992) Atmospherically resistant vegetation index (ARVI) for EOS-MODIS. *IEEE Trans Geosci Remote Sens* 30:261–270
- Ko DW, Kim D, Narantsetseg A, Kang S (2017) Comparison of field-and satellite-based vegetation cover estimation methods. *J Ecol Environ* 41(2):34–44
- Landis JR, Koch GG (1977) A one-way components of variance model for categorical data. *Biometrics*:671–679
- Lawrence RL, Ripple WJ (1998) Comparisons among vegetation indices and bandwise regression in a highly disturbed, heterogeneous landscape: Mount St. Helens, Washington. *Remote Sens Environ* 64(1):91–102
- Liang S (2005) *Quantitative remote sensing of land surfaces*. Wiley, Hoboken
- McGregor K, Lewis M (1996) Quantitative spectral change in chenopod shrublands. In: Hunt LP, Sinclair R (eds) *Focus on the future—the heat is on*, Proceedings of the 9th biennial conference of the Australian Rangeland Society, Port Augusta, SA, pp 153–154
- Meyer WB, Turner B (1994) Changes in land use and land cover. *Changes*. In: Meyer WB, Turner BL (eds) *Land use and land cover*. Cambridge University Press, p 549
- Mirik MSAA, Ansley RJ (2012) Comparison of ground-measured and image-classified mesquite (*Prosopis glandulosa*) canopy cover. *Rangel Ecol Manag* 65:85–95

- Mnsur S, Rotherham ID (2010) Using TM and ETM+ data to determine land cover land use changes in the Libyan Al-jabal Alakhdar region. In: Rotherham I. D., Agnoletti, M., Handley, C. (Eds.), *End of tradition? Part 2 commons: current management and problems (cultural severance and commons present)*. *Landsc Archaeol Ecol* 8:32–38
- O'Neill A (1996) Satellite-derived vegetation indices applied to semi-arid shrublands in Australia. *Aust Geogr* 27:185–199
- Omar Al Mukhtar University (2005) Study and evaluation natural vegetation in Al Jabal Al Akhdar area, Final report, Al Bieda, Libya (in Arabic)
- Pickup G, Chewings V, Nelson D (1993) Estimating changes in vegetation cover over time in arid rangelands using Landsat MSS data. *Remote Sens Environ* 43:243–263
- Pickup G, Bastin G, Chewings V (1994) Remote-sensing-based condition assessment for nonequilibrium rangelands under large-scale commercial grazing. *Ecol Appl* 4:497–517
- Pilliod DS, Arkle RS (2013) Performance of quantitative vegetation sampling methods across gradients of cover in Great Basin plant communities. *Rangel Ecol Manag* 66(6):634–647
- Qi J, Chehbouni A, Huete A, Kerr Y, Sorooshian S (1994) A modified soil adjusted vegetation index. *Remote Sens Environ* 48:119–126
- Ren H, Feng G (2015) Are soil-adjusted vegetation indices better than soil-unadjusted vegetation indices for above-ground green biomass estimation in arid and semi-arid grasslands? *Grass Forage Sci* 70:611–619
- Richardson MD, Karcher DE, Purcell LC (2001) Quantifying turfgrass cover using digital image analysis. *Crop Sci* 41:1884–1888
- Rondeaux G, Steven M, Baret F (1996) Optimization of soil-adjusted vegetation indices. *Remote Sens Environ* 55:95–107
- Roujean JL, Breon FM (1995) Estimating PAR absorbed by vegetation from bidirectional reflectance measurements. *Remote Sens Environ* 51(3):375–384
- Rwanga SS, Ndambuki J (2017) Accuracy assessment of land use/land cover classification using remote sensing and GIS. *Int J Geosci* 8:611
- Sant ED, Simonds GE, Ramsey RD, Larsen RT (2014) Assessment of sagebrush cover using remote sensing at multiple spatial and temporal scales. *Ecol Indic* 43:297–305
- Shupe SM, Marsh SE (2004) Cover-and density-based vegetation classifications of the Sonoran Desert using Landsat TM and ERS-1 SAR imagery. *Remote Sens Environ* 93:131–149
- Silleos NG, Alexandridis TK, Gitas IZ, Perakis K (2006) Vegetation indices: advances made in biomass estimation and vegetation monitoring in the last 30 years. *Geocarto Int* 21:21–28
- Simms DM, Waine TW, Taylor JC (2017) Improved estimates of opium cultivation in Afghanistan using imagery-based stratification. *Int. J. Remote Sens* 38(13):3785–3799 <https://doi.org/10.1080/01431161.2017.1303219>
- SWECO SC (1986) Final report, land survey, mapping and pasture survey for 250.000 hectares of South Jabel el Akhdar area, for Socialist People's Libyan Arab Jamahiriya Secretariat for Agricultural Reclamation and Land Development, Contract No. 17/90/81, Libya
- Tehrany MS, Kumar L, Drielsma MJ (2017) Review of native vegetation condition assessment concepts, methods and future trends. *J Nat Conserv* 40:12–23
- Thenkabail PS, Ward AD, Lyon JG, Merry CJ (1994) Thematic Mapper vegetation indices for determining soybean and corn growth parameters. *Photogramm Eng Remote Sens (USA)* 60: 437
- Tucker CJ (1979) Red and photographic infrared linear combinations for monitoring vegetation. *Remote Sens Environ* 8:127–150
- Tucker CJ (1980) A spectral method for determining the percentage of green herbage material in clipped samples. *Remote Sens Environ* 9:175–181
- Verrelst J, Schaepman ME, Koetz B, Kneubühler M (2008) Angular sensitivity analysis of vegetation indices derived from CHRIS/PROBA data. *Remote Sens Environ* 112:2341–2353
- White K, Brooks N, Drake N, Charlton M, MacLaren S (2003) Monitoring vegetation change in desert oases by remote sensing; a case study in the Libyan Fazzān. *Libyan Stud* 34:153–166

Abdulsalam Al-Bukhari is Lecturer of Rangeland Science at the Department of Forestry and Rangeland, Faculty of Natural Resources and Environmental Sciences, Omar Al-Mukhtar University, Al-Bayda, Libya. He received his M.Sc. in Environmental Sciences (Rangeland Ecology and Management) in 2010 from Omar Al-Mukhtar University, Al-Bayda, Libya. Dr. Al-Bukhari achieved his Ph.D. in Natural Resource Management from Cranfield University, Cranfield, UK, in 2019. He specialized in rangeland ecology and management. His main research interests focused on monitoring and assessment of rangeland degradation and the environmental information sciences (remote sensing and GIS). Dr. Al-Bukhari is a member of the Editorial Board for Al-Mukhtar Journal of Sciences.

Tim Brewer is a Senior Lecturer in Resource Survey at Cranfield University, UK. He is currently Director of Education for the School of Water, Energy and Environment. He has more than 30 years' experience in the following areas of expertise: developing geospatial training courses, deriving map based products from Geographic Information Systems (GIS), water harvesting suitability analysis using GIS, developing customised GIS solutions; mapping land cover/use by image interpretation within the UK and overseas; ground surveys in support of land cover classification; topographic mapping using analogue and softcopy photogrammetry, GPS survey, erosion survey and risk assessment.

Stephen Hallett is Chair of Applied Environmental Informatics at Cranfield University, UK. His research focuses on developing the scientific understanding of environmental risks and challenges relating to land resource management in the natural and built environment and understanding the role and opportunity data science and digital technologies offer in addressing research and development. Professor Hallett's work centres on natural ecosystems, agriculture and infrastructure and understanding the impact of a changing climate. His work draws on expertise in environmental big data, analytics, decision support, GIS/remote sensing, software development, 3D data visualisation, virtual/augmented reality, and geospatial decision-support systems applied across agricultural and environmental informatics; soil and land resource management; geohazards and urban infrastructure; and environmental risk mitigation and climate change.

Spatiotemporal Analysis of Vegetation Health Index (VHI) and Drought Patterns in Libya Based on Remote Sensing Time Series



Khalid I. Elfadli and Hamdi A. Zurqani 

Abstract Drought is one of the most important and complex climatic and environmental extreme events in terms of measuring, monitoring, and determining the related potential effects and hazards. In this study, a remote sensing-based Vegetation Health Index (VHI) was used to measure the drought conditions in vegetated areas of Libya. In order to ensure the high performance of this index, it was evaluated by a developed ground-based drought index called the Vegetation-Precipitation and Temperature Index (VPTI). The results showed a high level of confidence that VHI is scientifically reliable. The results of our experiment, which used datasets of growth seasons (Sep-May) during 2000–2014, showed that the average VHI did not exceed 43%. Thus, the country was closer to drought conditions. The country has also experienced three major spells of drought (2000–2002, 2009–2011, and 2012–2014), the most severe and prolonged of which was during the 2000/2001 and 2001/2002 seasons, reaching 18 months of moderate drought conditions. The winter and fall dynamics of VHI were responsible for 56% of reported droughts in the season, while the percentage of areas affected by drought reached 46% during the study period. The assessment and analysis of drought risks in Libya using a drought hazard mapping model found that 82% of the areas were subjected to high and very high drought risk.

Keywords North Africa · Drought indices · Temperature Condition Index (TCI) · Vegetation Condition Index (VCI) · Drought hazards

K. I. Elfadli
Libyan National Meteorological Center, Tripoli, Libya

H. A. Zurqani (✉)
University of Arkansas Agricultural Experiment Station, Arkansas Forest Resources Center,
College of Forestry, Agriculture and Natural Resources, University of Arkansas at Monticello,
Monticello, AR, USA
e-mail: Zurqani@uamont.edu; Hzurqani@uark.edu

1 Introduction

The twenty-first century began with a series of widespread, long, and intensive droughts around the world. Droughts of severe-to-exceptional intensity covered 7–16% of the world land and those of extreme intensity covered 2–6% (Kogan et al. 2013). Kogan and Guo (2016) detailed the few methods of drought detection and monitoring. Weather, climate, and hydrological data have been used traditionally as a drought tool. Precipitation, temperature, snowpack, reservoir level, groundwater, soil moisture, and crop yield are the most popular parameters for drought detection, monitoring, and impacts estimation. Weather/climate indices are another instrument, including the Palmer Drought Severity Index (PDSI, based on water balance), Standardized Precipitation Index (SPI, based on probability of precipitations), Standardized Precipitation and Evapotranspiration Index (SPEI, based on probability of temperature and precipitations), US Drought Monitor (USDM, percentile metrics of five composite weather parameters), Agricultural Index (yield anomaly), and others (Heim 2002).

There are a few significant reasons to use satellite data. First, the weather station network is sparse, especially in climate, ecosystem, and population marginal areas. For example, in Africa, the total number of 4 km^2 satellite observation pixels is 1800 times larger than the number of the weather observing stations (from the World Meteorological Organization's global telecommunication system). Currently, satellite technology has successfully filled the gaps left by weather station. Second, satellite data and indices provide cumulative numerical approximations of drought and its impacts. Third, in the past few years, advanced remote sensing techniques have proven their utility for operational drought management and impact estimation as a separate and additional tool to weather data (Kogan et al. 2013). Finally, satellite drought monitoring has been validated in many countries against *in situ* data (Kogan et al. 2012). Vegetation health is a comprehensive and accurate measure of vegetation conditions with a specific emphasis on drought detection and assessment of drought start/end time, area, intensity, duration, origination, and impact on the environment and socioeconomic activities (Kogan and Guo 2016).

The current chapter is intended to study drought in Libya by using a satellite-based indicator (from remote sensing data) called the Vegetation Health Index (VHI). The indicator is used to assess seasonal variations in vegetation conditions and drought dynamics of the studied area and is evaluated by comparison with similar ground-based drought indicators. This provides a foundation for studying and assessing long-term changes in drought resulting from human interactions or global climate change and alterations.

The objectives of this study are to (1) examine drought by using remote sensing techniques for the first time over Libya; and (2) fill important gaps in the global and regional pictures in order to identify the general features of drought, its patterns, and its spatiotemporal change.

2 Materials and Methods

2.1 Study Area

Libya is bordered by the Mediterranean Sea to the north, Egypt to the east, Sudan to the southeast, Niger and Chad to the south, and Tunisia and Algeria to the west (Zurqani, 2021). It covers an area of about 1,759,540 km², and the vegetation cover is about 7% of the country's total area (Zurqani et al. 2019). Most of the vegetated area is concentrated in the northern area of the country and lies within the rainy region, with 50 mm of annual rainfall. Smaller, irrigated vegetated areas are scattered outside of the rainy region to the south (about 0.1% of vegetated areas). The vegetated areas shown in Fig. 1 are assigned as a study field for the drought remote sensing analysis. Droughts often occur in rainy and cultivated areas; however, we are interested in vegetated areas for our investigation especially because Libya suffers from high variability in its annual and seasonal rainfall.

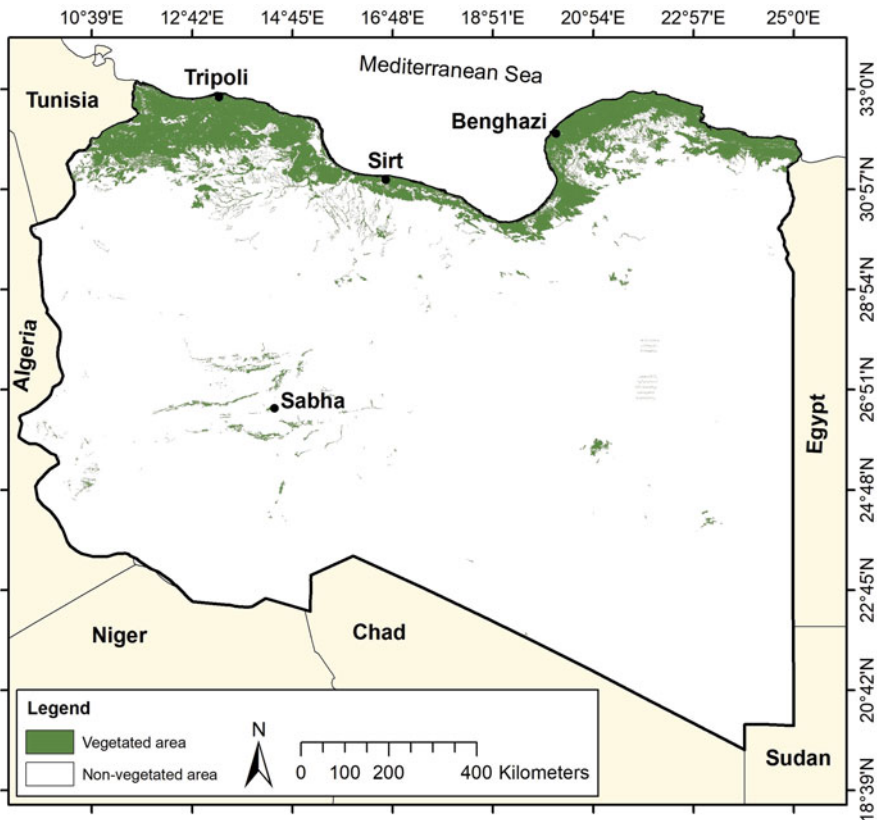


Fig. 1 Location of the study area

2.2 Remote Sensing Data

In this study, two sets of agroclimatological remote sensing data were used to achieve our target investigation goals. The data were derived from the National Oceanic and Atmospheric Administration (NOAA)'s Advanced Very High-Resolution Radiometer (AVHRR) and the Terra satellite's MODIS sensor. Nine tiles of the MODIS dataset (h18–h20, v05–v07), and data from 145–241 days of each year during 2000–2014 were used to cover the primary growing season of most vegetation types in Libya (Sep–May). The first dataset represents eight-day land surface temperature (LST) data with a 1-km resolution (MOD11A2). The LST is the radiative skin temperature of the ground. It depends on the albedo, the vegetated areas, and the soil moisture. The LST was calculated using radiative transfer simulations (Qin et al. 2001; Jiménez-Muñoz and Sobrino 2003). The measurement principle of LST can be given in simplified Planck's radiance function for brightness temperature as shown in Eq. (1):

$$LST = \frac{K_2}{\ln\left(\frac{K_1}{L_\lambda} + 1\right)} \quad (1)$$

where K_1 and K_2 are coefficients determined by the effective wavelength of a satellite sensor and L_λ is satellite-measured radiant intensity. The second dataset represents the vegetation indices (VI), including the Normalized Difference Vegetation Index (NDVI), which was calculated based on (MOD13Q1) data. The NDVI is a numerical indicator that uses the visible and near-infrared (NIR) bands of the electromagnetic spectrum and is adopted to analyze remote sensing measurements and assess whether the observed target contains live green vegetation or not. Generally, healthy vegetation will absorb most of the visible light that falls on it and reflect a large portion of the NIR light. Unhealthy or sparse vegetation reflects more visible light and less NIR light. Bare soils, on the other hand, reflect moderately in both the red and infrared portions of the electromagnetic spectrum (Holme et al. 1987). The NDVI algorithm subtracts the red reflectance values from the NIR and divides them by the sum of the NIR and red bands, as shown in Eq. (2):

$$NDVI = \frac{NIR - RED}{NIR + RED} \quad (2)$$

Theoretically, NDVI values are represented as a ratio ranging from -1 to 1 . In practice, extreme negative values represent water, values around zero represent bare soil, and values over 0.6 represent dense green vegetation.

2.3 Data Processing

Approximately 9000 raster images were downloaded to cover all of Libya during the study period of 2000–2014. Sets of calendar months from September to May (the season of potential drought) for the 14 seasons of the studied period were stacked together to calculate the Temperature Condition Index (TCI) and the Vegetation Condition Index (VCI) for each overlapped pixel (pix). The TCI and VCI characterize the thermal and moisture conditions of vegetation, respectively (Bhuiyan et al. 2006; Kogan 1995, 2001, 2002), and were computed using Eqs. (3) and (4):

$$TCI = 100 \times \frac{LST_{max} - LST_{pix}}{LST_{max} - LST_{min}} \quad (3)$$

$$VCI = 100 \times \frac{NDVI_{pix} - NDVI_{min}}{NDVI_{max} - NDVI_{min}} \quad (4)$$

where LST_{pix} , LST_{max} , and LST_{min} are the radiant temperature pixel of the monthly composite (8-days average) and the highest and lowest radiant temperature pixels of the monthly composite (8-days average) for multi-years, respectively; $NDVI_{pix}$, $NDVI_{max}$, and $NDVI_{min}$ are the normalized difference vegetation index pixel of the monthly composite (16-days average) and the highest and lowest normalized difference vegetation index pixels of the monthly composite (16-days average) for multi-years, respectively. Thermal conditions are particularly important when moisture deficiency is accompanied by high temperature, which increases the severity of agricultural drought and has a direct impact on vegetation health. The VCI and TCI values vary from zero (extremely unfavorable conditions) to 100 (optimal conditions). Thus, higher VCI and TCI values represent healthy and unstressed vegetation. The maximum amount of vegetation occurs in years with optimal climatic conditions, whereas the minimum vegetation amount occurs in years with extremely unfavorable climatic conditions (mostly dry and hot). Therefore, the absolute maximum and minimum values of $NDVI_{pix}$ and LST_{pix} , calculated for several years, contain the extreme climatic events (drought and no drought conditions). The VHI proposed by Kogan (1995, 1997) and Bayarjargal et al. (2006) was calculated based on the mathematical relationship shown in Eq. (5):

$$VHI = 0.5 \times (TCI) + 0.5 \times (VCI) \quad (5)$$

where VHI represents overall vegetation health. In this VHI computation, equal weight has been assumed for VCI and TCI, since moisture and thermal contributions during the vegetation cycle are currently not known in enough detail (Kogan 2001). We identified drought characteristics, trends, patterns, dynamics, and intra-drought seasonal variations, as well as hazard risk analysis, according to the classifications of Kogan (2001) and Bhuiyan et al. (2006) as shown in Tables 1, 2, 3, 4 and 5.

Table 1 VHI classification

VHI (class %)	VHI
0–10	Extreme drought
10–20	Severe drought
20–30	Moderate drought
30–40	Mild drought
40–100	No drought

Table 2 Drought variability and intensity classes

Variability %	Intensity %	Classes	Indices
0–25	60–80	Very low	I
25–50	40–60	Low	II
50–75	20–40	High	III
75–100	0–20	Very high	IV

Table 3 Drought frequency classed by VHI values

VHI (class %)	Frequency (class)	Frequency (code)
0–10	Drought event	1
10–20	Drought event	1
20–30	Drought event	1
30–40	Drought event	1
40–100	No drought	0

Table 4 Developed drought frequency indices

Frequency (seasons)	Frequency (class)	Frequency (Index)
0–03	Very low	I
04–07	Low	II
08–11	High	III
12–14	Very high	IV

Table 5 Developed consecutive (severity) drought index

Severity (seasons)	Severity (class)	Severity (Index)
0–03	Very low	I
04–07	Low	II
08–11	High	III
12–14	Very high	IV

To create hazard risk maps (model-1 and model-2) of drought that represent pixels more vulnerable and sensitive to drought, a table showing drought frequency, consecutive, variability, and intensity indices was established to classify the hazard risk index (Table 6).

Table 6 Developed hazard risk index

Frequency index	Intensity index	Variability index	Consecutive index	Hazard risk index	Hazard risk class
I, II, III	I, II	I	I	I	Very low
I, II, III	III, IV	I	I		
I, II, III	I, II, III, IV	II	I	II	Low
IV	I, II	I	I		
I, II	I, II	I	II		
I, II, III, IV	I, II, III, IV	III	I	III	High
I, II, III, IV	I, II, III, IV	II	II		
I, II, III, IV	I, II	I, II	III		
I, II, III, IV	I, II, III, IV	III, IV	I	IV	Very high
I, II, III, IV	I, II, III, IV	III, IV	II		
I, II, III, IV	I, II, III, IV	III, IV	III		
I, II, III, IV	I, II, III, IV	I, II, III, IV	IV		

Table 7 Description of the station-based drought indices

Drought index	Description	Method
VPTI	Vegetation-Precipitation and Temperature Index	$0.5*(ACPCI + XTCI)$
ACPCI	Accumulated Precipitation Condition Index	$(ACP_{ijk} - ACP_{i,min}) / (ACP_{i,max} - ACP_{i,min})$
XTCI	Max. Temperature Condition Index	$(XT_{i,max} - XT_{ijk}) / (XT_{i,max} - XT_{i,min})$

2.4 Evaluation Techniques

2.4.1 Station-Based Drought Indices

The assessment of drought conditions is more accurate when the variables of interest are measured *in situ*, i.e., recorded directly at a series of ground stations. In the present study, ground stations were selected to be uniformly and closely spaced in order to get the best information. However, in most cases, the costs associated with dense spatial coverage are high and developed countries rarely have the economic and human resources necessary to realize it. On the other hand, most modern satellites are able to provide continuous, consistent, and accurate measurements with high spatial coverage, which can be integrated with *in situ* observations or replace them entirely (Tonini et al. 2012). In this study, a special method of building up station-based drought indices was developed to evaluate the remote sensing-based drought indices of interest. These indices are described in Table 7.

VPTI is established under the same principle of VHI computation. Temperature and precipitation observations were used as raw data to build up the suggested indices. *ACP* is accumulated precipitation and represents the moisture condition of the soil, while *XT*, or daily maximum temperature, represents the thermal condition.

These were used to facilitate the scientific and practical conformity and evaluation of the VHI. We define ACP_{ijk} , XT_{ijk} --monthly ACP , XT for station i , in month j , for season k , respectively. $ACP_{i,min}$, $XT_{i,min}$ --multi-season minimum ACP , XT , respectively, and $ACP_{i,max}$, $XT_{i,max}$, max--multi-season maximum ACP , XT , respectively, for station i .

2.4.2 Vegetation Health Index (VHI) Validation

For the evaluation of the VHI, 32 available climatological stations (Table 8) distributed around the country, in particular in vegetated areas, were selected. The cumulative precipitation and mean maximum temperature each month, derived from daily time series of precipitation and maximum temperature for each station, were used to calculate the ground measuring drought indices during 2000–2014 from September to May.

The *in situ* drought indices (VPTI, ACP, ACPCI, and XTCI) were used and compared with VCI-TCI-derived VHI and VCI and TCI derived from NDVI and LST, respectively, using three goodness-of-fit measures—the correlation values (r-values), root mean square error (RMSE), and mean absolute error (MAE)—in 32 climate stations from September to May for the years 2000–2014 (for a total N: $7*14*32 = 3136$). The r-values, RMSE, and MAE were further used to evaluate the performance of VCI-TCI-derived VHI and were calculated using the following equations (6, 7, and 8):

Table 8 Climate station sites used in this study

Stations	Long.	Lat.	Stations	Long.	Lat.
Abonjaim	15.38	30.58	Kyhair	13.85	32.71
Agdabia	20.16	30.71	Misurata	15.05	32.31
Ahzyat	22.66	32.23	Mizzda	12.98	31.43
Azizia	13.03	32.53	Nalut	10.98	31.86
Bayda	21.73	32.75	Shahat	21.85	32.81
Benina	20.16	32.08	Sirt	16.58	31.20
Benwaleed	14.02	31.73	Sloug	20.25	31.66
Binjawwad	18.06	30.80	Tajoura	13.35	32.88
Darna	22.56	32.78	Trhouna	13.63	32.43
Elmarij	20.20	32.30	Tripoli A/P	13.15	32.66
Emssahed	25.08	31.58	Tubrok	23.91	32.10
Fhatayh	22.66	32.68	Yefren	12.53	32.06
Gryan	13.00	32.16	Zawya	12.77	32.75
Hadba	13.10	32.80	Zintan	12.23	31.93
Hon	15.95	29.13	Zletin	14.56	32.46
Khomes	14.28	32.61	Zuara	12.08	32.88

$$r = \frac{\sum_{i=1}^N (X_i - \bar{X})(Y_i - \bar{Y})}{\sqrt{\sum_{i=1}^N (X_i - \bar{X})^2} \sqrt{\sum_{i=1}^N (Y_i - \bar{Y})^2}} \tag{6}$$

$$RMSE = \sqrt{N^{-1} \sum_{i=1}^N (X_i - Y_i)^2} \tag{7}$$

$$MAE = N^{-1} \sum_{i=1}^N |X_i - Y_i| \tag{8}$$

where X_i is the remote sensing-based drought index for point i ; \bar{X} is the mean value of the remote sensing-based drought index; Y_i is the *in-situ* drought index for point i ; and \bar{Y} is the mean value of the *in-situ* drought index.

3 Results and Discussion

3.1 Seasonal Temporal Correlations of VHI

The seasonal station-based drought index performance statistics for all 32 selected climate stations are summarized in Tables 9, 10 and 11. In this study, we compared the correlations between the *in-situ* drought indices (VPTI, ACP, ACPCI, and XTCI)

Table 9 Comparisons of the r-value to different ground-measured and remote sensing-based single drought indices

Drought indices	VPTI	ACP	ACPCI	XTCI
VHI	0.800	0.750	0.698	0.765
VCI	0.594	0.597	0.394	0.570
TCI	0.592	0.572	0.594	0.586

Table 10 Comparisons of the RMSE to different ground-measured and remote sensing-based single drought indices

	VPTI	ACP	APCI	XTCI
VHI	6.221	25.312	10.652	11.299
VCI	18.026	9.297	12.231	26.665
TCI	10.695	30.554	15.491	10.834

Table 11 Comparisons of the MAE to different ground-measured and remote sensing-based single drought indices

	VPTI	ACP	APCI	XTCI
VHI	5.270	24.737	8.662	9.933
VCI	15.853	8.729	10.026	24.308
TCI	8.991	29.246	12.525	9.402

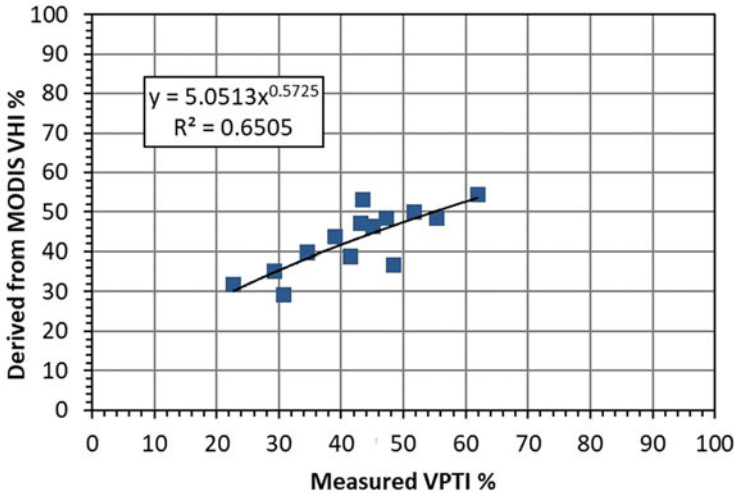


Fig. 2 Regression relationship between the seasonal grounds-measured index (VPTI) and VHI derived from MODIS data

and three remotely sensed drought indices (VHI, VCI, and TCI). Among the three remotely sensed drought indices, VHI ranked first in all three goodness-of-fit measures. As shown in Table 9, the VHI correlates best with VPTI, ACP, ACPCL, and XTCI ($r = 0.8, 0.75, 0.698, \text{ and } 0.765$, respectively), and Tables 10 and 11 indicate that it has a smaller error relative to VPTI, ACP, ACPCL, and XTCI (RMSE = 6.221, 25.312, 10.652, and 11.299, respectively; MAE = 5.270, 24.737, 8.662, and 9.933, respectively), than those of NDVI-derived VCI and LST-derived TCI.

Based on these results, it is clear that to rely heavily on the VPT index to assess and evaluate VH index and from the fact that a statistical relationship has been built up between them as in Fig. 2. The VPTI could be used to determine the VHI using regression analysis. Regression analysis between VHI and measured VPTI resulted in an R^2 value of 0.65. The power model of the VPTI–VHI relationship could be used to generate a seasonal VHI map on the country level as well.

Moreover, ACP was found to be more suitable for evaluating agricultural remote sensing–based drought indices (VCI) because the observed accumulated precipitation directly represents the moisture condition (moisture preserved by the soil); the changes in vegetation growth are buffered by soil moisture (Zhang and Jia 2013; Ji and Peters 2003).

Each seasonal cycle for VPTI and VHI has roughly the same pattern, and the same average and variability (43% and 11.5%, respectively) with a mean RMSE of 7%. This means that the seasonal cycles of VPTI and VHI droughts mostly have the same characteristics which, in turn, determines the features of the drought and its intensity in the study area.

On the other hand, the analysis of seasonal VPTI at the country level succeeded in reproducing the VHI's 14-season average (43%) and matching the number of drought seasons (83%), though three seasons (2001/2002, 2009/2010, 2011/2012) were not symmetrical at all. This is perhaps due to the low number of ground stations included in the study; it was observed that most climatic stations located north of the vegetated areas matched the seasonal pattern of the VHI.

3.2 Spatial and Temporal Characterization of VHI

The country's average (i.e., vegetated areas) VHI was about 43% for all 14 seasons (Appendices 1 and 2); that is, it exceeded the threshold of drought conditions by only 3% and, therefore, any changes in this indicator will be considered important on the temporal and spatial scale of this study. However, despite the intra-seasonal variability of VHI, which was about 18%, it is not expected to cause any significant change in potential drought patterns (Fig. 3).

During the whole study period (2000–2014) droughts occurred in six separated growing seasons (Sep–May). The season of 2000/2001 was the worst drought season experienced by the country with a VHI of about 29% (moderate drought). Conversely, in seven consecutive seasons (2002–2009) drought was absent completely. This long wet spell represented 50% of the length of the studied time period (Table 12). The wettest season was in 2011/2012 (as the whole country did not experience any drought condition).

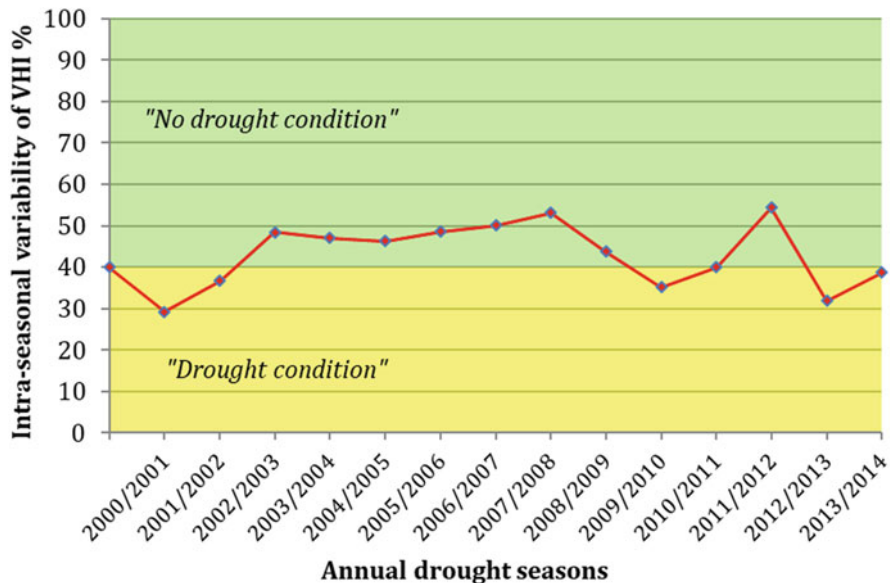


Fig. 3 Intra-seasonal VHI–drought variability for growing season (Sep–May) in Libya (2000–2014)

Table 12 Vegetation Health Index (VHI) values in (%) for different time scales

Season	Sep	Oct	Nov	Dec	Jan	Feb	Mar	Apr	May	Average	C.V	Fall	Winter	Spring	Average	C.V
2000/2001	29.0	43.7	27.3	22.2	20.3	30.5	15.7	39.2	35.9	29.3	31.2	33.3	24.4	30.2	29.3	15.5
2001/2002	30.3	29.3	45.1	52.4	42.3	34.8	20.9	36.1	38.9	36.7	25.5	34.9	43.1	32.0	36.7	15.8
2002/2003	58.7	51.6	55.1	37.8	36.1	61.8	40.7	49.9	43.9	48.4	19.1	55.1	45.2	44.8	48.4	12.1
2003/2004	67.0	25.6	34.5	51.6	47.5	35.9	31.2	59.3	71.0	47.1	34.7	42.4	45.0	53.8	47.1	12.7
2004/2005	63.4	32.2	54.2	45.7	57.3	49.0	32.8	54.6	27.5	46.3	27.4	50.0	50.7	38.3	46.3	15.0
2005/2006	57.1	57.3	45.6	50.7	58.9	57.4	32.7	42.6	34.7	48.6	20.9	53.4	55.7	36.7	48.6	21.3
2006/2007	57.8	50.4	66.8	50.2	40.9	38.8	38.3	61.9	45.9	50.1	20.5	58.3	43.3	48.7	50.1	15.1
2007/2008	50.9	51.0	52.5	52.4	61.4	59.7	39.8	58.3	52.2	53.1	12.0	51.5	57.8	50.1	53.1	7.7
2008/2009	44.4	63.8	44.5	52.8	40.6	42.6	31.1	38.0	35.8	43.7	22.2	50.9	45.3	35.0	43.7	18.5
2009/2010	53.3	42.6	45.6	20.1	22.3	39.3	14.5	31.6	47.0	35.2	38.8	47.2	27.2	31.0	35.2	30.2
2010/2011	46.1	40.8	23.4	22.1	24.7	54.8	33.6	56.6	57.7	40.0	36.6	36.7	33.9	49.3	40.0	20.5
2011/2012	48.5	74.9	68.2	50.3	63.3	47.6	41.6	47.7	47.3	54.4	21.0	63.8	53.7	45.5	54.4	16.9
2012/2013	44.1	24.2	23.9	44.4	41.6	33.3	17.7	22.7	35.5	31.9	31.8	30.7	39.7	25.3	31.9	22.8
2013/2014	40.5	24.6	44.4	47.1	34.9	25.9	42.5	44.3	44.5	38.7	21.6	36.5	36.0	43.8	38.7	11.2
Average	49.3	43.7	45.1	42.8	42.3	43.7	30.9	45.9	44.1	43.1	26.0	46.0	42.9	40.3	43.1	6.6
C.V	22.9	35.6	31.3	28.6	33.6	26.4	31.9	25.4	25.1	18.3	—	22.4	23.4	21.9	18.3	—

Three drought spells with mild VHI values occurred with a duration of two consecutive seasons: 2000/2001–2001/2002 with VHI of 33% per season (67% of severity), and 2012/2013–2013/2014 and 2009/2010–2010/2011 with VHI intensity of 35% (65% of severity) and 37% (63% of severity), respectively. The entire country was affected by drought during the 2000/2001 season, which was considered the most intense. This excluded the northwestern mountains region, which experienced drought in the next season when widespread drought dominated the northwestern region, while the rest of the country was mostly wet. During the drought spells of 2012/2013–2013/2014 and 2009/2010–2010/2011 seasons, most northwestern areas experienced drought conditions.

During the winter season of 2009/2010, Libya experienced a wide and severe drought in both the east and west vegetated areas with an average VHI of 27% (moderate drought). Spatially, this winter was the second worst relative to the whole studied period, whereas the fall season was the wettest with the highest VHI (47%). All areas were mostly dry during the spring season with an average VHI of 31% (moderate drought). VHI in March was the lowest in the period considered (14.5%, severe drought) whereas May had a wet VHI of 47%. In general, the worst dry seasons for the western region were 2012/2013 and 2000/2001, and the worst dry season for the eastern region was 2000/2001. In addition, the growing season variability during drought spells was significant (11%), whereas the variability of fall, winter, and spring were 19%, 21%, and 26%, respectively. In total, there were eight seasons left unaffected by drought at the national level. Furthermore, the eastern regions were more vulnerable to drought episodes than the western region; this may be because rainfall variability was greater in the eastern region than in the western region.

3.3 Drought-Climatic Profile Curve

Climatology of NDVI and BT is considered an essential part of the VHI algorithm (i.e., *VCI* and *TCI*) because the original parameters characterize two groups of environmental variables: long term (climate, ecosystems, soils, etc.) and short term (weather), to which drought belongs (Kogan and Guo 2016). The climatic profile curve of VHI, VCI, and TCI for the growing season (Sep–May) during the study period (2000–2014) is shown in Fig. 4.

It is clear that the contribution of TCI is stronger than that of VCI for VHI and dependent on the strength of the VHI by an average of 52%. This pattern is different from that of cold and rainy regions. The limits of VHI climatology fell between 31–49%, and between 52–32% and 47–31% for TCI and VCI, respectively. The VHI of upper limits was reported in September and that of the lower limits was reported in March. However, the temporal pattern of changes and fluctuation among the months was nearly flat (seasonal cycle was absent) with an average variability of about 10%, which is small. March was the only month characterized by drought. Specifically, the climatology of VHI in March was characterized by mild drought as a natural feature (i.e., normal condition) with a variability of 32%. The threshold was

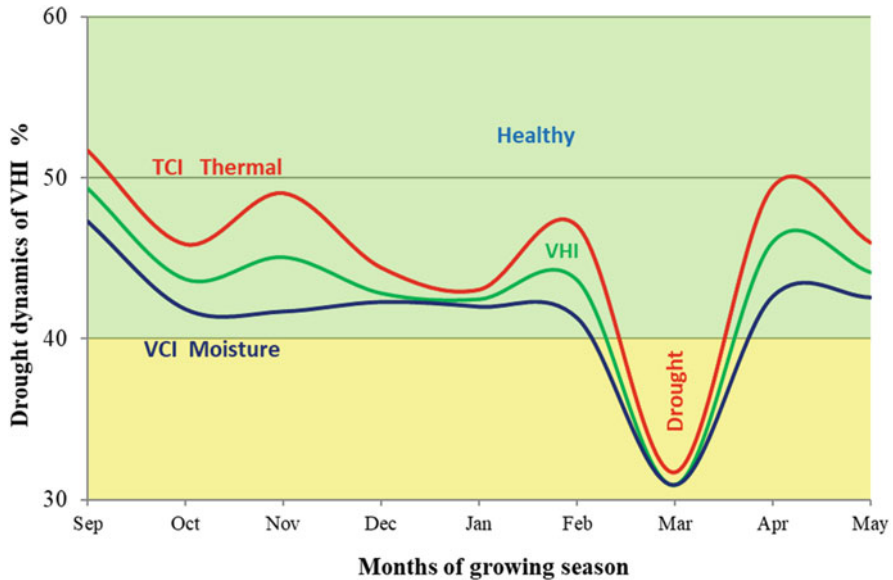


Fig. 4 Drought dynamics of VHI of growing season in Libya (2000–2014)

passed slightly in only three of the 14 months of March (29%); the absolute lowest value of VHI occurred during this month as well. The VHI was more stable in September, as shown in Fig. 5, with a coefficient of variations (C.V) of 23%. It was less stable during October and January, with C.Vs of 36% and 34%, respectively.

The month of May was more extreme (i.e., less stable), with the difference reaching 23% of the 75th percentile. The most and the least stable seasons were the spring and fall with 27% and 30% C.V, respectively.

Time series of monthly and seasonally VHI for the study period (126 months) were plotted in Figs. 6 and 7, with the absolute highest VHI of 74.8% occurring October 2011. Thirty-nine percent of the months experienced drought while 65% of drought months occurred during the six drought seasons. Thirty-eight percent of the drought months in the drought spells were winter months; January and February were controlled by the dynamics of the winter drought pattern by 75%. March and April had the same role in controlling the percentage for the spring in drought seasons as well.

Monthly and seasonal time series of VHI show the duration, onset, and offset of each drought spell as follows:

- First longest drought spell onset was in September 2000 (Fall 2000) with offset in May 2002 (Spring 2002), 18 months (6 seasons) in duration
- Second longest drought spell onset was in October 2012 (Fall 2012) with offset in February 2014 (Winter 2014) and 14 months (5 seasons) in duration
- Third longest drought spell onset was in December 2009 (Winter 2010) with offset in January 2011 (Winter 2011) and 11 months (4 seasons) in duration

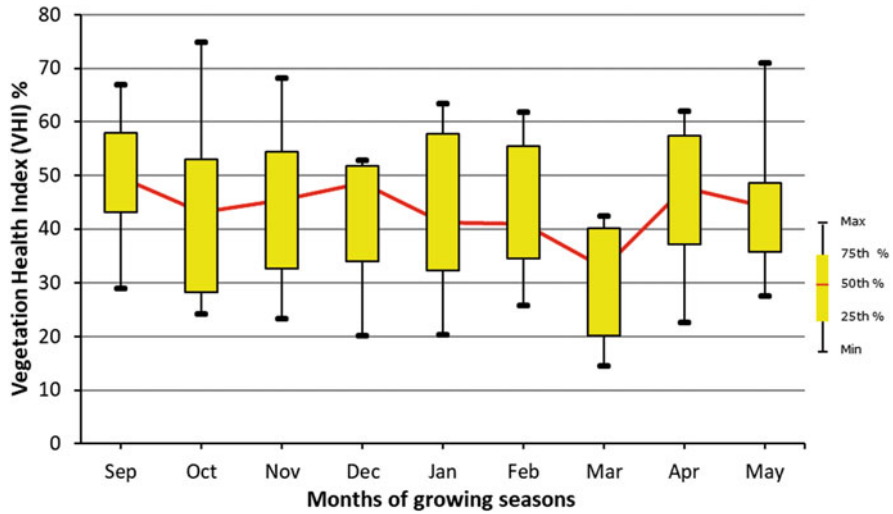


Fig. 5 Box plot diagram of VHI growing season in Libya (2000–2014)

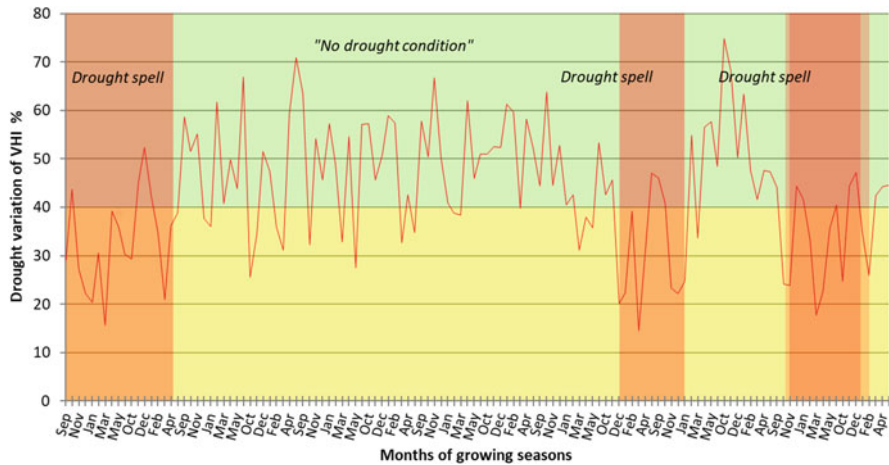


Fig. 6 Variation of VHI by months of growing seasons in Libya (2000–2014)

3.4 Vegetation Health Index (VHI) Trends

It was of interest to this study to recognize the important changes in the vegetated areas via time series analysis, as this helped us understand VHI dynamics and drought hazards within the studied area. To detect and estimate trends in time series of VHI values, we used statistical methods including the nonparametric Mann–Kendall test for testing for the presence of a monotonic increasing or decreasing trend and the nonparametric Sen’s slope estimator for estimating the slope of a linear trend. The results show that none of the trend slopes were statistically significant, which might

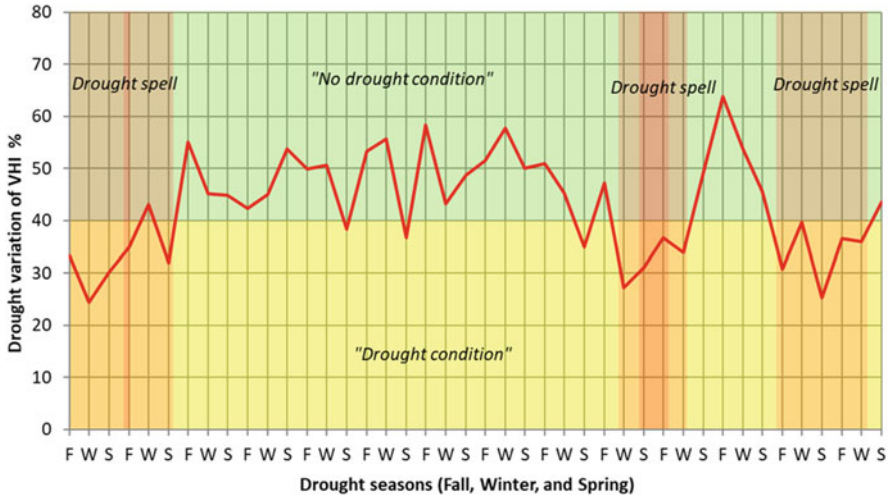


Fig. 7 Variation of VHI by seasons in Libya (2000–2014)

be due to the time series length, despite the rather low seasonal and intra-seasonal variability and small residuals (values remaining after the estimated slopes of VHI have been subtracted from actual VHI data). However, our findings are particularly important when studying the general characteristics of drought in Libya.

As shown in Fig. 8 and Table 13, seasonal VHI time series slopes show a positive trend with a rate change of 1.74% per decade. On a seasonal scale, the fall VHI trend was negative (−0.75% per decade); the lowest positive trend occurred during the winter season with 0.21% per decade while the spring season trend was 0.56% per decade, more than that of the winter. It should be noted that the absolute value of the increase in the trend is inversely proportional to the C.V: the seasonal, fall, winter, and spring variabilities were 18.3%, 22.4%, 23.4%, and 21.9%, respectively. Trends for six out of nine months were negative, and the lowest decreasing slope was in September (14.7% per decade). On the other hand, March had the highest upward trend by 7.6% per decade. In general, any potential changes in slope trends (because it is not significant) for any time scales are considered important, especially because the VHI of the country is somewhat small, making it more sensitive and prone to such drought conditions and risks.

3.5 Drought Frequency, Consecutive, Intensity and Variability Patterns

The frequency of droughts refers to how many times a pixel was subjected to drought episodes. In our case, this is the number of times out of 9 months (one season) multiplied by the 14 seasons the cell experienced in the study period. The resulting

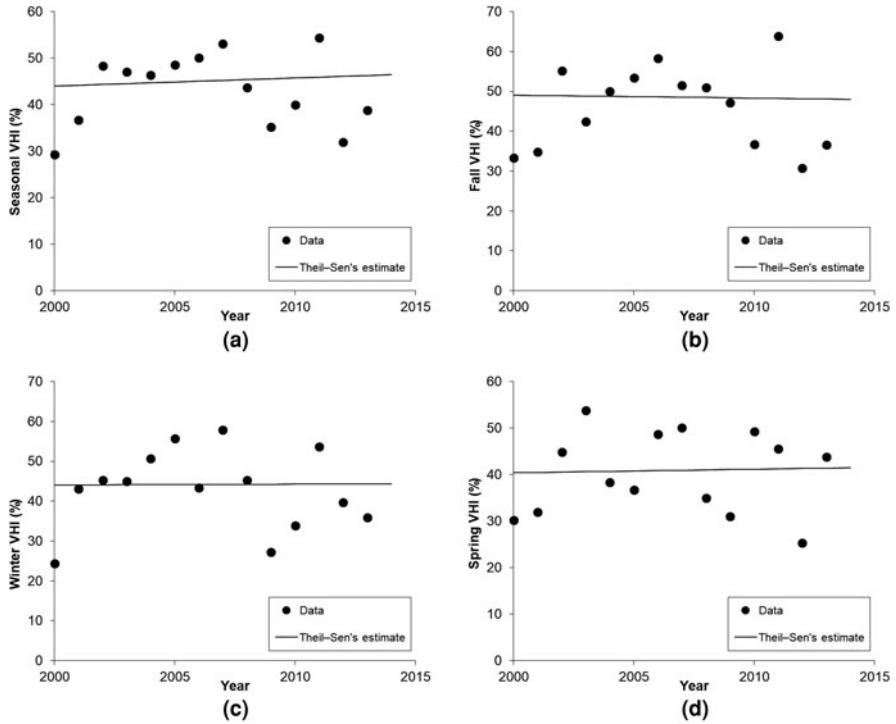


Fig. 8 Trends of VHI magnitude in Libya (2000–2014) (a) seasonally, and in the (b) fall, (c) winter, and (d) spring seasons

Table 13 Vegetation Health Index (VHI) trends in Libya (2000–2014)

Time series	Trend/decade	Residual average
Sep	-14.7	-2.8
Oct	-1.2	0.8
Nov	-0.7	-0.1
Dec	-0.7	-6.0
Jan	2.6	1.7
Feb	-2.9	2.1
Mar	7.6	-2.9
Apr	-5.6	-1.7
May	4.5	0.7
Seasonal	1.7	-2.0
Fall	-0.7	-2.5
Winter	0.2	-1.3
Spring	0.8	-0.6

map depicted in Fig. 9 shows the spatial patterns of drought frequency in the vegetated area of the country during the study period.

Using Table 14, we observed that the vast majority of vegetated areas (92%) falls under the low and very low drought frequency classes, where the prevailing drought frequency patterns are almost homogenous. We further found that the national spatial average of drought frequency occurred within the classes of (4–7) over 14 seasons, which is classified as a low drought frequency. This means that the pixel experienced a low frequency class of drought on a monthly basis within 4–7 seasons.

At a regional level, two studies that differ in terms of study period and extent of vegetated areas exist but were carried out with the same methodology. A drought frequency study in Egypt (2011–2012) showed that about 83% of vegetated areas fell in the very low and low classes (Yassmin 2014). This is consistent with our

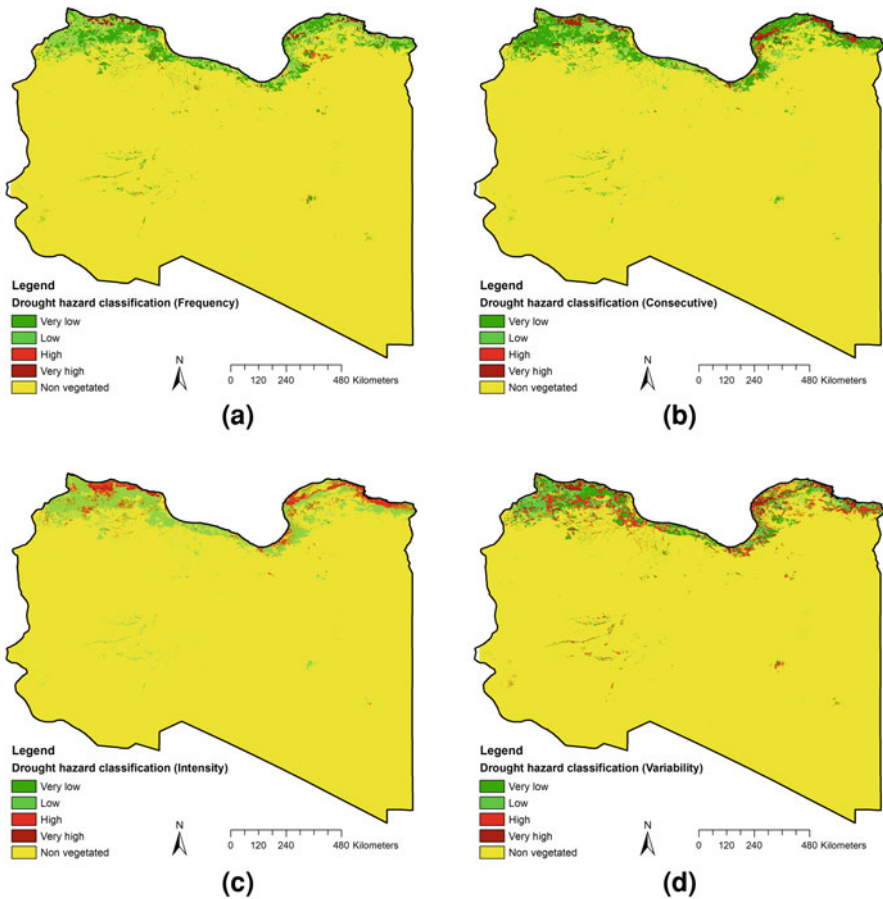


Fig. 9 Classification of drought components during the growing season (Sep–May) in Libya (2000–2014): (a) frequency, (b) consecutive, (c) intensity, and (d) variability

Table 14 Areas (%) within the vegetated area (Libya) exposed to drought risk

Severity level	frequency	consecutive	intensity	variability	Hazard model-01	Hazard model-02
Very low	45.8	61.3	0.1	0.0	26.6	0.0
Low	46.4	26.4	79.5	68.6	34.6	18.0
High	2.7	1.4	19.2	25.9	26.9	23.7
Very high	5.1	10.9	1.2	5.5	11.9	58.3

findings, despite the agriculture in the studied areas depending heavily on the waters of the Nile. In Tunisia, Algeria, and Morocco, most vegetated areas fell within the high classes of drought frequency (Erian et al. 2011) during 2000–2010.

Recurrent (consecutive) drought is characterized by frequency is shown in Fig. 9b. The closer the droughts are the higher the sequence index. Table 14 shows that about 88% out of vegetated areas percentage experienced lower classes of droughts, while about 12% showed higher classes, however, this proportion was relatively larger in the eastern parts of the country. In general, the spatial average of the low recurrent class was dominated and occurred 5 times over 14 seasons. In the same pattern, a low drought recurrent in Egypt was represented by about 92% (Yassmin 2014), which is largely agreed with the same distribution prevailing over Libya.

Drought intensity annotates the departure of a climate index from its normal value. The higher values of VHI, the less low drought intensity. Figure 9c and Table 14 showed that two different patterns of low (80% of areas) and high (20% of areas) drought intensities dominated symmetrically over the east and west of the country with a national spatial average of 40% (high class of intensity).

Furthermore, variability is the most important statistical measure to study the behavior of any climate variable on temporal and spatial scales. In principle, variability is a natural feature of each climatic element. In this study, the temporal variability analysis was evaluated for each pixel. The final produced map Fig. 9d showed that there are no areas affected by the very low variability class, as about 69% of the regions were classified as low variability drought, while about 31% of the areas are affected by the higher variability. It is also noticeable that the variability is higher in the northern region than the western region, especially in areas with more rainfall rates and a smaller daily range of temperature (DTR).

3.6 Drought Hazards Patterns

Spatial and temporal statistical analysis of droughts help to assess potential risks. Two models for producing drought hazard maps are presented in this section (Fig. 10) for evaluation and identification purposes for the affected areas.

The first hazard map model (scenario mostly optimistic) was produced by crossing the frequency and consecutive indices as described above. About 61%

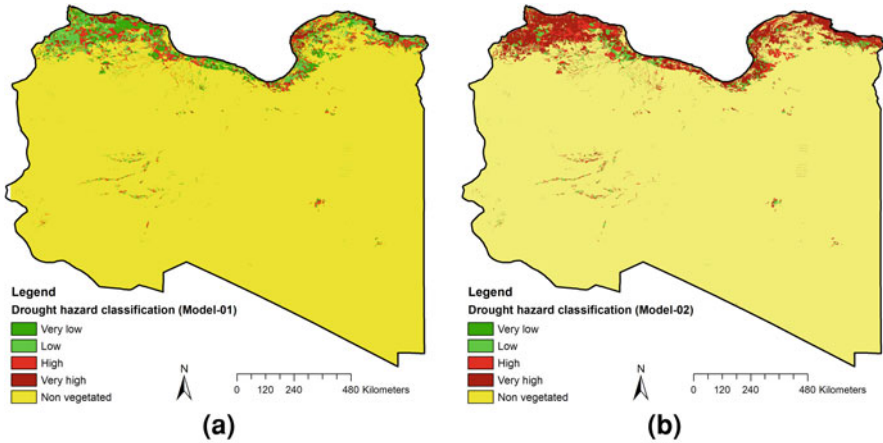


Fig. 10 Hazard classification of droughts during the growing season (Sep–May) over Libya (2000–2014): (a) Hazard model-01, and (b) Hazard model-02

and 39% of the vegetated areas are affected by low and high risks, respectively, as shown in Fig. 10a and Table 14. The eastern parts of the country were more threatened by drought hazards than other regions during the period of study.

The second model (model-02; scenario least optimistic) was produced by crossing the frequency, consecutive, intensity, and variability indices described earlier. The results are quite different as shown in Fig. 10b and Table 14; the vast majority of the areas (82%) was exposed to high drought hazards, 24% of which fell under the very high drought hazard risk. There were no areas that were exposed to very low drought hazard risk. Moreover, agricultural areas in the western regions experienced significantly more drought hazard risks.

At regional scale, the study of ACSAD we mentioned earlier (Erian et al. 2011) which dealt with the study and analysis of drought hazard risks over the “Arab world” through the risk maps that were built according to the basis of the first model of our map (model-01), but the name used was different (Drought Vulnerability map) rather than (Drought Hazards map). Here we review some results, especially for the neighboring countries east and west of Libya.

In Libya, this study showed that 6% and 2% of total surface area of the country were affected by high and low drought risks, respectively. This is somewhat consistent with the findings represented in the first hazards map model (hazard model-01). The study in Egypt (Yassmin 2014) showed nearly the same results as ours in Libya, except that about 52% of the cultivated areas were exposed to drought risks while the rest of the areas were not vulnerable to drought episodes, apparently depending on irrigation from the Nile. In addition, the total area exposed to drought risks in Tunisia, Algeria, and Morocco, to the west of Libya, were 52%, 21%, and 55%, respectively, thus showing that the entire region is under threat of persistent drought risks. In general, we support and favor the national results obtained from the second model (hazard model-02) for drought risk analysis of hazards because the

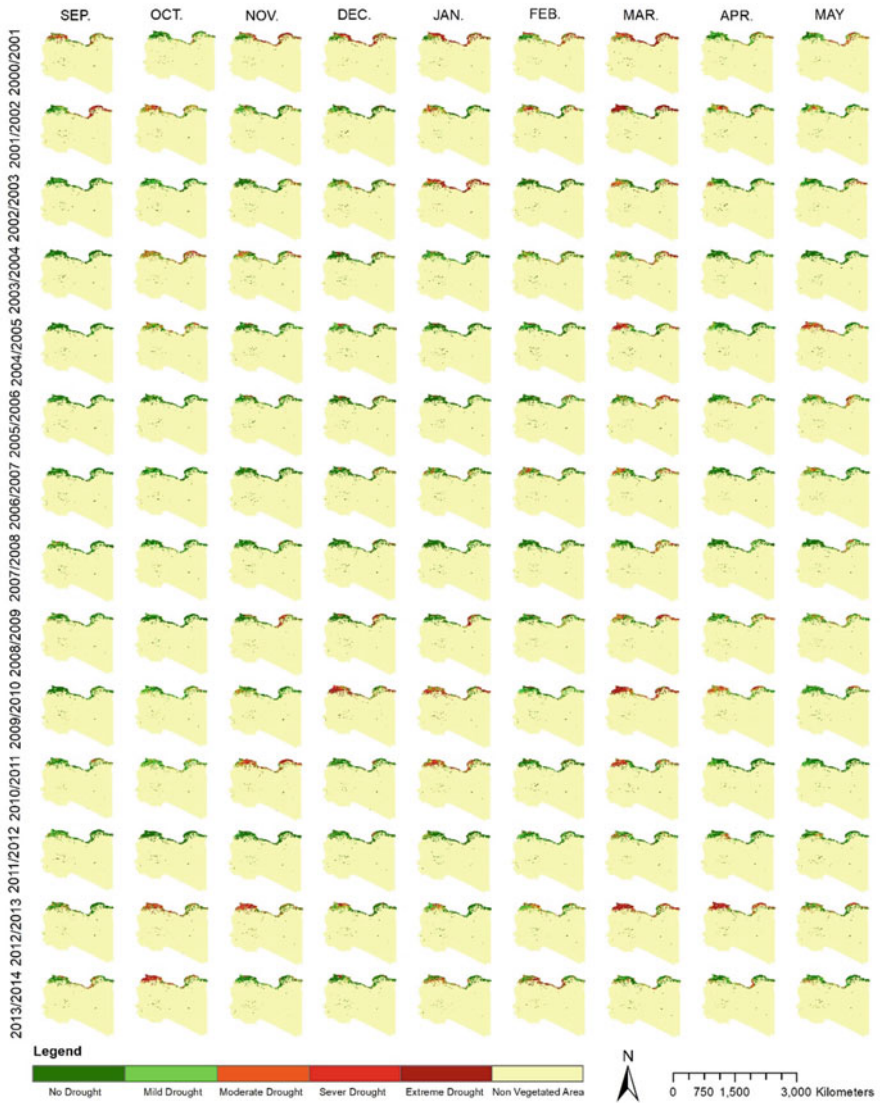
model includes important elements of the drought phenomenon. There were more areas exposed to drought risk in the second model than in the first model, which is more consistent with the dry and semi-dry agroclimatological classification of the country (FAO database). Thus, classification is the result of high rainfall variability of Libya.

4 Conclusion

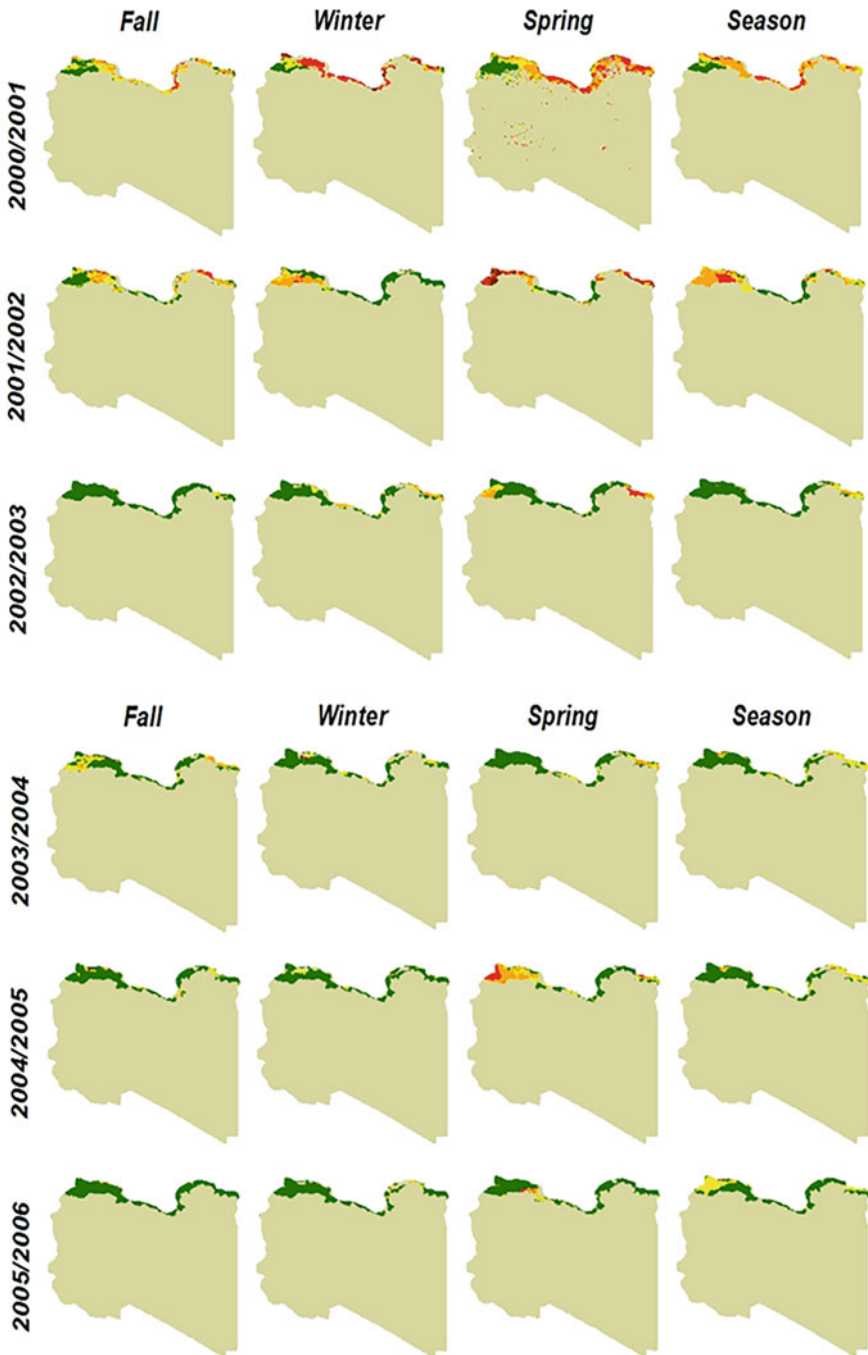
This chapter examined droughts in Libya during the growing season in 2000–2014 by using a remote sensing–based single drought index: VHI. The index was assessed in terms of performance, dynamics, and potential hazards at different spatial and temporal scales. Despite the area affected by drought reaching 46% of the total studied area during the study period, the overall drought pattern in Libya tended to be dominated by moderate and mild drought more than other categories. The contribution of TCI to VHI dynamics was found to be stronger than that of VCI, at a rate of 52%. Furthermore, the VHI showed that March is generally drought-prone compared to the other months, although the growth season inter-variability is somewhat small (10%). The first model of drought hazards map showed that about 61% and 39% of the vegetated areas were affected by low and high hazard risk classes, respectively. Furthermore, the eastern parts of the country were more threatened by drought hazards than other regions during the study period. The second model showed opposite results that are much closer to reality: most areas (82%) were exposed to high to very high drought hazards, 24% of which fell under the very high drought risk, and agricultural areas in the western region experienced more significant drought risks. This situation means the country is under persistent threat of drought risks. The remote sensing–based drought indices (VHI, VCI, and TCI) were correlated with the *in-situ* drought indices (VPTI, ACP, APCI, and XTCI) used in this study for assessing and evaluating the performance of VHI in Libya during the growing season (Sep–May). The VHI had the strongest correlation with stations-based drought indices in different periods of the growing season, and in a greater number of stations with higher r-values. This indicates that the VHI has potential for monitoring drought conditions in different parts of Libya. A statistical relationship has been established between VPTI and VHI, so that the Vegetation-Precipitation and Temperature Index (VPTI) could be used to retrieve remote sensing drought index (VHI) values using the regression model.

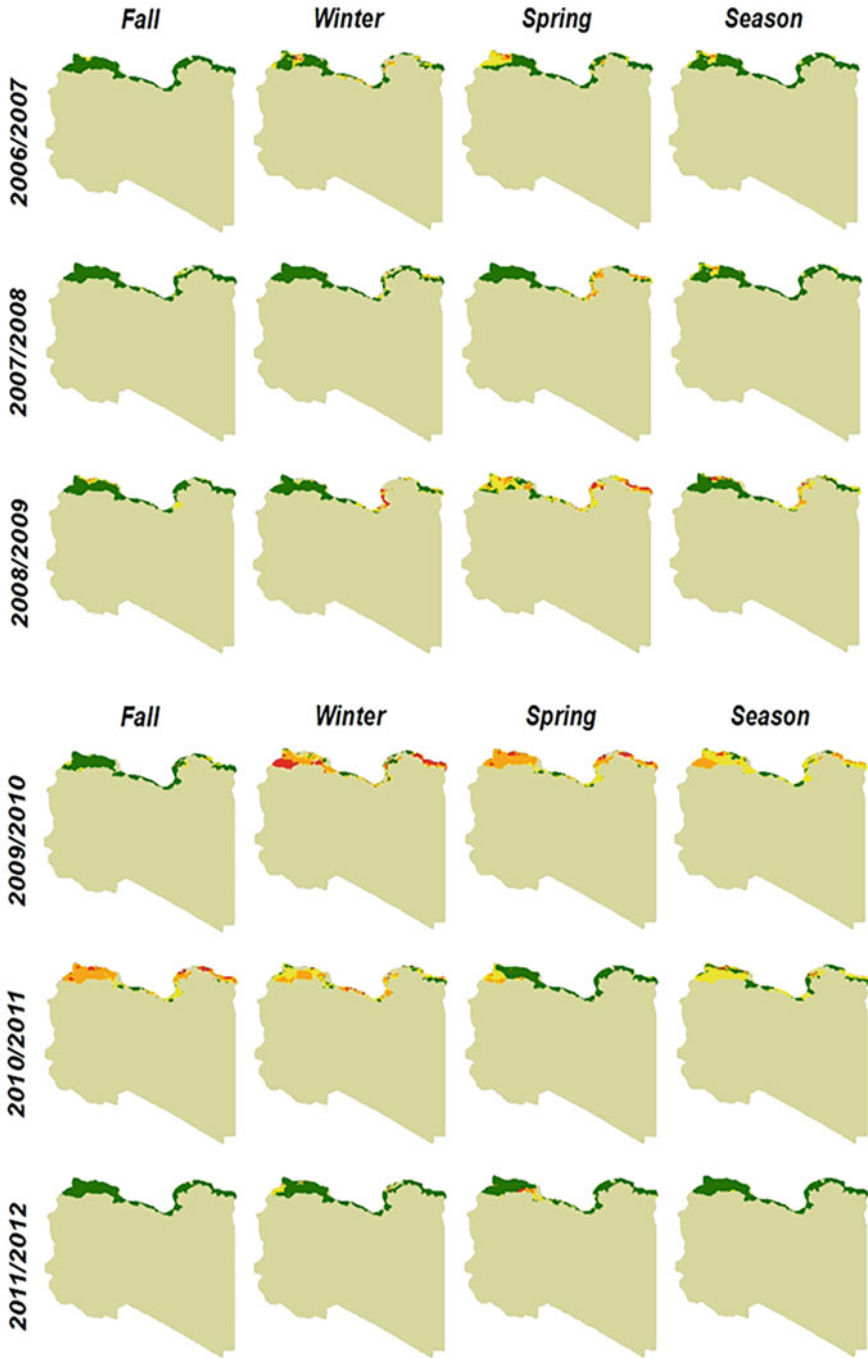
Author Contributions **Khalid I. Elfadli**: conceptualization, methodology, formal analysis, writing-original draft, visualization, validation, investigation. **Hamdi A. Zurqani**: conceptualization, methodology, supervision, software, data curation, formal analysis, validation, investigation, writing-original draft, visualization, writing—review and editing, review of analysis. All authors have read and agreed to the published version of the manuscript.

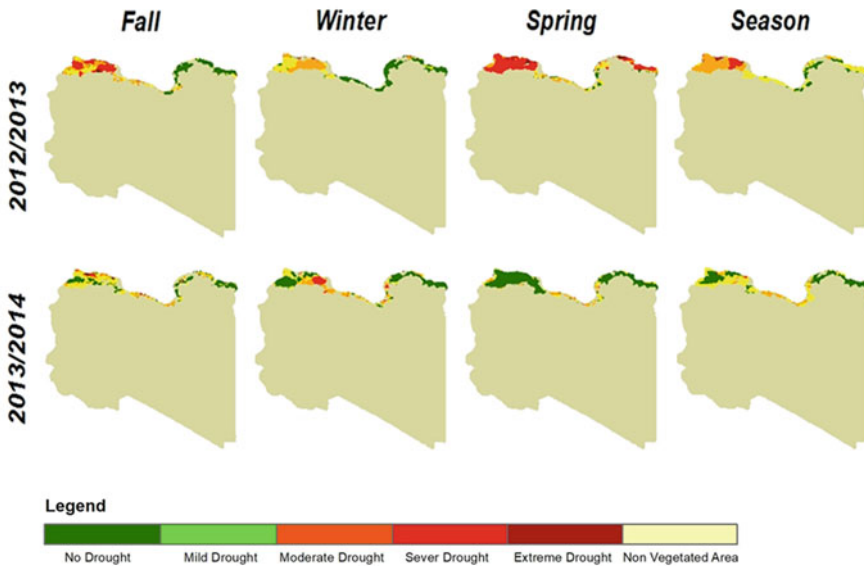
Appendix 1 Monthly Drought in Libya Expressed by VHI during the Study Period (2000–2014)



Appendix 2 Seasons and Seasonal Drought over Libya Expressed by VHI during the Study Period (2000-2014)







References

- Bayarjargal Y, Karnieli A, Bayasgalan M, Khudulmur S, Gandush C, Tucker CJ (2006) Acomparative study of NOAA-AVHRR derived drought indices using change vector analysis. *Remote Sens Environ* 105:9–22
- Bhuiyan C, Singh RP, Kogan FN (2006) Monitoring drought dynamics in the Aravalli region (India) using different indices based on ground and remote sensing data. *Int J Appl Earth Obs Geoinf* 8:289–302
- Erian W, Katlan B, Babah OB (2011) Drought vulnerability in the Arab region, case study- drought in Syria, (2000–2010). The Arab Center for the Studies of Arid Zones and Dry Lands – ACSAD, Damascus
- Heim R Jr (2002) A review of twentieth-century drought indices used in the United States. *BAMS* 83:1152
- Holme AMR, Burnside DG, Mitchell AA (1987) The development of a system for monitoring trend in range condition in the arid shrublands of Western Australia. *Aust Rangel J* 9:14–20
- Ji L, Peters AJ (2003) Assessing vegetation response to drought in the northern Great Plains using vegetation and drought indices. *Remote Sens Environ* 2003(87):85–98
- Jiménez-Muñoz JC, Sobrino JA (2003) A generalized single-channel method for retrieving land surface temperature from remote sensing data. *J Geophys Res* 108. <https://doi.org/10.1029/2003JD003480>
- Kogan F, Adamenko T, Guo W (2013) Global and regional drought dynamics in the climate warming era. *Remote Sens Lett* 4:364–372
- Kogan FN (1997) Global drought watch from space. *Am Meteorol Soc Bull* 78:621–636

- Kogan F, Salazar L, Roytman L (2012) Forecasting crop production using satellite based vegetation health indices in Kansas, United States. *Int J Remote Sens* 3:2798–2814. <https://doi.org/10.1080/01431161.2011.621464>
- Kogan FN (2001) Operational space technology for global vegetation assessment. *B Am Meteorol Soc* 82:1949–1964
- Kogan FN (2002) World droughts in the new millennium from AVHRR- based Vegetation Health Indices. *EOS Trans Am Geophys Union* 83:562–563
- Kogan FN (1995) Application of vegetation index and brightness temperature for drought detection. *Adv Space Res* 15:91–100
- Kogan FN, Guo W (2016) Early twenty-first-century droughts during the warmest climate. *Geomat Nat Haz Risk* 7(1):127–137
- Qin Z, Karnieli A, Berliner P (2001) A mono-window algorithm for retrieving land surface temperature from Landsat TM data and its application to the Israel-Egypt border region. *Int J Remote Sens* 22:3719–3746
- Tonini F, Giovanna JL, Hartwig H (2012) Mapping return levels of absolute NDVI variations for the assessment of drought risk in Ethiopia. *Int J Appl Earth Obs Geoinf* 18:564–572
- Yassmin H (2014) Drought monitoring and assessment over Egypt. Thesis submitted for the degree of MSc in Meteorology, Cairo University, Cairo, p 33
- Zhang A, Jia G (2013) Monitoring meteorological drought in semiarid regions using multi-sensor microwave remote sensing data. *Remote Sens Environ* 2013(134):12–23
- Zurqani HA, Mikhailova EA, Post CJ, Schlautman MA, Elhawej AR (2019) A review of Libyan soil databases for use within an ecosystem services framework. *Land* 8(5):82
- Zurqani HA (2021) Introduction. In: Zurqani HA (ed) *The soils of Libya*, World soils book series. Springer, Cham. https://doi.org/10.1007/978-3-030-66368-1_1

Khalid I. Elfadli is a climate expert, climate change advisor at Libyan National Meteorological Center (LNMC) since 1987, faculty member (cooperating) at technology college of Civil aviation and meteorology, a member of the national committee to combat desertification, and president of the general assembly of the southern organization for sustainable development and climate change (NGO), Tripoli, Libya. In addition, he is a member of the Climate Extremes Team of the World Meteorological Organization (WMO). Dr. Elfadli received and completed his M.Sc. and Ph.D. in 2012 and 2019 respectively, in (climate change science) from Cairo University, Egypt. He specialized in climate and climate change. Most of his scientific works and research are concerned with and focused on the following topics: climate extreme, drought and climate change; detection, trends, indices, impacts and projections, studies. He has been the head of the meteorology department at the aforementioned college and teaching courses and has supervised the graduation BA's and MA's degree students since 2012. He also contributes and participates in international scientific investigations of some climatic extremes and the annual global report of climate statement issued by WMO. He is now working as a scientific reviewer for Scientific African and, Water and climate change Journals on climate and climate change issues. He was also appointed as a focal point for Libya with the Intergovernmental Panel on Climate Change (IPCC).

Hamdi A. Zurqani is an Assistant Professor of Geospatial Science in Natural Resource Management and Conservation at the University of Arkansas Agricultural Experiment Station, Arkansas Forest Resources Center, University of Arkansas at Monticello, Monticello, AR, USA. He is also an FAA (i.e., Pt107) Certified sUAS/Drones Pilot, and has used this skill to enhance his knowledge of remote sensing and GIS. Dr. Zurqani is a recognized expert as a result of his internationally acclaimed work in the areas of environmental information science, remote sensing, geospatial analysis, land evaluation, sustainability, pedology, and soil science education. He has conducted research across the world, including the United States of America, and Africa, and has served as PI, co-PI, or co-investigator on several grants-funded research projects. Dr. Zurqani is highly collaborative as evidenced by his publications. He is the author and co-author of many peer-reviewed

publications, book chapters, and technical publications (including teaching laboratory manuals). He also edited two books with Springer Nature (i.e., “The Soils of Libya”, and “Environmental Applications of Remote Sensing and GIS in Libya”), and has published widely in many peer-review journals (e.g., International Journal of Applied Earth Observation and Geoinformation (Elsevier); Remote Sensing in Earth Systems Sciences (Springer Nature); Scientific Reports (Nature); Frontiers in Environmental Science (Frontiers); Geoderma (Elsevier); Land (MDPI); Urban Forestry & Urban Greening (Elsevier), and others). Dr. Zurqani is a member of the Editorial Board for Remote Sensing (MDPI) Journal, counseling outcome, and research evaluation. He also was appointed to serve as a Guest Editor for the Special Issue “Applications of Remote Sensing in Earth Observation and Geo-Information Science”. In addition, Dr. Zurqani conducted peer-review for many journals including Journal of Environmental Informatics, Applied Sciences, SN Applied Sciences, Remote Sensing, Geo-spatial Information Science, AgriEngineering, Sensors, Heliyon, Geosciences, Land, Soil Systems, Water, Agronomy, Agriculture, Resources, Sustainability, Arid Land Research and Management, Quaestiones Geographicae, Geocarto International, International Journal of Environmental Research and Public Health, Natural Hazards, and Conference of the Arabian Journal of Geosciences. Dr. Zurqani conducts cutting-edge research in the field of Environmental Information Science, Remote Sensing, Land use management/ planning, change detection of landscape degradation, and Geographic Information System (GIS) models. He has focused his research efforts on the development of novel applications for new technologies in analyzing spatial data, remote sensing, geostatistical modeling of environmental changes such as erosion, mapping and predicting soil salinity, and land use/ land cover changes. His new publications include: “Mapping and Quantifying Agricultural Irrigation in Heterogeneous Landscapes Using Google Earth Engine” in the Journal of Remote Sensing Applications: Society and Environment; “Evaluating the integrity of forested riparian buffers over a large area using LiDAR data and Google Earth Engine” in the Journal of Scientific Reports; “Mapping Urbanization Trends in a Forested Landscape Using Google Earth Engine” in the Journal of Remote Sensing in Earth Systems Sciences; “Geospatial analysis of land use change in the Savannah River Basin using Google Earth Engine” in the International Journal of Applied Earth Observation and Geoinformation; and “Application of Non-Hydraulic Delineation Method of Flood Hazard Areas Using LiDAR-Based Data” as well as “Assessing ecosystem services of atmospheric calcium and magnesium deposition for potential soil inorganic carbon sequestration” in the Geosciences Journal.

Integration of Remotely Sensed Data and Machine Learning Technique for Spatial Prediction of Selected Soil Properties in Northwestern Libya



Hamdi A. Zurqani 

Abstract Understanding the distribution of soil properties over the landscape is required for a variety of land resource management applications, modeling, and monitoring practices. The main aim of this research is to conduct a spatial prediction of selected topsoil properties such as soil pH, calcium carbonate (CaCO_3); exchangeable sodium percentage (ESP); and cation exchange capacity (CEC) using integrated remotely sensed data and machine learning approach in northwestern Libya. The results indicated that the coefficient of determination (R^2) varies from 0.22 to 0.42, the root mean square error (RMSE) ranges between 0.35 and 6.96, and the normalized root mean square error (NRMSE) ranges between 0.12 and 0.26 indicating less residual variance and thus a proper operation of the machine learning model used. Based on these results, it can be concluded that this approach is an effective and valid methodology for modeling and spatial mapping soil properties in this area, and this method could also be applied to other regions with similar characteristics.

Keywords Environmental covariates · Soil characteristics · Spatial prediction · Decision tree · Remote sensing · Google Earth Engine · Digital soil mapping

1 Introduction

Nutrients are essential for crop production and stable plant growth. Studying, modeling, and mapping the spatial distribution of soil properties is crucial for a more cost-effective soil nutrient management strategy (Suleymanov et al. 2021). In Libya, where land degradation and its consequences have been reported by numerous studies (Aburas et al. 2008; Abagandura and Park 2016; Zurqani et al. 2019;

H. A. Zurqani (✉)

University of Arkansas Agricultural Experiment Station, Arkansas Forest Resources Center, College of Forestry, Agriculture and Natural Resources, University of Arkansas at Monticello, Monticello, AR, USA

e-mail: Zurqani@uamont.edu; Hzurqani@uark.edu

Zurqani 2021), this information is increasingly required by governments and development partners to help improve land management.

In recent decades, digital soil mapping (DSM) methods have been actively used to study and map soils and their properties (Taghizadeh-Mehrjardi et al. 2016; Minasny and McBratney 2016). DSM methods require the integration of soil data and its environmental covariates and allow the creation of maps with greater accuracy, comparatively lower cost, and higher spatial resolution (Lucà and Buttafuoco 2018; Zurqani et al. 2018; Zeraatpisheh et al. 2019). These methods are particularly relevant to digital mapping of soil nutrients, as field and laboratory measurements of soil properties can be time-consuming and expensive (Zurqani et al. 2018).

Machine learning (ML) techniques are actively used for predicting and mapping soil properties (Mosleh et al. 2014; Forkuor et al. 2017; Zeraatpisheh et al. 2019; John et al. 2020; Suleymanov et al. 2021). Various ML models including multiple linear regression (MLR), artificial neural network (ANN), decision tree (DT), random forests (RF), and support vector machine (SVM) have successfully explained the relationships between soil properties and covariates to unknown locations (Hateffard et al. 2019; Taghizadeh-Mehrjardi et al. 2020; Suleymanov et al. 2021). It has been reported that the accuracy and spatial validity of soil maps derived from DT are higher than those obtained from traditional methods (Kheir et al. 2010; Taghizadeh-Mehrjardi et al. 2015; Hateffard et al. 2019). Predictive soil properties using decision tree analysis can increase predicting efficiency and accuracy by extracting relationships between soil parameters and environmental variables, which can be applied to predict soil properties for unmapped areas.

Considerable advances in remote sensing techniques and machine learning approaches allowed to accurately predict soil properties at unsampled locations. A large number of existing remote sensing data sets (e.g., SPOT, RapidEye, Landsat, Sentinel-2) have been used to extract remote sensing attributes as predictors for predicting soil properties (Mammadov et al. 2021; Forkuor et al. 2017; John et al. 2020; Taghizadeh-Mehrjardi et al. 2020; Mosleh et al. 2016). Furthermore, digital elevation models and their derivatives (e.g., elevation, slope, etc.) have also served as excellent data for studying and mapping the spatial distribution of soil nutrients (Hateffard et al. 2019; Mosleh et al. 2016; Suleymanov et al. 2021). John et al. (2020) reported that the combination of environmental auxiliary data such as remote sensing (RS) and digital elevation models (DEM) via predictive models provides a cost-effective, reproducible, and spontaneous approach for estimating the variability of soil properties.

However, the potentials of remote sensing data in improving knowledge of local-scale soil information in Libya have not been fully explored. This study investigated the use of satellite imagery data (i.e., Landsat), terrain/climatic data, and laboratory analyzed soil samples to map the spatial distribution of soil properties in the most arable land in northwestern Libya. The main aim of this research is to conduct a spatial prediction of selected topsoil properties such as soil pH, calcium carbonate (CaCO_3); exchangeable sodium percentage (ESP); and cation exchange capacity

(CEC) using integrated remotely sensed data and machine learning approach in northwestern Libya.

2 Material and Methods

2.1 Study Area

The study area is located between 12° 74' 0" to 13° 28' 4" E longitudes and 32° 91' 3" to 32° 22' 2" N latitudes and covers approximately 3700 km² in Tripoli region, in northwestern Libya (Fig. 1). It is part of the Jafara plain and considered to be the most important agricultural region in the country. Figure 1 displays the location of soil samples in northwestern Libya (Selkhozpromexport. 1980) and the dominant soil types (subgroup level) (U.S. Soil Taxonomy). The study area has a Mediterranean climate, with average monthly temperatures ranging from 13.2 to 27.9 °C and an average annual temperature of 20.7 °C (Zurqani et al. 2018). Most of the yearly rainfall occurs during the winter months (October to March) with great temporal and spatial variability (Zurqani and Ben Mahmoud 2021).

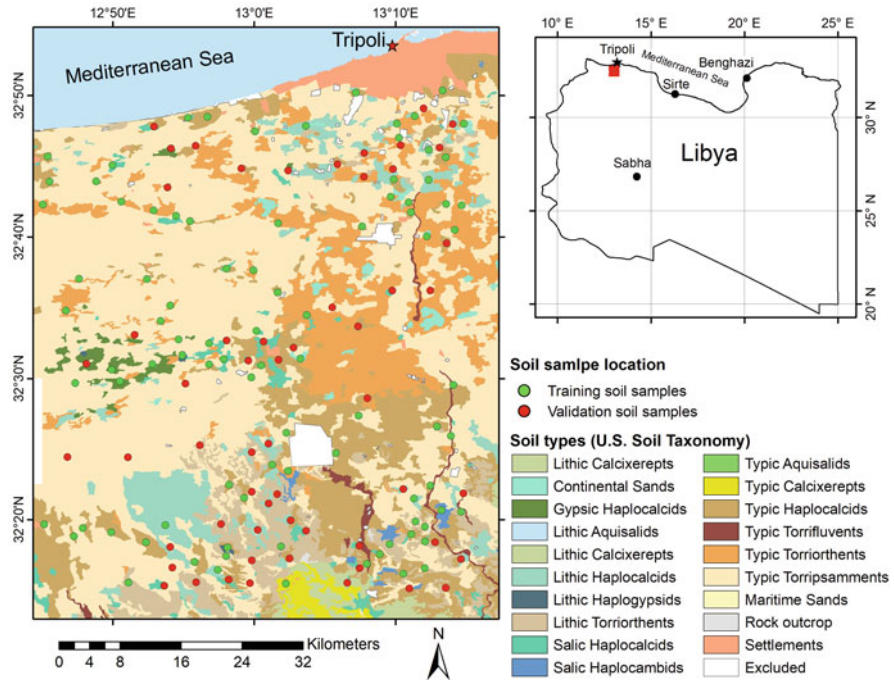


Fig. 1 Map of the study area and location of soil samples in northwestern Libya (Selkhozpromexport. 1980), and the dominant soil types (subgroup level) (U.S. Soil Taxonomy)

Most of the soils in the region are undeveloped or partly developed with Aridisols and Entisols being the main soil orders (Zurqani and Ben Mahmoud 2021). In addition, the major agricultural crops grown in this area are barley, wheat, and maize (Elaalem 2010).

2.2 Soil Samples Dataset

The reference soil dataset used in this study was obtained from a previous soil study conducted in northwestern Libya (Selkhozpromexport. 1980). The soil information was entered and organized in Excel format for a total of ($n = 147$) soil profiles (Elaalem 2010). The spatial distribution of 147 locations of these soil profiles are illustrated in Fig. 1. The information collected in this study represents soil surface properties (0–30 cm) for the used soil profiles that include soil pH, calcium carbonate (CaCO_3), exchangeable sodium percentage (ESP), and cation exchange capacity (CEC).

2.3 Environmental Covariates

Environmental covariates used in spatial prediction of selected soil properties in northwestern Libya include remotely sensed spectral data (RS) and derivatives of the digital elevation model (DEM). Google Earth Engine (GEE) provides a rapid analysis of remote sensing using Google’s computing infrastructure, which offers online datasets in near-real-time (Zurqani et al. 2018). In this study, all the satellite data pre-preprocessing was conducted in GEE Code Editor (<https://code.earthengine.google.com>). Remote sensing data was obtained from Landsat 5 Surface Reflectance images acquired between the 1st of April and the 29th of December 1984. These data have been atmospherically corrected using LEDAPS, and include a cloud, shadow, water, and snow mask produced using CFMASK, as well as a per-pixel saturation mask (Gorelick et al. 2017). Table 1 shows the wavelength, and spatial resolution of spectral bands, including the red, green, blue (RGB, ‘visible spectrum’), the near-infrared (NIR) bands, and 2 short-wave infrareds (SWIR) in Landsat 5 TM.

Table 1 Band specifications of Landsat 5 TM (U.S. Geological Survey (USGS) 2021)

Band	Wavelength (micrometers)	Resolution (meters)
Band 1 visible (blue)	(0.45–0.52 μm)	30 m
Band 2 visible (green)	(0.52–0.60 μm)	30 m
Band 3 visible (red)	(0.63–0.69 μm)	30 m
Band 4 near-infrared	(0.76–0.90 μm)	30 m
Band 5 shortwave-infrared 1	(1.55–1.75 μm)	30 m
Band 7 shortwave infrared 2	(2.08–2.35 μm)	30 m

Table 2 Environmental covariates used as predictors in the study area

Environmental covariates	Name of covariate	Formula	Reference
Remote sensing attributes (Landsat ETM) Source (GEE), provided by U.S. Geological Survey (USGS)	Normalized difference vegetation index (NDVI)	$(R - NIR) / (R + NIR)$	Hateffard et al. (2019)
	Normalized difference soil index (NDSI)	$(R - NIR) / (R + NIR)$	Deng et al. (2015)
	Brightness index (BI)	$[(R)^2 + (NIR)^2]^{0.5}$	Gholizadeh et al. (2018)
	Carbonate Index (CI)	(Red / Green)	Boettinger et al. (2008)
	Bare soil Index (BSI)	$((SWIR1 + Red) - (NIR + Blue)) / ((SWIR1 + Red) + (NIR + Blue))$	Mzid et al. (2021)
	Soil Adjusted Vegetation Index (SAVI)	$((NIR - Red) / (NIR + Red + L)) \times (1 + L) L = 0.5$	Gholizadeh et al. (2018)
	Modified Soil-adjusted Vegetation Index2 (MSAVI2)	$(2 * NIR + 1 - \sqrt{(2 * NIR + 1)^2 - 8 * (NIR - Red)}) / 2$	Gholizadeh et al. (2018)
Topographic attributes Source (GEE), provided by (NASA/USGS / JPL-Caltech)	DEM	–	Mosleh et al. (2016)
	Slope	–	Mosleh et al. (2016)

B blue band, *G* green band, *R* red band, *NIR* near infrared band of Landsat 5 images

The selected remote sensing auxiliary variables included Landsat image band 4 (B1–5, and 7), in addition to indices derived from spectral band combinations that including the normalized difference vegetation index (NDVI), normalized difference soil index (NDSI), brightness index (BI), carbonate index (CI), bare soil index (BSI), soil adjusted vegetation index (SAVI), and modified soil-adjusted vegetation index2 (MSAVI2) (Table 2).

Topography has a significant impact on soil development, and its orientation affects microclimate which in turn affects vegetation (Zurqani and Ben Mahmoud 2021). Therefore, terrain attributes including elevation and slope obtained from the digital elevation model (DEM) database with the cell size of 30 m × 30 m were also used as auxiliary variables (Table 2).

2.4 Modeling Approach

For the spatial prediction of selected soil properties in northwestern Libya, a decision tree classifier was selected as the classification algorithm in this study. In GEE, the DT classifier algorithm was applied in the regression mode to estimate the spatial distribution of the selected soil properties. In this approach, 80% of the total dataset were

randomly selected for DT model training, which left 20% of the dataset to be used as testing set. Each soil property was modeled independently using the selected environmental covariates (Table 2). Decision tree classifier algorithm is popular and has been widely and successfully used in the field of DSM many times, and it can be used for solving regression and classification problems too (Bui et al. 2006; Zhang et al. 2008; Hateffard et al. 2019; Esfandiarpour-Boroujeni et al. 2020). Decision tree algorithm belongs to the family of ensemble machine learning algorithms that predicts a response (in this case the respective soil parameters) based on a set of qualitative and quantitative predictor variables. DT is a non-parametric non-linear supervised learning algorithm that splits the data into subsets according to independent factors in the input dataset. The core parameter of decision tree is the node. In this study, 25 leaf nodes in each tree provided an optimum generalization of the model.

2.5 Model Validation and Variable Importance

In machine learning, the algorithm model needs to be trained to update each parameter in the model. Therefore, it is necessary to provide the training set as a training sample. At the same time, a testing set is needed to describe the generalization ability of the model and to test obtain the generalization error. The performance of the DT model in predicting the soil properties was assessed by using a cross-validation approach. There are different types of cross validation techniques (Dash and Swain 2020), but the overall concept remains the same; (1) divide the data into several subsets, (2) hold out a set at a time and train the model on the remaining set, and (3) test model on the hold out set. In this study, a k-fold-cross-validation with ten repetitions ($k = 10$) was applied to ensure model stability and reliability (Fig. 2). The advantage of using this method is that it performs reliably and is unbiased on smaller datasets (Zeraatpisheh et al. 2019).

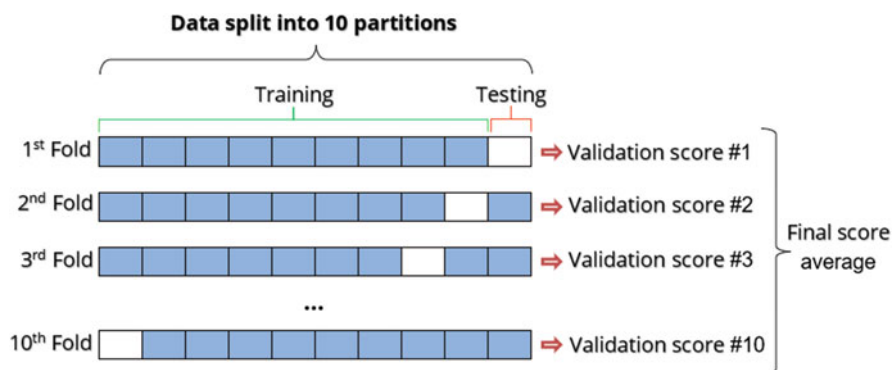


Fig. 2 Ten-fold-cross-validation diagram. The dataset was divided into ten parts, and nine of them were taken as training data in turn, and one was used as test data for testing. This procedure was repeated 10 times, each time setting a different fold aside

For each soil parameter, three quantitative criteria between measured and predicted values—coefficient of determination (R^2), root mean squared error (RMSE), and the normalized root mean squared error (NRMSE)—were calculated (see Eqs. 1, 2 and 3). These three error statistics indicate the robustness of the statistical linear relationship between the measured and predicted soil properties' values. Generally, values closer to one of R^2 and smaller values RMSE and NRMSE indicate better model performance.

$$R^2 = 1 - \left[\frac{\sum_{i=1}^n (p_i - o_i)^2}{\sum_{i=1}^n (p_i - o_i)^2} \right] \quad (1)$$

$$RMSE = \left[\frac{1}{n} \sum_{i=1}^n (p_i - o_i)^2 \right]^{1/2} \quad (2)$$

$$NRMSE = \frac{RMSE}{o_{i,max} - o_{i,min}} \quad (3)$$

where n is the number of locations for the observations/samples; o_i signifies the observed/measured values, p_i signifies the predicted/estimated values, and $o_{i,max}$ and $o_{i,min}$ are the maximum and minimum observed values, respectively. Variable importance measures of environmental covariates are also calculated by the DT classifier algorithm in GEE for each of the selected soil properties to quantify the most influential covariates used in the models. Variable importance is based on the number of times the variable was chosen as a predictor in the individual trees and weighted by the deviance the variable explained across all trees (Elith et al. 2008). Inspecting variable importance helps us understand which variables contribute to the model predictions, but not necessarily how they relate to the outcome. The decision tree technique uses Gini Index, also known as the Gini importance, to help determine which variables are most important. The importance of a variable is computed as the (normalized) total reduction (i.e., weighted information gain) of the criterion brought by that variable. The higher the value, the more important the variable.

3 Results and Discussion

3.1 Descriptive Statistics and Correlation Analysis

Summary statistics of soil properties in the study area are presented in Table 2. Soil pH ranging from 7.50 to 8.90, calcium carbonate (CaCO_3) ranging from 0.0% to 55.25%, exchangeable sodium percentage (ESP) ranging from 0.20% to 9.10%, and cation exchange capacity (CEC) ranging from 3 to 14.50 ($\text{Cmol}^+ \cdot \text{Kg}^{-1}$). The results showed that soil pH and CEC had the lowest variation, while ESP and CaCO_3 had the highest variation, respectively. Among all soil properties, CaCO_3 shows the

Table 3 Descriptive statistics of selected soil properties in the study area (n = 147)

Soil properties	Minimum	Maximum	Mean	Median	CV (%)	SD
Soil pH	7.50	8.90	8.28	8.30	3.29	0.27
CaCO ₃	0.00	55.25	7.23	5.30	104.85	7.58
ESP	0.20	9.10	1.71	1.54	64.89	1.11
CEC	3.00	14.50	6.33	5.90	35.80	2.27

CaCO₃ calcium carbonate, ESP exchangeable sodium percentage, CEC cation exchange capacity, CV coefficient of variation, SD standard deviation

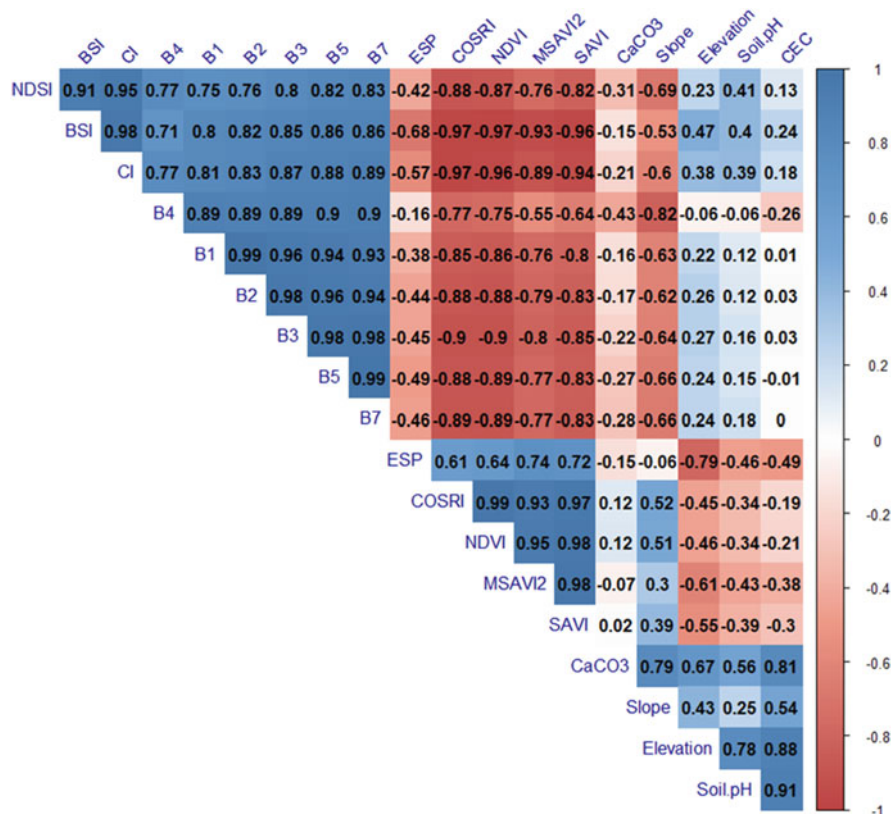


Fig. 3 Correlograms of soil properties and environmental covariates (values in cells show Pearson correlation coefficients). CaCO₃ calcium carbonate, ESP exchangeable sodium percentage, CEC cation exchange capacity, NDVI normalized difference vegetation index, NDSI normalized difference soil index, BI brightness index, CI carbonate index, BSI bare soil index, SAVI soil adjusted vegetation index, MSAVI2, modified soil-adjusted vegetation index2, and Landsat 5 image bands (B1–5, and 7) (Table 2)

highest CV value of 104.85%, which indicates a greater degree of relative variability of CaCO₃ values across the study area (Table 3).

The correlogram (Fig. 3) summarizes the relationships (i.e., correlations) between soil properties and environmental covariates (Landsat 5 image bands, spectral

indices, and terrain attributes). Positive correlations are displayed in blue and negative correlations in red. The intensity of the color is proportional to the correlation coefficient so the stronger the correlation (i.e., the closer to -1 or 1), the darker the boxes. Among all the variables, soil pH has a moderate positive correlation with BSI ($R = 0.40$), carbonate index ($R = 0.39$), NDSI ($R = 0.41$), and a strong positive correlation with elevation ($R = 0.78$), while ESP shows a strongest correlation with COSRI ($R = 0.61$), MSAVI2 ($R = 0.74$), NDVI ($R = 0.64$) and SAVI ($R = 0.72$). On the other hand, CaCO_3 and CEC did not show significant correlation with remote sensing attributes and only showed significant correlation (i.e., a strong positive correlation) with topographic attributes including elevation with ($R = 0.67$, and 0.88), and slope with ($R = 0.79$, and 0.54), respectively (Fig. 3). Forkuor et al. (2017) stated that Landsat spectral and topographic data can represent environmental covariates for spatial prediction of soil properties. These results are also consistent with other studies (Jafari et al. 2014; Mosleh et al. 2016; Zeraatpisheh et al. 2019). Similarly, Suleymanov et al. (2021) mentioned that topography had great potential to explain a large part of the variability in soil properties.

3.2 Measured vs. Predicted Values of the Selected Soil Properties Obtained from the Machine Learning Model

The performance of the DT model in predicting the soil properties was assessed by using k-fold-cross-validation approach as described in the material and methods section (2.5). According to the R^2 , RMSE, and NRMSE values (Table 4, Fig. 4a–d), where larger values of R^2 and smaller values RMSE and NRMSE indicate higher validity of the model performance. Cation exchange capacity (CEC) had the highest validity by giving an accurate ($R^2 = 0.42$), and (RMSE = 2.87). Calcium carbonate (CaCO_3) had a moderate validity with ($R^2 = 0.29$) and (RMSE 6.96), respectively. The model showed low coefficients of determination ($R^2 < 0.25$) and, consequently, no predictive capabilities were found for soil pH ($R^2 = 0.22$), or ESP ($R^2 = 0.22$). These elements are not predicted with satisfactory accuracy by the model. However, low coefficients of determination R^2 values may not necessarily lead to inaccurate predictions. Previous results also obtained poor models for predicting the spatial distribution of soil pH using machine learning approaches (Suleymanov et al. 2021; Mosleh et al. 2016). On the other hand, the lower values of NRMSE with range between 0.12 and 0.26 (Table 4) indicate less residual variance for these selected soil

Table 4 The values of error statistics obtained during the training, and validation process of the DT model for each soil property

Soil properties	R^2	RMSE	NRMSE
Soil pH	0.22	0.35	0.25
CaCO_3	0.29	6.96	0.12
ESP	0.22	1.67	0.18
CEC	0.42	2.87	0.26

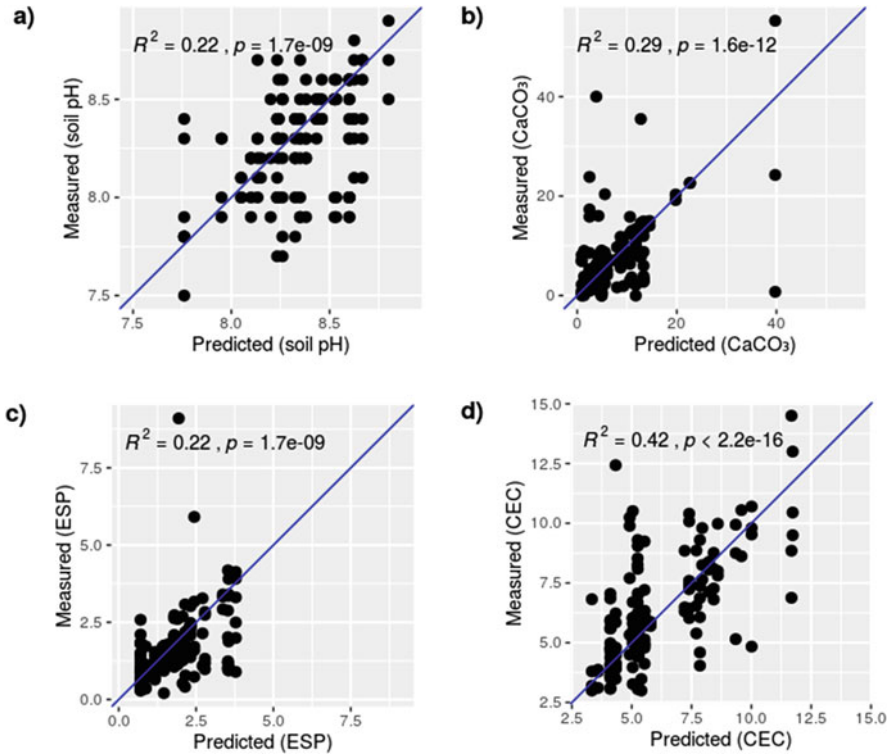


Fig. 4 Scatter plot for measured vs predicted values of selected soil properties; (a) soil pH; (b) calcium carbonate (CaCO₃); (c) exchangeable sodium percentage (ESP); and (d) cation exchange capacity (CEC)

properties (i.e., soil pH, CaCO₃, ESP, and CEC). The current study used validation techniques commonly reported in DSM. For example, a study conducted in a semiarid region, central Iran (Zeraatpisheh et al. 2019) calibrated and validated multiple machine learning models by using the k-fold cross-validation approach. Hateffard et al. (2019) assessed the performance of Artificial Neural Network (ANN) and Decision Tree (DT) models in the prediction of spatial variability of the soil properties in Alborz province, Iran. Their results revealed that the DT model showed higher performances than the ANN model in estimating the spatial variability of soil properties in the study area with (RMSE ranges between 0.38 and 13.74, and R^2 ranges between 0.59 and 0.73), which is in line with the results of (Kheir et al. 2010; Jafari et al. 2014; Almajmaie et al. 2017).

3.3 Environmental Covariates Importance

The variable importance of environmental covariates as identified by the DT classifier in GEE for each of the selected soil properties is shown in (Fig. 5a–d). Landsat 5 imagery blue band (B1) is a key attribute for predicting the soil pH and calcium carbonate (CaCO₃), while the shortwave-infrared 1 band (B5) is the best predictor variable for the exchangeable sodium percentage (ESP). Similar results were obtained by da Silva Chagas et al. (2016) and Hateffard et al. (2019) highlighting the importance of these bands in mapping soil properties. The variable importance of the DT model also showed that terrain elevation is the most important variable for explaining the variability of the exchangeable sodium percentage (ESP) and cation exchange capacity (CEC) in the study area. Ma et al. (2017) also indicated that elevation is the most important variable that has a significant impact on the spatial distribution of soil properties, which is in line with the results of (Taghizadeh-Mehrjardi et al. 2015; Mosleh et al. 2016).

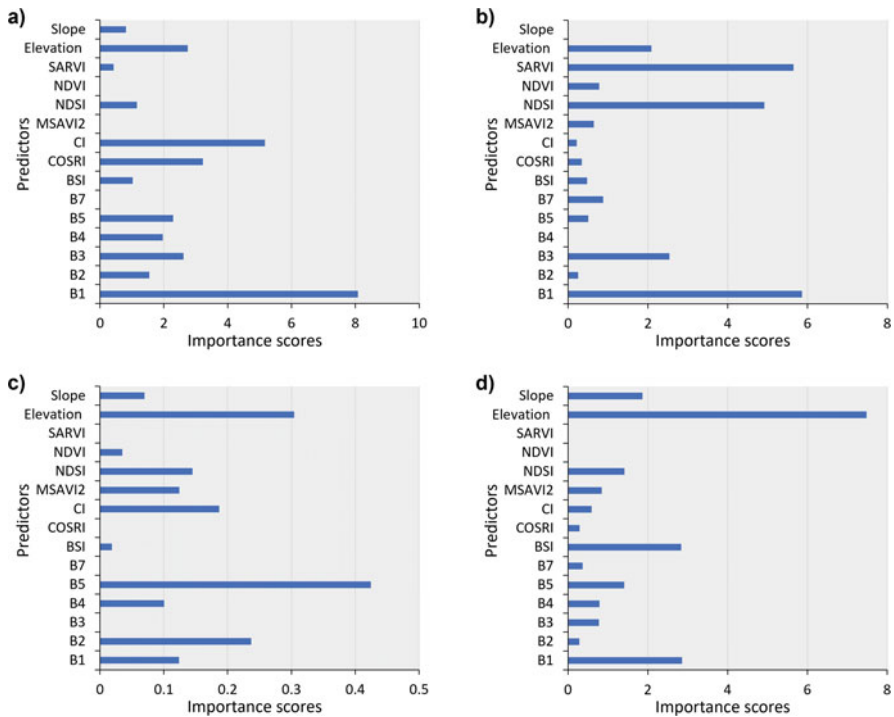


Fig. 5 Variable importance of environmental covariates as identified by DT classifier in GEE for each of the selected soil properties; (a) soil pH; (b) calcium carbonate (CaCO₃); (c) exchangeable sodium percentage (ESP); and (d) cation exchange capacity (CEC). NDVI normalized difference vegetation index, NDSI normalized difference soil index, BI brightness index, CI carbonate index, BSI bare soil index, SAVI soil adjusted vegetation index, MSAVI2 modified soil-adjusted vegetation index2, and Landsat 5 image bands (B1–5, and 7)

3.4 Spatial Distribution of the Selected Soil Properties Using the Machine Learning Model

Mapping soil properties is a preliminary step towards decision making such as the delineation of suitable crop growing areas and applying site-specific management. The spatial distribution maps of the selected soil properties generated by the DT model are presented in (Fig. 6a–d), which highlight the high and low concentrations of the soil pH, CaCO₃, ESP, and CEC within the topsoil (0–30 cm) depth in all the geographical locations of the study area. The predicted soil pH varied from 7.66–8.80, while the CaCO₃ showed high spatial variability ranging from 1.37% to 29.87% across the study area. The ESP and CEC ranging from 0.35 to 6.50 and 3.60–12.72 (Cmol⁺¹.Kg⁻¹), respectively (Fig. 6a–d). The spatial prediction of soil properties suggested that distribution of soil properties on the surface are highly variable due to variations in land management and land use in the region. These predicted maps can be used to identify areas with important soil fertility constraints (Liu et al. 2015; Suleymanov et al. 2021), to determine the soil degradation risk (Kheir et al. 2010; Mosleh et al. 2016), and to suggest suitable management options for better reclamation (Forkuor et al. 2017; Zeraatpisheh et al. 2019; Esfandiarpour-Boroujeni et al. 2020).

4 Conclusion

Accurate and detailed spatial soil information is essential for environmental modeling, risk assessment, and decision making. Large-scale mapping of soil properties is necessary for rational land management and agriculture reclamation measures. This study shows that is possible to use remote sensing and topography variables with a DT approach to predict soil properties in Libya. The use of such ML techniques can reduce soil sampling efforts, and therefore reduce soil mapping costs and preserve time and human resources. The reason for the high values of RMSE of CaCO₃, ESP, and CEC was likely because of the wide-ranging values in the soil dataset. The NRMSE was convenient for quantifying the degree of agreement between predicted and measured values where its lower values indicate less residual variance and thus a better performance of the model used. The most important variables for predicting the spatial distribution of soil properties were elevation, Landsat 5 imagery blue band (B1, and B5), and NDSI index. In Libya, digital soil mapping (DSM) methods have rarely been used, and there is still a great need for large scope DSM research within local geographical settings. However, the accuracies obtained in this study seem to be promising for current and future local scale digital soil mapping efforts as well as for the other regions in the world with similar soil and climate conditions.

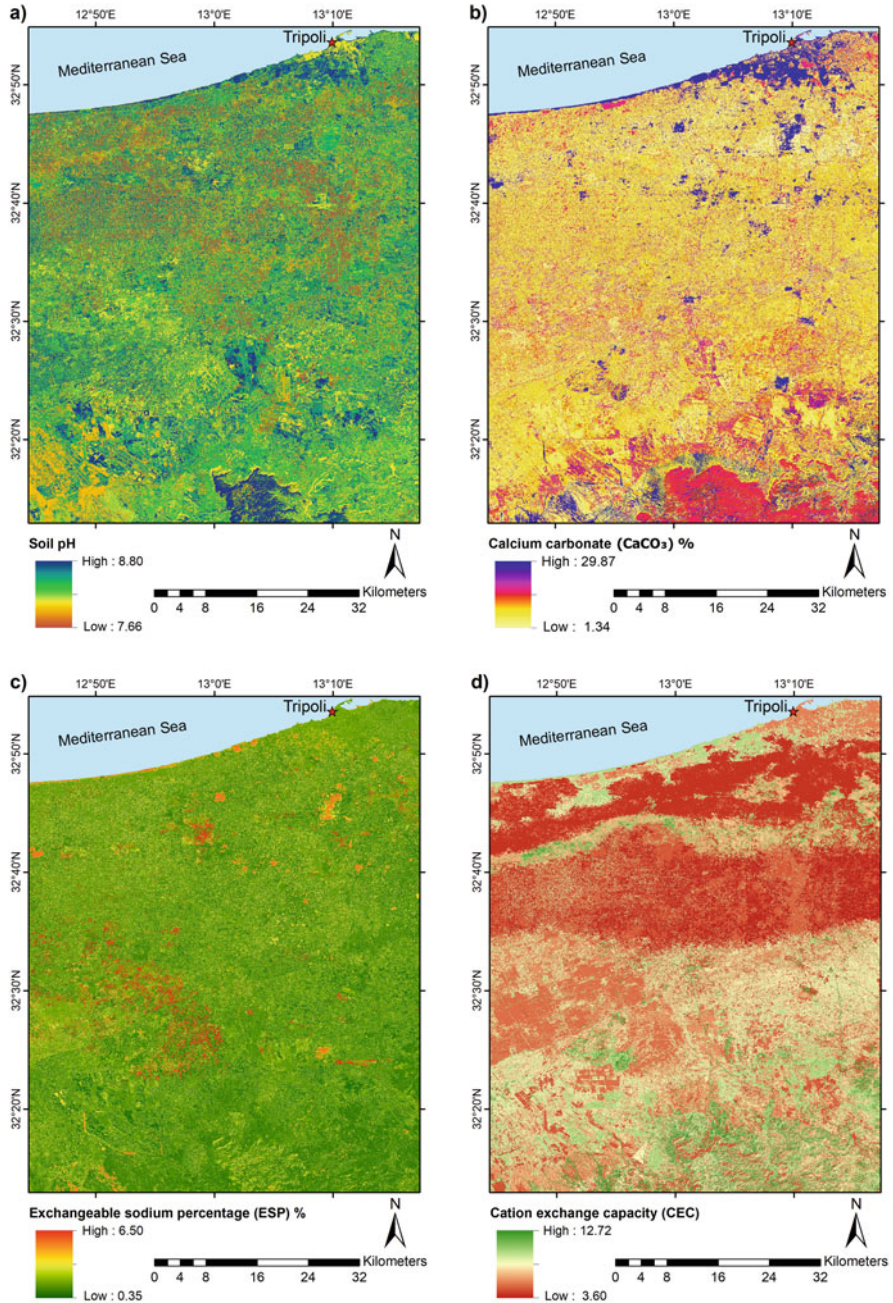


Fig. 6 Spatial distribution of each soil property in the study area based on the DT model; (a) soil pH; (b) calcium carbonate (CaCO₃); (c) exchangeable sodium percentage (ESP); and (d) cation exchange capacity (CEC)

Author Contributions Hamdi A. Zurqani: conceptualization, methodology, supervision, software, data curation, formal analysis, validation, investigation, writing—original draft, visualization, writing—review and editing, review of analysis. The author has read and agreed to the published version of the manuscript.

References

- Abagandura OG, Park D (2016) Libyan agriculture: a review of past efforts, current challenges and future prospects. *J Nat Sci Res* 6(18):57–67
- Aburas M, Payton R, Gowing J (2008) Assessment of soil erodibility, degradation and its relation to land use practices in Aljabal Alakhdar region, Libya. School of Agriculture, Food and Rural Development, Newcastle University, UK
- Almajmaie A, Hardie M, Doyle R, Birch C, Acuna T (2017) Influence of soil properties on the aggregate stability of cultivated sandy clay loams. *J Soils Sediments* 17(3):800–809
- Boettinger JL, Ramsey RD, Bodily JM, Cole NJ, Kienast-Brown S, Nield SJ, Saunders AM, Stum AK (2008) “Landsat spectral data for digital soil mapping.” In *Digital soil mapping with limited data* 193–202. Springer, Dordrecht, 2008. https://link.springer.com/chapter/10.1007/978-1-4020-8592-5_16
- Bui EN, Henderson BL, Viergever K (2006) Knowledge discovery from models of soil properties developed through data mining. *Ecol Model* 191(3–4):431–446
- da Silva Chagas C, de Carvalho Junior W, Bhering SB, Calderano Filho B (2016) Spatial prediction of soil surface texture in a semiarid region using random forest and multiple linear regressions. *Catena* 139:232–240
- Dash R, Swain SC (2020) A review on nearest-neighbor and support vector machine algorithms and its applications. In *AI in manufacturing and green technology: methods and applications* 83–88. CRC Press. <https://www.taylorfrancis.com/chapters/edit/10.1201/9781003032465-8/review-nearest-neighbor-support-vector-machine-algorithms-applications-ritesh-dash-sarat-chandra-swain>
- Deng Y, Wu C, Li M, Chen R (2015) RNDSI: a ratio normalized difference soil index for remote sensing of urban/suburban environments. *Int J Appl Earth Obs Geoinf* 39:40–48
- Elaalem M (2010) The application of land evaluation techniques in Jeffara Plain in Libya using fuzzy methods. Published PhD thesis, Leicester University
- Elith J, Leathwick JR, Hastie T (2008) A working guide to boosted regression trees. *J Anim Ecol* 77(4):802–813
- Esfandiarpour-Boroujeni I, Shamsabadi MS, Shirani H, Mosleh Z, Bodaghabadi MB, Salehi MH (2020) Comparison of error and uncertainty of decision tree and learning vector quantization models for predicting soil classes in areas with low altitude variations. *Catena* 191:104581
- Forkuor G, Hounkpatin OK, Welp G, Thiel M (2017) High resolution mapping of soil properties using remote sensing variables in south-western Burkina Faso: a comparison of machine learning and multiple linear regression models. *PLoS One* 12(1):e0170478
- Gholizadeh A, Žižala D, Saberioon M, Borůvka L (2018) Soil organic carbon and texture retrieving and mapping using proximal, airborne and Sentinel-2 spectral imaging. *Remote Sens Environ* 218:89–103
- Gorelick N, Hancher M, Dixon M, Ilyushchenko S, Thau D, Moore R (2017) Google Earth Engine: Planetary-scale geospatial analysis for everyone. *Remote sensing of Environment* 202:18–27
- Hateffard F, Dolati P, Heidari A, Zolfaghari AA (2019) Assessing the performance of decision tree and neural network models in mapping soil properties. *J Mt Sci* 16(8):1833–1847
- Jafari A, Khademi H, Finke PA, Van de Wauw J, Ayoubi S (2014) Spatial prediction of soil great groups by boosted regression trees using a limited point dataset in an arid region, southeastern Iran. *Geoderma* 232:148–163

- John K, Abraham Isong I, Michael Kebonye N, Okon Ayito E, Chapman Agyeman P, Marcus Afu S (2020) Using machine learning algorithms to estimate soil organic carbon variability with environmental variables and soil nutrient indicators in an alluvial soil. *Land* 9(12):487
- Kheir RB, Greve MH, Bøcher PK, Greve MB, Larsen R, McCloy K (2010) Predictive mapping of soil organic carbon in wet cultivated lands using classification-tree based models: the case study of Denmark. *J Environ Manag* 91(5):1150–1160
- Liu S, An N, Yang J, Dong S, Wang C, Yin Y (2015) Prediction of soil organic matter variability associated with different land use types in mountainous landscape in southwestern Yunnan province, China. *Catena* 133:137–144
- Lucà F, Buttafuoco G, Terranova O (2018) GIS and soil. In: Huang B (ed) *Comprehensive geographic information systems*. Elsevier, Oxford, pp 37–50
- Ma Y, Minasny B, Wu C (2017) Mapping key soil properties to support agricultural production in eastern China. *Geoderma Reg* 10:144–153
- Mammadov E, Nowosad J, Glaesser C (2021) Estimation and mapping of surface soil properties in the Caucasus Mountains, Azerbaijan using high-resolution remote sensing data. *Geoderma Regional* 26:00411
- Minasny B, McBratney AB (2016) Digital soil mapping: a brief history and some lessons. *Geoderma* 264:301–311
- Mosleh Z, Salehi MH, Jafari A, Borujeni IE, Mehnatkesh A (2016) The effectiveness of digital soil mapping to predict soil properties over low-relief areas. *Environ Monit Assess* 188(3):195
- Mosleh Z, Salehi MH, Jafari A, Borujeni IE, Mehnatkesh A (2016) The effectiveness of digital soil mapping to predict soil properties over low-relief areas. *Environ Monit Assess* 188(3):1–13
- Mzid N, Pignatti S, Huang W, Casa R (2021) An analysis of bare soil occurrence in arable croplands for remote sensing topsoil applications. *Remote Sens* 13(3):474
- Selkhozpromexport. (1980) *Soil studies in the Western zone of the socialist people's Libyan Arab Jamahiriya*. Secretariat for Agricultural Reclamation and Land Development, Tripoli
- Suleymanov A, Abakumov E, Suleymanov R, Gabbasova I, Komissarov M (2021) The soil nutrient digital mapping for precision agriculture cases in the trans-ural steppe zone of Russia using topographic attributes. *ISPRS Int J Geo Inf* 10(4):243
- Taghizadeh-Mehrjardi R, Nabiollahi K, Minasny B, Triantafyllis J (2015) Comparing data mining classifiers to predict spatial distribution of USDA-family soil groups in Baneh region. *Iran Geoderma* 253:67–77
- Taghizadeh-Mehrjardi R, Nabiollahi K, Kerry R (2016) Digital mapping of soil organic carbon at multiple depths using different data mining techniques in Baneh region, Iran. *Geoderma* 266:98–110
- Taghizadeh-Mehrjardi R, Schmidt K, Amirian-Chakan A, Rentschler T, Zeraatpisheh M, Sarmadian F, Valavi R, Davatgar N, Behrens T, Scholten T (2020) Improving the spatial prediction of soil organic carbon content in two contrasting climatic regions by stacking machine learning models and rescanning covariate space. *Remote Sens* 12(7):1095
- Terranova O (2018) GIS and Soil. In Huang, B. (Ed.), *Comprehensive Geographic Information Systems* 2:37–50. Oxford: Elsevier. <http://dx.doi.org/10.1016/B978-0-12-409548-9.09634-2> ISBN: 9780128046609
- U.S. Geological Survey (USGS) (2021) Landsat missions. https://www.usgs.gov/core-science-systems/nli/landsat/landsat-5?qt-science_support_page_related_con=0#qt-science_support_page_related_con. Accessed 5 May 2021
- Zeraatpisheh M, Ayoubi S, Jafari A, Tajik S, Finke P (2019) Digital mapping of soil properties using multiple machine learning in a semi-arid region, Central Iran. *Geoderma* 338:445–452
- Zhang X, Lin F, Jiang Y, Wang K, Wong MT (2008) Assessing soil Cu content and anthropogenic influences using decision tree analysis. *Environ Pollut* 156(3):1260–1267

- Zurqani HA (2021) *The Soils of Libya*. World Soils Book Series. Switzerland. Springer International Publishing AG. (1st ed.). ISBN-13: 978-3030663674
- Zurqani HA, Ben Mahmoud, KR (2021) Land cover land use and the vegetation distribution In: Zurqani HA (ed) *The Soils of Libya*. World Soils Book Series. Springer, Cham. https://doi.org/10.1007/978-3-030-66368-1_6
- Zurqani HA, Post CJ, Mikhailova EA, Schlautman MA, Sharp JL (2018) Geospatial analysis of land use change in the Savannah River Basin using Google Earth Engine. *Int J Appl Earth Obs Geoinf* 69:175–185
- Zurqani HA, Mikhailova EA, Post CJ, Schlautman MA, Elhawej AR (2019) A review of Libyan soil databases for use within an ecosystem services framework. *Land* 8(5):82

Hamdi A. Zurqani is an Assistant Professor of Geospatial Science in Natural Resource Management and Conservation at the University of Arkansas Agricultural Experiment Station, Arkansas Forest Resources Center, University of Arkansas at Monticello, Monticello, AR, USA. He is also an FAA (i.e., Pt107) Certified sUAS/Drones Pilot, and has used this skill to enhance his knowledge of remote sensing and GIS. Dr. Zurqani is a recognized expert as a result of his internationally acclaimed work in the areas of environmental information science, remote sensing, geospatial analysis, land evaluation, sustainability, pedology, and soil science education. He has conducted research across the world, including the United States of America, and Africa, and has served as PI, co-PI, or co-investigator on several grants-funded research projects. Dr. Zurqani is highly collaborative as evidenced by his publications. He is the author and coauthor of many peer-reviewed publications, book chapters, and technical publications (including teaching laboratory manuals). He also edited two books with Springer Nature (i.e., “*The Soils of Libya*”, and “*Environmental Applications of Remote Sensing and GIS in Libya*”), and has published widely in many peer-review journals (e.g., *International Journal of Applied Earth Observation and Geoinformation* (Elsevier); *Remote Sensing in Earth Systems Sciences* (Springer Nature); *Scientific Reports* (Nature); *Frontiers in Environmental Science* (Frontiers); *Geoderma* (Elsevier); *Land* (MDPI); *Urban Forestry & Urban Greening* (Elsevier), and others). Dr. Zurqani is a member of the Editorial Board for *Remote Sensing* (MDPI) Journal, counseling outcome, and research evaluation. He also was appointed to serve as a Guest Editor for the Special Issue “*Applications of Remote Sensing in Earth Observation and Geo-Information Science*”. In addition, Dr. Zurqani conducted peer-review for many journals including *Journal of Environmental Informatics*, *Applied Sciences*, *SN Applied Sciences*, *Remote Sensing*, *Geo-spatial Information Science*, *AgriEngineering*, *Sensors*, *Heliyon*, *Geosciences*, *Land*, *Soil Systems*, *Water*, *Agronomy*, *Agriculture*, *Resources*, *Sustainability*, *Arid Land Research and Management*, *Quaestiones Geographicae*, *Geocarto International*, *International Journal of Environmental Research and Public Health*, *Natural Hazards*, and *Conference of the Arabian Journal of Geosciences*. Dr. Zurqani conducts cutting-edge research in the field of *Environmental Information Science*, *Remote Sensing*, *Land use management/ planning*, *change detection of landscape degradation*, and *Geographic Information System (GIS) models*. He has focused his research efforts on the development of novel applications for new technologies in analyzing spatial data, remote sensing, geostatistical modeling of environmental changes such as erosion, mapping and predicting soil salinity, and land use/ land cover changes. His new publications include: “*Mapping and Quantifying Agricultural Irrigation in Heterogeneous Landscapes Using Google Earth Engine*” in the *Journal of Remote Sensing Applications: Society and Environment*; “*Evaluating the integrity of forested riparian buffers over a large area using LiDAR data and Google Earth Engine*” in the *Journal of Scientific Reports*; “*Mapping Urbanization Trends in a Forested Landscape Using Google Earth Engine*” in the *Journal of Remote Sensing in Earth Systems Sciences*; “*Geospatial analysis of land use change in the Savannah River Basin using Google Earth Engine*” in the *International Journal of Applied Earth Observation and Geoinformation*; and “*Application of Non-Hydraulic Delineation Method of Flood Hazard Areas Using LiDAR-Based Data*” as well as “*Assessing ecosystem services of atmospheric calcium and magnesium deposition for potential soil inorganic carbon sequestration*” in the *Geosciences Journal*.

Field and Laboratory Estimation of Soil Erodibility, Erosion and Degradation of the Semi-Arid Aljabal Alakhdar Region, Libya



Murad M. Aburas, Asama S. Alferjani, and Mohammed S. Yousef

Abstract The fragile ecosystems in this Mediterranean semi-arid region of eastern Libya are affected by soil degradation driven by soil erosion as a result of the introduction of intensive land use. In this chapter, field measurements were carried out using erosion plots and field observations in order to estimate soil loss and erodibility. Statistical relations and dynamic laboratory methods were applied to estimate soil erodibility values. Soil maps and GIS technology were also used to improve the evaluation of soil erosion risks. The study found apparent indications of soil degradation and accelerated erosion on the northern and southern slopes of Aljabal Alakhdar. The field erosion plots, and the rainfall simulation experiments showed that the moderate aggregate stability of Typic and Calcic Rhodoxeralfs soils significantly improved their resistance to water erosion compared to the Lithic Rhodoxeralfs soils. The study suggested that water stable aggregates can efficiently determine soil erodibility. In order to promote sustainable soil management, potential erosion risk maps identified sites with high, medium and slight classes of erosion hazards depending on soil types and slope characteristics. Accordingly, well designed soil conservation measures need to be applied to enhance soil depth and its holding capacity, so that soil productivity can be recovered and consequently prevent land degradation.

Keywords Arid and semi-arid region · Soil degradation · Erosion · Universal soil loss equation · GIS modelling · Geospatial analysis

1 Introduction

In the Libyan semi-arid Mediterranean region, erosion-related soil degradation has a considerable impact on vulnerable soils, which already experience shallowness and have been subjected to organic matter decline. The region of Al-Jabal al Akhdar

M. M. Aburas (✉) · A. S. Alferjani · M. S. Yousef
Department of Soil and Water, Faculty of Agriculture, University of Omar
Al-Mukhtar, Al Bayda, Libya
e-mail: Murad.aburas@omu.edu.ly

suffers from the most severe natural soil erosion in Libya. This phenomenon, according to FAO (1969) is because the relatively high rainfall promotes increased runoff. Some of the studies conducted in the region were very limited in terms of scale and time. However, since these studies applied direct measurements in the field, they were generally able to relate the problem of degradation to land use. Gebril (1995) observed that the agricultural activities by local people, such as clearance of vegetation, often lead to serious accelerated erosion, especially on the steeper slopes. There are several types of water erosion such as: splash, sheet, rill and gully erosion. The most serious types are sheet and rill erosion, which are responsible for most of the topsoil movement in the area. Gerbil's (1995) measurements of soil erosion by means of erosion pins in the Al-Jabal Alkhdar region showed that considerable soil material was transported by surface wash processes.

The study carried out by Selkhoz Prom Export (1980) was exceptional because it covered the whole region with very detailed investigation. The study reported that during the second half of the twentieth century, intensive forest fires and human-induced woodland removal to establish field and horticulture crops had taken place widely in the area. Some parts of the deforested land were utilized successfully, while the rest was left fallow for various practical reasons, resulting in severe erosion in much of the area. The study estimated that about 79% of Al-Jabal Alkhdar north of the 200 mm rain isoline (i.e., about 14,000 km²) was to some degree affected by water erosion, mainly types of sheet erosion and linear forms of gulling. According to this study the main factors affecting the development of erosion processes are: relatively heavy downpours of rain on the uplands, absence of adequate vegetation cover, particularly during heavy rainfall events and periods of strong winds, slopes of different steepness and length, low permeability of the fine textured lower horizons of deeply developed soils, small humus content, absence of suitable soil tillage technology and regulated grazing, and low soil moisture holding capacity.

Classification of soil erosion was made by the above mentioned body from data collected during large-scale soil surveys (1: 50,000) and soil erosion maps were produced. The description of the degree of soil erosion was made by comparison of the thickness of the A₁ and A_{1+B₁} horizons of an eroded soil with the thickness of the A₁ and A_{1+B₁} horizons of standard non-eroded soils used as benchmarks, although the establishment of pedogenetic benchmarks was not rigorously applied. Moreover, since this comprehensive and detailed investigation was carried out forty years ago, noticeable changes could have taken place in the region as a result of continued intensive human activities. Consequently, the reliability of the Selkhoz Prom soil erosion maps for the present environment is questionable.

Other studies have applied predictive relations in order to assess soil erodibility and erosion-related degradation. Those predictive relations were developed under different environmental conditions and used in the region without validation. Therefore, the accuracy of their results could be in doubt. GEFLI (1975) stated that in the major part of the Al-Jabal Alkhdar area soil erosion is limited (GEFLI 1975), although, in some plots with shallow soils erosion has occurred, in which reddish runoff has been noted during the heavy rains, particularly when the first rains fall after the dry season. The study estimated soil loss based on the universal soil loss

equation (USLE), where the rainfall erosivity factor (R) calculated from rainfall data and soil erodibility factor (K) were estimated by analogy with comparable soils studied in Tunisia. A weakness in this study was the estimation of soil erosion by applying a predictive equation USLE (Wischmeier et al. 1971) without validation and estimating K from soils in Tunisia instead of measuring the actual soil loss in the region. Field observations carried out in the GEFLI study noted few visible signs of soil erosion during the rainy season (1973/1974), while no traces of runoff were recorded within the study area and no rills were recorded. The study concluded that there was a very little, or no, danger of severe soil erosion for the deep soils. In contrast, slowly permeable, shallow and sloping soils can be affected and subjected to excessive soil losses.

OMU (2005) investigated soil erodibility for more than 50 sites across the Al-Jabal al Akhdar region using the K-USLE index. The results showed that most of the sites have medium erodibility. However, there were some highly erodible sites that were protected by good vegetation cover, which indicates the importance of the plant cover factor. In other words, severe erosion is likely to occur if these erodible soils lose the protection of the existing plant cover. As in the case of the GEFLI (1975) research, this study also applied the USLE predictive formula (Wischmeier et al. 1971) without validating the results against any direct measurements. It is argued here that a better understanding of soil degradation-related erodibility in this part of Libya is required in order to design appropriate soil conservation measures and that such measures must be better related to more sustainable land management practices.

There has been no previous attempt to develop indicators for soil erodibility estimation for the region of study in particular. This makes the investigation of soil erodibility and the causes of erosion-related soil degradation in this region a priority, with the aim of providing a formula to estimate soil erodibility in a spatial framework and relate this to the hazard of ecosystem degradation and to the local land use practices. This study aims to focus mainly on a better understanding of the physical processes of soil degradation, with particular emphasis on the assessment of soil erosion in relation to soil type and land use practices, and an evaluation of why conventional approaches to soil erosion prediction in Mediterranean environments often fail to fully reflect the degree of soil degradation observed in the field. The main objective is to develop a method of predicting soil erodibility based on easily measurable and appropriate soil properties.

2 Materials and Methods

2.1 Study Sites and Soil Description

The study was conducted on the northern and southern slopes of Al-Jabal Alkhdar (Fig. 1) using different criteria. The Mediterranean type climate has an annual rainfall range of 400–500 mm, falling mainly in the period from October to April.

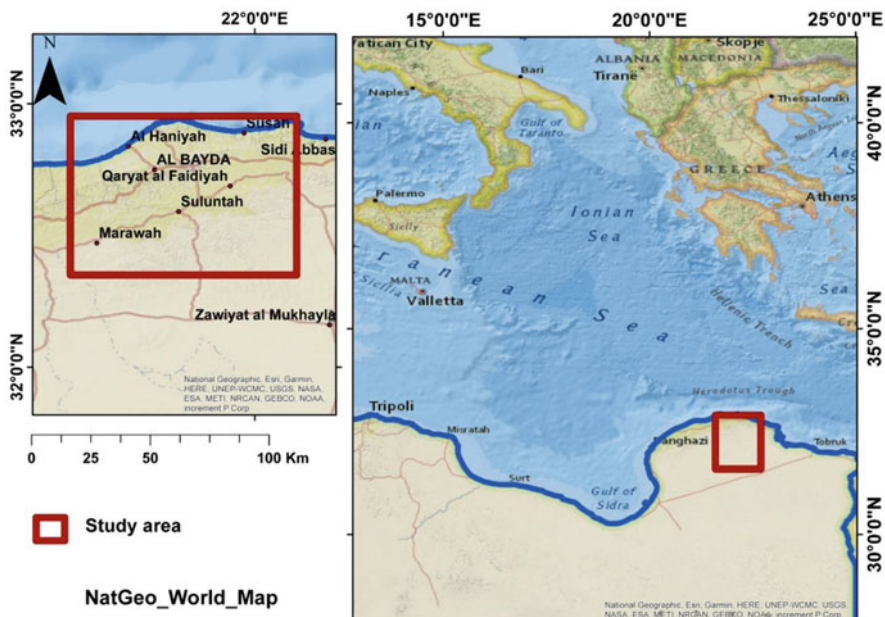


Fig. 1 Sites of study at the northern and southern slopes of Al-jabal Alkhdar

Parts of the area have been cleared of natural vegetation and are currently cultivated with rain-fed barley or are used for tomatoes and fruit production, with some fields left as fallow.

2.1.1 Field Erosion Plots Experiment, Northern Slopes

Erosion plots were established during the 1995–1997 seasons, at two locations in Al-Jabal Alkhdar; the first location, at Al-Hamama, lies on average slopes of 12%, and the second location, at Shahat, was located on average slopes of 9%. Each of the two locations was divided into three parts. The first part was covered with forest trees, the second was cultivated with barley after deforestation, and the third part was left fallow after forest removal. Three field plots (3 x 10 m each) were laid out randomly to evaluate soil loss by rain from a Mediterranean semi-arid Calcic, Typic, Lithic Rhodoxeralfs and Lithic Rendolls) soils (Fig. 2). Rain-gauge recorder was installed at each experiment location so that rain events data can be recorded.

Soil loss amounts (A) from the field plots were measured for each rain event as well as the whole season, and rainfall erosivity factor (R) values were calculated using the rain-gauge recorder data. Hence, soil erodibility factor values (K) were calculated using the basic eq. $A = R \cdot K$, where A is the annual soil loss (ton/ha), (Wischmeier et al. 1971).



Fig. 2 Soil erosion plots for soil loss measurements at the study locations; (a) Alhamama, and (b) Shahat

Table 1 The measured physical and chemical properties of the investigated soil classes (Mean \pm standard error)

Soil Property (Topsoil 0–15 cm)	Soil Class			
	Calcic Rhodoxeralfs	Typic Rhodoxeralfs	Lithic Rhodoxeralfs	Lithic Rendolls
Soil Depth, cm	65–85	60–80	25–35	20–35
Organic matter content (%)	2.40 \pm 0.199	2.92 \pm 0.273	2.17 \pm 0.203	3.19 \pm 0.234
Clay (%)	48.6 ^b \pm 2.16	58.4 ^a \pm 1.44	51.7 ^{ab} \pm 1.23	48.8 ^b \pm 1.59
Silt + Very fine sand (%)	40.1 \pm 1.27	37.4 \pm 0.96	44.2 \pm 1.01	44.8 \pm 1.73
W. stable aggs > 2 mm (%)	19.20 \pm 2.92	20.13 \pm 2.75	15.03 \pm 2.40	19.72 \pm 2.92
S. hydraulic cond. (mm hr. ⁻¹)	42 ^{ab} \pm 6.00	54 ^a \pm 7.38	36 ^{bc} \pm 5.71	30 ^c \pm 3.24
Bulk density (g cm ⁻³)	1.23 \pm 0.008	1.23 \pm 0.009	1.21 \pm 0.012	1.22 \pm 0.012
Soil reaction pH	7.92 \pm 0.068	7.77 \pm 0.058	7.82 \pm 0.037	7.95 \pm 0.039
CaCO ₃ (%)	6.38 ^a \pm 1.98	0.86 ^c \pm 0.261	0.93 ^c \pm 0.266	2.04 ^b \pm 0.541
CEC (cmol ⁺ Kg ⁻¹ soil)	–	18.22 ^a \pm 1.280	10.99 ^b \pm 0.753	–

Each value is the mean of 30 replicates. Soil subgroups classified according to the US Soil Taxonomy (Soil Survey Staff, 1999). The means were tested by Tukey multiple comparisons. Means with different letters are significantly different at the 5% level.

2.1.2 Estimation of Soil Erodibility by the Rainfall Simulation Experiment, the Northern Slopes

This study was carried out during the 2009 season on soil samples from the Al-Jabal Alkhdar region, Lussaita – Al Hamama area which lies between longitude 21° 30' to 21° 45' E and latitude 32° 45' to 33° 00' N at elevations ranging from 20 to 400 metres above sea level. The soil samples were taken from the A horizon (0–15 cm) of cultivated soils of the four soil classes under investigation, Table 1.

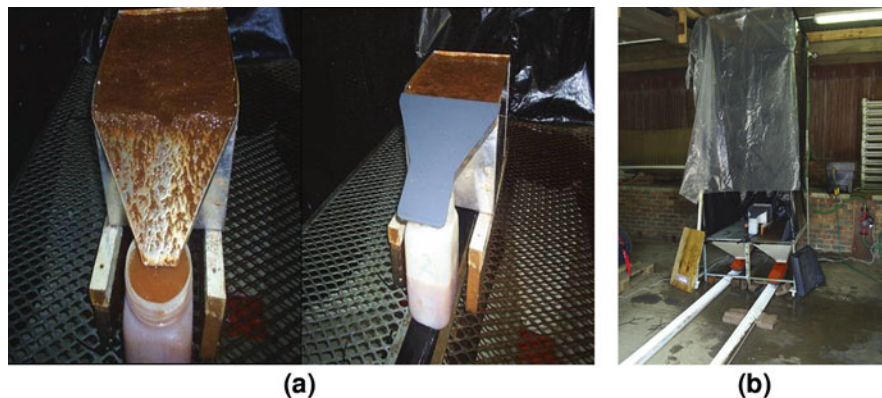


Fig. 3 Investigating soil susceptibility to erosion using the simulated rainfall test; (a) simulated runoff, and (b) rainfall simulator

These soil classes are Typical Carbonate Red Ferrisiallitic Soils (Calcic Rhodoxeralfs), Typical Leached Red Ferrisiallitic Soils (Typic Rhodoxeralfs), Leached Red Ferrisiallitic Soils with a truncated profile (Lithic Rhodoxeralfs), and Red Carbonate Rendzinas (Lithic Rendolls). Four replicates of each soil type were collected, with total of 16 samples. The samples were dried and sieved through a 5 mm sieve. The method used for this experiment is based on the work of Meyer (1958) and was also used by Aknaro (1983) and Macharia et al. (1997). The experiment used trays of soil 25x25x20 cm in size (Fig. 3); the soil layer (5 cm thick) was packed above 5 cm layer of sand, and a cloth material was placed between the two layers to separate them. A gravel layer of 5 cm was added below the sand layer to facilitate the free drainage of water from the bottom of the tray which was perforated. The soil surface had a slope of 5° towards the collection container. An easily hand rotated rainfall simulator was used with one Floodjet (3/8 K SS45) spray nozzle, as used by Blanquies et al. (2003). The nozzle was placed at 3 m height on the top of metal rig to provide a uniform rainfall on the soil tray which was located beneath the nozzle to form the most suitable spray angle. The nozzle was connected to the pump via a plastic pipe to carry the pressurized water to the nozzle at 4–7 psi (approximately 0.3–0.5 bar). The pressure was monitored using a pressure gauge and several regulators were placed across the pipe to allow full control of the flowing water. The four sides of the rig were protected by a windshield. In order to keep steady water flow, two tanks were connected to provide a total capacity of 400 litres and supplied with constant water flow from the mains water supply. A drainage system was placed beneath the rig to carry the used water away.

2.1.3 Soil Erodibility Estimation Using Dynamic Laboratory Tests, the Southern Slopes

The study was carried out during the seasons (2015–2017) to estimate soil susceptibility to water erosion and to assess erosion risk on the southern slopes of Al-Jabal Alkhdar. Five areas were selected from west to east: Meseliba (Taknes); Marawa; Sirat Alia (Gandulah), Grehat (Gandulah) and Qasar Mestashi (Salantah), as shown in Fig. 1 and Table 2. These areas are within the most degraded lands in Al-Jabal Alkhdar, where grazing and rainfed cultivation represent the basic activity for many residents. Also, the indicators of desertification in this area are clear as a result of uncontrolled human activities, soil erosion and consequently decreasing the quantity and quality of natural vegetation. The dynamic laboratory tests included experiments that simulate the detachment of soil aggregates, the tests are listed below:

- Water aggregate stability index: in this experiment, the wet sieving method was applied on surface soil samples. The method was reported by Morgan (1996) within soil erodibility indicators, and was used in the soil laboratory of Cranfield University in the United Kingdom on soil samples from Africa by Ekwue (1984), which was based on the work of Adams et al. (1958).
- Instability index: the index = $\% \text{ silt} + \text{clay} / (\% \text{ aggregates} > 0.2 \text{ mm after wet sieving}) - 0.9 (\% \text{ coarse sand})$. The index was reported in Combeau and Monnier (1961), and listed in Morgan (1996) as an indicator of soil erodibility.
- Detachability index: the index can be measured by dividing the residual weight on the sieve in experiment (a) on the shaking duration to obtain the rate of detachment in grams per minute. Higher residual weight in and lower detachment rate could indicate greater structure stability and resistance to erosion. The test was applied by Russell and Feng (1947), and pointed out by Kemper and others (1985).

Table 2 Some general characteristics of the southern slopes

Site	Geographic Coordinate		Slope degree °	Height (m)	Surface stoniness (%)	V. cover (%)	Soil depth (cm)	Land use type
	East	North						
Meseliba	32° 28.75	21° 19.36	4.5 south	460	10–15	< 15%	21.5	Grazing
Marawa	32° 28.57	21° 25.34	7.0 south	481	15–20%	< 20%	15.0	Rain-fed Agri grazing
Sirat alia	32° 28.81	21° 30.76	8.5 south	607	20–40%	20–30%	16.6	Grazing
Grehat	32° 28.35	21° 32.66	7.5 south	614	25–30%	20–25%	16.4	Rain-fed Agri grazing
Q. Mestashi	32° 29.12	21° 44.90	3.5 south	672	30–40%	15–20%	12.4	Grazing

2.2 *Erosion Risk Assessment of the Southern Slopes Using GIS*

Various types of data and satellite imagery were used for the present study; the method involved integration of different thematic layers such as soil map and DEM in GIS environment (ArcGIS10.3.1 software). The produced erosion risk maps were prepared to illustrate and classify potential soil erosion on the southern slopes of Al-Jabal Alkhdar using the following criterion:

1. Soils with good content of clay, organic matter and iron oxides and with medium and deep depth (such as Alfisols) are highly aggregated soils. In this case the risk of erosion under similar climate will depend on the degree and length of the slope, and often the risk of erosion ranges between slight to medium.
2. Soils with good content of clay and medium organic matter content, such as the shallow calcareous Mollisols, are also aggregated soils, but these soils are shallow with undeveloped profiles due to its formation on slopes. The shallow Mollisols are less resistant to erosion compared to the deep Alfisols, and the risk of erosion ranges between slight to severe according to the slope characteristics.
3. Soils with fragile, shallow and weak soil structure due to the low content of organic matter, such as the soils of arid lands Aridisols, will have erosion risk ranges between medium and severe according to the slope characteristics.

Note: the erosion hazards classification excludes climate and land use factors since all sites in this study are within the same climate and land use conditions.

3 Results and Discussion

3.1 *Erosion Plots Experiment, Northern Slopes of Al-Jabal Alkhdar*

The results showed that the largest soil and water losses occurred on the bare plots in both sites (Al-Hamama and Shahat) during the seasons 1995/1996 and 1996/1997. In Al-Hamama site, for example (Table 3), soil losses amounted to 1.62 and 4.14 tons/ha, organic matter 51.7 and 139.8 kg/ha, total nitrogen 3.7 and 10.1 kg/ha and available phosphorus as little as 3 and 4 g/ha in the first and second seasons, respectively. In comparison, the losses from the barley cultivated plots were less, with soil losses of 0.219 and 0.046 tons/ha, and organic matter losses of 0.7 and 1.4 kg/ha in the first and second seasons, respectively. Only traces of total nitrogen and available phosphorus were lost from Al-Hamama barely cultivated soil in both seasons. On the other hand, practically no losses occurred in the forest-covered plots, characterized by significantly higher organic matter, infiltration rates and aggregate stability. Losses from Shahat site were much lower than those from Al-Hamama site

Table 3 The annual losses of soil components and plant nutrients during the tow seasons of study at Al-Hamama site

Type of plot	The first season			The second season		
	A	B	C	A	B	C
Water runoff m ³ /ha	94.18	69.47	14.20	171.08	54.12	11.15
Total soil loss kg/ha	1620.00	219.00	12.00	4140.00	46.00	4.00
Clay loss kg/ha	792.16	113.40	0.00	1938.46	23.40	0.00
Silt loss kg/ha	611.48	83.70	0.00	1723.23	17.60	0.00
O. M. loss kg/ha	51.68	7.00	0.00	139.83	1.40	0.00
Nitrogen kg/ha	3.73	Traces	0.00	10.06	Traces	0.00
Phosphours kg/ha	Traces	Traces	0.00	Traces	Traces	0.00

A bare plots, B barley plots, C natural vegetation plots.

Table 4 Measured and estimated soil erodibility factor (K) values

Site	K _{measured}	K _{estimated}
Al-Hamama	0.02	0.18
Shahat	0.01	0.12

in both seasons, which were due to significantly higher soil depth and infiltration rates.

3.2 Soil Erodibility Assessment

Table 4 shows values of soil erodibility factor K which were measured directly using the field erosion plots data and applying the basic eq. ($A = R.K$), where A is the annual soils losses ton/ha and R is the rainfall erosivity factor calculated using the rain-gauge rainfall data. The Measured K values were compared to the estimated K values which were assessed using the nomograph suggested by Wischmeier et al. (1971) which is based on a statistical relation between specific soil properties. It appears clearly that the nomograph overestimates values of the soil erodibility factor, and the reason may be that it was not originally designed for conditions similar to the current study area. The question therefore arises whether soil erodibility can be predicted by using formulae based on selected soil properties that affect soil structure, particularly, organic matter, clay content, carbonate content and Fe and Al oxides (Diaz-Fierros and Benito 1996). According to Abu Hammad (2005) the factor is dynamic and affected significantly by dynamic soil properties that were in turn influenced by environmental factors. This conclusion can explain why erodibility overestimation was repeatedly reported when K-USLE index was applied in the Mediterranean.

The results shown in Table 5 could confirm the contribution of certain soil properties to soil resistance to erosion (or soil susceptibility to water erosion). Organic matter, soil particle size distribution, aggregate stability and infiltration rate were all correlated to soil resistance. Soil susceptibility to erosion (soil

Table 5 The correlation (r) between measured soil erodibility factor (K) values with some physical soil properties

The property	r value	t value
Infiltration rate cm\min	- 0.90	4.18 ^a
Instability index gm\min	0.90	4.23 ^a
Clay %	-0.92	4.69 ^a
Silt %	0.88	3.87 ^a

^a; significantly different at $p < 0.05$

erodibility) varied between soils according to these properties, and this can to some extent explain the significant differences in soil losses between the plots within the same site or between the sites. High clay content, moderate organic matter content, low content of silt, and very fine sand all contributed to a stable soil structure. The moderate aggregate stability of Typic and Calcic Rhodoxeralfs significantly improved their resistance to rain drop impact. These characteristics were reflected in moderate and stable infiltration rate, which is predicted to result in less water runoff and soil loss. On the other hand, relatively lower content of organic matter and higher content of silt and very fine sand have resulted lower aggregate stability and saturated hydraulic conductivity among the Lithic Rhodoxeralfs. Greater runoff and soil loss is expected on these soils, as they are more erodible and less resistant to the processes of erosion.

3.3 The Simulated Rainfall Test

As a dynamic property, soil erodibility values may vary with different rainfall characteristics. Table 6 shows soil losses from the four soil types under investigation under several levels of rainfall intensity and duration. Low values of soil loss were generally recorded in the experiment. This is consistent with the field observations and the previous field plot experiment data, all of which showed a low to moderate level of soil erosion. The Rendolls were unable to maintain their stability under simulated rainfall conditions, resulting in a significant decrease in hydraulic conductivity and increase in runoff and soil loss. These results for Lithic Rendolls agree with findings by other researchers that, due to the changeability in some erodibility-related properties such as wetting, sealing and crusting, the resistance of the soil surface to interrill erosion can vary during rainfall events (Kuhn and Bryan 2004).

The results showed soil erodibility values varied from 0.00 to 0.195 (t.MJ⁻¹) for soil losses in the range 0.00–4.04 t.ha⁻¹. The findings indicate that soil classes were differentiated relatively by the soil erodibility factor (Table 7, Fig. 4). Although all erodibility values fall within the low to low-moderate ranges, the statistical analysis indicates that soils have different levels of susceptibility. Calcic Rhodoxeralfs and Typic Rhodoxeralfs have the lowest soil erodibility while Lithic Rhodoxeralfs and Lithic Rendolls have higher erodibility. The relative erodibility of the four soils follows this order: Lithic Rendolls and Lithic Rhodoxeralfs greater than Calcic Rhodoxeralfs and Typic Rhodoxeralfs.

Table 6 Mean and standard deviation of measured soil loss values ($\text{kg}\cdot\text{m}^{-2}\cdot\text{hr}^{-1}$) for the rainfall simulation test on four soil types under different rainfall intensity and duration

Simulated rainfall intensity Rainfall duration † (min)	35 mm.hr. ⁻¹			50 mm.hr. ⁻¹			75 mm.hr. ⁻¹			Mean soil loss for each soil type
	20	30	50	20	30	50	20	30	50	
Calcic Rhodoxeralfs	0.001	0.005	0.002	0.009	0.048	0.043	0.039	0.109	0.156	0.046 ^b
Typic Rhodoxeralfs	0.001	0.001	0.001	0.008	0.029	0.034	0.035	0.060	0.148	0.035 ^b
Lithic Rhodoxeralfs	0.001	0.002	0.003	0.019	0.077	0.094	0.126	0.217	0.264	0.089 ^a
Lithic Rendolls	0.001	0.002	0.004	0.013	0.096	0.129	0.135	0.265	0.342	0.109 ^a
Mean soil loss ^a for each intensity	0.002 ^C			0.049 ^B			0.158 ^A			
Property										Significance
Soil class										
Rainfall duration (min ⁻¹)										***
Rainfall intensity (mm.hr. ⁻¹)										***
Soil class*Duration										Ns
Soil class*Intensity										***
Duration*Intensity										***
Soil class*Duration*Intensity										Ns

***; significantly different at $p < 0.001$, ns; not significantly different at $p < 0.05$

The means were tested by Tukey multiple comparisons. Means with the same letters and font are not significantly different. 0.001 represents any value of 0.001 kg or less.

Note: the data were transformed to SQR (square root) before being statistically analyzed

^aSL Soil loss, †: 20 min = dry run, 30 min = wet run 1, 50 min = wet run 2

Table 7 Mean values of the measured soil erodibility factor of the four soil classes

Soil Class	Erodibility Value (ton.MJ ⁻¹)†
Calcic Rhodoxeralf	0.031
Typic Rhodoxeralf	0.023
Lithic Rhodoxeralf	0.060
Lithic Rendoll	0.074

†The values of erodibility are the average of all durations and intensities excluding the intensity of 35 (mm.hr.⁻¹).

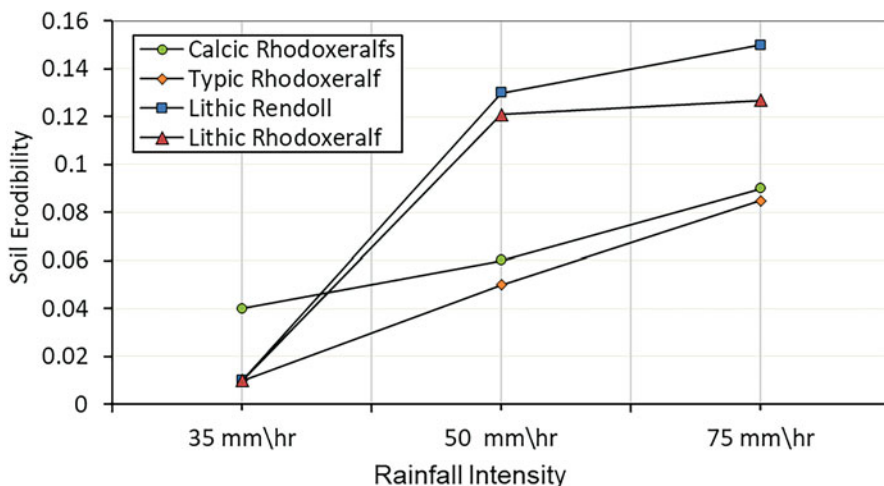


Fig. 4 The trend of erodibility of different soil types with the increase of rainfall intensity for 50 minutes rainfall duration

The lower soil loss and erodibility values associated with Typic Rhodoxeralfs and Calcic Rhodoxeralfs reflect the effect of higher hydraulic conductivity on these soils compared to Lithic Rendolls and Lithic Rhodoxeralfs soils. Furthermore, the moderate aggregate stability of these soils significantly improves their resistance to rain drop impact. This may also reflect the associated effects of higher clay content with moderate organic matter content and low content of silt + very fine sand (Table 1). Similar results were reported for Spain (Sanroque et al. 1990) and Ethiopia (Fufa et al. 2002; Adekalu et al. 2006) showing that structural stability and organic matter content are the properties most related to erodibility. Fine texture and strong, medium to coarse, angular and sub-angular blocky or prismatic structure were the factors behind the low erodibility of Red Mediterranean soils in Greece (Yassoglou et al. 1997).

In Spain, Diaz-Fierros and Benito (1996) stated that calcareous soils and Cambisols associated with Rendzinas have moderate to good stability and that organic matter was the main agent stabilizing soil structure. But in the present study this was not the case, as the field observations and the rainfall simulation tests showed them to be more easily eroded relative to Typic and Calcic

Rhodoxeralfs, which have similar levels of clay, organic matter and aggregate stability. The relationship between aggregate breakdown under raindrop impact and clay type, crusting, seal formation and decreasing infiltration may help to explain the change in erodibility and soil loss in Lithic Rendolls during rainfall events. Selkhoz Prom Export (1980) reported a relatively higher content of swelling clays in Lithic Rendolls than in Rhodoxeralfs. In Al-Jabal al Akhdar region of Libya, Rhodoxeralfs are rich in kaolinite and very poor in their content of smectite (Bin Mahmoud 1995). It seems that it is difficult to predict the behaviour of soils rich in swelling clays in relation to erodibility. The effects of drying and wetting can lead these minerals to greater swelling and shrinkage. Consequently, these soils cannot maintain their pore spaces during wetting and swelling resulting in progressively slower infiltration capacity (Morgan 1996).

In spite of the fact that soil erodibility is a dynamic property affected by rainfall characteristics, it can be suggested that relative soil erodibility will be affected mainly by the inherent soil properties. This hypothesis is confirmed by the fact that the order of average erodibility values of all soil types was the same in this experiment and maintained the same trend under different intensities of simulated rainfall (Fig. 4). Assouline and Ben-Hur (2006) reported that with gentle slopes; interrill soil erodibility values were constant and independent of the effect of rainfall intensity soon after the beginning of runoff. In the same way, Kinnell (2000) suggested that soil erodibility will be constant as soon as steady state occurs and sediment concentration stabilizes.

Table 8 shows the correlation coefficient between soil erodibility and various soil properties. The erodibility was significantly correlated with only two parameters, water stable aggregates (WSA% >2 mm) and saturated hydraulic conductivity (K_s $\text{cm}\cdot\text{min}^{-1}$), and both were negatively correlated. Although neither organic matter nor soil particle size (clay, silt + very fine sand) showed any significant correlation, the results suggest a combined positive effect of organic matter and clay content on the stability of soil structure, in addition to maintaining moderate hydraulic conductivity within the soil layers. Assouline and Ben-Hur (2006) found that erodibility values can vary due to surface sealing which causes noticeable changes in upper soil structure and permeability.

Table 8 The correlation coefficient (r) of measured soil erodibility with various soil parameters

Soil Property	Correlation coefficient (r)
Organic matter, %	-0.092
Water stable aggregate >2 mm (WSA),%	-0.555 ^a
Silt + Very fine sand, %	0.118
Clay, %	-0.267
Saturated hydraulic conductivity (K_s), $\text{cm}\cdot\text{min}^{-1}$	-0.548 ^a
CaCO_3 , %	0.070
pH	-0.024
Bulk density, $\text{g}\cdot\text{cm}^{-3}$	0.249

^a Significant at 0.01 level

Table 9 Regression equation of the relations between measured erodibility (K) and measured soil properties

Regression equation	R ²	Significance	SE
$K_3 = 0.117 - 0.00206 \text{ WSA} - 0.362 \text{ Ks}$	0.74	***	0.02

Table 10 Correlation matrix between soil erodibility indicators and some field parameters

	Final Inf. rate	Resist. to penetration	Soil depth	Bulk density
<i>The used indicators</i>	mm min ⁻¹	N m ⁻²	cm	g cm ⁻³
Aggregate St > 2 mm index	0.76**	-0.17	0.34	-0.68**
Aggregate St > 1 mm index	0.81**	-0.07	0.25	-0.73**
Aggregate St > 0.5 mm index	0.79**	0.01	0.17	-0.73**
Aggregate St t > 0.2 mm index	0.77**	0.05	0.13	-0.73**
The instability index	-0.65**	0.12	-0.23	0.60**
Detachability index 2 mm	-0.64**	-0.01	-0.19	0.69**
Detachability index 1 mm	-0.74**	0.12	-0.09	0.76**
Detachability index 0.5 mm	-0.70**	-0.21	0.01	0.75**

AgSt aggregates stability index, *Inf. R* final infiltration rate.

A regression analysis (Table 9) was used to find out the most relevant properties to soil erodibility assessment, using the most correlated soil properties to erodibility (Table 8). The regression analysis shows a significant relationship between a combination of water aggregate stability index (WSA% >2 mm) and saturated hydraulic conductivity (Ks cm.min⁻¹) with soil erodibility. Similarly, Le Bissonnais (1996) suggested that water stable aggregates can efficiently estimate soil erodibility if an improved method is used. Ben-Hur and Agassi (1997) found a significant correlation between final infiltration rate (FIR) and interrill erodibility (Ki), which suggests that the soil properties can be a useful estimate of erodibility.

3.4 The Dynamic Laboratory Tests of Water Aggregates Stability (Wet Sieving)

Statistical comparison was made using the correlation analysis to test the association between the dynamic soil erodibility indicators under investigation with some field parameters such as soil depth, soil resistance to penetration, final filtration rate and bulk density (Table 10). The dynamic laboratory indicators were significantly correlated with the field parameters of the southern slopes of Al-Jabal Alkhdar. The success of the dynamic indicators in the expression of erosion-related land degradation was reported in the literature, which considered that wet sieving-soil stability indices were capable of predicting soil erodibility and degradation due to their direct relationship to climate, soil properties, parent materials, vegetation and

Table 11 The multiple regression equations of the soil erodibility indicators and field parameters

The used indicators	The Regression Equation	R ²	P	SE
AgSt>2 mm index (A)	A = 60.5 + 45.3 IR - 38.7 B D + 0.562 SD	67.9	**	5.67
AgSt>1 mm index (B)	B = 70.3 + 68.8 IR - 40.7 BD + 0.280 SD	71.1	**	6.17
AgSt>0.5 mm index (C)	C = 81.4 + 68.1 IR - 44.0 BD + 0.039 SD	67.4	**	6.81
AgSt>0.2 mm index (D)	D = 88.4 + 69.1 IR - 45.5 BD - 0.081 SD	66.5	**	7.05
The instability index (E)	E = - 0.96 + 2.98 BD - 2.53 IR - 0.0296 SD	47.4	*	0.58
Detachability ind. 2 mm (F)	F = 0.784 + 0.904 BD - 0.401 IR - 0.00515 S D	66.4	**	0.09
Detachability ind.1 mm (G)	G = 0.375 + 1.06 BD - 0.808 IR + 0.000262 comp	73.3	**	0.11
Detachability ind. 0.5 mm (H)	H = 0.412 + 1.06 B D - 0.851 IR - 0.0003 comp	68.3	**	0.13

land use. Moreover, due to the proximity of simulations to the natural conditions of the field, these indices could play a very helpful tool for erosion risk assessment (Cerdeira 2000; Barthes et al. 2000; Rosse 2002). In particular, the dynamic stability indicators will be useful, low-cost and easy-to-apply tools to describe the risk of erosion when comparing different types of soils or land uses.

The multiple regression tests were applied to select the dynamic stability indicators that are most related to the field state. In Table 11 some of the field parameters were employed in set of regression equations to relate them to the dynamic indicators, and to test the indicators validity to estimate erodibility of the study area soils, and to determine that soil erodibility is a measurable and useful index for estimating actual soil erosion.

Table 11 showed that the following dynamic stability indicators, AgSt>1 mm index and Detachability index 1 mm, have the highest (R²) values when using the most relevant field parameters set together in the multiple regression equation. Therefore, the findings indicate a relative capability for the predictive formulae to broadly indicate erodibility in the field in the southern slopes of Al-Jabal Alkhdar. However, reflecting the reality of erosion-related soil degradation in the field is still questionable and needs further investigation. Le Bissonnais (1996) suggested that water stable aggregates can efficiently estimate soil erodibility if an improved method is used. Aggregates stability in the present study was measured using wet sieving, which may not have the same effect of rain drops on soil aggregates. Rejman et al. (1994) suggested that considerable improvement can be made in soil erodibility measurement if the indicator is measured by using a rainfall simulator rather than wet sieving. However, due to the large areas under investigation and the lack of resources, the wet sieving method was the most appropriate means to achieve some of the objectives of this study such as mapping soil erosion (erosion risk assessment).

3.5 Erosion Risk Assessment

The areas that need appropriate management to limit the phenomenon of erosion-related soil degradation and land desertification can be recognised from the potential erosion risk maps produced in this study (Figs. 5, 6, 7, 8 and 9). The maps classified the lands according to the severity of erosion and indicated the slopes that require extra measures to conserve soil and resist water and wind erosion on the slopes. The required measures would control surface runoff using appropriate barriers that help soil preservation, water harvesting and moisture retention. Consequently, plant environment, such as soil characteristics, fertility and productivity, and its diversity would be improved. Figure 10 shows the role of some soil conservation measures in improving the natural environment on the southern slopes of Al-Jabal Alkhdar.

From the erosion risk maps we notice that the areas with the highest erosion risks are found mainly within the shallow arid soils (Aridisols soil type in particular), however, Mollisols soil type (shallow Rendezina) were also vulnerable to noticeable degradation. But in both cases, it is often (the soil factor) linked to the steeper lands (slope factor) that were nearby active water ways that had the highest risk of erosion (Figs. 5, 6, 7, 8 and 9). As previously emphasized, this behaviour is expected within Aridisols soils because of their weak cohesion and resistance to erosion factors. As for the Rendezina soils, their shallow depth will always be a major weakness in their ability to resist erosion factors despite their relative cohesion and stability. However, as is the case in this example, most of the lands, especially the red

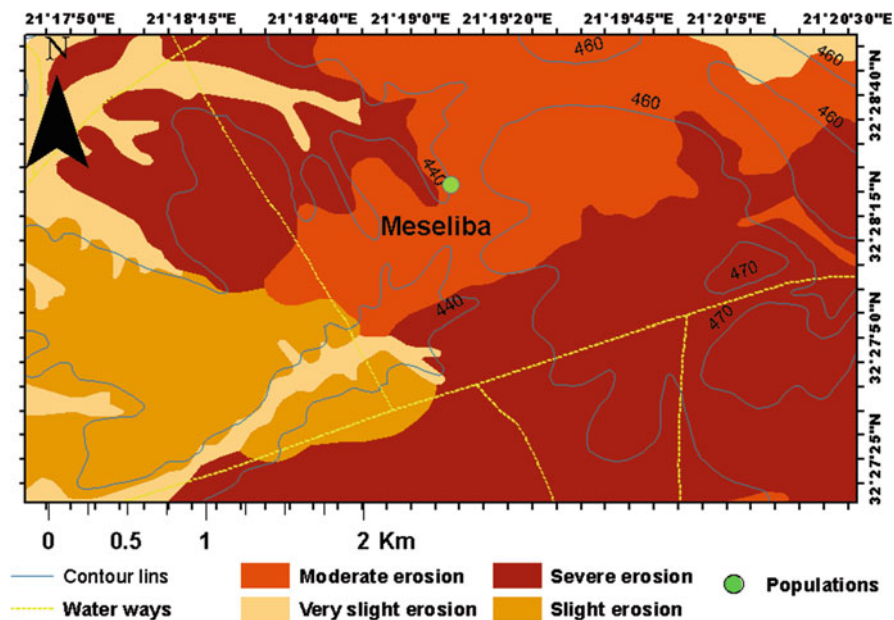


Fig. 5 Potential erosion risk classes, Meseliba area

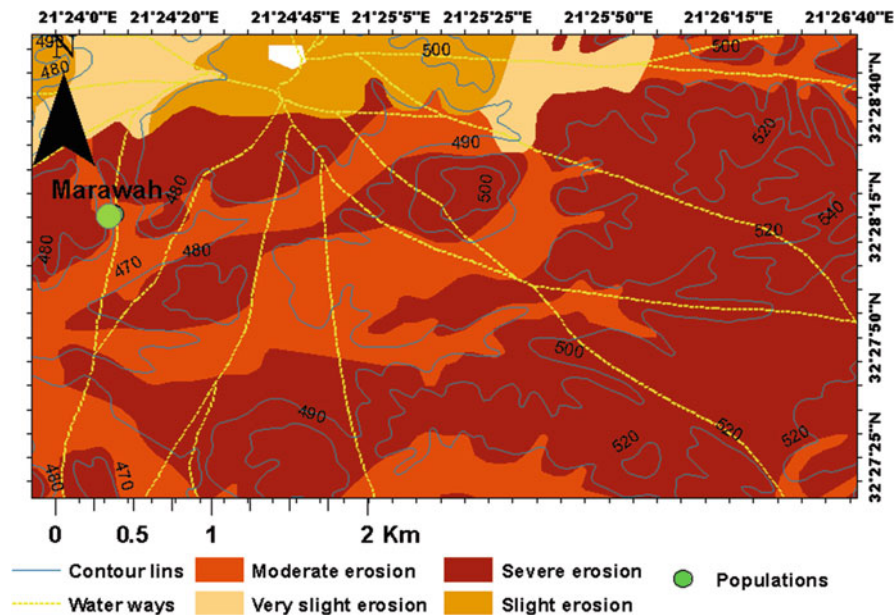


Fig. 6 Potential erosion risk classes, Marawa area

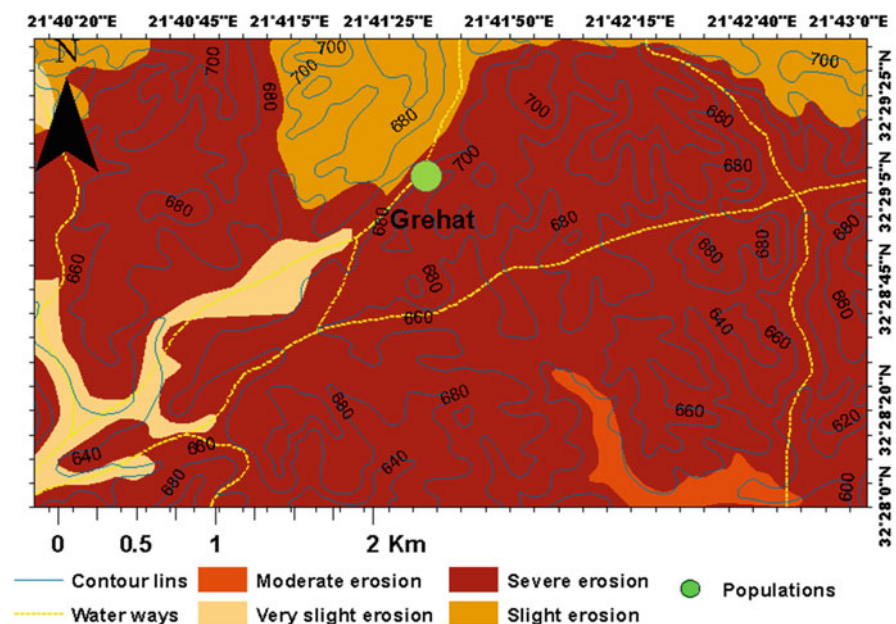


Fig. 7 Potential erosion risk classes, Grehat area

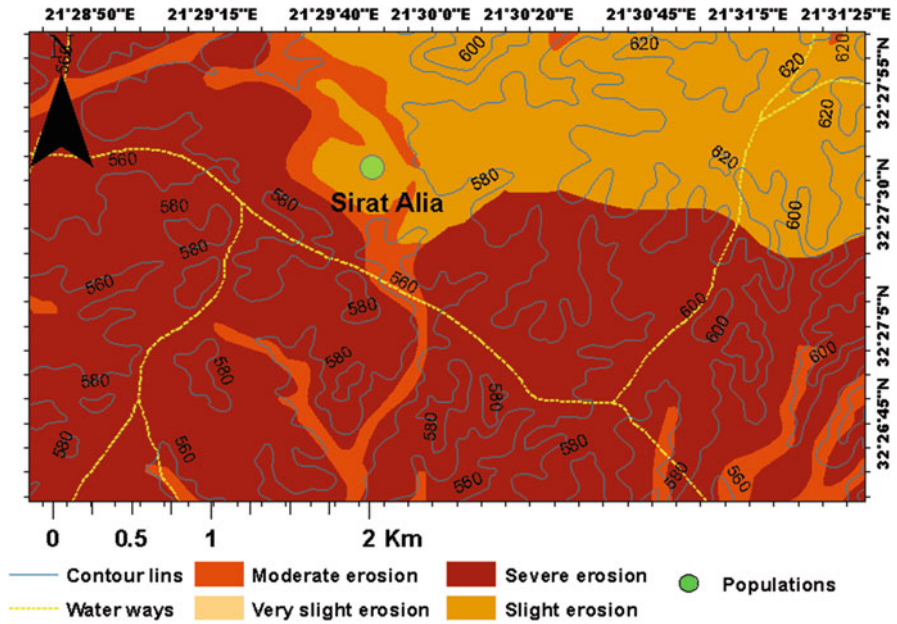


Fig. 8 Potential erosion risk classes, Sirt Alia area

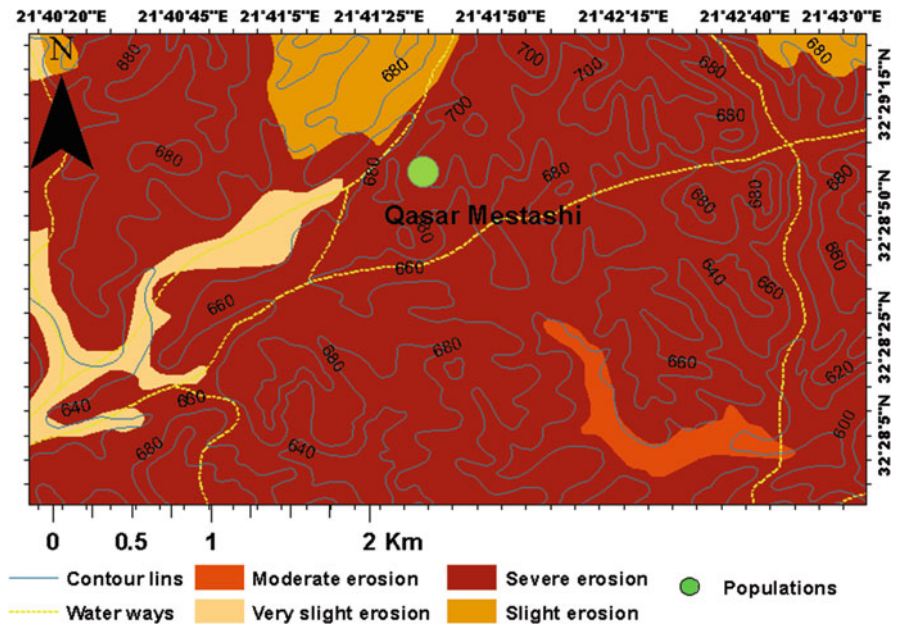


Fig. 9 Potential erosion risk classes, Mestashi area



Fig. 10 Effectiveness of soil conservation measures on the semi-arid southern slopes in improving soil quality and productivity in Marawa area; (a) tide-ridges, and (b) semi-circular bunds

Mediterranean soils, Alfisols, and a large proportion of Mollisols (Rendezina soils), fall within the degrees of erosion risk that can be controlled by applying some known agricultural and engineering soil conservation procedures. In this low-scale study, the assessment of soil erosion risk using GIS technology focused on the most accessible sites, however, the assessment can be expanded in future to most affected areas. The produced maps of potential erosion hazards will definitely help in highlighting the fragile areas that should maintain the natural plant vegetation, the areas that allowed for restricted and limited agricultural uses, and the areas that are flexible for a wide range of crops.

4 Conclusions

The validation of estimated K-USLE erodibility values against field observations and field plot data in the present research showed that the estimating formula overestimated soil erodibility under semi-arid Mediterranean Libyan conditions. In the present study, simulated rainfall tests found that aggregate stability and saturated hydraulic conductivity together explained most variations in measured soil erodibility of the soil types under investigation. Although soil properties play the main role in soil resistance to erosion, the rainfall simulation test showed that rainfall characteristics, intensity and duration, can contribute to the changeability of erodibility. It is very important to determine the dynamism of the erodibility factor in relation to the climate effect, which can greatly affect the accuracy of erodibility prediction. The dynamic nature of erodibility can also explain the unexpected lower resistance of Lithic Rendolls soils and it is concluded that change over time in these soils is probably due to the physical effects of swelling clays. The finding of this study suggest that the test for water stable aggregates (WSA) is a fairly reliable predictor of soil erodibility and relate to the fact that it is a parameter that combines the effects of

several soil particle binding agents. It achieves this by directly measuring the cohesive forces that determine soil stability against water erosion by simulating the destructive action of rainfall and water action through wet sieving. One of the most important aspects of this research was estimating soil erodibility on a spatial basis by using GIS technology with information on soil properties and distribution patterns derived from existing national soil survey maps and reports, and from the soil classification systems employed to describe soil map units. Mapping soil erodibility and erosion risks based on soil survey data can undoubtedly be a useful tool in soil conservation-related policies and land use planning in Libya. The present study has highlighted the importance of WSA% and Ks as parameters for estimating soil erodibility, however, considering their often limited availability, further investigation to find other more easily measured, or readily available, parameters should be encouraged, so that a wider-scale spatial prediction of soil erodibility can be achieved in Mediterranean soil environments.

Author Contributions **Murad M. Aburas:** conceptualization, methodology, supervision, software, data curation, formal analysis, validation, investigation, writing—original draft, visualization, writing—review and editing. **Asama S. Alferjani:** data curation, formal analysis. **Mohammed S. Yousef:** software, data curation, formal analysis, visualization. All authors have read and agreed to the published version of the manuscript.

References

- Abu Hammad AH, Lundervam H, Berresen T (2005) Adaptation of RUSLE in the Eastern part of the Mediterranean Region. *Environ Manag* 34(6):829–841
- Adams JE, Kirkham D, Scholtes WH (1958) Soil erodibility and other physical properties of some Iowa soils. *Iowa State Coll J Sci* 32(4):485–540
- Adekalu KO, Okunade DA, Osunbitan JA (2006) Compaction and mulching effects on soil loss and runoff from two southwestern Nigeria agricultural soils. *Geoderma* 137(1–2):226–230
- Akanro JO (1983) An experimental investigation to test the validity of Wischmeier's erodibility nomograph. M.Sc Thesis. Cranfield Institute of Technology, Silso College, UK
- Assouline S, Ben-Hur M (2006) Effects of rainfall intensity and slope gradient on the dynamics of interrill erosion during soil surface sealing. *Catena* 66(3):211–220
- Barthes B, Azontonde A, Boli BZ, Part C, Roose E (2000) Field-scale run-off and erosion in relation to topsoil aggregate stability in three tropical regions (Benin, Cameroon, Mexico). *Eur J Soil Sci* 51:485–496
- Ben-Hur M (2007) Soil mineralogy effects on runoff/rainfall ratio, soil erodibility and surface movement of pollutants. *Geophys Res Abstr* 9
- Ben-Hur M, Aggasi M (1997) Predicting interrill erodibility factor from measured infiltration rate. *Water Resour Res* 33(10):2409–2415
- Bin-Mahmoud KM (1995) The Libyan soils the National Council of scientific research, Tripoli, Libya
- Blanquies J, Scharff M, Hallock B (2003) The design and construction of a rainfall simulator. International erosion control association, 34th annual conference and expo. Las Vegas, Nevada, USA, February 24–28, 2003
- Cerda A (2000) Aggregate stability against water forces under different climates on agriculture land and scrubland in southern Bolivia. *Soil Tillage Res* 57(3):159–166

- Diaz-Fierros F, Benito E (1996) Rainwash erodibility of Spanish soils. In: Rubio JLC (ed) Soil degradation and desertification in Mediterranean environments. Logrono, Geofoma Ediciones, pp 91–105
- Ekwe E (1984) Experimental investigation on the effect of preparation of soil samples on measured values of soil erodibility. M.Sc Thesis. Cranfield Institute of Technology, Silsoe College, UK
- FAO (1969) Report to the government of Libya on development on tribal lands settlement project. FAO, Rome (SF 20)
- Fufa SD, Strauss P, Schneider W (2002) Comparison of erodibility of some Hararghe soils using rainfall simulation. *Commun Soil Sci Plant Anal* 33(3–4):333–348
- Gebril MA (1995) Water erosion on the northern of Al-Jabal Alkhdar of Libya. PhD thesis. Durham University. UK
- GEFLI (1975) Study of soil and water conservation in Jabal Lakhdar, Libya. Final report
- Kemper WD, Trout TJ, Brown MJ, Rosenau RC (1985) Furrow erosion and water and soil amangement. *Trans. ASAE* 28(5):1564–1572
- Kinnell PIA (2000) The effect of slope length on sediment concentrations associated with side-slope erosion. *Soil Sci Soc Am J* 64(3):1004–1008
- Kuhn NJ, Bryan RB (2004) Drying, soil surface condition and interrill erosion on two Ontario soils. *Catena* 57(2):113–133
- Le Bissonnais Y (1996) Aggregate stability and assessment of soil crustability and erodibility: I. Theory and methodology. *Eur J Soil Sci* 47(4):425–437
- Macharia DW, Moll W, Kamau PA (1997) Relation of some chemical properties to soil erodibility of some South Western Kenyan soils. *Afr Crop Sci J* 5(2):185–196
- Meyer LDM (1958) Rainfall simulator for runoff plots. *Agric Eng* 39(10):644–648
- Morgan RPC (1996) Soil erosion & conservation. Addison Wesley Longman Limited, London
- OMU (2005) Study and evaluation of the natural plant cover in Aljabal Alkhdar Region, Libya, final report (in Arabic). Omar Al-Mukhtar University, Elbieda
- Rejman J, Pawlowski M, Debicki R, Link M (1994) Stability of aggregates and erodibility of loss soil. *Polish J Soil Sci* 27(2):87–92
- Roose E (2002) Evaluating Monitoring and Forecasting Erosion. 12 th ISCO Conference. Beijing, China
- Russell MB, Feng CL (1947) Characterization of the stability of soil aggregates. *Soil Sci* 63(4): 299–304
- Sanroque P, Rubio JL, Lzqvierdo L (1990) Relationship among erodibility parent material and soil type in areas of the Valencia province (Spain). *Soil Technol* 3:373–384
- Selkhoz Prom E (1980) Soil studies in the eastern zone of Libya. Secretariat of Agriculture, Libya
- Wischmeier WH, Johnson CB, Cross BV (1971) A soil erodibility nomograph for farmland and construction sites. *J Soil Water Conserv* 26:189–193
- Yassoglou N, Kosmas C, Moustakas N (1997) The red soils, their origin, properties, use and management in Greece. *Catena* 28:261–278


Dr. Murad Milad Aburas is a professor of soil science at the Department of Soil and Water, Faculty of Agriculture, Omar Al-Mukhtar University, Elbeida, Libya. PhD degree in Agricultural and Environmental Science 2009 (soil and water conservation). Faculty of Agriculture, Science and Engineering, University of Newcastle upon Tyne, UK. The main interest is the field of soil conservation and management, with research interests such as: Erosion risk assessment, soil degradation investigation, application of soil conservation measures, sustainable land use and management. He has been teaching courses and has supervised the graduation of master's and bachelor's degree students since 2009.

Eng. Asama S. Alferjani is a soil expert at the Ministry of Justice in Libya. He completed his M. Sc. (Agricultural Sciences) in 2019, with the main research interest in soil erosion and degradation.

Eng. Mohammed S. Yousef is a teacher in the Ministry of Education in Libya, he is in the last stage of his Ph.D. research at Alexandria University, Egypt. He completed his M.Sc. (Agricultural Sciences) in 2016, with the main research interest in soil conservation measures.

DRAINMOD Applications to Design Drainage Systems in Libya Using Soil Salinity Data Predicted by GIS, Remote Sensing and Artificial Neural Networks



Murad Ellafi, Hamdi A. Zurqani , Lynda K. Deeks, and Robert W. Simmons

Abstract Soil salinity in irrigated agricultural regions is a growing problem. Saline soil conditions have reduced the value and productivity of considerable areas of land all over the globe. Direct methods of measuring soil salinity are time-consuming and expensive. Monitoring soil salinity can help to evaluate the effectiveness of having a drainage system installed. Therefore, research effort has been dedicated to developing indirect methods for predicting soil salinity. This study aims to (1) develop Artificial Neural Networks (ANNs) to predict the electrical conductivity of the saturated paste extract (EC_e), (2) evaluate the performance of a drainage system based on measured and predicted EC_e, and (3) develop soil salinity prediction maps to monitor the initial and simulated salinity under drained and undrained conditions. The Eshkeda Agricultural Project (EAP) and the Hammam Agricultural Project (HAP) are the focus of this research. Yearly satellite datasets for 1984, 1990, 2000, and 2010 were generated using the Landsat 5 Surface Reflectance bands median values for each measurement location in HAP and EAP. Two ANNs we developed to predict EC_e in 1990, 2000, and 2010. The input parameters for ANN1 were based on satellite image reflectance, while ANN2 used both reflectance and salinity indices. DRAINMOD was applied to simulate drained and undrained conditions in EAP and HAP. ANN2 was 45% more accurate than ANN1 according to the RMSE. The results also showed that a drainage system can reduce EC_e while increasing relative yield. Installing and maintaining an adequate drainage system can help increase crop yield and reduce salinity stress in saline agricultural regions. ANNs can be used as a tool to evaluate an existing drainage system and specify an area in need of improvement. This supports the frequently stated proposition that

M. Ellafi · L. K. Deeks · R. W. Simmons
Cranfield Soil and Agrifood Institute, Building 52a, Cranfield University, Bedfordshire,
MK, UK

H. A. Zurqani (✉)
University of Arkansas Agricultural Experiment Station, Arkansas Forest Resources Center,
College of Forestry, Agriculture and Natural Resources, University of Arkansas, Monticello,
AR, USA
e-mail: Zurqani@uamont.edu; Hzurqani@uark.edu

drainage, irrigation, and salinity control for arid lands should be considered as components of a water management system and the design of each component should be dependent on the design of the other components.

Keywords Arid regions · Saline soils · Irrigated agriculture · Agricultural drainage design · Spectral indices · K-fold cross-validation · Google Earth Engine.

1 Introduction

Since the 1950s, the water demand in Libya has exceeded the capacity of its water resources to support food production (Qadir et al. 2003). North Africa is considered to be one of the driest regions in the world, with only 5% of the total area of Libya receiving precipitation >100 mm per year (Brika 2018). Furthermore, the population has increased from 1.1 million in 1950 to 6.7 million in 2019 (United Nations 2019). This surge in population has put increased pressure on water resources making water scarcity one of the current greatest challenges facing Libya (Brika 2018). Since the 1970s, water resources have a high consideration of the Libyan governments and their development (Wheida and Verhoeven 2007).

Between 1961 and 2013, the Libyan government financially supported the agricultural sector in order to meet the increased demand on food and achieve sustainability (FAO 2016; Wheida and Verhoeven 2007). Despite 95% of the country being designated as desert, the support from the government helped to increase cultivated area from 1.9 million ha in 1961 to 2.2 million ha in 1996 (FAO 2018). However, this led to an increased use of groundwater (from non-renewable aquifers), exceeding safe groundwater abstraction volume by 1940 million cubic meter per year (FAO 2018). This increased abstraction has led to seawater intrusion advancing by 2 km inland in some coastal areas, and groundwater salinity increasing from 150 mg L⁻¹ in 1950 to 5000 mg L⁻¹ in 1990.

Across many irrigated lands in the world, excessive groundwater abstraction has led to higher soil salinity rates (Elhag 2016). Soil salinity is the process of enriching soil with soluble salts, which results in salt-affected soil. Saline soil conditions have reduced the value and production of considerable areas of land all over the globe (Elhag 2016). For example, in Jefara plain (north west Libya), two irrigation schemes built using artesian wells in the 1970s have recently been converted to pumping wells, resulting in some waterlogging, soil salinity and decrease in crop yields (CEDARE 2014). Soil salinity increases the irrigation water requirement (more water is needed to leach the salt), while decreasing the yields as a result of waterlogging and salinity (FAO 1994). Same issue (soil salinity, waterlogging and crop yields reduction) was observed in the southern portion of Libya as a result of inadequate drainage (FAO 2016).

Drainage systems have been installed in arid and semi-arid regions to control the water table levels and to leach the salt below the root zone. However, less than 30% of all irrigated land needing drainage has been effectively drained (Schultz et al. 2007), and the situation is worse in least developed countries. According to Smedema et al. (2000) the proportion of agricultural land drained in the least

developed countries is 5–10% compared to 25–30% in developed countries. In Libya, c. 9000 ha of irrigated land (which represents around 2% of all croplands in Libya) was estimated to be equipped with some form of drainage in 2000 (FAO 2016). This is due to a fundamental lack of expertise in-country and the high cost of drainage installation as well as the lack of contiguous input data for their design. Computer simulation models can reasonably measure the effects of different input variables while minimising costs and shortening the time to system design (Selvaperumal et al. 2020; Wang et al. 2006).

DRAINMOD is a widely applied model used to simulate the hydrology of poorly drained and high water table soils (Gupta et al. 1993; Kandil et al. 1995; Luo et al. 2009; Selvaperumal et al. 2020; Skaggs et al. 2012). DRAINMOD can also be used to predict salinity (soil salinity and salinity in drains), it does this by applying a mass balance approach for the total dissolved concentrations of salt in the soil profile at each time step (Kandil et al. 1995). From the prediction of soil salinity, DRAINMOD can be used to estimate the response of crop yield to soil salinity by plotting two linear lines, one a tolerance plateau at 100 percent relative yield up to a salinity threshold, and the other a concentration dependant line, the slope of which reflects the yield loss per unit rise in soil salinity (Maas and Hoffman 1977). DRAINMOD has been successfully applied to simulate the impact of water management and drainage system design on yield, drainage water quality, and soil salinity in many irrigated areas including Egypt (Kandil et al. 1995; Wahba et al. 2002), Turkey (Kale 2011), and Iran (Pourgholam-Amiji et al. 2021).

To be able to apply DRAINMOD for salinity control, the initial soil salinity is required as an input parameter (Kandil et al. 1995). A standard method used to determine soil salinity is from the electrical conductivity of the saturated paste extract (EC_e) (USDA 1954). The EC_e measure is considered as the most accurate for estimating crop response to salinity. However, this approach is time consuming, tedious, and requires personnel with skills and experience of calculating the saturation percentage (Kargas et al. 2018). In recent decades, satellite imageries have been used as a technique to predict and map soil salinity (Nguyen et al. 2020). Many researchers have developed and evaluated different salinity indices (Asfaw et al. 2018; Elhag 2016). These indices were then used to develop a prediction map to illustrate the location of the salt affected soils (Asfaw et al. 2018). Recently, artificial neural networks (ANNs) have been combined with Remote Sensing (RS) and Geographical Information System (GIS) to create more accurate soil salinity maps by using salinity indices and reflectance from satellite images as an input for the ANNs (Habibi et al. 2021; Shahabi et al. 2016).

Habibi et al. (2021) found that developing ANNs using salinity indices and reflectance from satellite images produced more accurate soil salinity maps compared to Multiple Linear Regression (MLR). Mousavi et al. (2017) applied salinity and vegetation spectral indices to evaluate the relationship between the EC_e parameter and spectral indices. They compared ANN and MLR salinity prediction models and reported that ANN was 46% more accurate. Shahabi et al. (2016) used ANN, Ordinary Kriging, and multiple regression techniques to estimate soil salinity. Environmental factors such as altitude, geographic aspect, slope length,

Topographic Wetness Index (TWI), and Normalized Difference Vegetation Index (NDVI) spectral parameters were employed. They found that ANN had a lower Mean Square Error (MSE) and a higher coefficient of determination (R^2) than the other two models.

The purpose of this research is to improve the prediction of ECe in order to increase the efficacy of drainage system design in data-poor areas by utilising salinity indices and reflectance from satellite images. The expectation is that this will provide a low-cost alternative to drainage system design, making it more accessible to farmers, planners, and decision-makers in the least developed countries. The objectives of this study were to: (1) develop an ANN to predict ECe, (2) evaluate the performance of drainage systems based on measured and predicted ECe, and (3) develop soil salinity prediction maps to monitor the initial and simulated salinity under drained and undrained conditions.

2 Material and Methods

2.1 Study Area and Soil Salinity Dataset

This research focuses on two agricultural projects in the southern part of Libya, Eshkeda Agricultural Project (EAP) and Hammam Agricultural Project (HAP). EAP is located north of Sabha ($27^{\circ}32'45''N$ $14^{\circ}16'7''E$) at an altitude of 320 meters above sea level (ASL). The EAP is 3000 hectares in size and is split into three subareas: The Western Area (2000 ha), the Central Area (600 ha), and the Eastern Area (370 ha). According to the installed irrigation wells, the land is divided into 25 districts, each with 12 farms of around 10 ha. HAP is located in the north-east side of Sokna Oasis ($29^{\circ}04'01''N$ $15^{\circ}47'05''E$) at an altitude of 270 meters ASL. The HAP encompasses 1200 ha and is split into 182 farms (6 – 8 ha each farm). The ECe data collected from the two agricultural project areas was measured on water extracted from the saturated soil paste (USDA 1954). In total, for the HAP, there were 169 ECe measurements (c. 1 measurement for every 7 ha) while for the EAP there were 354 ECe measurements (c. 1 measurement for every 8 ha). Figure 1 shows the location of the study area and the ECe measurements points for HAP and EAP.

2.2 Remote Sensing Data and Salinity Indexes

Google Earth Engine (GEE) provides a rapid analysis of Remote sensing using Google's computing infrastructure, which offers online datasets in near-real-time (Zurqani et al. 2018). In this study, all of the satellite data pre-processing was conducted in GEE Code Editor (<https://code.earthengine.google.com>). Yearly scenes were generated from January to December for 1984, 1990, 2000, and 2010

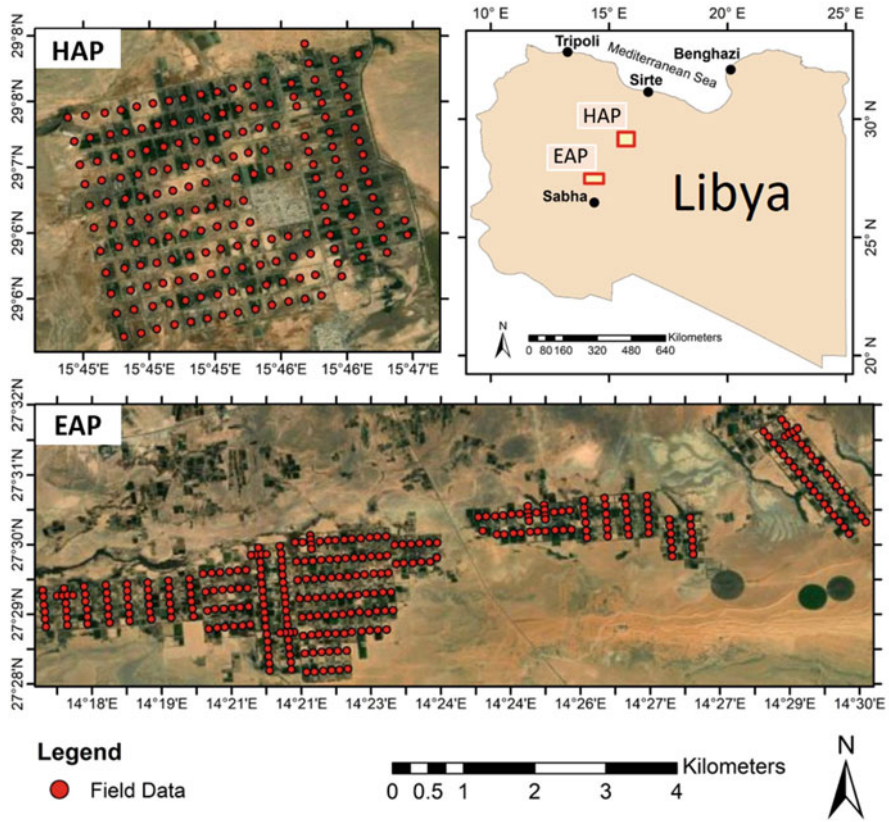


Fig. 1 The study area and soil salinity measurement locations. HAP is Hammam Agricultural Project, and EAP is Eshkeda Agricultural Project

using the median values of Landsat 5 Surface Reflectance bands for each measurement location in HAP, and EAP. These data have been atmospherically corrected using the Landsat Ecosystem Disturbance Adaptive Processing System (LEDAPS), and include a cloud, shadow, water, and snow mask produced using C Version of Function of Mask (CFMASK), as well as a per-pixel saturation mask (Gorelick et al. 2017). Table 1 gives detail of the wavelength, and spatial resolution of spectral bands, including the red, green, blue (RGB, ‘visible spectrum’), the near-infrared (NIR) bands, and 2 short-wave infrared (SWIR) bands in Landsat 5™.

In arid and semi-arid regions, several satellite salinity indices have been proposed locally based on environmental conditions (Bannari et al. 2008; Elhag 2016; Garajeh et al. 2021; Seifi et al. 2020). Based on previous studies, the most commonly utilised satellite salinity indices were selected and applied as input for ANN to predict soil salinity in the present study as detailed in Table 2.

Table 1 Band specifications of Landsat 5™ U.S. Geological Survey (USGS 2021)

Band	Wavelength (micrometres)	Resolution (meters)
Band 1 visible (blue)	(0.45–0.52 μm)	30 m
Band 2 visible (green)	(0.52–0.60 μm)	30 m
Band 3 visible (red)	(0.63–0.69 μm)	30 m
Band 4 near-infrared	(0.76–0.90 μm)	30 m
Band 5 shortwave-infrared	(1.55–1.75 μm)	30 m
Band 7 shortwave infrared	(2.08–2.35 μm)	30 m

Table 2 Spectral indices are derived from spectral reflectance at various bands and used for soil salinity prediction

Indicates	Acronym	Formula	References
Normalized difference salinity index	NDSI	$(R - NIR)/(R + NIR)$	Khan et al. (2005)
Brightness index	BI	$[(R)^2 + (NIR)^2]^{0.5}$	Khan et al. (2005)
Salinity index 1	SI1	$(G \times R)/B$	Douaoui et al. (2006)
Salinity index 2	SI2	$(B \times R)/G$	Khan et al. (2005)
Salinity index 3	SI3	B/R	Khan et al. (2005)
Salinity index 4	SI4	$(B \times R)^{0.5}$	Khan et al. (2005)
Salinity index 5	S5	$(G \times R)^{0.5}$	Khan et al. (2005)
Salinity index 6	SI6	$(R \times NIR)/G$	Khan et al. (2005)
Salinity index 7	SI7	$[(R)^2 + (G)^2]^{0.5}$	Douaoui et al. (2006)
Salinity index 8	SI8	$(B - R)/(B + R)$	Douaoui et al. (2006)
Salinity index 9	SI9	$[(G)^2 + (R)^2 + (NIR)^2]^{0.5}$	Abbas and Khan (2007)
Normalized difference vegetation index	NDVI	$(NIR - R)/(NIR + R)$	Khan et al. (2005)

B blue band, *G* green band, *R* red band, *NIR* near-infrared band of Landsat 5 images.

2.3 Artificial Neural Networks (ANNs)

ANNs typically have three layers. The first layer is the input layer, which includes the independent variables (input parameters), and the second layer is a hidden layer, which sits between the input and the output. The hidden layer containing a number of units (a grouping of independent variables). These units, often known as ‘neurons,’ are used to guide data processing in the input layer and to build computational links between the input and output layers. The output layer, which is the dependent variable, is the third layer. The structure of the ANNs developed in this research is depicted in Fig. 2.

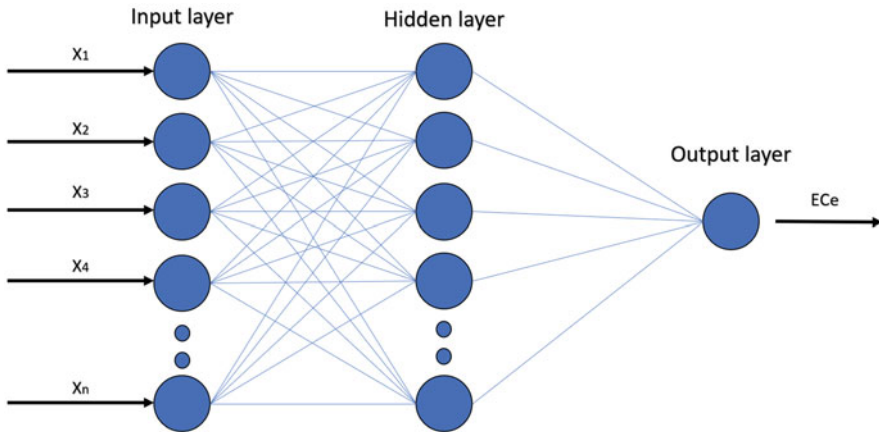


Fig. 2 the structure of artificial neural network applied in this study, adopted from Ellafi et al. (2021).

For this research, the ANNs were developed following the steps described by Ellafi et al. (2021). In summary, three steps were undertaken in the development of ANNs to predict ECe values. In the first step, the dataset from both study area were combined (the remote sensing data used as an input and the measured data as an output) make a total sample size of 523 samples with 19 input parameters and 1 output (Table 3 shows the summary of the dataset). In the second step, the training and testing dataset was defined. Ninety percent of the dataset was defined as a training dataset, leaving 10% as a testing dataset. In the third step, the appropriate network was defined using the sequential orthogonal approach (Ellafi et al. 2021; Sun 2012). Table 3 shows the two ANNs developed in this study and the input parameters used for each ANN to predict ECe in HAP and EAP. Two groups of input parameters were used, the first group has six input parameters (i.e. Band 1 Visible (Blue), Band 2 Visible (Green), Band 3 Visible (Red), Band 4 Near-Infrared, Band 5 shortwave-infrared, and Band 7 shortwave infrared). The second group has nineteen input parameters included Band 1 Visible (Blue), Band 2 Visible (Green), Band 3 Visible (Red), Band 4 Near-Infrared, Band 5 shortwave-infrared, Band 7 shortwave infrared, Normalized difference salinity index, Brightness index, Salinity index 1, Salinity index 2, Salinity index 3, Salinity index 4, Salinity index 5, Salinity index 6, Salinity index 7, Salinity index 8, Salinity index 9, and Normalized difference vegetation index. The purpose for having two groups of input parameters was to determine the smallest data set necessary to accurately estimate ECe.

The ability of the two ANN models developed in this study to accurately predict ECe was critically evaluated in two steps. Step 1 involved developing ANNs using the training dataset and then utilising the testing dataset to select the best performing ANN model in terms of predicting ECe using three statistical parameters. These were: (1) the coefficient of determination (R^2) between the observed and

Table 3 statistical summary of the dataset used in this research

Variable	Min	Max	Average	STDEV	Median	SE
BI	3405.57	6274.52	4341.46	432.63	4309.03	18.92
Blue	788	1760	1068.23	150.05	1038	6.56
Green	1265	2990	1737.3	275.03	1674	12.03
NDSI	-0.52	-0.03	-0.24	0.09	-0.24	0
NDVI	0.03	0.52	0.24	0.09	0.24	0
NIR	2798	4890	3686.49	339.82	3693	14.86
Red	1363	4125	2265.06	446.61	2187	19.53
SI1	2107.83	7007.81	3691.26	816.22	3509.47	35.69
SI2	849.05	2428.09	1391.66	247.82	1345.68	10.84
SI3	0.39	0.6	0.48	0.04	0.48	0
SI4	1036.36	2694.44	1554.47	259.61	1500.53	11.35
SI5	1313.09	3511.94	1983.07	351.17	1912.99	15.36
SI6	3763.52	6553.43	4776.9	462.21	4734.83	20.21
SI7	1859.57	5094.68	2855.45	519.83	2752.12	22.73
SI8	-0.44	-0.25	-0.35	0.03	-0.35	0
SI9	3651.36	6950.52	4678.68	489.03	4619.41	21.38
SWIR1	2101	20,000	3545.29	1236.48	3396	54.07
SWIR2	1145	5048	2443.2	709.66	2318	31.03
ECe	0.35	88	8.5	14.54	2.91	0.64

predicted ECe values for the testing dataset (e.g., best performance equals 1), (2) the mean square error (MSE), and (3) the root mean square error (RMSE) (Ellafi et al. 2021) which can be defined mathematically as:

$$R^2 = 1 - \frac{\sum_{i=1}^n (P_i - M_i)^2}{\sum_{i=1}^n (M_i - \bar{M}_i)^2} \quad (1)$$

$$MSE = \frac{1}{n} \sum_{i=1}^n (P_i - M_i)^2 \quad (2)$$

$$RMSE = \sqrt{\frac{\sum_{i=1}^n (P_i - M_i)^2}{n}} \quad (3)$$

Where n represents the number of soil samples, M_i is the measured ECe, P_i is the predicted ECe, and \bar{M}_i is the mean measured ECe.

In Step 2 the developed ANNs were tested by applying the K-fold cross validation technique (Bell 2015; Ghatak 2019). In the K-fold cross-validation the dataset was split into ten randomly generated subsets. Nine sub-sets were merged and used as the ‘training sub-set’ for each K-fold cross-validation, while one part was used as the ‘testing sub-set’. This procedure was iterated 10 times, each time “rotating out” a

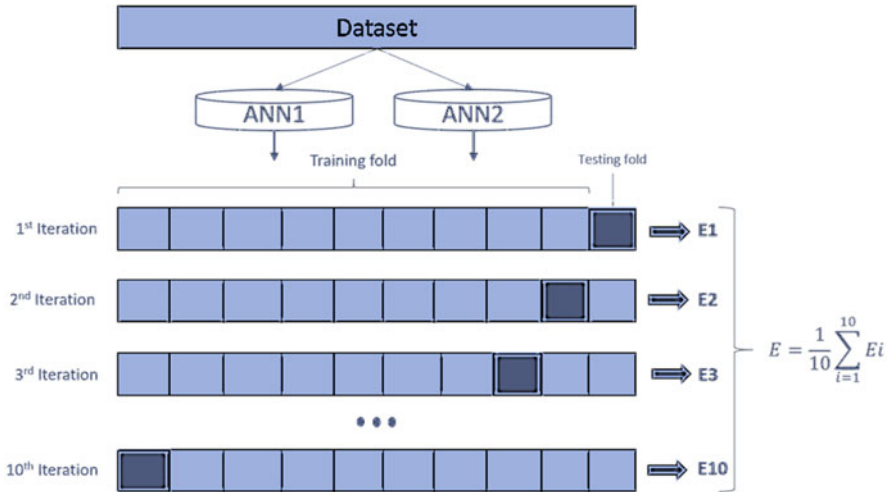


Fig. 3 A schematic illustration of K-fold cross-validation for K = 10. Where E1 – E10 are the Mean Square Error for each iteration. E is the mean average of E1 – E10

testing sub-set, ensuring that each sub-set used in each ANN was tested. Figure 3 illustrates the structure of the cross validation for the dataset divided into 10 subsets. The MSE mean average of the 10 iteration was taking and compared to the MSE gathered from Step 1. This approach was used to quantify the performance of the developed ANNs (ANN1 and ANN2).

Finally, the most accurate ANN based on Step1, and Step 2 were then applied to predict soil salinity in years 1990, 2000, and 2010 for EAP and HAP. The predicted values were then used to create soil salinity maps using the classification described by the Food and Agriculture Organization (FAO) (FAO 1988). The maps were then used to evaluate the salinity status in both EAP and HAP. Table 4 shows the soil salinity classes recognised by the FAO (FAO 1988).

2.4 DRAINMOD

DRAINMOD is a field scale computer simulation model for shallow water table soils, which was developed for agriculture fields to design and evaluate drainage systems (Skaggs et al. 2012). The model needs a range of input parameters (i.e., climatic, soil-water, drainage design, and crop information). The input data for DRAINMOD were gathered during site studies of soil properties in EAP (Cornelius-Brochier 1981; Italconsult 1976) and HAP (Danenco 1980; Holzmann-Wakuti 1974). The impervious layer depth in EAP and HAP was also determined by site studies. Crop data for Beans, Maize, Soybeans, and Wheat were gathered in

Table 4 soil salinity classes and crop growth

Soil salinity class	Soil salinity (ECe in dS m ⁻¹)	Effect on crop plants
Non saline	0–2	Salinity effects negligible
Slightly saline	2–4	Yields of sensitive crops may be restricted
Moderately saline	4–8	Yields of many crops are restricted
Strongly saline	8–16	Only tolerant crops yield satisfactorily
Very strongly saline	> 16	Only a few very tolerant crops yield satisfactorily

Where ECe is the electrical conductivity of the saturated paste extract, dS/m is a ECe unit are Deci Siemens per meter.

accordance with the recommendations from the following studies (Evans et al. 1991; Kandil et al. 1995; Maas and Hoffman 1977). This crop rotation was chosen because it is common in Egypt's Nile Delta (an arid area, with similar climate conditions to EAP and HAP). Additionally, the Libyan General Water Authority (GWA) recommends growing Beans, Maize, Soybeans, and Wheat in EAP and HAP (GWA 1999). The climatic data required to run DRAINMOD was generated from the closest meteorological stations to EAP (Sabha meteorological station located 50 km south of EAP) and HAP (Hon meteorological station located 15 km east of HAP) for the period from 1981–2010. Table 5 provides a summary of the input data applied in DRAINMOD.

DRAINMOD required the initial soil salinity as an input parameter for the 30-year simulations (1981–2010) in HAP and EAP. As there were 523 ECe measurement, representative values were needed to reduce the number of simulations. Therefore, the measured values of ECe were categorised based on FAO soil salinity classes (see Table 4). The average value of each category was assumed as a representative value of that class and used as an input for DRAINMOD. Therefore, DRAINMOD was run five times in each project for the period 1981–2010. Two scenarios were assumed in DRAINMOD. The first scenario assumed that a drainage system was installed and maintained properly. The second scenario assumed there to be no drainage system installed (Undrained). DRAINMOD does not have an option to simulate without including the drainage design parameters (drain depth and spacing). Therefore, by having a wider distance between drains (i.e. 500 m) the undrained assumption can be achieved. The median ECe values for the four years, 1981, 1990, 2000, and 2010, were selected to create soil salinity maps for scenarios in EAP and HAP. Finally, the maps were used to evaluate the importance of installing drainage system for salinity control. The relative yield for the 30-year simulations (1981–2010) in HAP and EAP were obtained for both scenarios.

Table 5 Summary of the input data required to run the DRAINMOD 30-year simulation

Input parameter	EAP	HAP		
Drainage design				
Drain spacing (m)	50	50		
Drain depth (cm)	100	100		
Depth of restricting layer (cm)	150	150		
Effective radius (cm)	1.5	1.5		
Drainage coefficient (cm d ⁻¹)	2.5	2.5		
Initial water table depth (cm)	50	50		
Soil property				
Saturated hydraulic conductivity above drains (m d ⁻¹)	2.6	5.6		
Saturated hydraulic conductivity below drains (m d ⁻¹)	11.2	4.5		
Saturated water content (cm ³ cm ⁻³)	0.35	0.35		
Water content at lower limit (cm ³ cm ⁻³)	0.08	0.04		
Required drainage for field work (cm)	3.9	3.9		
Weather data				
Daily ET0 (mm d ⁻¹)	Data generated from Sabha meteorological station*			
Daily rainfall (mm d ⁻¹)	Data generated from hon meteorological station*			
Crop information	Observed precipitation at Sabha station			
	Beans	Maize	Soybeans	Wheat
	10	10	10	9
	640	1088	4000	3800
Soil salinity threshold (mg l ⁻¹)	2.97 × 10 ⁻²	1.88 × 10 ⁻²	2.50 × 10 ⁻²	7.10 × 10 ⁻³
Slope for higher soil salinity values (% per mg l ⁻¹)	2.97 × 10 ⁻²	1.88 × 10 ⁻²	2.50 × 10 ⁻²	7.10 × 10 ⁻³
		Observed precipitation at hon station		
	Beans	Maize	Soybeans	Wheat
	10	10	10	9
	640	1088	4000	3800
	2.96 × 10 ⁻²	1.88 × 10 ⁻²	2.50 × 10 ⁻²	7.10 × 10 ⁻³

(continued)

Table 5 (continued)

Input parameter	EAP				HAP				
	100	100	100	100	100	100	100	100	100
Relative yield without deficit stress (%)	7.20	1.22	7.2	1.22	7.20	1.22	7.20	1.22	1.22
Slope for yield versus deficit stress-day-index	100	100	100	100	100	100	100	100	100
Relative yield without wet stress (%)	0.65	0.71	0.65	0.71	0.65	0.71	0.65	0.71	0.71
Slope for yield versus wet stress-day-index	1.25								
Irrigation water salinity (dS m ⁻¹)									3.91
Soil salinity									
Average salinity 0-2 in dS m ⁻¹									1.2
Average salinity 2-4 in dS m ⁻¹									2.9
Average salinity 4-8 in dS m ⁻¹									5.7
Average salinity 8-16 in dS m ⁻¹									11.8
Average salinity > 16 in dS m ⁻¹									40.7

* Sabha meteorological station is the closest station to Eshkeda agricultural project (EAP), Hon meteorological station is the nearest station to Hammam agricultural project (HAP).

2.5 Software and Programming Used

The data was analysed using several software packages. The remote sensing data was analysed using Google Earth Engine (GEE) platform. The development of the ANNs utilised a neuralnet package in R (Stefan and Guenther 2019). ArcGIS 10.7. was used to create soil salinity maps. DRAINMOD was used to simulate and design drainage systems for salinity control.

3 Results

3.1 Performance of Artificial Neural Networks to Predict Soil Salinity

Table 6 summarizes the structure of the ANN1 and ANN2 developed in this research, as well as their step one performance evaluation. In both (training and testing) ANN1 and ANN2 were able to predict, based on R^2 , between 0.72–0.90 of the variability in E_c. As hypothesised, the ANN models performed better when training data was used rather than testing data. According to the performance results in Table 6, ANN2 performed better than ANN1 in both phases (training and testing). The R^2 in ANN2 ranged from 0.86–0.90, while in ANN1 ranged from 0.72–0.78.

The results of Step 2 K-fold cross-validation are shown in Fig. 4. Figure 4 shows the median RMSE across 10 randomly generated subsets (dark line within the boxplot) when the size of the training set is fixed at 470 samples. The RMSE for ANN1 ranged between 6.7–11.3 dS m⁻¹, while in ANN2 RMSE ranged between 4.8–10.7 dS m⁻¹. Figure 5 shows the accuracy of ANN1 and ANN2 in predicting E_c in the training and testing datasets. The 1:1 line indicates the line of complete agreement between predicted and measured E_c values. It is worth noting that the

Table 6 structure performance evaluation of ANN1 and ANN2 implemented in EAP and HAP

Model name	Training				
	Model structure*	Number of samples	RMSE (dS m ⁻¹)	MSE (dS m ⁻¹)	R ²
ANN1	6:5:5:1	470	6.74	45.43	0.78
ANN2	18:15:15:1	470	4.60	21.02	0.90
Model name	Testing				
	Model structure*	Number of samples	RMSE (dS m ⁻¹)	MSE (dS m ⁻¹)	R ²
ANN1	6:5:5:1	53	9.19	84.50	0.72
ANN2	18:15:15:1	53	6.35	40.36	0.86

Where: (*) is the model structure of the ANNs, for example 6:5:5:1, 6 is the number of neurons representing the input parameters, 5:5 two hidden layers with 5 neurons in each layer, and 1 is the output of the model.

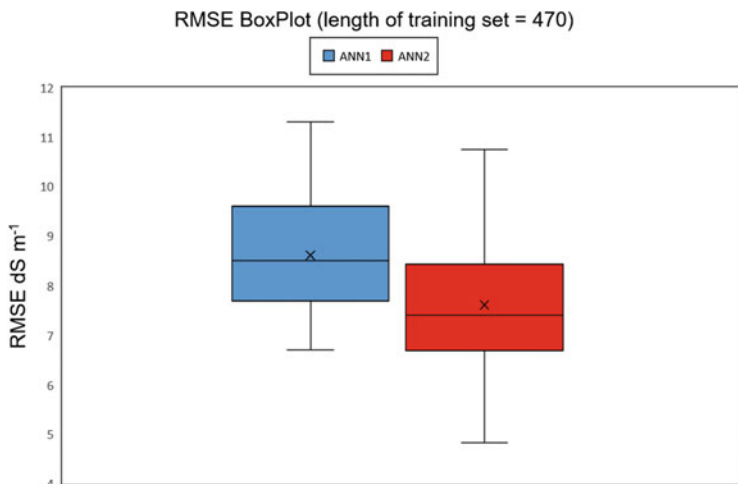


Fig. 4 Boxplots of the median Root Mean Square Error (RMSE) for the Artificial Neural Networks (ANN1 and ANN2) developed to predict soil salinity

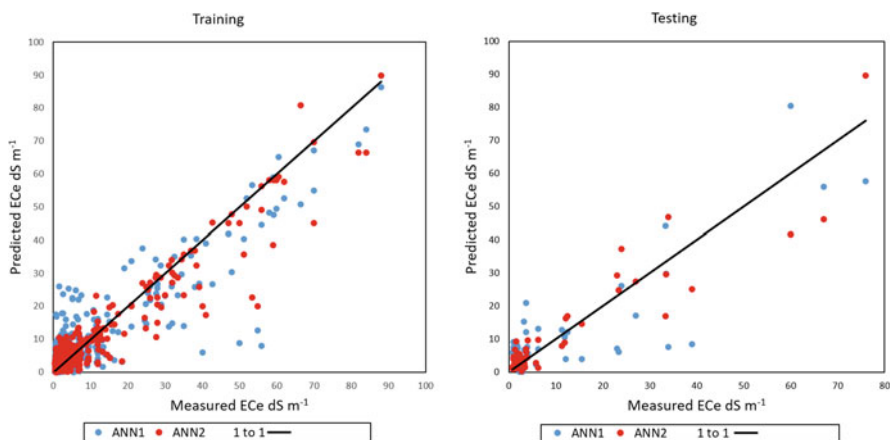


Fig. 5 Predicted Electrical conductivity of the saturated paste extract (ECe in dS m⁻¹) versus measured ECe in both training and testing dataset

predicted ECe values for ANN1 and ANN2 are close to the 1:1 line. The results indicate that ANN2 was noticeably better at predicting the observed ECe values compared to ANN1 applied to training and testing dataset (see Fig. 5 and Table 6). In general, in both ANN1 and ANN2, there were noticeable outliers in the predicted values of soil sample based on ECe (10–40 dS m⁻¹). The outliers occurred on both sides of the 1:1 line and were relatively discrete (Fig. 5). As expected, the predicted values of ANN1 and ANN2 in the training dataset were closer to the 1:1 line compared to the ANN1 and ANN2 in the testing dataset.

3.2 Potential Relative Yield Simulated By DRAINMOD and Soil Salinity Prediction Maps in EAP and HAP

The results of potential relative yields of the four simulated crops results for the 30-year simulation under drained and undrained scenarios are shown in Fig. 6 for EAP and HAP. In EAP, the simulated relative yield under drained conditions ranged between 70–100% (see Fig. 6d), while in HAP the simulated relative yield ranged between 30–100% (Fig. 6b). In HAP, beans and maize got the relative yield ranging between 30–70%, while soybeans and wheat obtained relative yield ranging between 88–100%. For the undrained scenarios in EAP and HAP (Fig. 6a and c), there was a reduction in relative yield in all crops. The first reduction was noticed on beans, maize, and soybeans with relative yield ranging between 0–5% (see Fig. 6a and c). According to the simulation results in Fig. 6a and c, wheat was the only crops to consistently produce a yield under undrained conditions. However, the expected relative yield under undrained conditions ranged between 6–38%. Figure 6 also shows a rapid decrease in yield for wheat from around 38% in 1981 to under 10% 1997 in both EAP and HAP.

Figure 7 shows the salinity prediction maps of EAP, as predicted with a drainage system installed, without a drainage system installed (DRAINMOD simulation) and based on a prediction using the current salinity condition (ANN2). In Fig. 7 maps (a), (b), (c), and (d) show the median soil salinity levels in EAP under the current

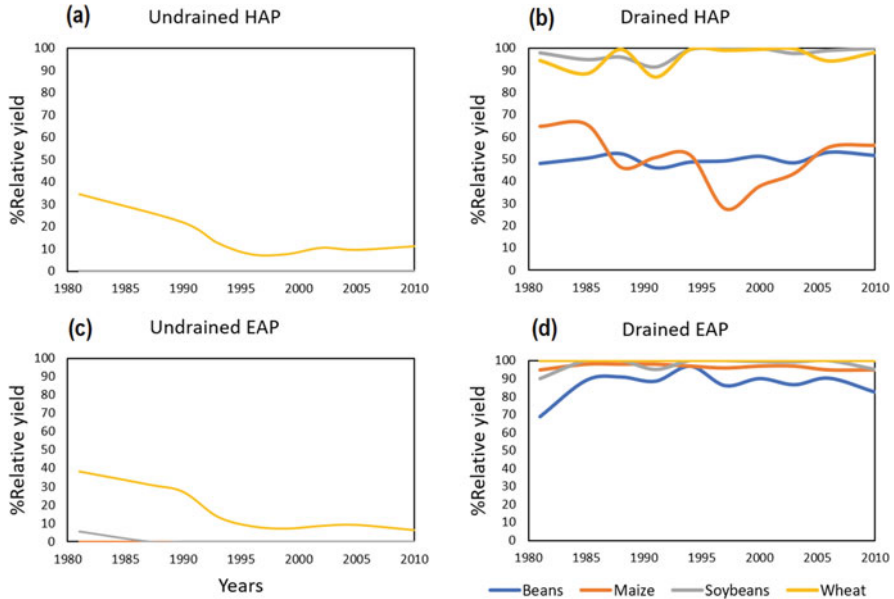


Fig. 6 Relative yield results as a percentage for beans, maize, soybeans, and wheat under drained and undrained condition for Eshkeda Agricultural Project (EAP) and Hammam Agricultural Project (HAP) for 30-year simulation

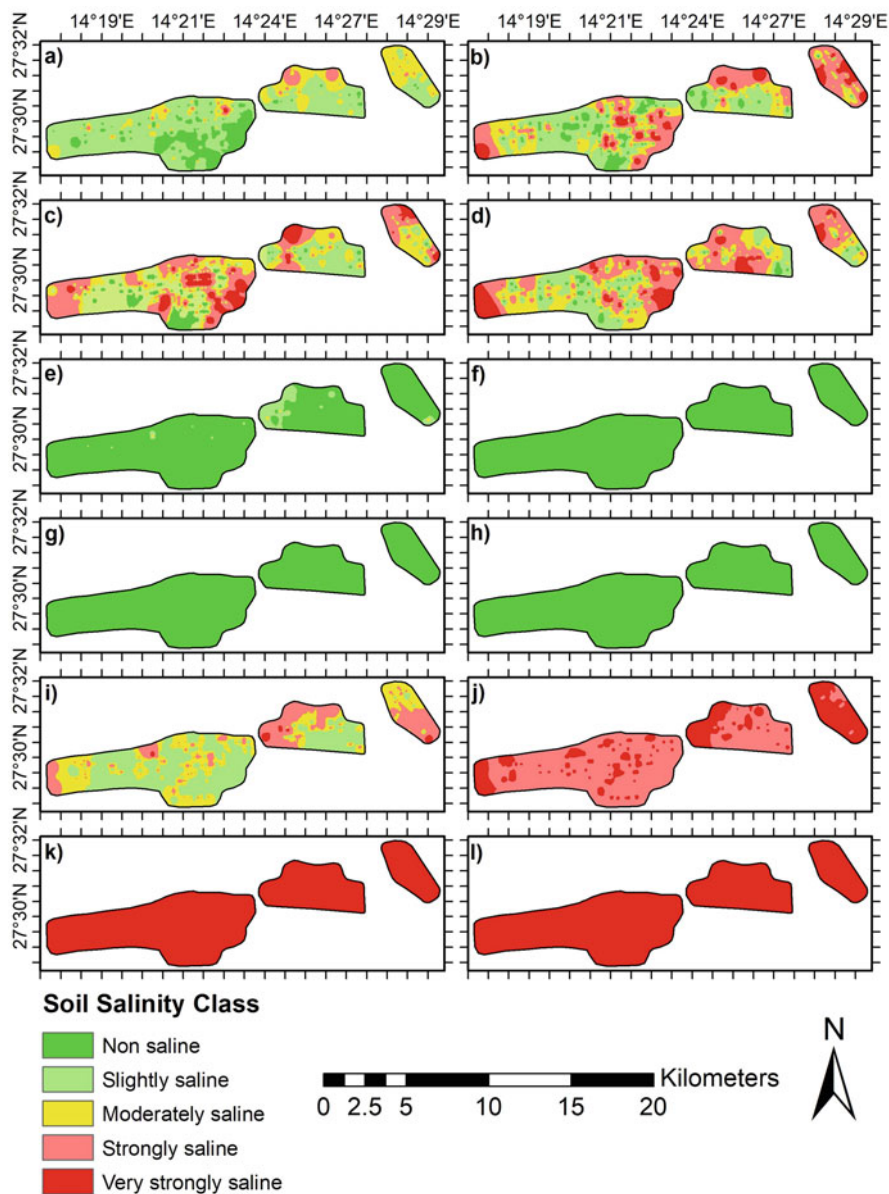


Fig. 7 The median soil salinity levels in Eshkeda Agricultural Project (EAP). Where (a) is the median soil salinity levels in 1981 predicted by the second Artificial Neural Network (ANN2). (b) the median soil salinity levels in 1990 predicted by ANN2. (c) the median soil salinity levels in 2000 predicted by ANN2. (d) the median soil salinity levels in 2010 predicted by ANN2. (e) the median soil salinity levels in 1981 simulated by DRAINMOD for drained scenario. (f) the median soil salinity levels in 1990 simulated by DRAINMOD for drained scenario. (g) the median soil salinity levels in 2000 simulated by DRAINMOD for drained scenario. (h) the median soil salinity levels in 2010 simulated by DRAINMOD for drained scenario. (i) the median soil salinity levels in 1981 simulated by DRAINMOD for undrained scenario. (j) the median soil salinity levels in 1990 simulated by DRAINMOD for undrained scenario. (k) the median soil salinity levels in 2000 simulated by DRAINMOD for undrained scenario. (l) the median soil salinity levels in 2010 simulated by DRAINMOD for undrained scenario

conditions predicted by ANN2 in 1981, 1990, 2000, and 2010 respectively. From these maps, an increase in soil salinity is noted in 1990 (Fig. 7b), 2000 (Fig. 7c), and 2010 (Fig. 7d) compared to 1981 (Fig. 7a) (see the red spots in maps Fig. 7b, c and d). Fig. 7e, f, g and h show the median salinity conditions simulated by DRAINMOD under drained conditions for years 1981, 1990, 2000, 2010 respectively. From these maps, it is notable that the majority of the area is classified as non-saline, with only a few locations in Fig. 7e classified as slightly saline. In comparison, the maps shown in Fig. 7i, j, k and l, represent the median salinity conditions simulated by DRAINMOD under undrained conditions for years 1981, 1990, 2000, 2010 respectively. From these maps, an increase in soil salinity is evident in maps shown in Fig. 7k and l compared to Fig. 7i. For example, maps shown in Fig. 7k (in 2000) and 7l (in 2010) are classified as very strongly saline soils, while the map shown in Fig. 7i (in 1981) has a higher proportion of the area classified as slightly saline.

Figure 8 shows the soil salinity prediction maps, with drainage system installed, without drainage system installed (DRAINMOD simulation) and predicting the current salinity condition (ANN2) for HAP. The maps in Fig. 8 are shown in three groups. The first group includes maps shown in Fig. 8a, b, c and d, these maps represent the predicted salinity levels based on ANN2 in 1981, 1990, 2000, and 2010 respectively. These maps show, salinity status to be mainly classified as either strongly saline or very strongly saline. Also, there is a slight increase in the proportion of the mapped area that is classified as very strongly saline class in the map in Fig. 8d (representing 2010) compared to maps in Figs. 8a, b and c. The second group of maps (Fig. 8e, 8f, 8g and 8h) show the median salinity conditions simulated by DRAINMOD under drained conditions for years 1981, 1990, 2000, 2010 respectively. From these maps, it is noticeable that the soil salinity in all maps is classified as slightly saline. The third group of maps (Fig. 8i, 8j, 8k and 8l), show the median salinity conditions simulated by DRAINMOD under undrained conditions for the years 1981, 1990, 2000, 2010 respectively. In these maps, only two classes are represented, strongly saline and very strongly saline. Also, it is notable that maps in Fig. 8j, 8k and 8l are only classified as have very strongly saline class.

4 Discussion

4.1 Development of ANNs

Using spectral variables to invert soil salt content requires a good mathematical regression model. Artificial neural networks have been widely used in predicting soil properties and modelling (Ellafi et al. 2021; Gholami et al. 2021; Wang et al. 2021; Yang et al. 2020). Wang et al. (2021) developed an ANN that could predict soil salinity with an accuracy of 0.57 in R^2 within the testing dataset. Wang et al. (2021) claim that the low R^2 accuracy is due to the limited number of samples used to develop the ANN (only 160 samples). In contrast, in this study 523 samples were used to develop ANN1 and ANN2 and the accuracy ranged between 0.72–0.86 in R^2

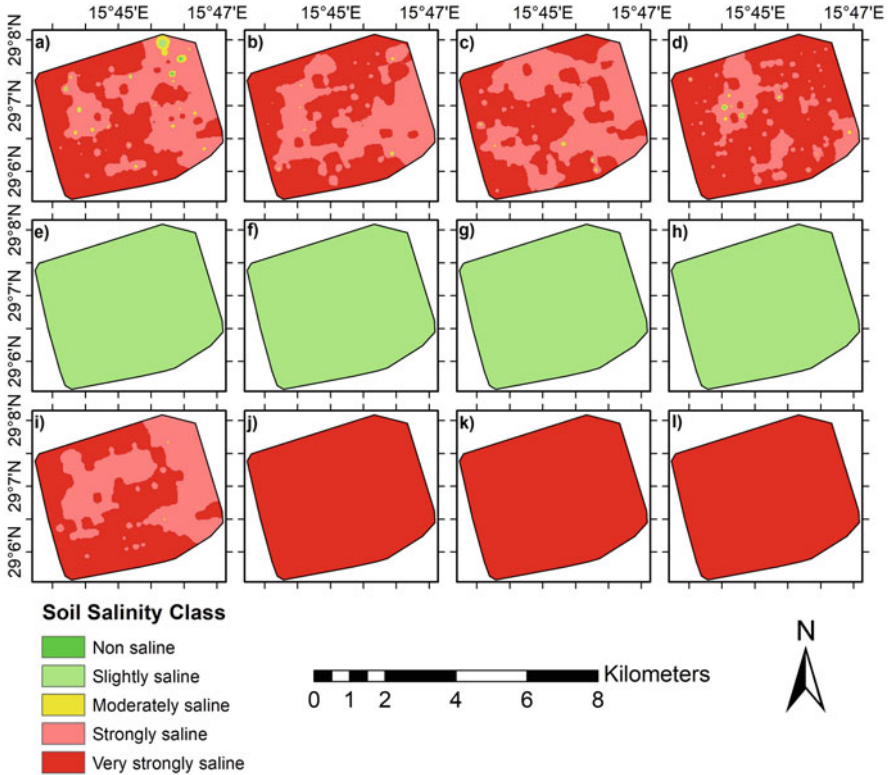


Fig. 8 the median soil salinity levels in Hammam Agricultural Project (HAP). Where (a) is the median soil salinity levels in 1981 predicted by the second Artificial Neural Network (ANN2). (b) the median soil salinity levels in 1990 predicted by ANN2. (c) the median soil salinity levels in 2000 predicted by ANN2. (d) the median soil salinity levels in 2010 predicted by ANN2. (e) the median soil salinity levels in 1981 simulated by DRAINMOD for drained scenario. (f) the median soil salinity levels in 1990 simulated by DRAINMOD for drained scenario. (g) the median soil salinity levels in 2000 simulated by DRAINMOD for drained scenario. (h) the median soil salinity levels in 2010 simulated by DRAINMOD for drained scenario. (i) the median soil salinity levels in 1981 simulated by DRAINMOD for undrained scenario. (j) the median soil salinity levels in 1990 simulated by DRAINMOD for undrained scenario. (k) the median soil salinity levels in 2000 simulated by DRAINMOD for undrained scenario. (l) the median soil salinity levels in 2010 simulated by DRAINMOD for undrained scenario

(see Table 6). Therefore, the results from this research support the findings from Wang et al. (2021), with respect to the performance of the developed ANN being dependent on the number samples in the training process. Also, the size of the dataset and the range of values within that dataset will also influence the performance of the ANN. If the value range is small, the variance will be small and the offset will be big, making the prediction in the training set much precises than the testing set.

The results of this study showed that ANN2 was 45% more accurate than ANN1 according to the RMSE in the testing set (ANN1 = 9.19 dS m⁻¹, and ANN2 = 6.35

dS m^{-1}). This finding resonates with that of Shahabi et al. (2016). Shahabi et al. (2016) found that the choice of bands and salinity indices as input variables in the ANN model was important and helped to improve the accuracy of the prediction from 0.62 to 0.82 in R^2 .

Additionally, Akramkhanov and Vlek (2012) and Ghorbani et al. (2019) highlighted the advantages of neural networks over other nonlinear techniques for measuring soil surface salinity. Akramkhanov and Vlek (2012) reported an R^2 of 0.83 for salinity prediction, whereas Ghorbani et al. (2019) claimed an accuracy of 0.82. Their studies are virtually identical to the current study in terms of the proposed technique and the accuracy of the results. Mohamed et al. (2018) and Morgan et al. (2018) validate the advantages of using bands including visible blue, green, red and Near-Infrared bands in combination with a neural network to map soil salinity, which corroborates our findings. Morgan et al. (2018) used NDVI spectral indices with ANN to produce a salinity map with 0.94 in R^2 . Jin et al. (2015) emphasised the importance of using spectral indices from satellite images to create a salinity map as one of the most effective and significant elements in desertification. They agreed that by utilising these indices, soil salinity may be detected, and the kind of salinity determined.

4.2 DRAINMOD Applications

The results of the simulated drained conditions (see Fig. 6b and d), even though drainage systems were assumed to be installed in EAP and HAP, resulted in different relative yields of the crops between the two projects (EAP has much higher yield compared to HAP). For example, the average relative yield in EAP was higher than HAP by 37%, 47%, 0.4% and 4% for beans, maize, soybeans and wheat respectively. The reduction in yield, in HAP, was probably caused by the quality of irrigation water applied (3.91 dS m^{-1}) compared to the irrigation water quality in EAP (1.25 dS m^{-1}). According to the Food and Agriculture Organisation (FAO), if the irrigation water quality (IWQ) applied for wheat exceeds 3.8 dS m^{-1} but less than 5 dS m^{-1} the expected yield will be above 90% but less than 100%, which was true in HAP where IWQ was 3.91 dS m^{-1} and the average yield was 96%. Also, the results of this study showed that an average relative yield of 100% was obtained for wheat in EAP when IWQ was at 1.25 dS m^{-1} (FAO 1994). The same was true for the other crops (beans, maize and soybeans) simulated in this study, where the obtained yield matched the predicted yield for a specific IWQ. For more information about the influence of IWQ on crop tolerance and crop yield see the Water Quality for Agriculture by FAO (FAO 1994).

The results of undrained conditions in EAP and HAP (Fig. 6a and c) show that the predicted yield for beans, maize and soybeans were 0% (except for the years between 1981 and 1985 in EAP where the relative yield ranged between 1–7%). Only wheat was considered able to grow and to produce a predicted yield in EAP and HAP. However, a declining trend in the relative yield is showing in Fig. 6a and c.

That decline results in a 30% reduction in predicted yield in both EAP and HAP. According to Kale (2012) the reason for this is most likely due to the aggravated problems of waterlogging and salinity. Which is true as showing in Fig. 6 and the predicted soil salinity maps in Fig. 7 and 8 in EAP and HAP (maps j, k and l in Fig. 7 and 8 show a noticeable increase of soil salinity for the years 1990, 2000, and 2010 in both EAP and HAP). On drained soils the relative yield of wheat was at least 50% higher compared to the undrained soils. Which is a considerable advantage and shows the importance of installing a drainage system. Based on simulated results and field measurements, Kale (2012) claimed that installing a drainage system in a semi-arid area in Turkey, increased the overall yield of wheat and beans by 36%. The selection of a crop to grow in a specific area is also an important consideration and should be done by monitoring the soil salinity, IWQ and the condition of drainage system installed.

4.3 Soil Salinity Mapping

Maps shown in Fig. 7 a, b, c and d and 8 a, b, c and d, show the current soil salinity situation in EAP and HAP for the years 1981, 1990, 2000, and 2010 respectively. From these maps, it can be noticed that the current drainage systems in both projects did not help to reduce the salinity stress. According to the World Bank Organisation (WBO), it is a common problem in least developed countries, because of the lack of financial resources for drainage system design, operation, and management, as well as a lack of stakeholder participation (rather than drainage users) (WBO 2000), (which is true for EAP and HAP). Ahmed and Ramadan (2007) studied the irrigation water quality in EAP and suggested that installing and maintaining an adequate drainage system would help to reduce the salinity problem in the project. Ramadan and Elssaidi (2017) have also done research on the soil salinity issues in the region including EAP and their recommendation was to improve the drainage system to lower the shallow water table and grow more tolerant crops. In addition, Ramadan and Elssaidi (2017), suggested that a model needed to be developed to predict soil salinity in the region including EAP.

The situation is similar in HAP, where the drainage is not maintained properly resulting in high soil salinity status. In 2003, the General Water Authority in Libya (GWA) found that open ditches at HAP were blocked and causing waterlogging and salinity problems (GWA 2003). Later on GWA contracted a local company to help with cleaning and unblock those ditches (GWA 2003). The National Committee to Combat Desertification in Libya (NCCD) evaluated the situation at HAP and they found the main problems facing the farmers at HAP are similar to the ones in EAP. The first problem is the soil salinity as the salt spot can be easily seen on the soil surface. The second problem is the shallow water table caused by over irrigation by the farmers (trying to flush the salt). The over irrigating caused another problem which is water scarcity (pumping from non-rechargeable aquifer). Finally, the current drainage system is ineffective (NCCD 2005). Experts from the General

Water Authority in Libya visited the HAP in 2007, and their recommendations were to design and install a new drainage system as the current one was ineffective (GWA 2007).

Maps in in Figs. 7 and 8 (e, f, g and h) show how the salinity situation would be if a drainage system were installed and maintained properly in EAP and HAP for the simulated years 1981, 1990, 2000, 2010 respectively. From these maps the importance of having a proper drainage system is noticeable. In EAP and HAP, the soil salinity decreased and the salinity classes in all the project converted to non-saline soils (in EAP, see Fig. 7) and slightly saline soils (in HAP, see Fig. 8). Also, it helped to improve the potential crop yield (see Fig. 6). The maps in Fig. 7 and 8 (i, j, k, and l) show the simulation results of how the salinity situation will be in EAP and HAP if no drainage system were installed for the years 1981, 1990, 2000, and 2010 respectively. For both projects, it is notable that the salinity levels increased, and the soil salinity class became very strongly saline at the end of the simulations (see Fig. 7 and 8). Also, as a result of the that, a massive reduction of crop yields was noted (see Fig. 6). These findings highlight the importance of installing a drainage system to reduce salinity issues and increase production. In addition, the findings of this study clearly illustrate the relationship between drainage design and soil salinity. This supports the frequently stated proposition that drainage, irrigation, and salinity control for arid lands should be considered as components of a water management system and that the design of each component should be dependent on the design of the other components.

5 Conclusions

Artificial neural networks (ANNs) as an indirect method of predicting soil salinity from the reflections of the satellite images have been successfully applied by researchers (Ghorbani et al. 2019; Habibi et al. 2021; Mohamed et al. 2018; Morgan et al. 2018; Shahabi et al. 2016). ANNs were applied to predict soil salinity in two case study drainage schemes in the south of Libya. It was shown that artificial neural networks developed from the reflection bands of satellite images and the derived salinity indices were capable of making highly accurate predictions of soil salinity. Additionally, predictions of soil salinity based on ANN generated using both reflection bands and salinity indices were slightly more comparable to observed soil salinity than predictions based only on reflection bands. The more accurate ANN were then successfully applied to predict the soil salinity status in different years to evaluate the effectiveness of the current drainage systems in two case study. In addition, DRAINMOD was applied to simulate the crop yield and salinity levels under drained and undrained conditions. The results suggest that having an effective drainage system installed and maintained properly can help to improve the potential crop yield and control the salinity stress in agricultural lands. Also, the results suggest that ANNs can be used as a tool to evaluate an existing drainage system and specify an area in need of improvement. However, further research is needed to

evaluate the productivity of existing agricultural projects under salinity stress using ANNs combined with the applications of DRAINMOD in other least developed countries. These tools are of value to farmers and decision-makers, helping them to evaluate the most appropriate drainage design to maximise crop production.

Author Contributions **Murad Ellafi:** conceptualization, methodology, formal analysis, writing—original draft, visualization, validation, investigation. **Hamdi A. Zurqani:** conceptualization, methodology, supervision, software, data curation, formal analysis, validation, investigation, writing—original draft, visualization, writing—review and editing, review of analysis. **Lynda K. Deeks:** Supervision, writing—review and editing, review of analysis. **Robert W. Simmons:** Supervision, writing—review and editing, review of analysis. All authors have read and agreed to the published version of the manuscript.

References

- Abbas A, Khan S (2007) Using remote sensing techniques for appraisal of irrigated soil salinity. In: MODSIM 2007 international congress on modelling and simulation. Modelling and Simulation Society of Australia and New Zealand, Bright
- Ahmed O, Ramadan A (2007) The effect of irrigation water on soil deterioration in the region of Wadi Ashati. In: Desert and desertification conference. Sabha University, Sabha, pp 1–10
- Akramkhanov A, Vlek PLG (2012) The assessment of spatial distribution of soil salinity risk using neural network. *Environ Monit Assess* 184:2475–2485. <https://doi.org/10.1007/s10661-011-2132-5>
- Asfaw E, Suryabagavan KV, Argaw M (2018) Soil salinity modeling and mapping using remote sensing and GIS: the case of Wonji sugar cane irrigation farm. *Ethiopia J Saudi Soc Agric Sci* 17:250–258. <https://doi.org/10.1016/j.jssas.2016.05.003>
- Bannari A, Guedon AM, El-Harti A, Cherkaoui FZ, El-Ghmari A (2008) Characterization of slightly and moderately saline and sodic soils in irrigated agricultural land using simulated data of advanced land imaging (EO-1) sensor. *Commun Soil Sci Plant Anal* 39:2795–2811. <https://doi.org/10.1080/00103620802432717>
- Bell J (2015) Machine learning with R, 2nd edn. Machine Learning. PACKT, Birmingham. <https://doi.org/10.1002/9781119642183.ch14>
- Brika B (2018) Water resources and desalination in Libya: a review. *PRO* 2:586. <https://doi.org/10.3390/proceedings2110586>
- CEDARE (2014) Libya Water Sector M&E Rapid Assessment Report. Monitoring & evaluation for water in North Africa (MEWINA) Project
- Cornelius-Brochier JV (1981) Wadi Al Shatti: drainage design. Tripoli, Libya
- Danenco (1980) Technical study for Jufra el Hamam project. Copenhagen, Denmark
- Douaoui AEK, Nicolas H, Walter C (2006) Detecting salinity hazards within a semiarid context by means of combining soil and remote-sensing data. *Geoderma* 134:217–230. <https://doi.org/10.1016/j.geoderma.2005.10.009>
- Elhag M (2016) Evaluation of different soil salinity mapping using remote sensing techniques in arid ecosystems. *Saudi Arabia J Sensors* 2016:1–8
- Ellafi MA, Deeks LK, Simmons RW (2021) Application of artificial neural networks to the design of subsurface drainage systems in Libyan agricultural projects. *J Hydrol Reg Stud* 35:1–17. <https://doi.org/10.1016/j.ejrh.2021.100832>
- Evans RO, Skaggs RW, Sneed RE (1991) Stress day index models to predict corn and soybean relative yield under high water table conditions. *J Am Soc Agric Eng* 34:1997–2005

- FAO (1988) Salt-Affected Soils and their Management [WWW Document]. Food Agric. Organ. URL <http://www.fao.org/docrep/x5871e/x5871e00.htm#Contents>. Accessed 5 Feb 18
- FAO (1994) Water quality for agriculture, Rev. 1. ed. FAO Irrigation and Drainage Paper 29, Rome, Italy
- FAO (2016) Country profile - Libya. Rome, Italy. <https://doi.org/10.1787/9487b828-en>
- FAO (2018) FAOSTAT statistical database
- Garajeh MK, Malakyar F, Weng Q, Feizizadeh B, Blaschke T, Lakes T (2021) An automated deep learning convolutional neural network algorithm applied for soil salinity distribution mapping in Lake Urmia. *Iran Sci Total Environ* 778:1–16. <https://doi.org/10.1016/j.scitotenv.2021.146253>
- Ghatak A (2019) Deep learning with R, Deep Learning with R. <https://doi.org/10.1007/978-981-13-5850-0>
- Gholami V, Sahour H, Hadian Amri MA (2021) Soil erosion modeling using erosion pins and artificial neural networks. *Catena* 196:1–11. <https://doi.org/10.1016/j.catena.2020.104902>
- Ghorbani MA, Deo RC, Kashani MH, Shahabi M, Ghorbani S (2019) Artificial intelligence-based fast and efficient hybrid approach for spatial modelling of soil electrical conductivity. *Soil Tillage Res* 186:152–164. <https://doi.org/10.1016/j.still.2018.09.012>
- Gorelick N, Hancher M, Dixon M, Ilyushchenko S, Thau D, Moore R (2017) Google earth engine: planetary-scale geospatial analysis for everyone. *Remote Sens Environ* 202:18–27. <https://doi.org/10.1016/j.rse.2017.06.031>
- Gupta GP, Prasher SO, Chieng ST, Mathur IN (1993) Application of DRAINMOD under semi-arid conditions. *Agric Water Manag* 24:63–80
- GWA (1999) Water and irrigation requirements for the most important crops in Libya [unpublished report]. Tripoli
- GWA (2003) Report on the Hammam agricultural project and the current drainage system in Jufra district. Tripoli, Libya
- GWA (2007) A field visit to Hammam agricultural project to investigate the Sokna flood. Tripoli, Libya
- Habibi V, Ahmadi H, Jafari M, Moeini A (2021) Mapping soil salinity using a combined spectral and topographical indices with artificial neural network. *PLoS One* 16:1–13. <https://doi.org/10.1371/journal.pone.0228494>
- Holzmann-Wakuti (1974) Hydrogeology of the Joufrah project area. Tripoli, Libya
- Italconsult (1976) Fezzan land reclamation project: Wadi-Shati Eshkeda area. Italy, Rome
- Jin P, Li P, Wang Q, Pu Z (2015) Developing and applying novel spectral feature parameters for classifying soil salt types in arid land. *Ecol Indic* 54:116–123. <https://doi.org/10.1016/j.ecolind.2015.02.028>
- Kale S (2011) Field-evaluation of DRAINMOD-S for predicting soil and drainage water salinity under semi-arid conditions in Turkey. *Spanish J Agric Res* 9:1142–1155
- Kale S (2012) Impact of drained and un-drained soil conditions on water table depths, soil salinity and crop yields. *African J Agric Res* 7:2935–2945. <https://doi.org/10.5897/AJAR12.101>
- Kandil H, Skaggs RW, Abdel Dayem S, Aiad Y (1995) DRAINMOD-S : water management model for irrigated arid lands , crop yield and applications. *Irrig Drain Syst* 9:239–258
- Kargas G, Chatzigiakoumis I, Kollias A, Spiliotis D, Kerkides P (2018) An investigation of the relationship between the electrical conductivity of the soil saturated paste extract E_{Ce} with the respective values of the mass soil/water ratios 1:1 and 1:5 (EC_{1:1} and EC_{1:5}). *PRO* 2:661. <https://doi.org/10.3390/proceedings2110661>
- Khan NM, Rastoskuev VV, Sato Y, Shiozawa S (2005) Assessment of hydrosaline land degradation by using a simple approach of remote sensing indicators. *Agric Water Manag* 77:96–109. <https://doi.org/10.1016/j.agwat.2004.09.038>
- Luo W, Jing WH, Jia ZH, Li J, Pan YX (2009) The effect of PET calculations in DRAINMOD on drain- age and crop yields predictions in a subhumid vertisol soil district. *Sci China Ser E Technol Sci* 52:1–5. <https://doi.org/10.1007/s11431-009-0349-0>
- Maas EV, Hoffman GJ (1977) Crop salt tolerance - current assessment. *ASCE J Irrig Drain Div* 103: 115–134. <https://doi.org/10.1061/jrcea4.0001137>

- Mohamed ES, Saleh AM, Belal AB, Gad AA (2018) Application of near-infrared reflectance for quantitative assessment of soil properties. *Egypt J Remote Sens Sp Sci* 21:1–14. <https://doi.org/10.1016/j.ejrs.2017.02.001>
- Morgan RS, El-hady MA, Rahim IS (2018) Soil salinity mapping utilizing sentinel-2 and neural networks. *Indian. J Agric Res* 52:524–529. <https://doi.org/10.18805/IJARe.A-316>
- Mousavi SZ, Habibnejad M, Kaviani A, Solaimani K, Khormali F (2017) Digital mapping of topsoil salinity using remote sensing indices in Agh-Ghala plain. *Iran ECOPERSIA* 5:1771–1786
- NCCD (2005) The national plan to combat desertification. Tripoli, Libya
- Nguyen K, Liou Y, Tran H, Hoang P, Nguyen T (2020) Soil salinity assessment by using near-infrared channel and vegetation soil salinity index derived from Landsat 8 OLI data : a case study in the Tra Vinh Province, Mekong Delta, Vietnam. *Prog Earth Planet Sci* 7:1–16
- Pourgholam-Amiji M, Liaghat A, Ghameshlou AN, Khoshravesh M (2021) The evaluation of DRAINMOD-S and AquaCrop models for simulating the salt concentration in soil profiles in areas with a saline and shallow water table. *J Hydrol* 598:1–10. <https://doi.org/10.1016/j.jhydrol.2021.126259>
- Qadir M, Boers TM, Schubert S, Ghafoor A, Murtaza G (2003) Agricultural water management in water-starved countries: challenges and opportunities. *Agric Water Manag* 62:165–185. [https://doi.org/10.1016/S0378-3774\(03\)00146-X](https://doi.org/10.1016/S0378-3774(03)00146-X)
- Ramadan A, Elssaidi MA (2017) Salinization of agricultural soils as development issues in Wadi Al-Shatti region. *J Mar Sci Environ Technol* 3:29–45
- Schultz B, Zimmer D, Voltman WF (2007) Drainage under increasing and changing requirements. *Irrig Drain* 56:S3–S22. <https://doi.org/10.1002/ird>
- Seifi M, Ahmadi A, Neyshabouri M-R, Taghizadeh-Mehrjardi R, Bahrami H-A (2020) Remote and Vis-NIR spectra sensing potential for soil salinization estimation in the eastern coast of Urmia hyper saline lake. *Iran Remote Sens Appl* 20:1–9. <https://doi.org/10.1016/j.rsase.2020.100398>
- Selvaperumal A, Thiyagarajan G, Vallalkannan S, Muthuchamy I (2020) DRAINMOD – calibration and validation for prediction of drainage coefficient and water table depth. 39:65–74. <https://doi.org/10.9734/CJAST/2020/v39i930607>
- Shahabi M, Jafarzadeh AA, Neyshabouri MR, Ghorbani MA, Valizadeh Kamran K (2016) Spatial modeling of soil salinity using multiple linear regression, ordinary kriging and artificial neural network methods. *Arch Agron Soil Sci* 63:151–160. <https://doi.org/10.1080/03650340.2016.1193162>
- Skaggs RW, Youssef MA, Chescheir GM (2012) DRAINMOD: model use, calibration, and validation. *Trans ASABE* 55:1509–1522. <https://doi.org/10.13031/2013.42259>
- Smedema LK, Abdel-Dayem S, Ochs WJ (2000) Drainage and agricultural development. *Irrig Drain Syst* 14:223–235. <https://doi.org/10.1023/A:1026570823692>
- Stefan F, Guenther F (2019) Package ‘neuralnet’ [WWW Document]. URL <https://cran.r-project.org/web/packages/neuralnet/neuralnet.pdf>. Accessed 13 May 2020
- Sun J (2012) Learning algorithm and hidden node selection scheme for local coupled feedforward neural network classifier. *Neurocomputing* 79:158–163. <https://doi.org/10.1016/j.neucom.2011.09.019>
- United Nations, 2019. World Population Prospects: The 2019 Revision, Online Edition [WWW Document]. United Nations Popul. Div. URL <http://data.un.org/Data.aspx?q=LIBYA&d=PopDiv&f=variableID%3A12%3BcrID%3A434>. Accessed 7 Sept 2021
- USDA (1954) Diagnosis and improvement of saline and alkaline soils. *Agric Handb* 60(18):348. <https://doi.org/10.2136/sssaj1954.03615995001800030032x>
- USGS (2021) U.S. Geological Survey [WWW Document]. Landsat Mission. URL https://www.usgs.gov/core-science-systems/nli/landsat/landsat-5?qt-science_support_page_related_con=#qt-science_support_page_related_con. Accessed 14 Apr 2021
- Wahba MAS, Kandil H, Gobran A (2002) Evaluation of DRAINMOD-S for simulating water table management under semi-arid conditions. *Irrig Drain* 51:213–226. <https://doi.org/10.1002/ird.54>

- Wang X, Mosley CT, Frankenberger JR, Klavdivko EJ (2006) Subsurface drain flow and crop yield predictions for different drain spacings using DRAINMOD. *Agric Water Manag* 79:113–136. <https://doi.org/10.1016/j.agwat.2005.02.002>
- Wang J, Peng J, Li H, Yin C, Liu W, Wang T, Zhang H (2021) Soil salinity mapping using machine learning algorithms with the Sentinel-2 MSI in arid areas. *China Remote Sens* 13. <https://doi.org/10.3390/rs13020305>
- WBO (2000) Drainage in developing countries: a review of institutional arrangements. Wageningen, The Netherlands
- Wheida E, Verhoeven R (2007) An alternative solution of the water shortage problem in Libya. *Water Resour Manag* 21:961–982. <https://doi.org/10.1007/s11269-006-9067-6>
- Yang J, Wang X, Wang R, Wang H (2020) Combination of convolutional neural networks and recurrent neural networks for predicting soil properties using Vis–NIR spectroscopy. *Geoderma* 380:1–16. <https://doi.org/10.1016/j.geoderma.2020.114616>
- Zurqani HA, Post CJ, Mikhailova EA, Schlautman MA, Sharp JL (2018) Geospatial analysis of land use change in the Savannah River basin using Google earth engine. *Int J Appl Earth Obs Geoinf* 69:175–185. <https://doi.org/10.1016/j.jag.2017.12.006>

Mr. Murad Ellafi is a PhD student in agricultural water management at Cranfield University. After gaining his bachelor’s degree in Agricultural Sciences (Soil and Water Science) from the University of Tripoli, Libya in 2010, Mr. Ellafi worked as a Teaching Assistant between 2012 and 2015. Mr. Ellafi gained his MSc in Environmental Water Management from Cranfield University in 2018. His MSc thesis was focused on understanding drain-aquifer interactions in low-lying agricultural drainage systems in east England. Mr. Ellafi’s current PhD research is focusing on applying machine learning to predict input parameters required for drainage design in arid and semi-arid areas.

Dr. Hamdi A. Zurqani is an Assistant Professor of Geospatial Science in Natural Resource Management and Conservation at the University of Arkansas Agricultural Experiment Station, Arkansas Forest Resources Center, University of Arkansas at Monticello, Monticello, AR, USA. He is also an FAA (i.e., Pt107) Certified sUAS/Drones Pilot, and has used this skill to enhance his knowledge of remote sensing and GIS. Dr. Zurqani is a recognized expert as a result of his internationally acclaimed work in the areas of environmental information science, remote sensing, geospatial analysis, land evaluation, sustainability, pedology, and soil science education. He has conducted research across the world, including the United States of America, and Africa, and has served as PI, co-PI, or co-investigator on several grants-funded research projects. Dr. Zurqani is highly collaborative as evidenced by his publications. He is the author and co-author of many peer-reviewed publications, book chapters, and technical publications (including teaching laboratory manuals). He also edited two books with Springer Nature (i.e., “The Soils of Libya”, and “Environmental Applications of Remote Sensing and GIS in Libya”), and has published widely in many peer-review journals (e.g., *International Journal of Applied Earth Observation and Geoinformation* (Elsevier); *Remote Sensing in Earth Systems Sciences* (Springer Nature); *Scientific Reports* (Nature); *Frontiers in Environmental Science* (Frontiers); *Geoderma* (Elsevier); *Land* (MDPI); *Urban Forestry & Urban Greening* (Elsevier), and others). Dr. Zurqani is a member of the Editorial Board for *Remote Sensing* (MDPI) Journal, counseling outcome, and research evaluation. He also was appointed to serve as a Guest Editor for the Special Issue “Applications of Remote Sensing in Earth Observation and Geo-Information Science”. In addition, Dr. Zurqani conducted peer-review for many journals including *Journal of Environmental Informatics*, *Applied Sciences*, *SN Applied Sciences*, *Remote Sensing*, *Geo-spatial Information Science*, *AgriEngineering*, *Sensors*, *Heliyon*, *Geosciences*, *Land*, *Soil Systems*, *Water*, *Agronomy*, *Agriculture*, *Resources*, *Sustainability*, *Arid Land Research and Management*, *Quaestiones Geographicae*, *Geocarto International*, *International Journal of Environmental Research and Public Health*, *Natural Hazards*, and *Conference of the Arabian Journal of Geosciences*. Dr. Zurqani conducts cutting-edge research in the field of

Environmental Information Science, Remote Sensing, Land use management/planning, change detection of landscape degradation, and Geographic Information System (GIS) models. He has focused his research efforts on the development of novel applications for new technologies in analyzing spatial data, remote sensing, geostatistical modeling of environmental changes such as erosion, mapping and predicting soil salinity, and land use/land cover changes. His new publications include: "Mapping and Quantifying Agricultural Irrigation in Heterogeneous Landscapes Using Google Earth Engine" in the *Journal of Remote Sensing Applications: Society and Environment*; "Evaluating the integrity of forested riparian buffers over a large area using LiDAR data and Google Earth Engine" in the *Journal of Scientific Reports*; "Mapping Urbanization Trends in a Forested Landscape Using Google Earth Engine" in the *Journal of Remote Sensing in Earth Systems Sciences*; "Geospatial analysis of land use change in the Savannah River Basin using Google Earth Engine" in the *International Journal of Applied Earth Observation and Geoinformation*; and "Application of Non-Hydraulic Delineation Method of Flood Hazard Areas Using LiDAR-Based Data" as well as "Assessing ecosystem services of atmospheric calcium and magnesium deposition for potential soil inorganic carbon sequestration" in the *Geosciences Journal*.

Dr. Lynda K. Deeks is an experienced soil physicist/hydrologist at Cranfield University. She graduated in Geography from the University of Plymouth, UK, and subsequently studied for a PhD in Physical Geography at the University of Plymouth. Her PhD, investigated preferential and matrix flow in a mole drained soil block and led on to Post-Doctoral positions based at the University of Plymouth and the Scottish Crop Research Institute, Dundee. She joined Cranfield University in 2003, and undertakes research and teaches in research areas related to soil hydrology, soil quality/health and sustainable soil management.

Dr. Robert W. Simmons is a Reader in sustainable soil management and has been at Cranfield University since 2008. Dr. Simmons gained his Masters in Agricultural Engineering (Soil Conservation option) from Silsoe College, Cranfield University in 1992. He went on to gain a PhD from the University of Kent which investigated the use of polyacrylamide soil conditioners to mitigate soil surface crusting in 1998. Dr. Simmons then spent ten years (1998 = 2008) working in South and Southeast Asia seven of which were for the International Water Management Institute. Rob is an excellent field and research scientist, working with farmers, agronomists, NGOs and government agencies. His research continues to address some of the fundamental sustainable soil management challenges facing UK and global agriculture today. Throughout his career, Dr. Simmons has used his research to inform his teaching of agricultural and environmental engineers. He continues to inspire students with his brand of enthusiastic and practical 'know-how', underpinned by robust scientific evidence.

Surface Water Potential and Suitable Sites Identification for RWH in the Semi-Arid and Arid Watershed of Wadi Sammalus, Northeast Libya Using GIS and Remote Sensing Approach



Salah Hamad and Nilanchal Patel

Abstract The watershed under investigation is located in northeast Libya and lies in arid (downstream) and semi-arid (upstream) regions with an aerial extent of 1511 km². Rainfed agriculture and grazing form the regular economic activities of the local community, and they face challenges related to scarce water resources and soil loss due to less rainfall and higher runoff and evaporation. Exploiting Rainwater Harvesting (RWH) is one of the most promising solutions to these challenges. In this study, remote sensing (RS) and geographic information system (GIS) approaches have been employed in assessing the potential surface water and identifying potential RWH sites, which are both critical tasks for effective water resource management. The runoff was estimated using Soil Conservation Service Curve Number (SCS-CN) method, where the CN is computed by the LULC map generated from Landsat 8 OLI imagery that was intersected with the HSG layer. Moreover, due to the unavailability of rainfall data in the study area, the precipitation data from Multi-satellite Retrievals for Global Precipitation Measurement (IMERG GPM) was used in the runoff calculation, where the average ten-year runoff volume was estimated as 26.5 Mm³. The RWH suitability sites were delineated based on the Analytical Hierarchy Process (AHP) method, where the criteria selection was performed based on a literature review, followed by weighted overlay analysis to determine the layer of suitable sites. The results showed that optimal and suitable sites cover 2.5% and 9% of the watershed, while the rest of the watershed is covered by moderate, marginal, and unsuitable sites covering 17.7%, 25%, and 45.7%, respectively. The watershed is found to have the potential to support RWH for soil and water conservation. Also, the RWH structures map was generated according to the indigenous dominant types.

S. Hamad (✉)

Faculty of Natural Resources and Environmental Science, Omar Al Mukhtar University,
Al Baydah, Libya

e-mail: Salah.Hamad@omu.edu.ly

N. Patel

Department of Remote Sensing, Birla Institute of Technology Mesra, Ranchi, India

e-mail: npatel@bitmesra.ac.in

Keywords Rainwater harvesting (RWH) · Soil conservation service curve number (SCS-CN) · Analytical hierarchy process (AHP) · Multi-satellite retrievals for global precipitation measurement (IMERG GPM) · Al Jabal Al Akhdar

1 Introduction

Water resources are under pressure due to unprecedented urban growth, unsustainable consumption, climate change, and weak institutional and regulatory governance, which further exacerbate water scarcity. Also, water scarcity erodes community socio-economic sustainability since it represents a limiting factor in development. Therefore the calls for new water planning and management measures are crucial to avoid escalating conflicts and to reverse environmental degradation (Ragab and Prudhomme 2002; Odhiambo 2017). In particular, arid and semi-arid regions all over the world are suffering from severe water scarcity, as water imbalances their ecosystems which is further aggravated by the rising challenges of exacerbating climate change. Additionally, the arid ecosystems are fragile due to periodic droughts and over-exploitation of natural resources, which are mostly affected during periods of drought and vulnerable to the precipitation reduction foreseen by different climate change scenarios; also the arid and semi-arid watersheds are more sensitive to hydrological processes and water resource sustainability compared with humid regions (Kadam et al. 2019; Goyal et al. 2013). Among the various measures used to combat water scarcity and to cope with climate change in arid and semi-arid watersheds is the Rainwater Harvesting (RWH), which is one of the resource conservations measures that has emerged as one of the efficient strategies for increasing groundwater and surface resources. Whereas RWH pledged to supplement surface water and groundwater to cope with the climate-change imbalance between water supply and demand, it also provides adequate amounts of water that may not be sufficient to meet the growing demand, but can help mitigate rising demand. Also, RWH can be considered as a potential method of inducing collection, storage, delivery, conservation of local surface runoff, and use of rainwater for various purposes, which can alleviate the water scarcity and soil loss in arid and semi-arid regions (Stec and Kordana 2015; Boers 1994; Rikalovic et al. 2014). On the other hand, RWH can also facilitate the process of concentration of runoff from a large area within the catchment. The concentrated runoff may be used later on in a smaller space. Besides, RWH encourages the production of more crops in rainfed areas by using the harvested water to increase and stabilize the region's production levels, and provide enough water suitable for domestic use and cattle watering. The success of RWH technology depends heavily on the identification of appropriate sites and their technical design and also to several spatial and environmental factors and considerations (Matomela et al. 2020; Alwan et al. 2020; Bakir and Xingnan 2008; Al-Adamat et al. 2012). One of the essential steps in implementing RWH is the estimation of the potential runoff as the success of RWH depends strongly on the quantity of water that can be collected under the given climatic conditions, in addition to the environmental factors. Proper

understanding of the spatial and temporal hydrological characteristics of a watershed is critical to the management of the watershed and also, its natural resources such as water, soil, and vegetation (Sayl et al. 2019; Matomela et al. 2019). Modeling the rainfall-runoff process forms the integral part of watershed management (Sindhu et al. 2013). However, there are many different methods for estimating the runoff in the watershed; one of the most widely used is the Soil Conservation Service Curve Number (SCS-CN) method, which has been developed by the Soil Conservation Service of the U.S. Department of Agriculture in 1954 (Currently known as the Natural Resources Conservation Service) in the National Engineering Handbook (NEH-4, Section 4) and has been revised with time (Mishra and Singh 2003). SCS-CN is commonly used to compute direct surface runoff from rainfall events using CN derived from watershed spatial characteristics. CN is an index developed by the Natural Resource Conservation Service (NRCS), and represents the potential for storm water runoff within a drainage area. Estimating runoff from rainfall over watershed is a complicated process since the process takes into account many factors affecting direct runoff generation such as physiography, precipitation, and land cover. Both Geographic information system (GIS) techniques and remote sensing (RS) data are integrated with SCS-CN, where the (DEM) data is used for watershed delineation and extraction of topographic characteristics and satellite images for land cover mapping, in addition to soil data. The satellite precipitation estimates can be used in the runoff computation in case of absence or scarcity in recorded rainfall data.

Selecting a potential site for RWH techniques is vital in arid and semi-arid regions since it contributes to the increase of water availability and maximize the land productivity (Alwan et al. 2020). The identification of suitable sites for RWH consists of four steps: a selection of appropriate criteria, classification of suitability for each factor, GIS analysis, and site identification (Adham et al. 2018). Several methodologies and criteria introduced for the RWH site suitability mostly depend on using Multi-Criteria Decision-Making (MCDM) and Analytical Hierarchy Process (AHP) based on the weighted overlay and fuzzy logic using geospatial techniques. The concept of Multi-criteria analysis is a part of decision analysis that provides a set of procedures for analyzing complex decision problems. By dividing the decision problem into small understandable parts, i.e., criteria, it is possible to examine each piece and logically combine them to produce a meaningful solution (Malczewski 1999). Based on the weighted sum, the AHP finds a suitable location for carrying out RWH activities using selected criteria that provide a suitable and straightforward tool for selecting the optimal sites for RWH, and the generated suitability map can yield good quality results while selecting the appropriate criteria (Kadam et al. 2019; Wu et al. 2018; Badhe et al. 2020; Ammar et al. 2016). In MCDM, GIS and RS technologies have been applied by many researchers to investigate land suitability for RWH (Shalamzari et al. 2019). Nevertheless, little attention has been paid to the performance of these methods in selecting suitable sites (Ammar et al. 2016).

This research concerns the Wadi Sammalus watershed located in northeast Libya in which the Libyan Secretariat of Agriculture Land Reclamation carried out a water resources study of southern flanks of Al Jabal Al Akhdar during the period 1974-

1976, which was implemented by the Frnlab consultant office (Frnlab 1974; Frnlab 1976). Rainfall-runoff measurements were undertaken during the years (1978–1980) in specific parts of the watershed by the Arlab consultant office during the complementary investigation of surface water, groundwater, and climatological survey (Arlab 1983). Since that time, hydrological data have not been recorded until the present time, nor even the implementation of what was planned from the studies. Thus, to support the essential background and knowledge for watershed we determined Spatio-temporal hydrological characteristics which are crucial for better management, planning, and development. Runoff, rainfall information, and spatial characteristics are required for the site suitability analysis to implement RWH techniques for flood protection and soil conservation measures. In this context, the present research was conducted to estimate surface runoff using the SCS-CN method and identify suitable water harvesting site using the AHP method in Wadi Sammalus of the watershed employing GIS techniques and RS.

2 Materials and Methods

2.1 Study Area

Libya's surface water resources are limited to the northern coastal areas, which experience sufficient rainfall. The highest precipitation rate for the entire country with an annual average of more than 500 mm occurs in Al Jabal Al Akhdar, which is a series of ridges, lies along the north-eastern coast of the country. Al Jabal Al Akhdar, as shown in (Fig. 1) is divided topographically into two parts such as the northern slopes in which the watersheds flow to the north (Mediterranean Sea), and the southern slopes in which the watersheds flow to the south through long, wide, flat wadi those gradually disappear to become large spreading zones. Only small

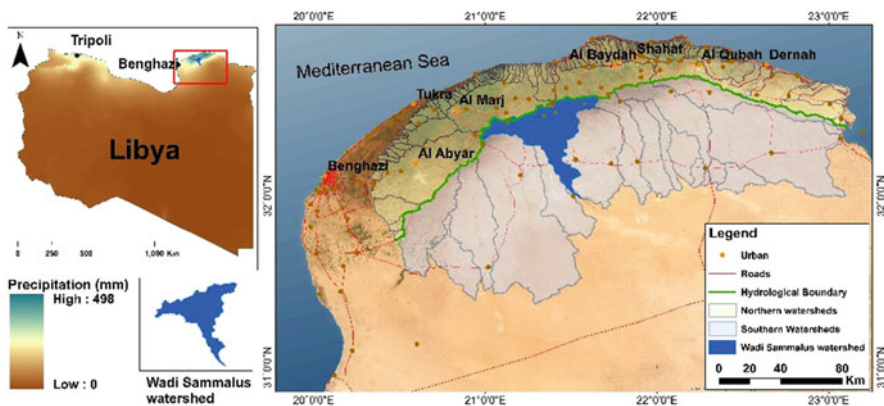


Fig. 1 Location of Wadi Sammalus watershed. (Adopted from: Fick and Hijmans 2017)

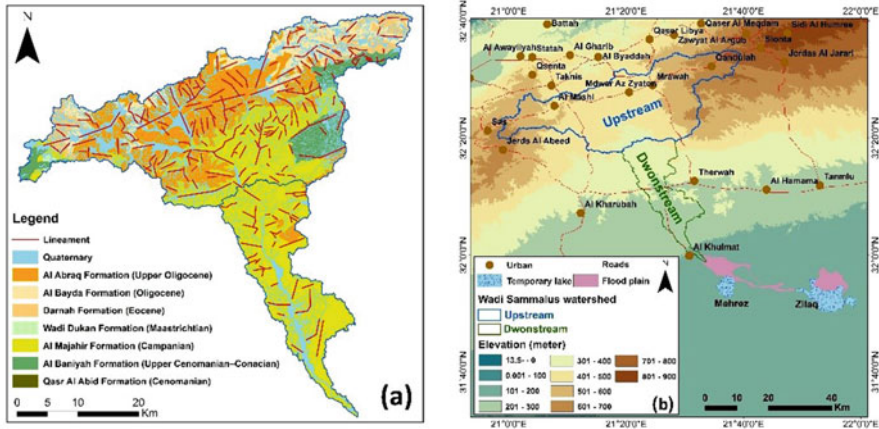


Fig. 2 (a) Geological map Wadi Sammalus watershed (Adopted from: IRC 1974), and (b) Elevation map. (Adopted from: USGS 2000)

quantities of the seasonal runoff are collected when it occurs, and the rest, unfortunately, evaporates in the south or mingle with the Mediterranean Sea. Moreover, meteorological and hydrological data are scarce. These factors led to challenges in the assessment and estimation of available water resources, and consequently, lack of investment and development in surface water. Nevertheless, previous hydrological studies performed during the seventies and eighties indicated the presence of considerable potential of surface water which can be inferred from the Wadi’s runoff (GWA. 2006).

The wadi Sammalus watershed in which the present study was performed is one of the south Al Jabal Al Akhdar watersheds. The exposed geological formation in the study area mainly consists of marine carbonate rocks from the Late Cretaceous age to Quaternary, as shown in (Fig. 2a). The first study refers to the delineation of watersheds using the United States Geological Survey (USGS) topographic maps produced in 1963 (Frnlab 1974, 1976; Arlab 1983). Lack of hydrological data has led to uncertain knowledge of surface water followed by improper management and inadequate concentrations of the available surface water in Al Jabal Al Akhdar (Hamad 2019). The watershed, as shown in (Fig. 2b), is located within the southern slope watersheds of Jabal Al Akhdar. It covers an area of approximately 1511.2 km². According to a Pan-African high-resolution Standardized Precipitation-Evapotranspiration Index (SPIE) drought (Peng et al. 2020), the upstream region is moderately wet, while the downstream part is moderately dry. Therefore, based on the physiographical and climatic characteristics the watershed is divided into two areas; the upstream with an aerial extent of 1062.34 km² which lies in the semi-arid zone that receives the most considerable rainfall, and the downstream with an area of 448.66 km² which lies in the arid region. It is broad in the upstream sector and narrows downstream to form a semi-rectangular shape.

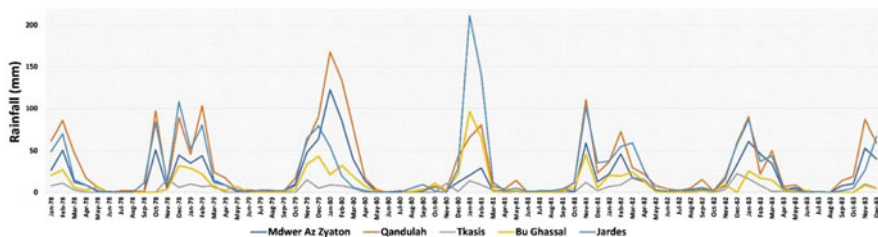


Fig. 3 Time series of rain gauges records. (Adopted from: Arlab 1983)

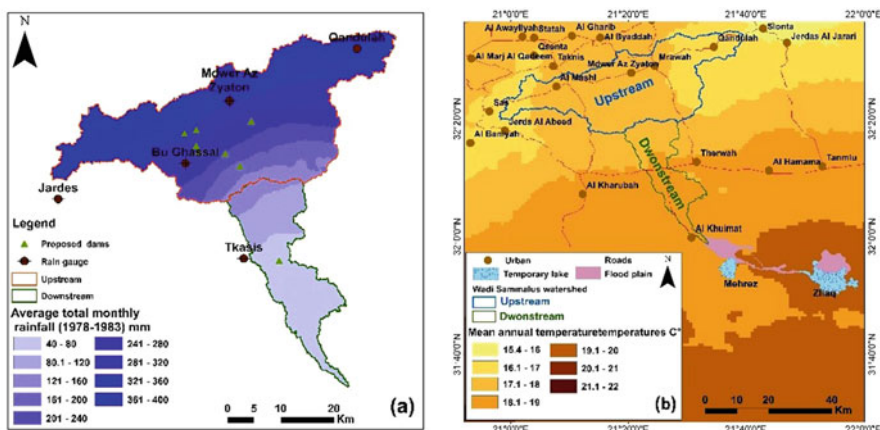


Fig. 4 (a) Precipitation map (Adopted from: Arlab 1983), (b) Temperature map. (Adopted from: Fick and Hijmans 2017)

The air masses over the Mediterranean Sea forms an area of convergence between the air of Eurasian and Saharan origin, which is often rendered unstable by the sea. The result is the occurrence of frequent cyclonic precipitation over Al Jabal Al Akhdar, enhanced by orographic uplift, which may be intense (Allan et al. 1975). The precipitation mainly occurs from October to April, and the maximum rainfall values are observed in December and January. Extended dry periods frequently occur within the wet seasons. Precipitation is characterized by spatial and temporal variability as ascertained by the rain gauge data (Fig.3) (Arlab 1983).

Runoff occurs during the rainy winters from November to April, where the average annual precipitation ranges from 350 mm in the northern parts to 60 mm in the south (Fig. 4a). The runoff concentrates from the upstream parts in the main wadi channel downstream, which is 95.5 km long. During the extreme runoff events, the flood continues to fill the flood plains and temporary lakes, which represent low areas south of the flood plains known locally as *Balat* in which the is water harvested for dry seasons in open trenches of 1 km long and 43 m wide. Some of the runoff in upstream is controlled by the check dams and cisterns, and further collected by the underground storage tanks which are both popular RWH structures and are mostly

practiced in the southern Al Jabal Al Akhdar region constructed through different times. Still, unfortunately, most of the runoff flows to reach the downstream and spread across the flood plains, and are mostly lost by the evaporation due to higher temperatures in the south, as shown in (Fig. 4b), where the mean annual temperature (15-22 °C) increases southward. The coldest months are January and February (7-11 °C) and the warmest are June to August when the maximum temperatures reach over 40 °C (Hamad 2019). In the upstream, local communities practice rain-fed agriculture and grazing. Few people practice irrigation of different crops as they can drill water wells, which are highly expensive because of the deep groundwater. On the other hand, the downstream areas are characterized by grazing in the pasture land along with a few parcels of agriculture that depends on the seasonal floods.

2.2 Methodology

The method of study is summarized in the workflow stepwise, as shown in the flow chart (Fig. 5) based on the data given in (Table 1).

2.3 Stream Orders, Drainage Density and Slope

2.3.1 Stream Orders

The drainage basin analysis begins by designating the stream orders, which is a hierarchical ranking of streams proposed by (Strahler 1964). There are no tributaries to streams of the first order. The second-order streams and third-order streams develop from the confluence of the lower order streams, respectively, and so on (Chopra et al. 2005). Stream order analysis for mapping RWH is critical since streams of lower orders have higher permeability and infiltration and vice versa. Besides, dendritic drainage patterns indicate homogeneous soil texture and a lack of structural control (Adham et al. 2018; Sayl et al. 2019).

2.3.2 Drainage Density

Drainage density (Dd) is defined by (Horton 1945) as the total length of the streams divided by the area of the watershed (Dingman 1978). The higher Dd is an essential indicator of higher volumes of runoff and fast peaks of floods, whereas high Dd is the typical characteristic of sparse vegetation, impermeable soils, and mountainous terrain (Pallard et al. 2009; Bhat et al. 2019). The smaller the Dd of a watershed, the slower the surface flow and runoff, but in the meantime, infiltration increases (Şen 2008). Analysis of Dd has significant relevance for RWH potential as the lower the drainage density, the lower RWH potential (Sayl et al. 2019).

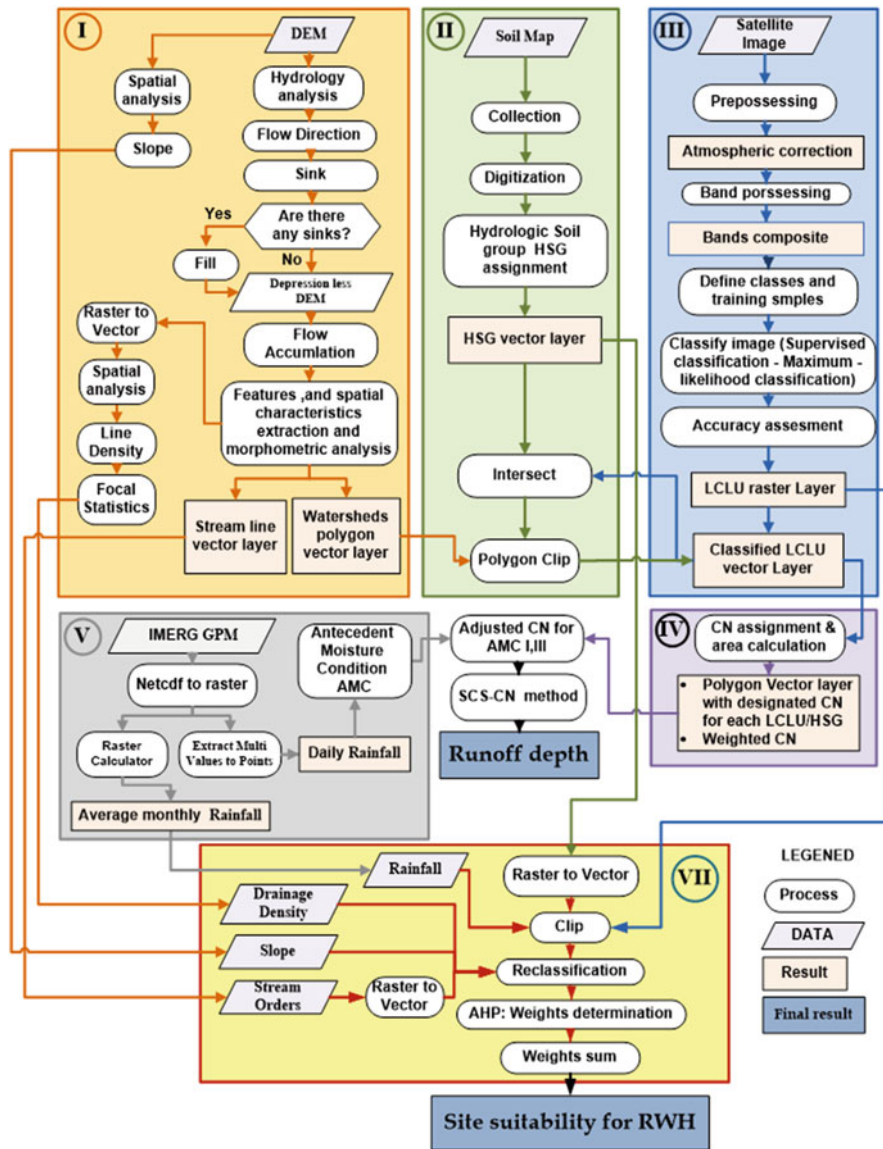


Fig. 5 Workflow steps of research implementation

Table 1 Data used for research implementation

Data	Description
Digital elevation model (DEM)	Digital elevation - shuttle radar topography Mission (SRTM) 1 arc-second global Units: meters, Spatial resolution: 30 m, C-band wavelength: 5.6 cm (USGS 2000)
Satellite image	Landsat 8 OLI [operational land imager] and TIRS [thermal infrared sensor] Spatial resolution: 15 - 30 m, multispectral. Path: 183 Rows: 38 (USGS 2013)
Soil	Soil Maps scale 1:50,000, (SELKHOZPROMEXPORT 1980) Libyan SOTER (ACSAD. 2005) Soil study in the vegetation cover of Al Jabal Al Akhdar report, Omer Al-Mukhtar University 2005 (OMU 2005)
Temperature	WorldCLIM database of high spatial resolution global weather and climate data (Fick and Hijmans 2017).
Precipitation	Integrated Multi-satellite Retrievals for Global Precipitation Measurement(Huffman et al. 2019) GPM IMERG final precipitation L3 1 month 0.1-degree x 0.1-degree V06 (GPM_3IMERGM 06) GPM IMERG late precipitation L3 1 day 0.1-degree x 0.1-degree V06 (GPM_3IMERGDL 06)

2.3.3 Slope

Slope affects the efficacy of water conservation, as the surface runoff depends on the slope of an area. The steeper the slope, the faster is the surface flow arrival to the outlet (Şen 2008). The slope of a hill determines the availability of moisture because it determines the amount of runoff. Topography affects the cultivation of vegetables, therefore affecting water conservation. Linear profiles on the topsoil have widespread plant cover compared to the concave profiles on which the plant cover at the bottom of the slopes is much more distributed (Nganga et al. 2019; Martín-Moreno et al. 2016). The slope directly affects runoff generation and the transformation of the rainfall to runoff. The slope should be as gentle as possible; the occurrence of a higher slope leads to rapid and higher runoff rates and increased erosion rate (potential soil loss) thereby decreasing the scope of RWH (Rai et al. 2017; Shadmehri Toosi et al. 2020).

Stream orders, stream length, and drainage density were generated using the Digital Elevation Model (DEM) that were processed according to the workflow in step I (Fig. 5) using the hydrology toolset provided in ESRI ArcGIS software Spatial Analyst extension (ESRI 2016). The Dd was computed by linear density computation function in ESRI ArcGIS software Spatial Analyst extension and was followed by the implementation of Focal Statistics, which computes the statistic of each input cell location within a designated neighborhood around it. The slope was generated through DEM using the slope function in ESRI ArcGIS software.

2.4 Runoff Estimation

2.4.1 Soil and the Landcover /Land Use (LULC)

Although soil and LULC are an essential part of the SCS-CN method, also both are vital in determining the suitability of the RWH. Soil permeability is an important parameter that controls the infiltration ratio and water storage in the soil layers. Due to their capacity to hold a higher water content, the fine and medium-textured soils are more suitable for RWH. The potential soils for RWH should have a greater water retention capacity. Soils with a high content of clay have a relatively higher runoff depth and do not allow more infiltration, while sandy soils have lower runoff and greater infiltration (Glendenning et al. 2012; Ibrahim et al. 2019). The LULC is one of the essential criteria for selecting suitable sites for RWH as the watershed's hydrological response is affected by the LULC change and rainfall. The soil and LULC and their temporal and spatial variability are considered the most critical factors affecting the intensity and frequency of surface runoff and soil erosion (Table 2). Also, inappropriate LULC or poor soil may accelerate water runoff and soil erosion dynamics leading to unsustainable land degradation processes (Lucas-Borja et al. 2019; García-Ruiz 2010; Nunes et al. 2011; Dunjón et al. 2004).

Table 2 Hydrologic soil groups (HSGs) (USDA 2009)

HSG	Soil texture class	Runoff potential
A	Sand	Low
B	Sandy loam, Loamy sand	Moderately low
C	Clay loam, Silty clay loam, Sandy clay loam, Loam, Silty loam, Silt	Moderately high
D	Clay, Silty clay, Sandy clay	High

For the study area soil data (Table 1) represents the Soil Terrain Digital Database (ACSAD 2005) which was compiled by the Libyan General Water Authority and the Arab Center for Studies of Arid Zones (ACSAD) in 2005. In addition, the study also includes the soil maps (in scale of 1:50,000) prepared by the Libyan Secretariat of Agriculture (SELKHOZPROMEXPORT 1980), where the soil data is processed as illustrated in the workflow step II in (Fig. 5). HSG was assigned according to (USDA 2009). LULC classification is one of the most widely used applications in RS. Classification of LULC was carried out, as illustrated in the workflow step III of the (Fig. 5) using Landsat 8 OLI, that was processed in Quantum GIS (QGIS) Semi-Automatic Classification Plug-in (SCP) which carry out semi-automatic classification employing both supervised and unsupervised techniques. The pre-processing of the images was accomplished using DOS1 for atmospheric correction and the classification process was performed using supervised Maximum-likelihood (ML) algorithm (Congedo 2016). Since the SCS-CN method is susceptible to CN value, which is basically a coefficient that relates the rainfall to runoff and depends upon the LULC and HSG (Ahmad and Verma 2018), therefore it is essential to determine this parameter accurately. The LULC and HSG thematic layers were intersected, and each polygon in the output layer was assigned the designated CN value according to NEH-4 (1997) standard lookup tables (NRCS 1986; USDA 2004).

2.5 Precipitation

Rainfall is one of the essential variables in rainfall-runoff modeling, where watershed hydrological modeling requires reliable rainfall data in both time and space to maintain the watershed's rapid hydrologic response. Average annual rainfall data is one of the prerequisites for RWH structures. More precipitation on an area leads to higher RWH potential (Ammar et al. 2016; Shadmehri Toosi et al. 2020; Gilewski and Nawalany 2018).

The precipitation for the study area is unavailable except for the period previously mentioned (Arlab 1983). Therefore, the study used satellite precipitation products (SPPs), which recently gained importance and more attention because they represent high space-time variability. The SPPs are advantageous over ungauged watersheds, especially in mountainous and oceanic regions (Gado et al. 2017; Soo et al. 2020; De Coning and Poolman 2011). The commonly used data sources of SPPs are the

Integrated Multi-satellite Retrievals for Global Precipitation Measurement (IMERG GPM), which is the successor of the Tropical Rainfall Measuring Mission (TRMM) mission that has provided high-quality precipitation estimates for almost two decades (Huffman et al. 2019; Gilewski and Nawalany 2018). Accordingly, the study relied on data of IMERG GPM as given in (Table 1) and was processed as illustrated in the workflow step V in (Fig. 5).

2.6 Computation of Runoff by SCS-CN Method

The SCS-CN method depends mainly on the rainfall parameter P to estimate the runoff depth Q. However, the SCS curve number aims to determine the ability of soils to allow infiltration of water concerning LULC and antecedent soil moisture condition (AMC). The AMC plays an important role in determining peak flow along with rainfall, catchment shape, and drainage density, therefore, AMC refers to the wetness of the soil surface and/or the available amount of moisture in the soil profile, and also the saturation degree before the start of the storm. Three AMC (I, II & III) represent different soil conditions and rainfall and are related to the dormant and growing seasons, as given in (Table 3). AMC-I represents the lowest runoff potential due to very dry soils, AMC-II represents the average moisture condition of the soil, and AMC- III corresponds to the highest runoff potential, which occurs practically when the watershed soil is saturated by antecedent rains (Nayak et al. 2020; Amutha and Porchelvan 2009; Mishra and Singh 2003). Runoff potential can also be classified according to CN_w as high runoff potential if CNII ranges from 75 to 100, moderate runoff if CNII ranges from 50 to 75, and low potential if CNII ranges from 26 to 50 (Ahmad and Verma 2018).

After the assignment of CN values based on LULC and HSG, as shown in workflow step IV and V in (Fig. 5), which is applied only to AMC-II that is further used to derive CN values for AMC-I and III. Correction factors are therefore necessary in case the weighted curve number CN_w is adjusted to the AMC condition using the following equations (Rodhe 2012; Viji et al. 2015).

$$CN_I = \frac{4.2 * CN_{II}}{10 - (0.058 * CN_{II})} \quad (1)$$

Table 3 Antecedent Moisture Conditions (NRCS 1986)

AMC	Total 5-day Antecedent rain fall (mm)	
	Dormant season	Growing season
I	Less than 12.7	Less than 35.6
II	12.7 to 27.9	35.6 to 53.3
III	More than 27.9	More than 53.3

$$CN_{III} = \frac{23 * CN_{II}}{10 + 0.13 * CN_{II}} \quad (2)$$

The weighted curve number CN_w is calculated according to the following equation:

$$CN_w = \sum CN_i * \frac{A_i}{A} \quad (3)$$

where CN_i the curve number for each LULC and HSG polygon, A_i is the area of each LULC and soil group polygon for given CN_i, and A is the total area of the watershed. The SCS-CN equation for calculation of runoff depth is as follows:

$$Q = \frac{(P - 0.2S)^2}{(P + 0.8S)} \quad (4)$$

where Q is the runoff depth, P is the rainfall, and S is the potential maximum soil retention, which is calculated from CN value as follows:

$$S = \frac{25400}{CN} - 254 \quad (5)$$

2.7 RWH Site Suitability

2.7.1 Site Suitability

Site suitability for RWH depends on the determination of the best site from a set of potential sites by analyzing all the characteristics of the candidate sites (Mugo and Odera 2019). RWH suitability site analysis was carried out following the workflow step VII (Fig. 5) in which different weights were assigned to the different criteria. The weights were ranked and assigned relative importance values according to Saaty's scale of importance (Saaty 2008). This resulted in a suitability layer with the ranks of the potential sites ranging from 1 to 9. Sites with a value of 1 are considered unsuitable and those with a value of 9 are considered highly suitable. The literature review showed that various scholars used different criteria. Nevertheless, they mostly agreed on the necessity to include slope, land cover, soil texture, runoff, and/or rainfall. For the study area, the criteria for locating the specific potential sites for RWH were selected according to the prevailing conditions and literature review (Shadmehri Toosi et al. 2020; Adham et al. 2018; Buraihi and Shariff 2015; Krois and Schulte 2014; Ahmad and Verma 2018). Six spatial and environmental criteria were taken into account, as given in (Table 4). Previous studies showed that

Table 4 Influence, category and weights of the selected criteria

Criterion	Influence%	Category	Weightage
Slope Percent	20	0-4.27	1
		4.28-10.36	9
		10.37-17.98	7
		17.99-27.73	5
		27.74-77.4	1
Rainfall (mm)	20	<200	1
		200-250	5
		250-300	7
		300-360	9
Soil texture	15	Clay	9
		Silty clay	7
		Sandy clay	4
		Sandy clayey loam and sandy loam	3
Landcover	15	Agriculture	9
		Forest (Evergreen)	3
		Grassland/Shrubland	7
		Barren land	5
		Built-up	Restricted
Stream order	15	> 6	9
		6	8
		5	5
		< 4	1
Drainage density Km/km ²	15	< 0.01	1
		0.01-0.05	5
		0.05-0.1	7
		0.1-0.5	8
		> 0.5	9

consideration of only biophysical criteria as a primary factor does not guarantee the success of RWH structures. Although there is less consensus about the socio-economic factors as a secondary criterion, studies revealed that insufficient insight into the socio-economic aspects was one of the significant reasons that RWH sites failed to function appropriately in arid and semi-arid regions (Shadmehri Toosi et al. 2020). In the case of the study area, the social and economic criteria were not taken into account, not because of their insignificance but due to the spatial distribution of the population and urban activities, which are concentrated towards the higher parts of the upstream region. The rest of the watershed areas are entirely uninhabited without infrastructure and utilities. The ArcGIS weighted overlay tool was used to generate the final suitability thematic layer (ESRI 2016).

2.8 RWH Structures

The indigenous dominant type of RWH structures that have been successfully implemented in the study area by the local communities and Libyan government throughout the time comprise the cistern, check dams, gully plug, and terraces. The cistern is an impermeable underground reservoir on the shallow ground for the collection of rainwater and typically built out of stone or brick masonry, or concrete, with lime mortar or cement plaster (Konar 2007). Check dams and gully plugs are constructed in the Wadi channel for mitigating and reducing soil erosion by lowering the runoff velocity and to encouraging sediment to settle and stabilize gully heads. They are used extensively as a watershed management measures to address water and soil conservation issues. They have also proved as traditional RWH techniques with significant contributions to the sustainability and profitability of agricultural watersheds in many regions (Zeng et al. 2009; Rahmati et al. 2019; Hassanli and Beecham 2013; Oweis et al. 2012). Terracing is both a soil and water conservation measure designed to reduce erosion and remove excess surface water. It consists of an earth embankment with a channel constructed across the slope at a fixed vertical interval and at an acceptable horizontal slope (Blanco-Canqui and Lal 2010). The specific suitability of individual RWH structures generated by spatial analysis based on literature review, environmental characteristics, and local experiences in the study area are given in Table 5.

3 Results and Discussion

3.1 Spatial and Morphometric Analysis Characteristics

The various spatial parameters derived from the Digital Elevation Model (DEM) are given in Table 6. The overall area of Wadi Samalous Watershed 1511 km².

Table 5 Criteria of RWH structures (Mahmood et al. 2020; Ammar et al. 2016; Ahmad and Verma 2018)

	Wadi Sammalus Watershed	Slope (%)	Runoff potential	Stream order	Landcover	HSG
1	Cistern	< 5	Low	1-2	Agriculture, barren, shrub and scrubland	C
2	Check dams	<15	Moderate /high	3-4	Agriculture barren, shrub and scrubland	C and D
3	Gully plug	15-20	High	5-6	Hilly agriculture, barren, shrub and scrubland	C and D
4	Terracing	5-30	High	1	Hilly sparse vegetation, barren, shrub and scrubland	C and D

3.2 Stream Order

The stream order (Nu) in the study area varies from first order to seventh order, as shown in Fig. 6 and Table 7, where large numbers of streams are found in the first, second, and third orders. The first-order streams account for 77% of the total number of streams. The drainage network represents a dendritic pattern which reflects the homogeneity in the subsurface lithology. The highest stream length (Lu) is observed in the first order accounting for 51% of the stream lengths, which decreases as the stream order increases.

3.3 Drainage Density

The Dd computed in the study area, as shown in Fig. 6b ranges from 0.212 to 2.45, which is classified according to (Smith 1950) as coarse to very coarse that indicates high susceptibility to flooding and soil erosion.

3.4 Slope

The slope for the study area was generated from DEM, as shown in Fig. 6c which ranges from 16% to more than 30% in hilly regions of the northeast and northwest part of upstream, which is classified as moderate to steep slope. In comparison, the other areas of the watershed tend to be relatively moderate to gentle slope ranging from 1% to 10% except for Wadis channels sides and a few isolated hills.

3.5 Soil and LULC

Generally, the soils downstream are covered by dense gravel pavement, the deposits in the Wadi beds, and the alluvial plains range from coarse alluvium with a gravel pavement on the surface to silty alluvium with a surface of fine texture. The landscape is also characterized by weathered limestone hills with thin soil cover and a high proportion of bedrock outcropping. In the upstream, the Wadis are covered by the variable thickness of red or brown soil. The most common texture is silty loam found mainly at the bottom and slopes of the Wadi. Soils with a high content of clay, silty clay loam, and clay loam are primarily found on hills and are darker as compared to the dry ones found downstream (SELKHOZPROMEXPORT 1980; OMU 2005; ACSAD 2005). Soil data were mapped and classified according to HSG classification as given in Table 8 and Fig. 7a and b, where it is noticed that the Reddish brown lithosol soil is predominant among other soils, C (24.5%) and D (75.5%).

Table 6 Main spatial parameters of Wadi Samalous watershed

Wadi Sammalus Watershed	Area km ²	Perimeter Km	MIN Elevation M	MAX Elevation M	Average Elevation M	Average Slope %	Max Slope %	Average Aspect
Upstream	1062.34	341.52	350	774	501	8	36	S (202)
Downstream	448.66	224	177	486	322	5	35.3	S (180)

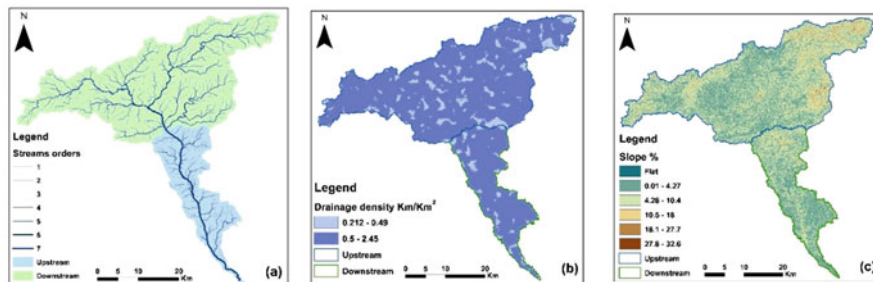


Fig. 6 (a) Stream orders, (b) Drainage density, and (c) Slope (c)

Table 7 Stream orders and lengths

Parameter	Orders						
	1	2	3	4	5	6	7
Stream order (Nu)	2633	574	149	32	5	2	1
Stream Length (Lu) km	1502	726	352	187	78	22	59.4

Table 8 Soil types of Wadi Samalous watershed

Soil type	Area km ²	Area %	HSG
Automorphic solonchaks	17.00	1.13	D
Brown arid differentiated soils	12.01	0.79	D
Brown lithosols	10.50	0.69	D
Cinnamonic lithosols	9.00	0.60	D
Dark rendzinas	74.46	4.93	D
Raddish brown arid differentiated soils	68.89	4.56	D
Raddish brown arid slightly differentiated	30.66	2.03	D
Raddish brown lithosols	829.75	54.91	D
Red ferrisiallitic soils	174.03	11.52	C
Red ferrisiallitic soils of a truncated profile	88.26	5.84	D
Red rendzinas	161.41	10.68	C
Siallitic cinnamon typical soils	35.02	2.32	C
Total area	1511	100	

The LULC was classified from Landsat8 OLI into six classes (Barren land, Built-up, Forest, Grassland/Shrubland, Irrigated agriculture) and Rainfed agriculture, as shown in Fig. 8a, and the area calculated for each class is given in Table 9. It is observed that 41% (or 620.30 km²) of the total watershed area falls into barren land and 27.62% (or 417.40 km²) to Grassland/Shrubland. All the classes of the LULC are dominant in the upstream region, while only (Barren land, Built-up, Grassland/Shrubland) and Rainfed agriculture are dominant in the downstream area. The HSG and LLC layers were intersected using ArcGIS software, and the CN values were assigned as given in Table 10 and Fig. 8b. Moreover, the weighted curve number CN II was calculated according to Eq. 3, and its value is 78.26. The CN I and CN II values calculated from CN II are 53.5, 86.23, respectively.

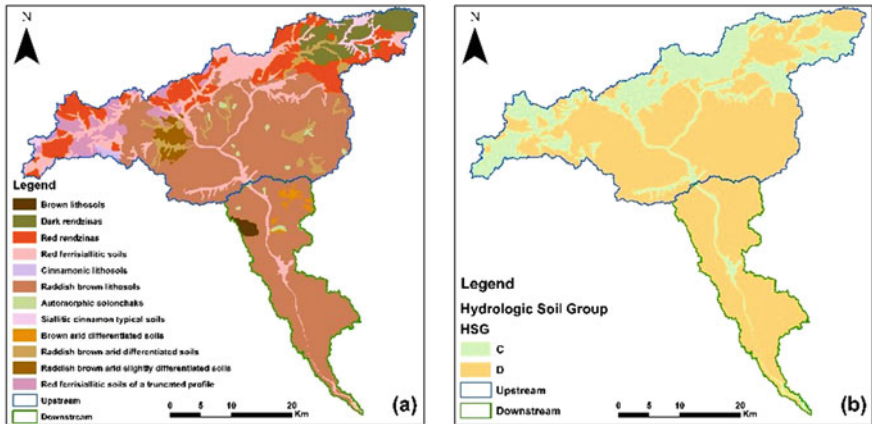


Fig.7 (a) Soil types map, and (b) HSG map

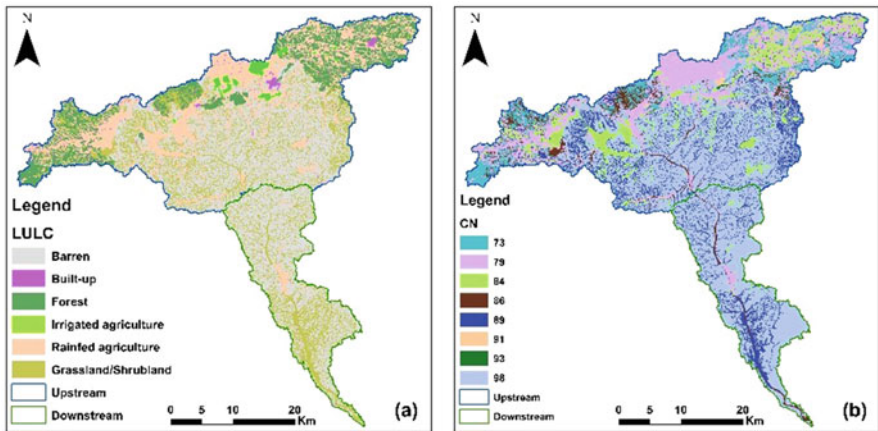


Fig. 8 LULC map (a), Curve Number map (b)

3.6 Rainfall

The analysis of IMERG GPM data for the period 2009-2019 is presented in Figs. 9 and 10. The result showed that the average total rainfall in the upstream varies from 150 to 400 mm, while it varies from 50 to 100 mm downstream. Both mountainous, forested areas receive the highest rainfall in the northeastern and northwestern limbs of the watershed. In contrast, the lower part of the upstream and the downstream regions receive the lowest rainfall. The average total rainfall for the period 2009-2019 is found to be 350.6 mm in the upstream and 131.74 mm in the downstream area.

Table 9 LULC classes of Wadi Samalous watershed

LULC	Area km ²	Area %
Barren	620.30	41.05
Built-up	12.70	0.84
Forest	169.20	11.20
Grassland/Shrubland	417.40	27.62
Irrigated agriculture	10.30	0.68
Rainfed agriculture	281.10	18.60
Total	1511	100.0

Table 10 Weighted Curve Number of Wadi Samalous watershed

LULC	HSG	CN	Area Km2	CN value for AMC conditions
Barren	C	98	45.88	AMC I = 53.5 AMC II = 78.23 AMC III = 86.23
Barren	D	98	574.48	
Built-up	C	91	8.40	
Built-up	D	93	4.30	
Forest	C	73	96.8	
Forest	D	79	72.42	
Grassland/Shrubland	C	86	149.20	
Grassland/Shrubland	D	89	268.09	
Irrigated agriculture	C	79	3.20	
Irrigated agriculture	D	84	7.10	
Rainfed agriculture	C	79	151.13	
Rainfed agriculture	D	84	130.00	
Total			1511	

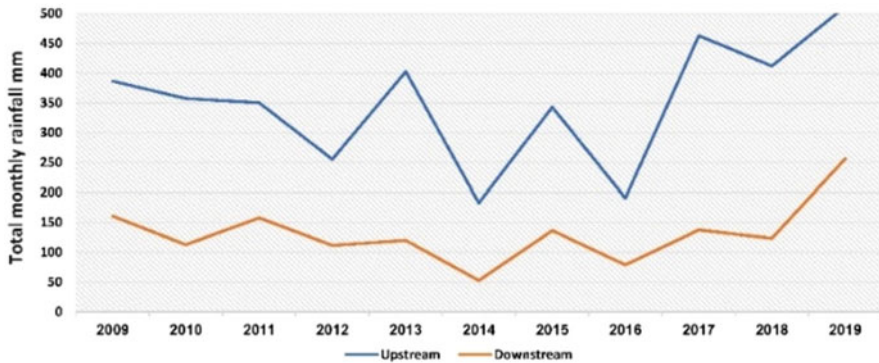


Fig. 9 The total monthly rainfall IMERG GPM (2015–2019)

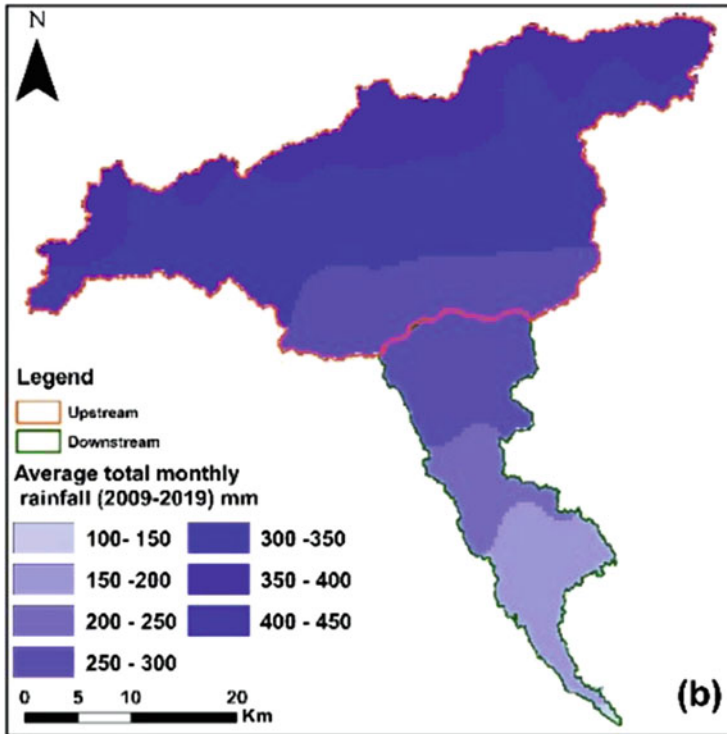


Fig. 10 Average total monthly rainfall (2009–2019)

3.7 *Runoff Estimation*

IMERG GPM precipitation data covering the period 2009–2019 were used to calculate the runoff depth using the SCS-CN method. The upstream runoff depth for Wadi Samalous watershed was calculated based on eqs. 4 and 5 for conditions AMC I, II, and III, as shown in Fig.11a. The estimated annual runoff d is given in Table 11. The runoff depth varies between 11.20 and 35.79 mm (2009–2019). The average ten-year runoff volume is 26.5 Mm³, representing 7.6% of the average annual rainfall during 2009–2019. The rainfall-runoff relationship showed a correlation coefficient of 0.89, as shown in Fig.11b.

3.8 *RWH Site Suitability*

The site suitability analysis was carried out to identify suitable sites for RWH according to the workflow shown in Fig. 3 (Step VI), where each representative thematic layer of the criterion was reclassified based on the relevant weighting given

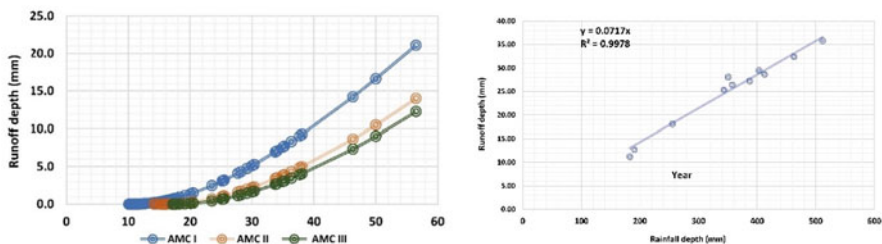


Fig. 11 (a) Solution of runoff equation for AMC conditions, and (b) rainfall and calculated runoff relation

Table 11 Annual runoff depth and volume

Year	Rainfall (mm)	Runoff depth (mm)	Runoff volume (m ³)
2009	386.90	27.21	28,906,164.434
2010	357.70	26.40	28,040,595.871
2011	350.40	28.06	29,814,346.302
2012	255.50	18.08	19,208,505.048
2013	402.96	29.47	31,310,207.426
2014	182.50	11.20	11,895,347.322
2015	343.10	25.33	26,914,373.044
2016	190.53	12.70	13,488,652.680
2017	462.82	32.38	34,399,499.683
2018	412.45	28.65	30,437,657.736
2019	511.73	35.79	38,022,295.39
Average	386.90	25.03	26,585,240.45

in Table 4, and the result is depicted in Fig.12. The final RWH suitability map produced is shown in Fig.13a, which depicts five potential RWH sites viz. optimal, highly, moderate, marginally, not suitable. The result of the site suitability analysis indicates that the optimal and highly suitable sites for RWH are concentrated in the upstream area (Table 12). The outcome indicated that 2.5% and 9% of the study area represent optimal and high suitable for RWH, while 17.7%, 25%, and 45.7% of the site were classified as moderate, marginally, and not suitable, respectively. The map of suitable sites for different RWH structure types is shown in Fig.13b and the frequency of each RWH structure type is given in Table 13.

4 Conclusion

Seasonal surface water resources in Libya are limited only to the northern coastal areas, which have great potential, especially in the Al Jabal Al Akhdar region, which is characterized by the highest rainfall rate of the country compared to the rest of Libya. Unfortunately, this resource is not well managed, and there is a lack of rainfall

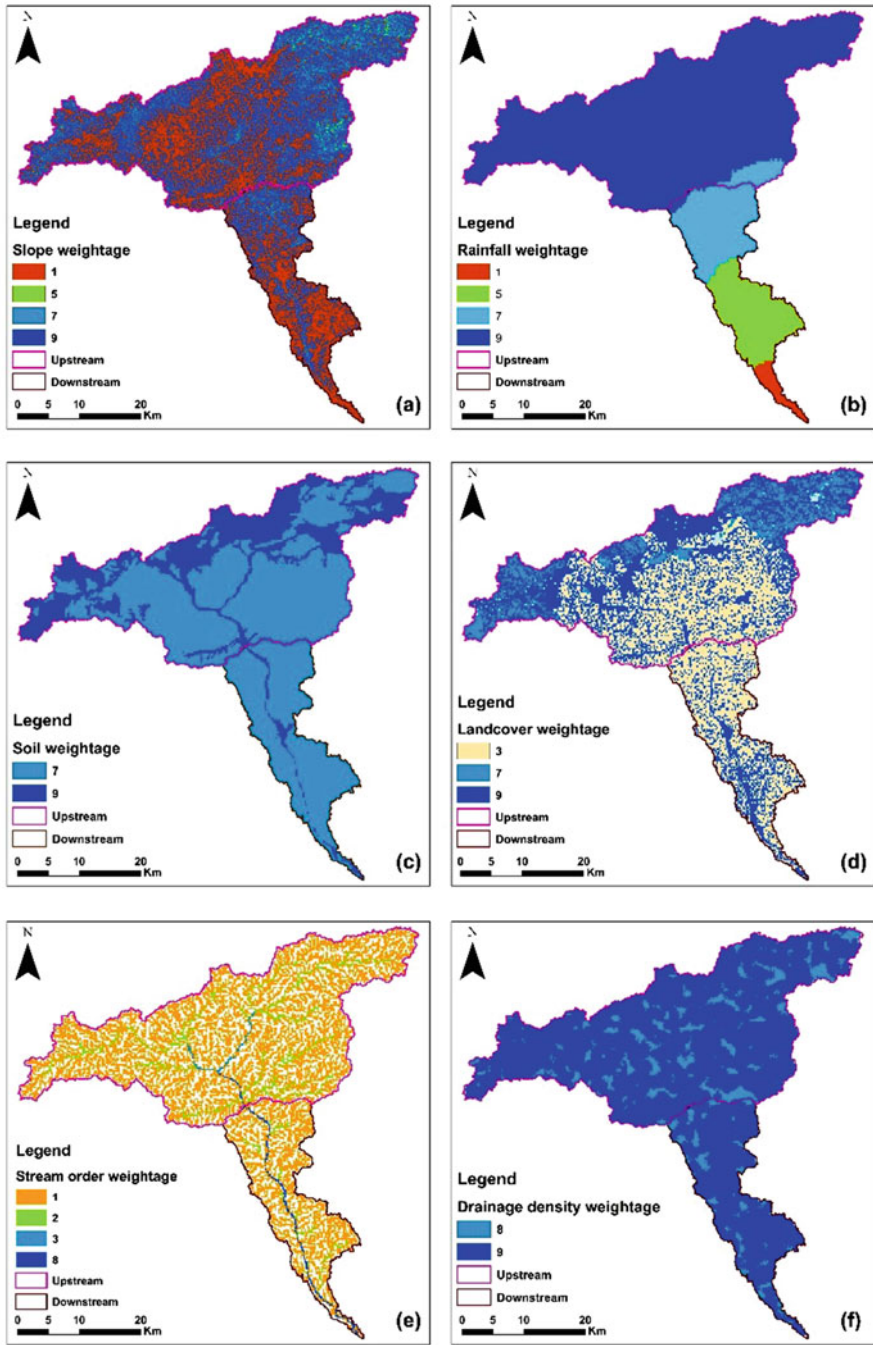


Fig. 12 Factor layers for the determination of suitable areas for RWH structures

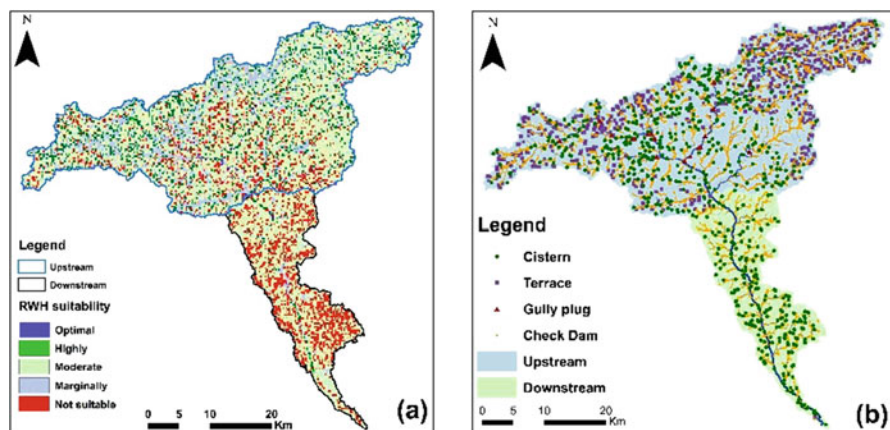


Fig. 13 (a) RWH suitability map, and (b) suitable sites for RWH structures

Table 12 Area and percentage of RWH suitability categories

Suitability categories	Area km ²	Area %
Optimal	38.5	2.5
Highly	136.7	9.0
Moderate	267.1	17.7
Marginally	377.5	25.0
Not suitable	691.2	45.7
Total	1511	100.0

Table 13 Number of suitable sites for RWH structures

	RWH structures	Upstream	Downstream
1	Cistern	470	217
2	Check dams	2176	1079
3	Gully plug	18	–
4	Terracing	612	–

and runoff data. This study aimed at estimating the potential for surface water and identifying suitable RWH sites using GIS techniques and RS data in the watershed of Wadi Samalus, northeast Libya. Surface water potential was evaluated through the runoff estimation using the SCS-CN method combined with GIS and RS data. LULC map was produced by classification of Landsat 8 OLI imagery and spatially intersected with the soil map showing the various HSG groups. CN values for different conditions of AMCs are 53.5 for AMC-I, 78.26 for AMC-II, and 86.23 for AMC-III. Since the rainfall data is unavailable for the study area, the precipitation data of IMERG GPM was used in the runoff computation. The average ten-year runoff volume was estimated as 26.5 Mm³, which represents 7.6% of the average annual rainfall amounting to 350.6 mm during 2009–2019. Identification of suitable sites for RWH was carried out based on the AHP method, where six criteria were selected (slope, rainfall, soil texture, LULC, stream order, and drainage density), and

the relative weights and influence were assigned based on the literature review. The result shows that the optimal and highly suitable RWH sites are concentrated in the upstream area. The analysis also indicated that 2.5% and 9% of the study area represent optimal and high suitability for RWH, while 17.7%, 25%, and 45.7% of the site were classified as moderate, marginally, and not suitable, respectively. The map of suitable sites for RWH structure types was generated showing the indigenous dominant type of RWH.

Furthermore, the methodology of the study could be implemented in the other Al Jabal Al Akhdar watersheds, and it was recommended to use more than one source of rainfall data for the future assessment and validation of the estimated runoff depth and volume since the observed rainfall measurements were not available during this study. In addition, the study does not recommend the construction of large storage dams in the study area due to their impacts on the environmental and socio-economic systems in the region. Whereas downstream pastures depend on the surface runoff, for prevention of soil erosion and nutrient loss which are the main challenges, low-height check dams are recommended across the main Wadi channel.

Moreover, the indigenous practice of RWH in the study area is highly imperative to limit natural resource degradation and confront the impact of climate change. The environmental, social, and economic suitability are the key drivers of RWH's implementation. Therefore, RWH's broad-based approach must be based entirely on integrated watershed management by setting up a policy for initial interventions to activate RWH in terms of legislation, administration, institutional preparation, and involvement of stakeholders to achieve sustainability and development of local community capacity.

Author Contributions **Salah Hamad:** conceptualization, methodology, software, data collection, spatial analysis, interpretation, writing-original draft, modeling, assessment, field investigation. **Nilanchal Patel:** review and editing. All authors have read and agreed to the published version of the manuscript.

References

- ACSAD (2005) Soil Terrain digital database (Libyan SOTER,2005). Arab Center for the Studies of Arid Zones and Dry Lands
- Adham A, Sayl KN, Abed R, Abdeladhim MA, Wesseling JG, Riksen M, Fleskens L, Karim U, Ritsema CJ (2018) A GIS-based approach for identifying potential sites for harvesting rainwater in the Western Desert of Iraq. *Int Soil Water Conserv Res* 6(4):297–304. <https://doi.org/10.1016/j.iswcr.2018.07.003>
- Ahmad I, Verma MK (2018) Application of analytic hierarchy process in water resources planning: a GIS based approach in the identification of suitable site for water storage. *Water Resour Manag* 32:5093–5114. <https://doi.org/10.1007/s11269-018-2135-x>
- Al-Adamat R, AlAyyash S, Al-Amoush H, Al-Meshan O, Rawajfih Z, Shdeifat A, Al-Harahsheh A, Al-Farajat M (2012) The combination of indigenous knowledge and geo-informatics for water harvesting siting in the Jordanian Badia. *J Geogr Inf Syst* 4(4):366–376. <https://doi.org/10.4236/jgis.2012.44042>

- Allan JA, McLachlan KS, Edith. (1975) Libya: agriculture and economic development. *Am Geograp Soc* 65(1):128–129
- Alwan IA, Aziz NA, Hamoodi MN (2020) Potential water harvesting sites identification using spatial multi-criteria evaluation in Maysan Province, Iraq. *ISPRS Int J Geo-Info* 9(4):235. <https://doi.org/10.3390/ijgi9040235>
- Ammar A, Riksen M, Ouessar M, Ritsema C (2016) Identification of suitable sites for rainwater harvesting structures in arid and semi-arid regions: a review. *Int Soil Water Conserv Res* 4(2): 108–120. <https://doi.org/10.1016/j.iswcr.2016.03.001>
- Amutha R, Porchelvan P (2009) Estimation of surface runoff in malattar sub-watershed using SCS-cn method. *J Indian Soc Remote Sensing* 37:291. <https://doi.org/10.1007/s12524-009-0017-7>
- Arlab (1983) Complementary investigation of surface water, groundwater, and climatological survey in Southern Flanks of Al Jabal Al Akhdar. Secretariat of Agriculture Land Reclamation Secretariat of Agriculture Land Reclamation. Tripoli-Libya
- Badhe Y, Medhe R, Shelar T (2020) Site suitability analysis for water conservation using AHP and GIS techniques: a case study of upper Sina River catchment, Ahmednagar (India). *Hydrospatial Anal* 3(2):49–59. <https://doi.org/10.21523/gc3.19030201>
- Bakir M, Xingnan Z (2008) GIS and remote sensing applications for rainwater harvesting in the Syrian Desert (Al-Badia). In: Proceedings of twelfth international water technology conference, IWTC12, Alexandria, pp 73–82
- Bhat MS, Alam A, Ahmad S, Farooq H, Ahmad B (2019) Flood hazard assessment of upper Jhelum basin using morphometric parameters. *Environ Earth Sci* 78:54. <https://doi.org/10.1007/s12665-019-8046-1>
- Blanco-Canqui H, Lal R (2010) Principles of soil conservation and management. <https://doi.org/10.1007/978-1-4020-8709-7>
- Boers TM (1994) Rainwater harvesting in Arid and Semi-Arid Zones. Agricultural University. Promotor(en): R.A. Feddes. - Wageningen: ILRI - ISBN 9789070754365 - 133
- Buraihi FH, Shariff ARM (2015) Selection of rainwater harvesting sites by using remote sensing and GIS techniques: a case study of Kirkuk, Iraq. *Jurnal Teknol* 76(15). <https://doi.org/10.11113/jt.v76.5955>
- Chopra R, Dhiman RD, Sharma PK (2005) Morphometric analysis of sub-watersheds in Gurdaspur district, Punjab using remote sensing and GIS techniques. *J Indian Soc Remote Sensing* 33:531. <https://doi.org/10.1007/BF02990738>
- Congedo L (2016) Semi-automatic classification plugin semi-automatic classification plugin documentation. Technical Report. <https://doi.org/10.13140/RG.2.2.29474.02242/1>
- De Coning E, Poolman E (2011) South African weather service operational satellite based precipitation estimation technique: applications and improvements. *Hydrol Earth Syst Sci* 15(4): 1131–1145. <https://doi.org/10.5194/hess-15-1131-2011>
- Dingman SL (1978) Drainage density and streamflow: a closer look. *Water Resour Res* 14(6): 1183–1187. <https://doi.org/10.1029/WR014i006p01183>
- Dunjó G, Pardini G, Gispert M (2004) The role of land use-land cover on runoff generation and sediment yield at a microplot scale, in a small Mediterranean catchment. *J Arid Environ* 57(2): 239–256. [https://doi.org/10.1016/S0140-1963\(03\)00097-1](https://doi.org/10.1016/S0140-1963(03)00097-1)
- ESRI (2016) Geoprocessing tool reference. Online; Environmental Systems Research Institute. <https://desktop.arcgis.com/en/arcmap/10.3/tools/spatial-analyst-toolbox/an-overview-of-the-hydrology-tools.htm>
- Fick SE, Hijmans RJ (2017) WorldClim 2: new 1-km spatial resolution climate surfaces for global land areas. *Int J Climatol* 37(12):4302–4315. <https://doi.org/10.1002/joc.5086>
- Frnlab (1974) Water resources study of Southern Flanks of Al Jabal Al Akhdar Phase I. Libyan Secretariat of Agriculture Land Reclamation Secretariat of Agriculture Land Reclamation. Tripoli-Libya
- Frnlab (1976) Water resources study of Southern Flanks of Al Jabal Al Akhdar Phase I. Libyan Secretariat of Agriculture Land Reclamation Secretariat of Agriculture Land Reclamation. Tripoli-Libya

- Gado TA, Hsu K, Sorooshian S (2017) Rainfall frequency analysis for ungauged sites using satellite precipitation products. *J Hydrol* 554:646–655. <https://doi.org/10.1016/j.jhydrol.2017.09.043>
- García-Ruiz JM (2010) The effects of land uses on soil erosion in Spain: a review. *Catena* 81(1): 1–11. <https://doi.org/10.1016/j.catena.2010.01.001>
- Gilewski P, Nawalany M (2018) Inter-comparison of rain-gauge, radar, and satellite (IMERG GPM) precipitation estimates performance for rainfall-runoff modeling in a mountainous catchment in Poland. *Water (Switzerland)* 10(11):1–23. <https://doi.org/10.3390/w10111665>
- Glendenning CJ, Van Ogtrop FF, Mishra AK, Vervoort RW (2012) Balancing watershed and local scale impacts of rain water harvesting in India - a review. *Agric Water Manag* 107:1–13. <https://doi.org/10.1016/j.agwat.2012.01.011>
- Goyal RK, Khan MA, Bhati TK et al (2013) Watershed Management for Development of hot arid zone of India. *Arid Zone Res Inst Jodhpur India* 003:46
- GWA (2006) Water resources status of Libya. General Water Authority. Tripoli-Libya
- Hamad S (2019) Spatial characteristics of the southern Al Jabal Al Akhdar watersheds: remote sensing approach. *Hydrospatial Anal* 3(1):37–48. <https://doi.org/10.21523/gcj3.19030104>
- Hassanli AM, Beecham S (2013) Criteria for optimizing check dam location and maintenance requirements. In *Check Dams, morphological adjustments and erosion control in torrential stream*, pp 11–31
- Horton RE (1945) Erosional development of streams and their drainage basins: Hydrophysical approach to quantitative morphology. *Bull Geol Soc Am*. [https://doi.org/10.1130/0016-7606\(1945\)56\[275:EDOSAT\]2.0.CO;2](https://doi.org/10.1130/0016-7606(1945)56[275:EDOSAT]2.0.CO;2)
- Huffman GJ, Stocker EF, Bolvin DT, Nelkin EJ, Jackson T (2019) GPM IMERG early precipitation L3 half hourly 0.1 degree x 0.1 degree V06. Goddard Earth Sciences Data and Information Services Center (GES DISC). <https://doi.org/10.5067/GPM/IMERG/3B-HH-E/06>
- Ibrahim GRF, Rasul A, Hamid AA, Ali ZF, Dewana AA (2019) Suitable site selection for rainwater harvesting and storage case study using Dohuk governorate. *Water (Switzerland)* 1(4):864. <https://doi.org/10.3390/w11040864>
- IRC (1974) Geological maps of Libya. Industrial Research Center
- Kadam A, Karnewar AS, Umrikar B, Sankhua RN (2019) Hydrological response-based watershed prioritization in semiarid, basaltic region of western India using frequency ratio, fuzzy logic and AHP method. *Environ Dev Sustain* 21(4):1809–1833. <https://doi.org/10.1007/s10668-018-0104-4>
- Konar M (2007) Rainwater harvesting in rural India - Taankas in the Thar Desert. *Waterlines* 25(4): 22–24. <https://doi.org/10.3362/0262-8104.2007.022>
- Krois J, Schulte A (2014) GIS-based multi-criteria evaluation to identify potential sites for soil and water conservation techniques in the Ronquillo watershed, northern Peru. *Appl Geogr* 51:131–142. <https://doi.org/10.1016/j.apgeog.2014.04.006>
- Lucas-Borja ME, Zema DA, Antonio Plaza-álvarez P, Zupanc V, Baartman J, Sagra J, González-Romero J, Moya D, de las Heras, J. (2019) Effects of different land uses (abandoned farmland, intensive agriculture and forest) on soil hydrological properties in southern Spain. *Water (Switzerland)* 11(3):503. <https://doi.org/10.3390/w11030503>
- Mahmood K, Qaiser A, Farooq S, Nisa M, un. (2020) RS- and GIS-based modeling for optimum site selection in rain water harvesting system: an SCS-CN approach. *Acta Geophys* 68(4): 1175–1185. <https://doi.org/10.1007/s11600-020-00460-x>
- Malczewski J (1999) GIS and multicriteria decision analysis (Vol. 1). Wiley. <https://www.wiley.com/en-us/GIS+and+Multicriteria+Decision+Analysis-p-9780471329442>
- Martín-Moreno C, Martín Duque JF, Nicolau Ibarra JM, Hernando Rodríguez N, Sanz Santos MÁ, Sánchez Castillo L (2016) Effects of topography and surface soil cover on erosion for mining reclamation: the experimental spoil heap at El Machorro mine (Central Spain). *Land Degrad Dev* 27(2):145–159. <https://doi.org/10.1002/ldr.2232>
- Matomela N, Tianxin L, Morahanye L, Bishoge OK, Ikhumhen HO (2019) Rainfall-runoff estimation of Bojiang lake watershed using SCS-CN model coupled with GIS for watershed management. *J Appl Adv Res* 4(1):16. <https://doi.org/10.21839/jaar.2019.v4i1.263>

- Matomela N, Li T, Ikhumhen HO (2020) Siting of rainwater harvesting potential sites in arid or semi-arid watersheds using GIS-based techniques. *Environ Proces* 7(2020):631–652. <https://doi.org/10.1007/s40710-020-00434-7>
- Mishra SK, Singh VP (2003) Soil conservation service curve number (SCS-CN) methodology. Water Sci Technol Library. <https://doi.org/10.1007/978-94-017-0147-1>
- Mugo GM, Odera PA (2019) Site selection for rainwater harvesting structures in Kiambu County-Kenya. *Egyptian J Remote Sensing Space Sci* 22(2):155–164. <https://doi.org/10.1016/j.ejrs.2018.05.003>
- Nayak RR, Krishnaswamy J, Vaidyanathan S (2020) Exotic plantations increase risks of flooding in mountainous landscapes. pp. 1–25. <https://doi.org/10.1002/essoar.10503675.2>
- Nganga BW, Ngetich KO, Adamtey N, Milka K, Ngetich KF (2019) Application of GIS on the identification of suitable areas for water conservation Technologies in the Upper Tana Watershed of the central highlands of Kenya. *Int J Plant Soil Sci* 30(1):1–20. <https://doi.org/10.9734/ijpss/2019/v30i130166>
- NRCS (1986) Urban hydrology for small watersheds (Natural Resources Conservation Service (ed.); 2nd ed.). USDA, United States Department Agriculture
- Nunes AN, de Almeida AC, Coelho COA (2011) Impacts of land use and cover type on runoff and soil erosion in a marginal area of Portugal. *Appl Geogr* 31(2):687–699. <https://doi.org/10.1016/j.apgeog.2010.12.006>
- Odhiambo GO (2017) Water scarcity in the Arabian Peninsula and socio-economic implications. *Appl Water Sci* 7(5):2479–2492. <https://doi.org/10.1007/s13201-016-0440-1>
- OMU (2005) Studying and evaluating the natural vegetation in Al-Jabal Al-Akhdar area (In Arabic), Omer Al Mukhtar University
- Oweis TY, Prinz D, Hachum AY (2012) Rainwater harvesting for agriculture in the dry areas. In *Rainwater harvesting for agriculture in the Dry Areas*. <https://doi.org/10.1201/b12351>
- Pallard B, Castellarin A, Montanari A (2009) A look at the links between drainage density and flood statistics. *Hydrol Earth Syst Sci* 13(2009):1019–1029. <https://doi.org/10.5194/hess-13-1019-2009>
- Peng J, Dadson S, Hirpa F, Dyer E, Lees T, Miralles DG, Vicente-Serrano SM, Funk C (2020) A pan-African high-resolution drought index dataset. *Earth Syst Sci Data* 12(2020):753–769. <https://doi.org/10.5194/essd-12-753-2020>
- Ragab R, Prudhomme C (2002) Climate change and water resources management in arid and semi-arid regions: prospective and challenges for the 21st century. *Biosyst Eng* 81(1):3–34. <https://doi.org/10.1006/bioe.2001.0013>
- Rahmati O, Kalantari Z, Samadi M, Uuemaa E (2019) GIS-based site selection for check dams in watersheds: considering Geomorphometric and Topo-hydrological factors. *Sustainability* 11(5639). <https://doi.org/10.3390/su11205639>
- Rai PK, Mohan K, Mishra S, Ahmad A, Mishra VN (2017) A GIS-based approach in drainage morphometric analysis of Kanhar River Basin, India. *Appl Water Sci* 7(2017):217–232. <https://doi.org/10.1007/s13201-014-0238-y>
- Rikalovic A, Cosic I, Lazarevic D (2014) GIS based multi-criteria analysis for industrial site selection. *Procedia Eng* 69(2014):1054–1063. <https://doi.org/10.1016/j.proeng.2014.03.090>
- Rodhe A (2012) Physical models for classroom teaching in hydrology. *Hydrol Earth Syst Sci* 16:3075–3082. <https://doi.org/10.5194/hess-16-3075-2012>
- Saaty TL (2008) Decision making with the analytic hierarchy process. *Int J Serv Sci* 1(83). <https://doi.org/10.1504/IJSSCI.2008.017590>
- Sayl KN, Muhammad NS, El-Shafie A (2019) Identification of potential sites for runoff water harvesting. *Proc Inst Civil Eng Water Manag* 172(3):135–148. <https://doi.org/10.1680/jwama.16.00109>
- SELKHOZPROMEXPORT (1980) Soil studies in the Eastern Zone of the socialist people. Agricultural Reclamation and Land Development, SPLAJ. VNESHORGREKLAMA" Publishing House, USSR
- Şen Z (2008) *Wadi Hydrology*. CRC Press, Boca Raton. <https://doi.org/10.1201/9781420061550>
- Shadmehri Toosi A, Ghasemi Tousi E, Ghassemi SA, Cheshomi A, Alaghmand S (2020) A multi-criteria decision analysis approach towards efficient rainwater harvesting. *J Hydrol* 582(2020): 124501. <https://doi.org/10.1016/j.jhydrol.2019.124501>

- Shalamzari MJ, Zhang W, Gholami A, Zhang Z (2019) Runoff harvesting site suitability analysis for wildlife in sub-desert regions. *Water (Switzerland)* 11:1944. <https://doi.org/10.3390/w11091944>
- Sindhu D, Shivakumar BL, Ravikumar AS (2013) Estimation of surface runoff in Nallur Amanikere. *Int J Res Eng Technol* 2(13):404–409
- Smith KG (1950) Standards for grading texture of erosional topography. *Am J Sci.* <https://doi.org/10.2475/ajs.248.9.655>
- Soo EZX, Wan Jaafar WZ, Lai SH, Othman F, Elshafie A, Islam T, Srivastava P, Othman Hadi HS (2020) Precision of raw and bias-adjusted satellite precipitation estimations (TRMM, IMERG, CMORPH, and PERSIANN) over extreme flood events: case study in Langat river basin, Malaysia. *J Water Climate Change jwc2020180*:1–21. <https://doi.org/10.2166/wcc.2020.180>
- Stec A, Kordana S (2015) Analysis of profitability of rainwater harvesting, gray water recycling and drain water heat recovery systems. *Resour Conserv Recycl* 105(A):84–94. <https://doi.org/10.1016/j.resconrec.2015.10.006>
- Strahler A (1964) Quantitative geomorphology of drainage basins and channel networks. In: Chow E, V. (eds) *Handbook of applied hydrology*. McGraw Hill, New York, pp 439–476
- USDA (2004) Hydrologic soil-cover complexes Part 630. In *Hydrology national engineering handbook*. United States Department of Agriculture. p. 20
- USDA (2009) Hydrologic soil groups. In *National engineering handbook*. The U.S. Department of Agriculture (USDA). p. 13
- USGS (2000) EROS archive - Digital elevation - Shuttle Radar Topography Mission (SRTM) 1 Arc-Second Global. Earth Resources Observation and Science (EROS) Center. <https://doi.org/10.5066/F7PR7TFT>
- USGS (2013) USGS EROS Archive - Landsat Archives - Landsat 8 OLI (Operational Land Imager) and TIRS (Thermal Infrared Sensor) Level-1 Data Products. Earth Resources Observation and Science (EROS) Center. <https://doi.org/10.5066/F71835S6>
- Viji R, Prasanna PR, Ilangovan R (2015) Gis based SCS - CN method for estimating runoff in Kundahpalam watershed, Nilgries District, Tamilnadu. *Earth Sciences Research Journal* 19(1): 59–64. <https://doi.org/10.15446/esrj.v19n1.44714>
- Wu RS, Molina GLL, Hussain F (2018) Optimal sites identification for rainwater harvesting in Northeastern Guatemala by analytical hierarchy process. *Water Resour Manag* 32(12): 4139–4153. <https://doi.org/10.1007/s11269-018-2050-1>
- Zeng QL, Yue ZQ, Yang ZF, Zhang XJ (2009) A case study of long-term field performance of check-dams in mitigation of soil erosion in Jiangjia stream, China. *Environ Geol* 58(4): 897–911. <https://doi.org/10.1007/s00254-008-1570-z>

Mr. Salah Hamad is an assistant professor of Hydrology and Geoinformation Science at the Department of Natural resources, Faculty of Natural resources and environmental science, University of Omer Al-Mukhtar, Al Bayda, Libya. He received his M.Sc. (Geographic information systems and science) in 2008 from Salzburg University, Salzburg, Austria. Mr. Salah Hamad has been teaching undergraduate courses and has supervised the graduation of bachelor's degree students since 2010. He is interested in GIS mapping and spatial analysis, particularly geoinformatics research with geodata documentation, applying various GIS and remote sensing techniques in conventional water resources management, engineering, and related aspects of earth science.

Dr. Nilanchal Patel is a professor of Remote Sensing at the Department of Remote Sensing, Birla Institute of Technology Mesra, Ranchi, India. He received his M.Sc. in (Applied Geology) in 1985 from (M.Tech.), India. Dr. Nilanchal Patel completed his Ph.D. in (Remote Sensing, Digital Image Processing) from the Indian Institute of Technology, Kanpur, India, in 1992. He specialized in research comprised a broad spectrum of disciplines such as remote sensing, GIS, climate change, snow cover dynamics, urbanization pattern analysis, traffic and transport, land degradation, vegetation, data mining, image processing, environment, and forests, rainfall-runoff modeling.

Stepwise Approach for Morphometric Modeling of Wadi Zamzam Watershed in North-Western Libya Using GIS and Remote Sensing Techniques



Ali M. Salim, Ibtisam A. Albira, and Safa A. Ebsheer

Abstract Watershed studies are helpful in creating spatial development plans for watersheds, maintaining and developing natural resources, and devising early warning, evacuation, and relief strategies to mitigate the consequences of flooding. This study aims to delineate the spatial boundaries of the Wadi Zamzam watershed in Libya and establish a geographical database of its morphometric, geological and climatic characteristics by using global information systems and remote sensing techniques based on the digital elevation model, the geological map of Libya, and climatic data. Moreover, climatic maps of the area were produced by using spatial analysis tools and spatial interpolation. Morphometric equations were applied to determine the morphological characteristics of the watershed: height, degree and direction of its slope, and the areal characteristics represented in its area, length, width and perimeter. Furthermore, the study also determined the characteristics of the water network, riverbeds, their numbers and lengths, and the bifurcation ratio. It also extracted shape properties such as the ratio of elongation, circularity, and form factor in the Wadi Zamzam watershed. The Wadi Zamzam watershed covers 38,444.4 km², with a perimeter of 2419.7 km and a form factor of 0.14. The drainage density was 1.49, and the height was 0–832 m. The study produced digital geological and climatic maps, including maps of the soil, water network, height and slope of the Wadi Zamzam watershed, and its vegetation cover.

Keywords Morphometry · Basin hydrology · Digital elevation model · Water resource management · Water network · Linear morphometric parameters

A. M. Salim · I. A. Albira (✉)

Department of Geography, Faculty of Education, University of Misurata, Misurata, Libya
e-mail: Ibtisam.albira@edu.misuratau.edu.ly

S. A. Ebsheer

Ministry of Education, Misurata, Libya

1 Introduction

Watersheds are important natural resources particularly in arid and semi-arid areas. They are pillars of sustainable development based on sustainable exploitation of natural resources in light of the climatic changes the world is witnessing. These changes have resulted in a decrease in the amount of rain, an increase in drought, and the recurrence of heat waves. Consequently, water and land resources have deteriorated, drought and desertification have spread, and land has been degraded in watersheds. Morphometric modeling, an essential component of sustainable environmental development, relies on studying watersheds by determining their spatial extension and building geographical databases of their morphometric, geological and climatic characteristics using geographic information systems (GIS) and remote sensing techniques. This is needed for optimizing the use of water resources by the construction of dams, preservation of vegetation, and development of land as pastures, reserves, natural tourism areas, and rain-fed farming grounds. Spatial techniques are used to study watersheds and their characteristics (area, shape, and water network) in order to construct high-resolution digital maps of the morphometric, geological and climatic characteristics of the watersheds. The digital elevation model, satellite images and the mathematical equations of Strahler (1957) and Horton (1945) are widely used to that end.

Watershed development projects protect and conserve the environment and contribute to livelihood security (Panhalkar et al. 2012). Setting watershed priorities is one of the most important aspects of planning for their development and implementation of management strategies (Zende et al. 2012). In arid regions, flash floods cause significant loss in infrastructure, property and human life (El Bayomi 2010). However, water from floods could be exploited as a resource, such as satisfying part of the increased water demand in such areas. Morphometric studies represent one of the most important components of geomorphological studies. The tools used in such studies have been considerably enhanced since the last years of the twentieth century by the use of GIS and remote sensing. This has led to a deeper understanding of the morphology of river watersheds and the geological, natural and climatic factors affecting their formation. GIS recently emerged as an important tool in morphometric studies using spatial analysis or model building to extract morphometric characteristics. For example, Tamang et al. (2012) carried out morphometric analysis and prioritization of the seven mini watersheds in the Rongli watershed in the eastern district in Sikkim state, India using remote sensing and GIS techniques.

The Wadi Zamzam watershed is one of the important watersheds in Libya. It is characterized by the diversity of its natural and soil characteristics, climatic conditions and agricultural resources. Thus, it represents a geographically distinct spatial unit that should be studied in detail to determine its morphometric characteristics in order to develop it spatially as a water resource for use in agriculture, grazing and tourism. Morphometric modeling of the Wadi Zamzam watershed involves mathematical analysis of the water drainage network to determine its morphometric characteristics and derive related digital maps, and to understand its natural

characteristics such as climate, soil and vegetation cover. This concept dates back to Horton (1945), but its application has progressed from the use of paper maps and aerial photographs to satellite images and field studies.

This chapter aims to highlight the role of GIS and remote sensing in determining and extracting the morphometric characteristics of the Wadi Zamzam watershed, as well as to provide a step-by-step approach for its modeling and production of digital maps of its morphometric, climatic and vegetation characteristics. The importance of the study lies in its use of modern spatial techniques to determine the morphometric and climatic characteristics, which has not been done before for this watershed. The findings will be useful in the management and development of its natural resources by the construction of dams and ground reservoirs, and implementation of agricultural and pastoral projects.

2 The Study Area

The Wadi Zamzam watershed covers an area estimated at 38444.4 km². is a large watershed located in the north-western region of Libya, southeast of the city of Misurata, and generally flows from southwest to northeast into the wetland Sabkhat Al-Hisha, from where it proceeds to the Mediterranean Sea. It is bordered on the west and northwest by the watershed of Wadi Suf Al-Jin, on the south and east by the watershed of Wadi Bay AlKabir, and on the south and southwest by Hamada Al-Hamra. It is located between latitudes 28.22° and 31.45° north, and longitudes 12.06° and 15.35° east (Fig. 1).

3 Material and Methods

A quantitative analytical approach was used to analyze the data by applying mathematical equations to extract the morphometric characteristics of the Wadi Zamzam watershed. To that end, the digital elevation model (DEM) was used, along with measurements of area, shape, circularity ratio, watershed length, width, circumference, height, hypsometric parameter, drainage density, and river repetition. Accurate digital maps of the watershed and its morphometric, geological and climatic characteristics were produced, as well as soil and vegetation maps based on GIS technology.

The data were collected from a satellite image from Landsat 8, 30 m of the Wadi Zamzam watershed area, and a geological map of Libya (Industrial Research Centre 2009). From the National Atlas (Planning Ministry 1978) were obtained an oil map, other maps, and climatic data (Fig. 2). GIS was used to locate the Wadi Zamzam watershed, extract the water network, determine its characteristics, and produce digital morphometric, climatic, geological, and soil maps.

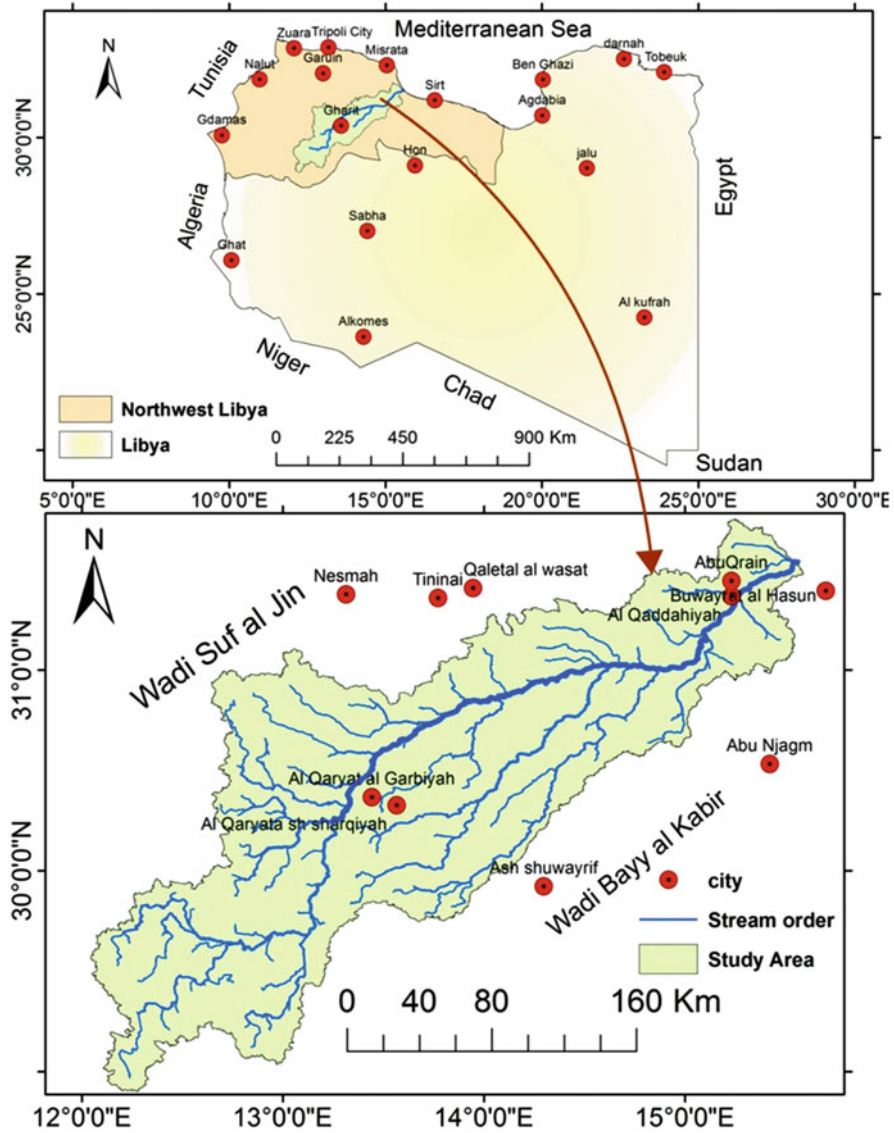


Fig. 1 Location of the study area: Wadi Zamzam watershed. (Adapted from Planning Ministry 1978)

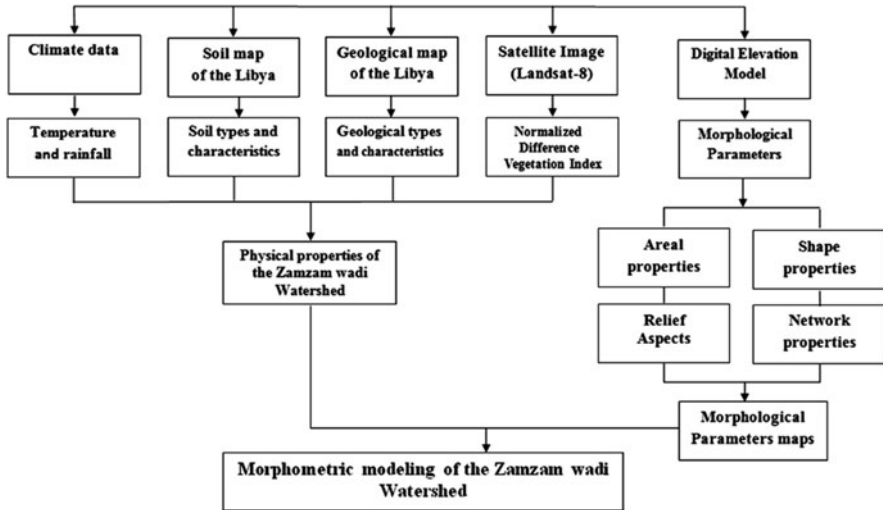


Fig. 2 Flowchart of the research approach

4 Results and Discussion

4.1 The Geology of the Study Area

The Wadi Zamzam watershed contains various rock formations and geological structures extending from the Upper Cretaceous to the Quaternary period (Fig. 3).

4.1.1 Quaternary Deposits

These undivided deposits are mainly alluvial deposits, as well as wind and water deposits, covering 696.7 km² (1.8%) of the watershed area. They are present at the estuary in the northern parts, and in the southeast (Table 1).

4.1.2 Holocene Deposits

The deposits of this age include wetland (sabkha) deposits and Wadi deposits, which cover 312.6 km² (0.81%) of the watershed area. These include deposits of gypsum and salts in the form of clay and sandy loam deposits with sodium chloride. Deposits of wadis, low terraces, and wind and water deposits constitute 1.67% of the total area of the Wadi Zamzam watershed. The deposits are distributed in the central and northern parts of the study area.

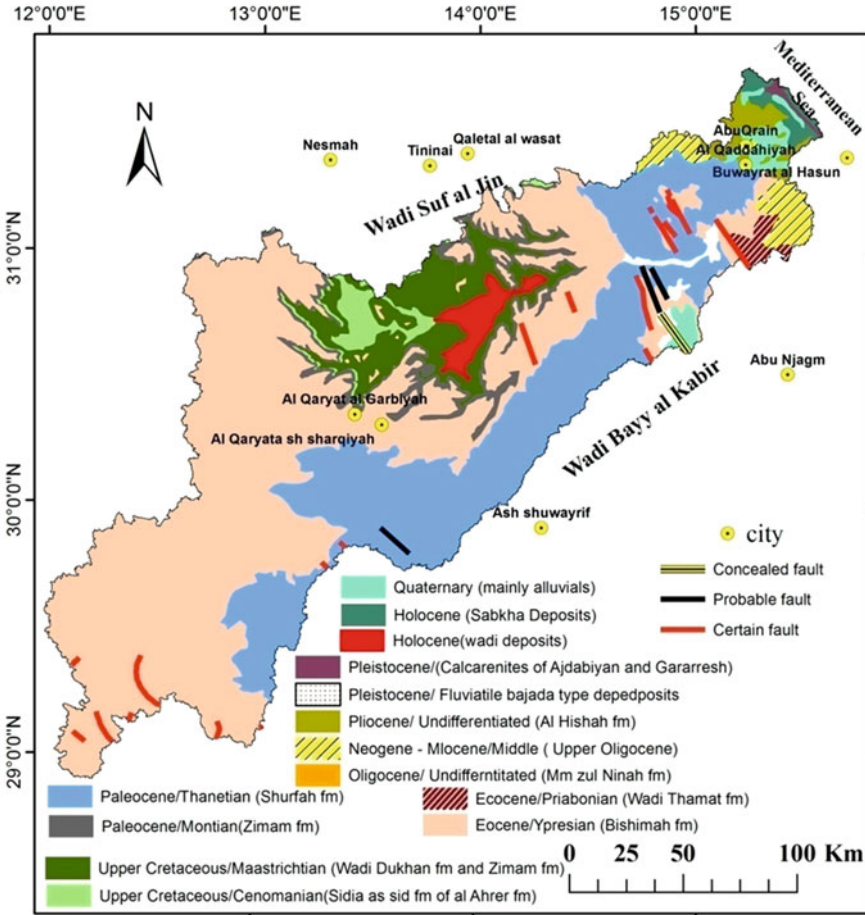


Fig. 3 Geological map of the Wadi Zamzam watershed. (Adapted from Industrial Research Center 2009)

4.1.3 Pleistocene Deposits

These deposits consist of beach deposits and cohesive sand dunes (Calcarnites, Ajdabiya and Gargaresh formations) and cover 129.5 km² (0.34%) of the watershed area. Fluviatile bajad type deposits and high terrace deposits cover about 177.9 km² (0.46% of the total area of the Wadi Zamzam watershed). These deposits are found in the far northern region and some southeastern locations.

Table 1 Geographical distribution of geological formations in Wadi Zamzam watershed

Geological period		Geological formation	Area (km ²)	%
Quaternary		Undivided quaternary deposits	696.7	1.81
Holocene		Sabkha (wetlands) deposits	312.6	0.81
		Wadi deposits	642.4	1.67
Pleistocene		Calcareous of Ajdabiyah and Gargaresh formations	129.5	0.34
		Fluvial bajad type deposits and high terraces deposits	177.9	0.46
Pliocene		Al-Hisha formation	517.9	1.35
Neogene–Palaeogene		Upper Oligocene of Al Faydiyah formation	794.5	2.07
Palaeogene–Oligocene		Undifferentiated Oligocene Mm Zul Ninah formation	141.5	0.37
Eocene	Priabonian	Wadi Thamat formation	271.7	0.71
	Ypresian	Bishimah formation	19,861.7	51.66
Paleocene	Thanetian	Shurfah formation	9875.9	25.69
	Montian	Zimam formation	1473.8	3.83
Cretaceous	Maastrichtian	Zimam formation, Wadi Dukhan formation	2830.7	7.36
Upper cretaceous	Cenomanian	Sidi as-Sid formation, Qasr al Ahrar formation	717.6	1.87
Total			38,444.4	100.00

4.1.4 Pliocene Deposits

The Pliocene deposits consist of marine to continental argillaceous sandstone with layers of gypsum from the formation of Al-Assah, delta sands with sandstone intrusion, and gypsum Calcarnites from Al-Hisha formation. The Pliocene deposits cover 517.9 km² (1.35%) of the watershed area and are predominant in the northwest (Table 1, Fig. 3).

4.1.5 Neogene, Paleogene, Middle Miocene, and Upper Oligocene Deposits

These deposits consist of calcite and limestone containing fossils. They are present in combination with gypsum and alkaline salts in the formation of Al-Faydiyah. The deposits cover an area of 794.5 km² (2.07%) of the total area of the Wadi Zamzam watershed and are present in the northeastern and northwestern regions.

4.1.6 Paleogene-Oligocene Deposits

The Paleogene-Oligocene deposits contain gypsum mudstone, Marlstone, and calcite. They contain vertebral fossils of earth formation, conglomerates, clay and

mudstone interlaced with gypsum, marl limestone, and limestone containing fossils of freshwater mollusks from the Ma Zul Ninah Formation and other continental or near-shore deposits in the Sirt watershed. These deposits cover 141.5 km^2 (0.37% of the watershed area) and are found in small areas in the southeastern regions.

4.1.7 Eocene Deposits

Priabonian Deposits

These deposits include limestone containing fossils, gypsum clays, and marl chalk limestone from the Wadi Thamat formation. The deposits cover 271.7 km^2 (0.71%) and are found in the northeastern regions, south of the Neogene deposits.

Ypresian Deposits

These deposits contain formations of chalk limestone, dolomite, calcite, chalk siliceous limestone, marl, and limestone of the Al- Bishimah Formation. With an area of 1861.7 km^2 , they represent 51.7% of the total area of the Wadi Zamzam watershed. They are located in various parts of the study area.

4.1.8 Paleocene Deposits

Thanetian Deposits

The Thanetian Formations include dolomite limestone containing fossils with intrusion of marl limestone, and deposits of chalk, chalk limestone, dolomitic limestone and marl, in addition to limestone and chalky limestone from Al- Shurfah formation. This formation is located in an area estimated at 9875.9 km^2 , which represents 25.7% of the study area. It is a continuous zone extending from the northwest to the southeast.

Montian Deposits

The deposits of this age contain limestone of incompatible stratification, and formations of dolomitic limestone alternating with chalky limestone from the Zimam formation. They cover about 1473.8 km^2 (3.8%) of the Zamzam watershed area and appear as veins in the central parts of the study area.

4.1.9 Cretaceous Deposits

Maastrichtian Deposits

These deposits vary between clay stone and gypsum marley, organic limestone and calcarenite. There are also interspersed sandstone, sandy marl and dolomitic limestone from the Zimam Formation, and dolomite and dolomitic limestone from the Wadi Dukhan Formation. These formations constitute 7.4% of the watershed area (2830.7 km²) and are located in the central parts (Fig. 3).

Cenomanian Deposits

The Cenomanian deposits include limestone and dolomitic limestone with intrusions of marl in the lower part, and clay, marl and gypsum in the upper part of the Sidi as-Sid formation. Marl and rare formations of marl limestone from the Qasr al Ahrar formation date back to the Upper Cinomani. These deposits cover about 717.6 km² (1.87%) of the geological formations of Wadi Kaam watershed and occupy the central areas of the Wadi Zamzam watershed (Industrial Research Center 2009).

4.1.10 Tectonic Geology

The Wadi Zamzam watershed contains faults of different lengths and directions dating back to the third geological period, as described below.

Certain Faults

These are the most prevalent in the Wadi Zamzam watershed and exist in its northern, central and southern parts. There are about 21 faults, some of which run from the northwest to the southeast. Others run from north to south or from east to west. Their total length is 225.6 km, and their lengths range from 1.8 to 26.7 km.

Probable Faults

These faults consist of three tectonic faults located in the northern, southeastern and central parts of the watershed, with a total length of 54.8 km and a range of 15.6–22.1 km (Fig. 3).

Concealed Faults

There is one concealed fault 20.8 km long extending from east to west in the northeastern region (Industrial Research Centre 2009).

4.2 The Soil

The soil in the Wadi Zamzam watershed varies in terms of its characteristics and geographical distribution. Soil is formed as a result of the different elements of climate and rock formations, and with the type of plant and animal life prevalent in the area. Knowledge of the porosity and permeability of the soil types in watersheds is of great importance in determining the sites for building dams and storing water in underground reservoirs and tanks, as well as for establishing agricultural and pastoral lands. The soil types in Wadi Zamzam watershed are depicted in Fig. 4.

4.2.1 Saline Soil (Sabkha)

Saline soil covers the northern parts of the Wadi Zamzam watershed at its estuary in Sabkhat Al-Hisha at the Mediterranean Sea. The salts appear on the surface as a thin layer, especially in the summer, and contain easily soluble salts such as chlorides of sodium, calcium and magnesium. Saline soil covers 917.2 km², *i.e.*, 2.39% of the watershed area (Table 2).

4.2.2 Sedimentary Soil

This soil is found in the streams, estuaries and banks of wadis. It is characterized by the presence of limestone rocks in the Wadi Zamzam watershed in the form of simple stratigraphic deposits due to water sedimentation. It covers 2522.3 km² (6.56% of the watershed area) and is present in some central and northwestern regions.

4.2.3 Dry Soil

This soil is formed under the combined influence of the Mediterranean climate and the semi-desert climate. It covers 2399.2 km² (6.24%) of the of the Wadi Zamzam watershed area and includes two types.

1. Shallow newly formed soil over cohesive stone materials with sedimentary soil deposited by water. It exists in the northern parts south of the saline soil and covers an area of 469.5 km² (1.22%).

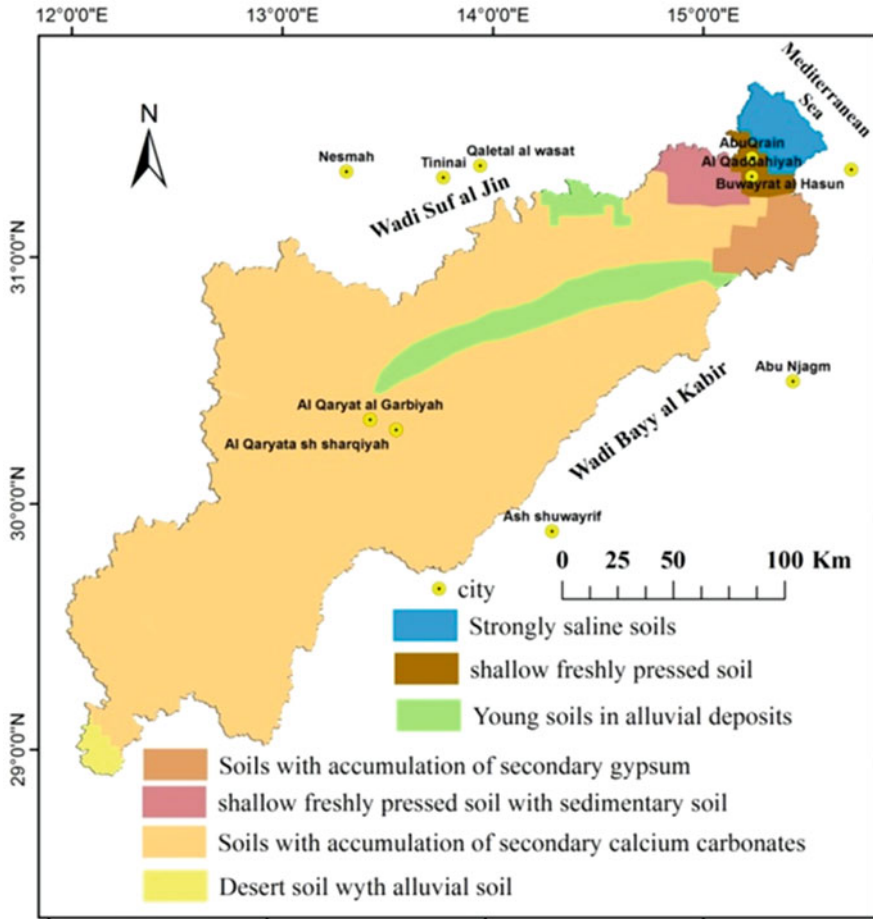


Fig. 4 The soil in the Wadi Zamzam watershed. (Adapted from Planning Ministry 1978)

2. Shallow newly formed soil over cohesive stone materials together with shallow newly formed soil over non-cohesive stone materials with limestone rocks on the surface. This soil type is present in the northeastern parts on 1086.2 km² (2.83% of the total study area).

4.2.4 Desert Soil

Desert soil occupies 84.8% of the Wadi Zamzam watershed area. The major type is characterized by the presence of a layer of limestone with a layer of gypsum and covers 32,313.2 km² of the watershed area (84.1%). Desert and sedimentary soils deposited by water and containing limestone rocks on their surface are located in the

Table 2 Soil types and their distribution in the Wadi Zamzam watershed

Type of soil		Location in the watershed	Area (km ²)	%
Strongly saline soils		Northern parts	917.2	2.39
Young soils in alluvial deposits		Central and northwestern parts	2522.3	6.56
Dry soil	Shallow freshly pressed soil	Northern parts, south of saline soil	469.5	1.22
	Soils with accumulation of secondary gypsum	Northeastern parts	1086.2	2.83
	Shallow freshly pressed soil with sedimentary soil	Northwestern parts near the estuary	843.5	2.19
Desert soil	Soils with accumulation of secondary calcium carbonates	Prevalent in most of Wadi Zamzam watershed	32,313.2	84.05
	Desert soil with alluvial soil	Southwestern parts	292.5	0.76
Total			38,444.4	100.00

extreme south and cover only 292.5 km² of the study area (Planning Ministry, 1978) (Fig. 4, Table 2).

4.3 *Vegetation in the Wadi Zamzam Watershed*

The study area ranges from arid to semi-arid. It is characterized by a poor vegetation cover, except in some areas with suitable soil and rain. The plants vary from evergreen perennials such as al-Ratum, Sidr, Sibat, *Artemisia campesteris*, Al-Jadah to annual plants that grow and bloom after the rainy season and then fade away, such as chamomile and chrysanthemum.

4.4 *Climatic Characteristics of the Wadi Zamzam Watershed*

The climatic characteristics of the Wadi Zamzam watershed vary from one location to another, and they are affected by the atmospheric depressions affecting the climate of Libya in general between September and May. The study area is affected by the Mediterranean climate in the northern parts and the semi-arid and desert climate in the central and southern regions. The average annual rainfall decreases towards the south and southwest. The average annual rainfall during 1958–2019 was 188.7 mm in the Abu Qrain area, 186.7 mm in the Al-Qudahiyah area, 149.2 mm in the Zamzam area, and 122.2 mm in the Al-Qaryat area (Fig. 5a). The peak of rainfall was during December to February due to the larger number of air depressions affecting Libya.

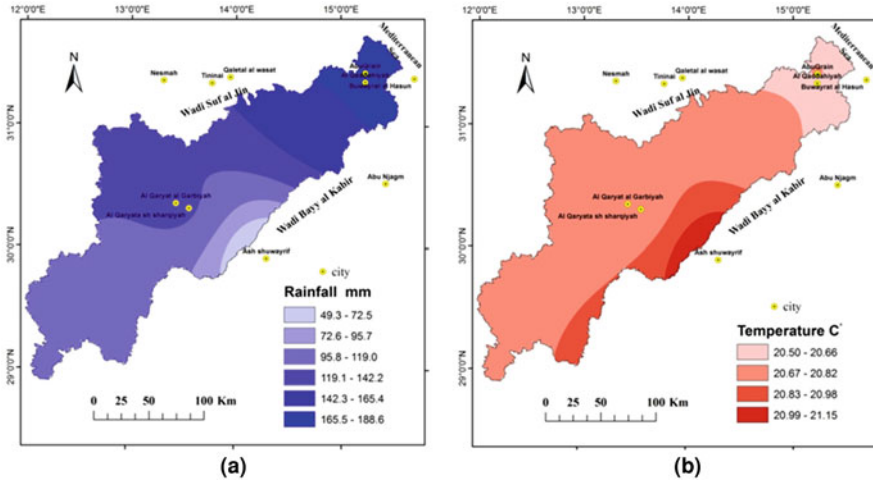


Fig. 5 (a) Average annual rainfall. (b) Annual temperature average in the Wadi Zamzam watershed

The annual average temperature during 1958–2019 in the watershed region ranged between 20.5 and 21.2 °C: 20.5–20.7 °C in the coastal areas (Al-Qudahiya and Abu Qarin), and 20.67–20.98 °C in the central and southern regions of the Qaryat area (Fig. 5b). The highest average temperature was recorded in southern and southeastern regions near Ash-Shuwayrif area.

The annual averages of minimum and maximum temperatures varies with location. During 1958–2019, the annual averages of minimum temperatures ranged between 13.7 °C and 14.6 °C, with the highest average in Abu Qarin area and the lowest in Qaryat area. This difference is due to the desert climate and the influence of the Mediterranean Sea. On the other hand, the annual averages of maximum temperatures ranged between 26.4 °C and 28.6 °C during the same period (Fig. 6). In the coastal areas, they were between 26.6 °C and 26.7 °C in Al-Qudahiya and Abu Qarin, respectively, and about 27.3 °C in the Al-Qaryat area.

4.5 Morphometric Parameters in the Wadi Zamzam Watershed

The morphometric parameters can be grouped in four categories: topographic, areal, relief, and network properties. Geomorphological studies of watersheds differ in the number of parameters used. However, according to Koshak and Dawod (2011), the studies of Horton (1945) and Strahler (1957) have remained the main references for most morphometric studies conducted during this century by using geographic information systems and remote sensing. Therefore, the morphometric parameters used in this study were as follows.

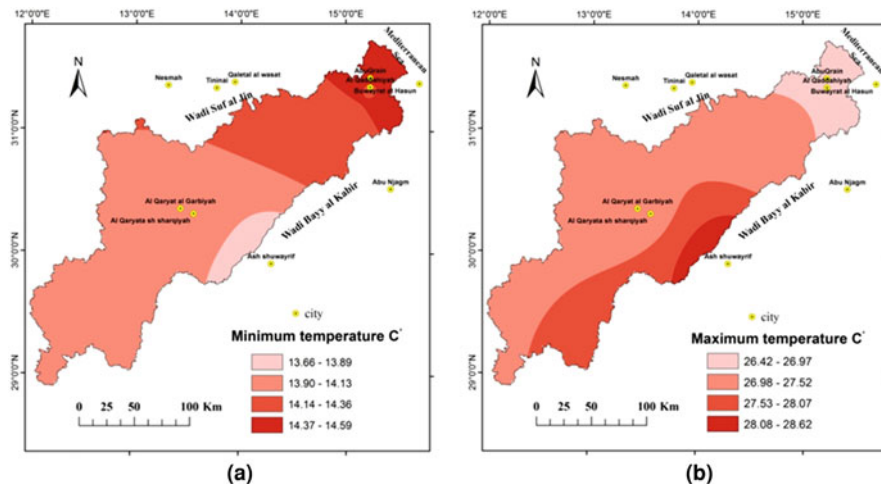


Fig. 6 (a) Minimum and (b) maximum average temperatures in the Wadi Zamzam watershed during 1958–2019

1. Areal parameters: Area, perimeter, length and width of the watershed, measured by using geographic information systems;
2. Shape parameters: Elongation ratio, circularity ratio, Lemniscate ratio and form factor, calculated by using mathematical equations;
3. Relief parameters: Watershed relief, relief ratio, degree of ruggedness, texture, and hypsometric integral;
4. Water network parameters: The order, lengths and numbers of streams were extracted using geographic information systems. Mathematical formulae were used to determine the percentages of streams, bifurcation rate, drainage density, stream frequency, and intensity of drainage (Table 3).

4.5.1 Areal Parameters

Watershed Area (A)

The watershed area directly affects the surface runoff, its volume, and the amount of sediment transported (Schumm 1963). The area of the Wadi Zamzam watershed is considered stable due to cessation of rain activity affecting water erosion, together with expansion of the watershed area since the rainy age, and the diversity of rock composition, and time. Wadi Zamzam flows from the southwest to the northeast on topographies differing in geology, climate and geomorphology. It is considered a large watershed, with an estimated area of 38,444.4 km² (Table 4).

Table 3 Formulae used to calculate morphometric parameters of the watershed

Morphometric parameter	Formula	Description	References
Areal parameters			
Area (A)		GIS (km ²)	GIS
Perimeter (P)		GIS (km)	
Length (L _b)		GIS (km) (Schumm 1956)	
Shape parameters			
Form factor	$R_f = A / (L_b)^2$	A = watershed area (km ²) L _b = watershed maximum length	Horton (1945)
Elongation ratio	$R_e = 1.128 * \sqrt{A} / L_b$	A = watershed area (km ²) L _b = watershed maximum length	Schumm (1956)
Circularity ratio	$R_c = 4 * 3.14 * A / L_p^2$	A = watershed area (km ²) L _p ² = watershed perimeter squared	Miller (1953) and Strahler (1964)
Lemniscate ratio (k)	$k = L_p^2 / 4 * A$	A = watershed area (km ²) L _p ² = watershed perimeter squared	Chorley et al. (1957)
Relief parameters			
Watershed relief (B _r)	Br = Z-z	The difference between the highest and lowest points in a water watershed	Strahler (1957)
Ruggedness number (Rn)	Rn = Br*Dd	D _d = drainage density H = watershed relief (B _r = H - h)	
Relief ratio (Rr)	Rr = H / Lb	H = watershed relief (Bh = H - h) L _b = watershed length	Schumm (1963)
Drainage texture (T)	T = Nu / P	Nu = Total stream number P = watershed perimeter	Horton (1945)
Hypsometric integral (Hi)	$H_i = (\bar{H} - h) / (H - h)$	\bar{H} = mean elevation H = maximum elevation in watershed h = minimum elevation in watershed	Strahler (1957)
Water network parameters			
Stream order (u)		Hierarchical order, GIS	Horton (1945)
Stream length (L)		Length of the stream (km) GIS	
Stream number (N _u)		Number of the streams (No) GIS	
Mean stream length (L _{sm})	$L_{sm} = Lu / Nu$	Lu = Total stream length of order u Nu = Total no. of stream segments of order u	Schumm (1956)
Stream length ratio (R _L)	$R_L = Lu / Lu-1$	Lu-1 = Total stream Length of its next lower order	
Bifurcation ratio (R _b)	$R_b = Nu / Nu + 1$	Nu = Total number of stream segments of order 'u' Nu+1 = number of segments of the next higher order	
Stream frequency (F _s)	Fs = N / A.	N = Total number of streams A = watershed area (km ²)	Horton (1945)
Drainage density (D _d)	D _d = L/A	L = Total length of streams A = watershed area (km ²)	
Length of overland flow (L _{of})	$L_{of} = 1 / 2 D_d$	D _d = drainage density	
Drainage intensity (D _i)	Di = Fs / Dd	Fs = stream frequency D _d = drainage density	Salim (2016)

Table 4 Morphometric parameters in Wadi Zamzam watershed

Areal parameters				
Area (km ²)	Perimeter (km)	Length (km)	Width (km)	
38,444.4	2419.7	440.5	190.5	
Shape parameters				
Form factor	Elongation ratio	Circularity ratio	Lemniscate ratio	Compactness coefficient
0.20	0.50	0.08	1.26	3.51
Relief parameters				
Watershed relief	Relief ratio	Ruggedness number	Hypsometric integral	Drainage texture
830	1.88	1.24	69.67	15.6
Water network parameters				
Drainage density	Stream frequency	Drainage intensity	Infiltration number	Length of overland flow
1.50	0.98	0.65	1.53	0.75

Watershed Perimeter (P)

The watershed perimeter represents the water-dividing line separating the watershed from neighboring watersheds. The perimeter of the Wadi Zamzam watershed is 2419.7 km (Table 4) and is characterized by a zigzag contour and a large number of its streams of the first order, which has resulted in an increase in its spatial extension and geomorphological activity during the fourth geological period.

Watershed Length (Lb)

This is the longitudinal distance from the farthest point on its perimeter at the estuary to the farthest point at its estuary in line with the main stream. Watershed length is one of the most significant factors that affect the surface runoff in the watershed and the occurrence of floods due to the rapid arrival of water to the estuary, besides other factors such as the slope, geological structure, soil type and climate (Schumm 1956). The length of the Wadi Zamzam watershed (about 440.5 km) was estimated using geographic information systems from the farthest point in the southwest, passing through the centre of the watershed, to its estuary within the water-dividing area.

Watershed Width

Watershed width is an important factor affecting water flow, infiltration and evaporation. It represents the latitudinal distance from the two farthest points on its perimeter, and thus determines the area that receives rain (Mahsoub 1997; Burqan 2015). The width of the Wadi Zamzam watershed was estimated at about 190.5 km (Table 4).

4.5.2 Shape Parameters

Form Factor

Form factor is important in morphometric studies because it shows the extent of regularity and consistency of the watershed. It is calculated as the relationship between the area of the watershed and the square of its length; its value falls in the range of 0–1. Small values indicate an elongated watershed (Miller 1953; Kanth and Hassan 2012). Values above 0.78 indicate the circularity of a watershed, the speed of the surface runoff, and flood force. According to the rock composition and prevailing climate, the form factor can vary among sub-watersheds (*e.g.*, watersheds of the first or second order). The value of the form factor of Wadi Zamzam is 0.20 (Table 4), which indicates elongation of the watershed. An increase in the length of the Wadi Zamzam watershed was noted. Furthermore, there is an increase in the number of its first-order streams and in the length of the watershed compared to its width.

Elongation Ratio

This is the ratio between the diameter of a circle having the same area as that of the watershed and the maximum length of the watershed (Schumm 1956). Values are in the range of 0–1. A ratio close to zero indicates elongation of a watershed, delay in the arrival of the surface water runoff to the estuary, decrease of a flood's impact due to the watershed's length, and increase in evaporation and infiltration, especially in dry and semi-arid climates. Watersheds are classified as rectangular if the elongation ratio is 0.6–0.7 and elongated if it is ≤ 0.5 , in which case it indicates a young watershed age (Pareta and Pareta 2011; Mahsoub and Rady 1989). The elongation ratio of the Wadi Zamzam watershed is 0.50, which indicates elongation of the watershed, continuation of geomorphological activity, and youthful stage.

Circularity Ratio

This ratio, suggested by Melton (1958), is the ratio between the area of a watershed and the area of a circle having the same perimeter as that of the watershed (Salim 2016). The circularity ratio varies between the main watershed and the sub-watersheds and is in the range of 0–1. A ratio close to one indicates circularity of the watershed, strong surface water runoff, rapid and intense flooding after a rainstorm, active erosive cycle, alter age stage, weakness of the rocky structure, and high sedimentary output (Kanth and Hassan 2012; Salim 2016; Salama 2007). The Wadi Zamzam watershed has a circularity ratio of 0.08, indicating continuation of the erosive cycle, transformation from a circular to a rectangular shape, and active geomorphological processes.

Lemniscate Ratio

This is one of the most important parameters, and as there are no fully-rounded watersheds, it is useful for assessing the shape of the water. This ratio is highly relied on in morphometric studies. It is calculated by dividing the square of the watershed length by four and multiplying by the area (Chorley et al. 1957; Gouda et al. 1991). Low values indicate the Lemniscate of the watershed. The Wadi Zamzam watershed has a Lemniscate ratio of 1.26 (Table 4), which indicates elongation of the watershed, activity of its geomorphological processes, and its youthful stage.

Compactness Coefficient

This coefficient is used as an indicator of the distance between the water-dividing line and the center of the watershed. This parameter expresses the extent to which the perimeter of the watershed is symmetrical, relief or regular with the area, and describes the shape of the watershed. High values indicate activity of the erosive cycle and increased tortuosity and irregularity, whereas low values indicate progress of the erosive cycle. It is calculated according to the following equation: $C_c = 0.2841 \times A^{0.5}$ (Pareta and Pareta 2011), where C_c = coefficient of compactness, A = watershed area (km^2), and 0.2841 is a constant. The coefficient in the Wadi Zamzam watershed is 3.51 (Table 4). This high value indicates that the watershed is in the youth stage and characterized by active erosion processes, tortuosity of surroundings, and irregularity.

4.5.3 Relief Parameter

Watershed Relief

Watershed relief is the difference between the highest and the lowest points in the watershed, measured in meters. It is helpful in studying erosion processes in a watershed and the impact of tectonic processes. It also has a role in determining the factors affecting the formation of the watershed and the erosive stage it has reached. Furthermore, it shows the slope of the watershed, which affects the speed and volume of the surface runoff and the sedimentary output. It also indicates the drainage density, stream pattern, hypsometric integral, and elongation ratio (Gouda et al. 1991; Salama 2007). The highest point in the Wadi Zamzam watershed, determined by using the digital elevation model and GIS, was about 832 m in the source areas, and the lowest point was about 2 m in the mouth area, giving a watershed relief of about 830 m (Table 4, Fig. 7). The slope in different areas of the Wadi Zamzam watershed ranged between zero and 62.5° (Fig. 8).

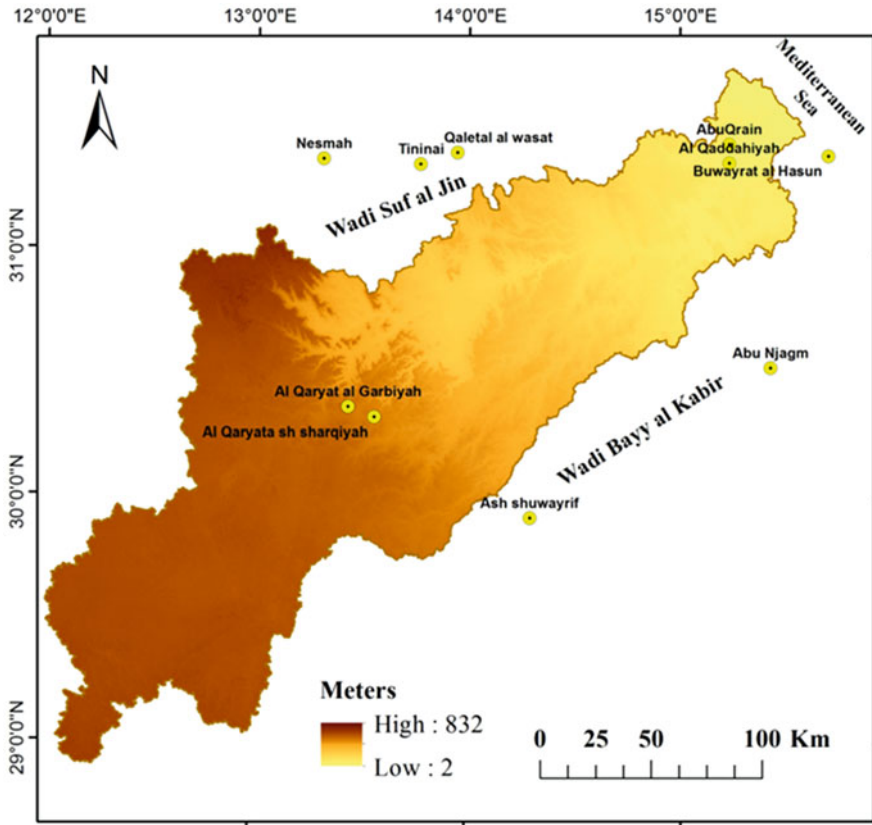


Fig. 7 Digital elevation model of the Wadi Zamzam watershed

Relief Ratio

This ratio is calculated by dividing the relief of the watershed (m) by its length (km), the relief ratio indicates the overall slope of the watershed surface. It affects other morphometric characteristics in the watershed, and the percentage of relief increases as the difference between the highest point and lowest point in the watershed increases (Strahler 1957; Gouda et al. 1991). The relief ratio in the Wadi Zamzam watershed is about 1.88, which indicates low drainage density.

Ruggedness Number

The degree of ruggedness reflects the relationship between the relief of the watershed and the density of the water network. Its value increases with increasing watershed relief and generally ranges from 0.06 in the plains to more than 1.0 in rugged mountainous areas (Strahler 1964). A high degree of ruggedness in a watershed

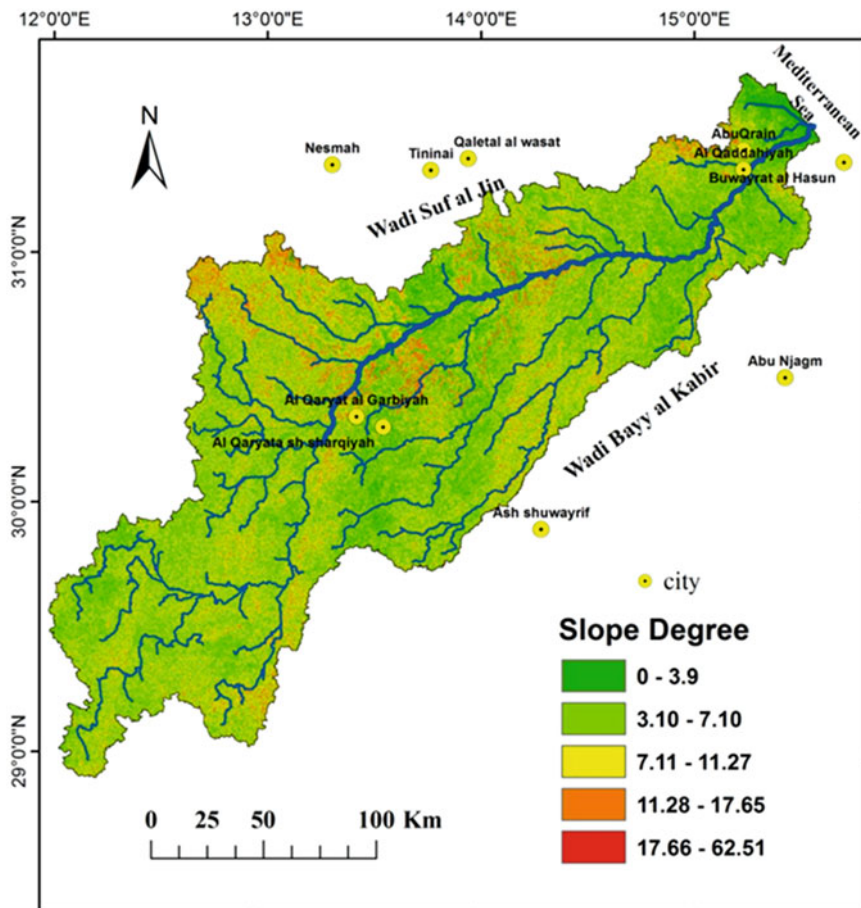


Fig. 8 The slope in Wadi Zamzam watershed

indicates activity of water erosion and high transport and sedimentary output due to the watershed relief and its slope, as well as increase in surface runoff, its volume and its density, which increase the possibility of flooding (Burqan 2015; Rayan 2014). The degree of ruggedness in the Wadi Zamzam watershed was about 1.24 (Table 4), indicating that it runs in a moderately rugged area with a slight slope, resulting in low drainage density, water erosion and sedimentary output.

Hypsometric Analysis

This accurate, quantitative, cartographic scale shows the erosive stage that a wadi has reached based on the relationship between the relative areas and the relative heights in the watershed. The hypsometric integral illustrates the relationship

between the relative height and the relative area. The former is the ratio between the height of any contour line in the watershed and the maximum height in the watershed. The latter is the ratio of the area confined between any contour line and the perimeter of the watershed to the total area of the watershed. The hypsometric integral is affected by the geology of the watershed, its rock structure, its type, and the climate (Pérez-Peña et al. 2009). Several methods have been proposed to measure the hypsometric parameter in watersheds (Strahler 1952; Miller 1953; Schumm 1956). We used Strahler's method to derive the hypsometric integral and curve because of its simplicity, ease of application, and accuracy in determining the stage of the erosive cycle.

Hypsometric Integral It is an accurate morphometric scale for measuring the time interval cut from the sculptural cycle of the Zamzam Valley drainage basin.

This accurate morphometric scale measures the time cut-off from the erosive cycle by determining the relationship between the watershed area (km^2) and its topography (m). High values of the hypsometric integral indicate an increase in the watershed area due to the high density of drainage and the decrease in topography, pointing to progression of the age stage in the watershed. There is a direct relationship between the hypsometric integral values and the time cut-off from the watershed erosive cycle. A watershed is in the aging phase when the hypsometric integral ≤ 0.4 , the maturity phase if it is 0.4–0.6, and the youth stage if it is 0.61–0.80 (Strahler 1957; Gouda et al. 1991; Salim 2016). Wadi Zamzam has a hypsometric integral of 0.7, which means that 30% of its rock mass has been eroded.

Hypsometric Curve This curve graphically measures the erosive stage of the watershed by calculating the area between consecutive contour lines, converting it to an aggregate relative area plotted on the X-axis, and converting the difference between the highest and the lowest points in the watershed to an aggregate percentage plotted on the Y-axis in the form of a descending aggregate curve. It is possible to compare hypsometric curves of different watersheds or different secondary watersheds within the same main watershed (Al-Maghazi 2015; Gouda et al. 1991). According to the classification of Strahler (1957), the Wadi Zamzam watershed is in the young stage (Fig. 9). With a hypsometric integral >0.6 , the watershed is in the first stage of the erosive cycle, when the watershed erodes the topography of its surface towards the level of the base (Fig. 10).

Drainage Texture

This is the degree to which the watershed surface intersects with the water drainage network, and how close or far apart they are. The texture of the watershed is affected by the type of prevailing climate, the amount of rain, the relief of the watershed, the rock texture, the vegetation cover and its density, and the soil. According to one classification (Smith 1950), watersheds are classified according to the texture and to the degree of intersection of their surface with streams as follows.

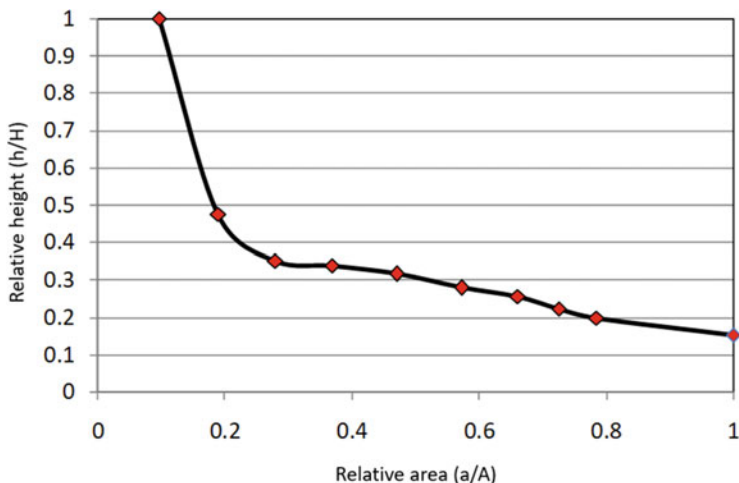
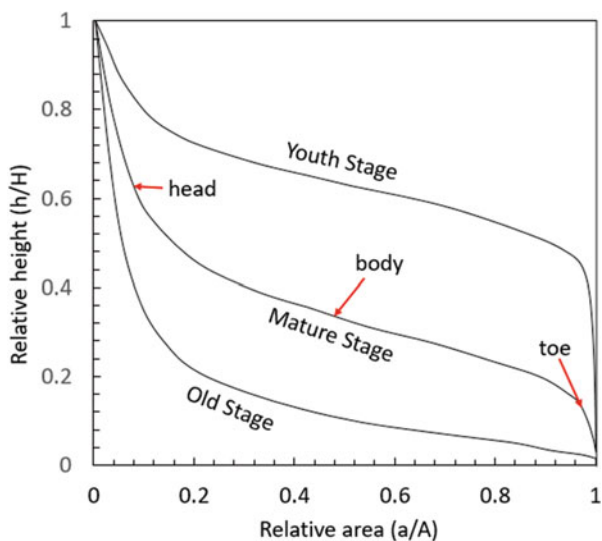


Fig. 9 Hypsometric curve of the Wadi Zamzam watershed c

Fig. 10 Hypsometric curves for the stages of youth, maturity and old age in watersheds. Adapted from (Strahler 1957)



1. Coarse: The texture is <4 degrees.
2. Medium texture: The degree of intersection of their surface with streams is 4–10.
3. Fine texture: The texture degree is >10. A study of 45 watersheds in the USA found that the textures ranged from 1.17 for the roughest watersheds to 23,840 for the most interrupted watersheds. The wadi Zamzam Watershed has a fine texture (15.6°).

4.5.4 Water Network Parameter

Stream Order (u) and Stream Number (N_u)

The ordering system of Horton (1945) as modified by Strahler (1957) was used to classify the streams in the Wadi Zamzam watershed (Fig. 11). In this scheme, confluence of streams of the first order feed into second-order streams, and so on. When a tributary of a lower order meets a higher order, it does not affect the arrangement until reaching the main stream that represents the highest order in the watershed. Based on this, the Wadi Zamzam watershed is of the eighth order (Table 5 and Fig. 12).

The total number of streams in the watershed and the number in each order have a direct impact on the volume of river discharge and the erosive stage of the watershed. They were counted by using GIS. According to Horton’s principle (Horton 1932), the number of streams is negatively correlated with the order. There are about 37,800 streams in the Wadi Zamzam watershed. Of these, 29,058 are first order streams (76.8%), 6757 are second order (17.9%), and 1536 third order (4.1%) (Table 5). While the reliefs in the rest of the orders ranged between 0.93–0.003 and their numbers ranged between 352 in the fourth order to the main stream in the eighth order (Table 5).

Stream Length (L_u) and Mean Stream Length (L_{sm})

The stream length is a measure of the hydrological characteristics of the underlying rock formations and the drainage degree (Chadha and Neupane 2011). The length of the streams refers to the sum of the stream lengths in the watershed’s water network (Salama 2007) or to the sum of their lengths in the secondary watersheds or in a stream order. The total length of the water network in the Wadi Zamzam watershed is 57,654.3 km. The longest order was the first order, reaching 28,626.9 km (49.7%

Fig. 11 Ordering system. Adapted from (Strahler 1957)

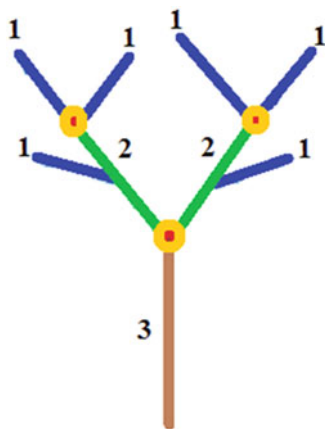


Table 5 Linear morphometric parameters of the drainage network of the Wadi Zamzam watershed drainage

Stream order (u)	Stream number (Nu)	%	Stream length (Lu)	%	Sum of streams for pairs of orders	Bifurcation ratio (R _b)	Number	Mean stream length (L _{sm})	Stream Length Ratio (R _L)	Mean bifurcation ratio (R _{bm})
1	29,058	76.87	28,627	49.65	–	–	–	0.985	–	4.78
2	6757	17.88	14,394	24.97	35,815	4.30	154,004.5	2.13	0.502	–
3	1536	4.06	7330	12.71	8293	4.39	36,406.3	4.77	0.509	–
4	352	0.93	3689	6.40	1888	4.36	8231.7	10.84	0.503	–
5	74	0.20	1704	2.96	426	4.76	2027.8	23.03	0.462	–
6	20	0.05	1193	2.07	94	3.7	347.8	59.65	0.700	4.32
7	2	0.01	343	0.60	22	10	220	171.1	0.288	–
8	1	0.00	374	0.65	23	2	46	373.9	1.089	–
Total	37,800	100	57,654.3	100	46,561	–	201,284.1	–	–	–

Probable bifurcation rate = $201,284.1/46,561 = 4.32$

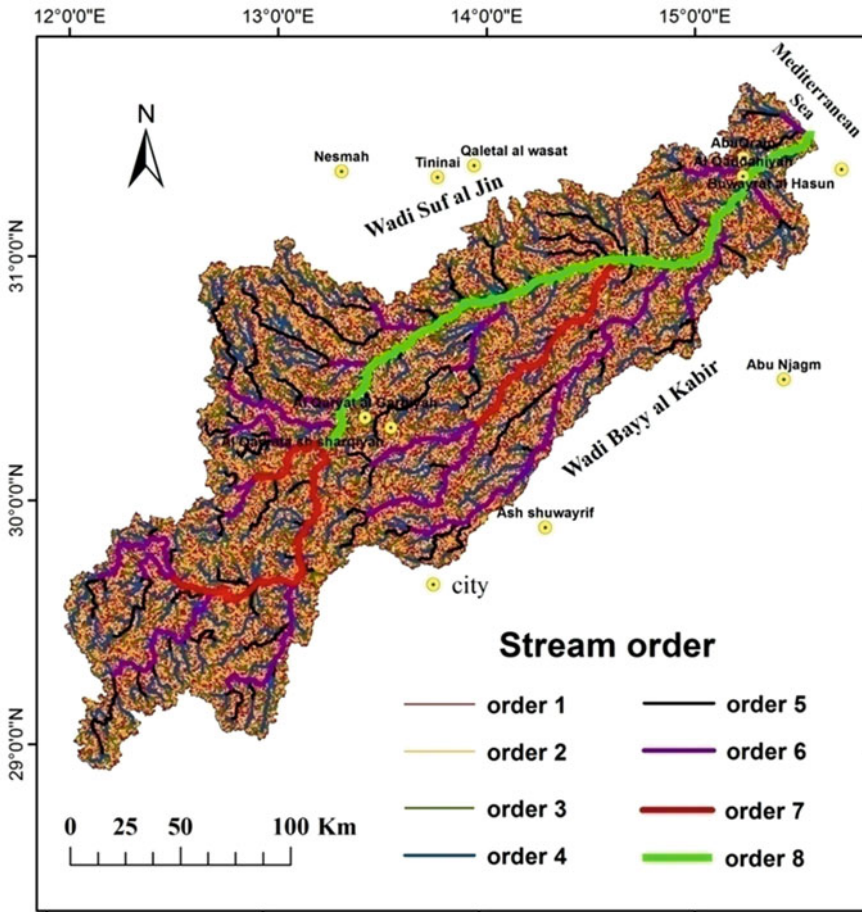


Fig. 12 Stream orders in the Wadi Zamzam watershed

of the total stream length), followed by the second order (14,393.6 km, 25.0%). The third order (7330.1 km) accounted for 12.7% of all streams, and the fourth order (3688.9 km) for 6.40%. The fifth to eighth orders (total 3614.8 km) represent 6.3% of the total stream length.

We noted that as one proceeds from one order to the next higher one, total length decreases. The average length of the streams in the Wadi Zamzam watershed was about 1.53 km. As expected from the confluence of streams, the number of streams and their lengths have a negative exponential relationship with the order number of the streams. According to Horton (1945), the relationship between stream length and stream order are geometrically related. The average lengths of the first three orders were about 1.0, 2.1 and 4.8 km, respectively, and reached 171.7 and 373.9 km in the seventh the eighth orders, respectively (Table 5, and Fig. 13). The lengths of the streams in a watershed and their proximity to each other are affected by the rock

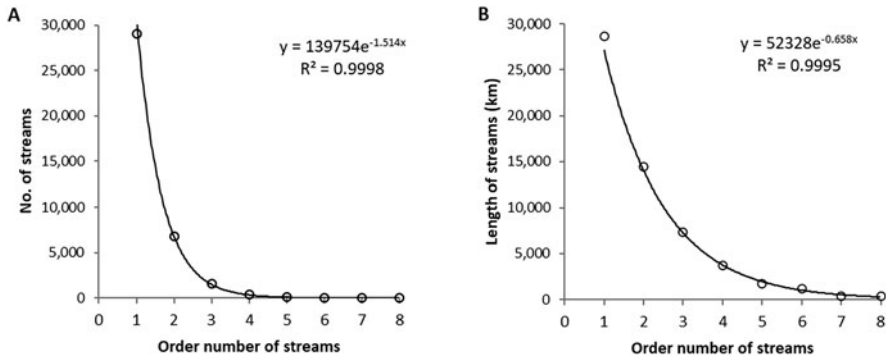


Fig. 13 Regression of the number of streams (a) and their lengths (b) with their order number in Wadi Zamzam watershed. (The trendlines were computed in Microsoft Excel)

composition, its hardness degree, and its structural integrity in terms of the presence of cracks, breaks and faults (Gouda et al. 1991). The stream length ratio in the Wadi Zamzam watershed varies between 0.288 and 1.089 due to the variation in the watershed's topography and the slope.

Bifurcation Ratio (R_b)

The bifurcation ratio represents the branching pattern of a drainage network (Hajam et al. 2013). It is the ratio between the number of streams in a certain order and the number of streams in the next order. This ratio is an important morphometric parameter of river drainage and the risk of flooding. The bifurcation ratio is inversely related to the discharge (Table 5). The bifurcation ratio in the Wadi Zamzam watershed in stream orders 1–6 ranges from 3.7 to 4.76. The reason for this narrow range is the homogeneity of the geological formations, soil quality, and climate characteristics. This is in line with an early report that homogeneous watersheds have bifurcation ratios of 3–5 (Horton 1945). However, in the seventh order streams, the ratio reached 10, only to decrease to 2 in streams of the eighth order due to differences in the geological components, soil and climate, and the decrease in the number of streams in the estuary. The mean bifurcation ratio in the Wadi Zamzam watershed was 4.78 and the probable bifurcation rate 4.32 (Table 5).

Drainage Density (D_d)

Drainage density represents the relationship between the total lengths of the streams and the area of the watershed or sub-watersheds. This parameter indicates the extent of convergence and divergence of the streams within the watershed and provides a clear picture of the distribution or spread of the water network in the watershed, as the density increases with the increase of the stream lengths. The drainage density is

affected by the amount of precipitation, the quality of the soil, its permeability, the amount of infiltration, evaporation rates, vegetation cover and its density, and the rock composition. The drainage density in the Wadi Zamzam watershed was calculated as 1.5 km/km^2 (Table 4), which is very low according to the Smith classification (Smith 1950). The reason for this low value is the highly permeable desert soil covering a large area of the Wadi Zamzam watershed and the dry and semi-arid climate, as well as the limestone formations and deposits and their associated seepage dating back to the ages of the Thanetian and Ypresian deposits covering a wide area of the watershed.

Stream Frequency (F_s)

The stream frequency is the ratio between the number of streams and the watershed area (Burqan 2015; Gouda et al. 1991; Smith 1950). It affects the volume of runoff in the watershed and the occurrence of flooding. High values indicate the possibility of water collecting in large quantities and the occurrence of flooding. Its value in the Wadi Zamzam watershed is about $0.98 \text{ streams/km}^2$. This low value is due to factors affecting the drainage density in addition to the watershed area factor.

Drainage Intensity (D_i)

Drainage intensity is the relation between the river frequency and the drainage density in the watershed. It indicates the activity of water erosion (Table 4). The drainage intensity in the Wadi Zamzam watershed was low (0.65) due to the dry climate and the lack of rain.

Infiltration Number (I_f)

The infiltration number is an indicator of the speed of water flow in the watershed, the leakage of water into the ground, and the drainage density. High values indicate rapid flow, absence of leakage, and impermeability of the rocks. Drainage density decreases with increasing leakage and infiltration and with the presence of permeable rocks. It is calculated by multiplying the discharge density by the river frequency (Burqan 2015). The infiltration number in the Wadi Zamzam watershed is 1.53.

Length of Overland Flow (L_{of})

This parameter represents the relationship between the total length of the watershed, its diameter, and the quantities that flow in its streams. L_{of} is affected by the strength of rainstorms, the slope, the quality of the soil, and the rock composition. According

to Horton 1945, it is defined as half the drainage density in the watershed and ranges from zero to one. The length of overland flow is 0.75 in the Wadi Zamzam watershed, which runs in a low relief area.

5 Conclusion

Geographic information systems, production of digital maps and morphometric analyses are important for studying floods, especially flash floods, and their effects on population centers and agricultural production sites. This study shows that the Wadi Zamzam watershed has an elongated shape, has a slight slope, and is located in a moderately rugged area. It is of the eighth degree and is in its young stage of the erosive cycle. Its drainage density is very low, which means that water erosion and sedimentary output are both low. The results of this study are useful in planning and implementing spatial development in the watershed, managing and developing its natural resources, and developing early warning, evacuation and relief plans to mitigate the impact of floods. The study recommends the establishment of weather monitoring stations in the watershed, especially in the upstream areas.

Author Contributions **Ali M. Salim:** conceptualization, methodology, software, data curation, formal analysis, writing—original draft, visualization, validation, investigation. **Ibtisam A. Albira:** conceptualization, supervision, translation, writing—review, and editing. **Safa A. Ebsheer:** formal analysis. All authors have read and agreed to the published version of the manuscript.

References

- Al-Maghazi BAR (2015) Studying the morphometric characteristics of the Wadi Al-Hay watershed using geographic information systems: a study in applied geomorphology. (Master Thesis). Islamic University, Gaza
- Burqan AM (2015) Studying the morphometric characteristics of the Wadi Gaza watershed and the water harvesting of its upper watershed using geographic information systems. (Master Thesis). An-Najah University, Nablus. https://scholar.najah.edu/sites/default/files/Mohammed%20Abdullah%20Adil%20Burgan_0.pdf
- Chadha D, Neupane B (2011) Significance of geomorphic analysis of watershed for optimization of recharge structures. UNESCO, New Delhi
- Chorley RJ, Malm DE, Pogorzelski HA (1957) A new standard for estimating drainage basin shape. *Am J Sci* 255(2):138–141
- El Bayomi G (2010) Morphometric analysis in Esna Basin, using remote sensing and GIS techniques. Paper presented at the US-Egypt workshop on space technology and geo-information for sustainable development, Cairo, Egypt
- Gouda GH, Ashour MM, Desouky SA, Trapp MM, Marghani AM, Mustafa MR (1991) Geomorphological analysis tools. University Knowledge House, Alexandria
- Hajam RA, Hamid A, Bhat S (2013) Application of morphometric analysis for geo-hydrological studies using geo-spatial technology—a case study of Vishav Drainage Basin. *Hydrol Curr Res* 4(3):1–12

- Horton RE (1932) Drainage-basin characteristics. *EOS Trans Am Geophys Union* 13(1):350–361
- Horton RE (1945) Erosional development of streams and their drainage watersheds; hydrophysical approach to quantitative morphology. *Geological Society of America Bulletin* (vol 56, pp 275–370). doi: Retrieved fro: [https://doi.org/10.1130/0016-7606\(1945\)56\[275:EDOSAT\]2.0.CO;2](https://doi.org/10.1130/0016-7606(1945)56[275:EDOSAT]2.0.CO;2)
- Industrial Research Center (2009) Geological map of Libya. Tripoli, Libya
- Kanth T, Hassan Z (2012) Morphometric analysis and prioritization of watersheds for soil and water resource management in Wular catchment using geo-spatial tools. *Int J Geol Earth Environ Sci* 2(1):30–41
- Koshak N, Dawod G (2011) A GIS morphometric analysis of hydrological catchments within Makkah Metropolitan area, Saudi Arabia. *Int J Geomatics Geosci* 2(2):544–554
- Mahsoub MS, Rady MM (1989) Geomorphological processes. Dar Al Thaqaqa, Cairo
- Mahsoub MS (1997) Geomorphology of landforms. Dar al-Fikr al-Arabi, Cairo
- Miller VC (1953) A quantitative geomorphic study of drainage watershed characteristics in the Clinch Mountain area Virginia and Tennessee. Columbia University, New York
- Panhalkar S, Mali S, Pawar C (2012) Morphometric analysis and watershed development prioritization of Hiranyakeshi Basin in Maharashtra. *India Int J Environ Sci* 3(1):525–534
- Pareta K, Pareta U (2011) Hydromorphogeological study of Karawan watershed using GIS and remote sensing techniques. *Int Scie Res J* 3(4):243–268
- Pérez-Peña JV, Azañón JM, Azor A (2009) CalHypso: an ArcGIS extension to calculate hypsometric curves and their statistical moments. Applications to drainage watershed analysis in SE Spain. *Comput Geosci* 35(6):1214–1223
- Planning Ministry. Survey Department (1978) National atlas. Tripoli, Libya
- Rayan WK (2014) Morphometric characteristics of Wadi Al-Fara' watershed – Palestine using geographic information systems and digital elevation models. (Master Thesis). Islamic University, Gaza
- Salama HR (2007) The origins of geomorphology, 1st edn. Dar Al-Masira, Amman
- Salim AM (2016) Morphometric characteristics analysis of the Wadi Kaam Watershed – Libya using geographic information systems. Paper presented at the international conference for spatial technologies -GEOTEC 2, Tripoli- Libya, 6–8 December
- Schumm SA (1956) Evolution of drainage systems and slopes in badlands at Perth Amboy, New Jersey. *Geol Soc Am Bull* 67(5):597–646
- Schumm SA (1963) Sinuosity of alluvial rivers on the Great Plains. *Geol Soc Am Bull* 74(9): 1089–1100
- Smith KG (1950) Standards for grading texture of erosional topography. *Am J Sci* 248(9):655–668
- Strahler AN (1952) Hypsometric (area-altitude) analysis of erosional topography. *Geol Soc Am Bull* 63(11):1117–1142
- Strahler AN (1957) Quantitative analysis of watershed geomorphology. *Trans Am Geophys Union* 38(6):913–920
- Strahler AN (1964) Part II. Quantitative geomorphology of drainage watersheds and channel networks. *Handbook of applied hydrology*. McGraw-Hill, New York, pp 4–39
- Tamang D, Dhakal D, Shresta D, Sharma N (2012) Morphometric analysis and prioritization of miniwatersheds in Rongli watershed, Sikkim (India) using remote sensing and GIS techniques. *Int J Fundam Appl Sci* 1(3):61–66
- Zende AM, Atal KR, Nagarajan R, Deshpande PK (2012) GIS based morphometric analysis of nine major sub-watersheds of Yerala River, Western Maharashtra, India. Paper presented at the 2nd international conference on advances in civil engineering, Tirupati, India, 7th Sept.–8th Sept

Dr. Ali M. Salim is an assistant professor of climatic geography at the Department of Geography, Faculty of Education, University of Misurata, Misurata, Libya. He received MSc (agricultural geography and development) in 2005 from the University of Elmergib, Libya. He completed his PhD (climate geography) in 2016 from the University of Jordan, Jordan. He has specialized in climatic issues. His main research interests are climate change, its trends, and its effects on humans in Libya. He has been teaching courses and has supervised master's and bachelor's degree students since 2008. He is a member of the Libyan Association for Geographical Information Systems and Remote Sensing and a member of the Consultation Committee of the Libyan Journal of Geographical Studies.

Dr. Ibtisam A. Albira is a lecturer of environmental studies at the Department of Geography, Faculty of Education, University of Misurata, Misurata, Libya. She received MSc (environmental geography) in 2007 from the University of Misurata, Misurata, Libya. She completed her PhD (environmental studies) in 2019 from the UM University of Malaya, Malaysia. She specialized in environmental pollution issues. Her main research interests focused on solid waste management and site selection, and environmental pollution. She has been teaching courses and has supervised the bachelor's degree students since 2008.

Ms. Safa A. Ebsheer is a geography teacher working in the education sector. She received her bachelor's degree from the Department of Geography, Faculty of Education, University of Misurata, Misurata, Libya, in 2016.

Geospatial Mapping and Analysis of the 2019 Flood Disaster Extent and Impact in the City of Ghat in Southwestern Libya Using Google Earth Engine and Deep Learning Technique



Hamdi A. Zurqani , Abdulsalam Al-Bukhari, Alsaket O. Aldaikh, Khalid I. Elfadli, and Ali A. Bataw

Abstract Flooding impacts from heavy rainfall, thunderstorm, and other natural hazards are a significant concern in many areas of the world. The objectives of this study were to: (1) develop a framework to identify flood-affected areas after storm impact; (2) map the flooded areas caused by the heavy rainfall and thunderstorm in the region; and (3) assess the major effect of the storm on the land cover during the flood period. The flood extent extraction analysis results indicated that approximately 2255.67 hectares of the study area were flooded during the wave of the heavy rainfall and thunderstorm event in June 2019, causing flooding and damage in several locations around the city. During this event, 70% of urban areas and roads were affected by floods, followed by half of the shrubs area inundated. About 30% of agriculture, tree canopy, and barren land were flooded overall land cover classes,

H. A. Zurqani (✉)

University of Arkansas Agricultural Experiment Station, Arkansas Forest Resources Center, College of Forestry, Agriculture and Natural Resources, University of Arkansas at Monticello, Monticello, AR, USA

e-mail: Zurqani@uamont.edu; Hzurqani@uark.edu

A. Al-Bukhari

Department of Forest and Rangeland, Faculty of Natural Resources and Environmental Sciences, Omar Al-Mukhtar University, Al-Bayda, Libya

A. O. Aldaikh

Department of Forest and Rangeland, Faculty of Natural Resources and Environmental Sciences, University of Omar Al-Mukhtar, Al-Bayda, Libya

K. I. Elfadli

Libyan National Meteorological Center, Tripoli, Libya

A. A. Bataw

Department of Zoology, Faculty of Sciences, University of Omar Al-Mukhtar, Al-Bayda, Libya

while the sand dunes had less area affected. These results not only indicate flood risk on the land cover but also demonstrate the advantage of utilizing Google Earth Engine and the public archive database in its platform to track and monitor the natural hazards over time.

Keywords North Africa · Remote sensing · Geographic information systems (GIS) · Machine learning · Flood mapping · Land cover classification

1 Introduction

Natural disasters are considered the leading cause of irrecoverable damages worldwide, and several societies are still vulnerable to flash floods despite the proliferation of advanced technologies. Therefore, flash floods continue to claim many people's lives worldwide and cause severe damage to property, infrastructure, and incur economic losses (Colombo et al. 2002). In the arid regions, flash floods are among the most devastating natural hazards of human casualties and damages (Abdel-Fattah et al. 2015). In arid and semi-arid areas, flash floods significantly affect human life and the ecosystem balance through soil erosion and sediment exchange between different regions (Yousif and Hussien 2020). The arid environment usually dries up throughout the year except after sudden heavy rains that often lead to flash floods (United Nations 2021). A flash flood can be defined as a quick progressing excessive rainfall in a short time not accompanied by apparent signs and fall on steep, shallow, low permeability soils, bared rocks, and low cover vegetation (Lin 1999). This, combined with the short time available to respond, increases the risk to people and property (Sene 2012).

The most frequent natural disaster in the Middle East and North Africa (MNA) is flooding. About 213 flood events have hit 15 MNA countries from 1900 to 2011, causing the death of about 19,000 people, affecting 8.6 million others (Banerjee et al. 2014). Floods are common in Morocco where many flash flood events occurred in 1995, 2002, and 2008, which led to the death of 230, 25, and 13, inundating many houses and cutting off the main roads (Moawad et al. 2016). In Algeria 2001, in the Bab El Oued neighborhood, more than 700 lost their lives, and thousands were homeless due to flash floods (Korichi et al. 2016). In Egypt, flash floods frequently occur in many regions; however, the worst during the past few decades occurred in 1994 in Drunka Village and 2010 in Wadi El Arish. These events left 15 dead, and hundreds injured with breathing problems caused by the flames from exploding oil tanks washed away by the floods (Ashour 2002; Moawad et al. 2016). About 2000 homes were completely or partially destroyed. Cars, trucks, trees, roads, power lines, and water systems were washed away. Damage was estimated at 137 million Egyptian pounds (Moawad 2013).

In Mali in 2012, floods have inundated homes, and food crops in the southern regions of Segou, Koulikoro, Sikasso, Kayes, and Mopti, where more than 2800 homes have collapsed, nearly 9000 people were displaced, and five people were killed (OCHA 2012). In Chad 2012, floods caused the displacement of hundreds of thousands and have swamped 255,720 hectares of croplands (IRIN 2013). In Jeddah 2009 and 2011, flash floods hit the city, which cost approximately 10 billion Saudi Riyal (around 3 billion USD), causing significant destruction to city infrastructures such as highways, settlement, and livelihood as a consequence of a combination of natural and anthropogenic factors (Youssef et al. 2016).

Libya is among arid countries that face flash floods. The rainfall in Libya is inconsistent due to the influence of the Sahara and Mediterranean conditions. The common thunderstorms are intensive and short in duration (United Nations 2021). These rainstorms observed in Libya over the western, southern, and eastern regions lead to flash flooding. In the Jabal Al-Akhdar region, floods occurred on 27 September 2018 in Mikhili village, causing damage to infrastructure (Zamot and Afkareen 2020). In southwestern Libya, severe flooding inundated the Ghat district in June 2019, causing casualties, including four fatalities and 30 minor injuries (OCHA 2019). Thousands of homes and structures were inundated affecting 20,000 people, with farmlands, roads, and schools severely damaged. The government allocated LYD10 million (USD7.1 million) for the initial cost of relief and recovery (Podlaha et al. 2019). Flash floods are among the most frequent and costly natural disasters in terms of human and economic loss in some arid regions (Abdel-Fattah et al. 2015); for example, in Libya from 1990 to 2006, the cost of damages caused by floods was about 27 million Euro (Llasat et al. 2010).

Floods in the desert are generally unforeseeable and uncommon (Reid et al. 1994). The meteorological measurements in these areas are often rainfall (Dolman et al. 1997). Therefore, flood in these regions varies from year to year in terms of frequency and severity that cause the floods (Warner 2004). Desert rainfall is often more spatially variable than the other regions (Moawad et al. 2016). Unfortunately, there is often a lack of data on critical hydrological processes in arid areas. This limits the ability to understand the flash flood process and use this knowledge to minimize its threat (Abdel-Fattah et al. 2015). Remote sensing (RS) and geographic information system (GIS) techniques can be applied in flood modeling and prediction (Billa et al. 2005; Youssef et al. 2011; Youssef et al. 2015; Haq et al. 2012). Also, the relationship between the land-use changes and the flood hazards can be analyzed using GIS (Chang et al. 2009).

The present study assesses the flood event of June 2019 which affected the Ghat municipality in the Fezzan region of southwestern Libya, utilizing pre-processed Sentinel-2 imagery available through the Google Earth Engine (GEE) platform. Then, it uses the flood hazard layer for inundation statistics and damage assessment. The main objectives of this study were to: (1) develop a framework to identify flood-affected areas after storm impact; (2) map the flooded areas caused by the heavy rainfall and thunderstorm in the region; and (3) assess the significant effect of the storm on the land cover during the flood period.

2 Materials and Methods

2.1 Study Area

In June 2019, a wave of heavy rainfall and thunderstorm had hit Ghat municipality in the Fezzan region of southwestern Libya. The rainfall commenced on 28 May 2019 and intensified on 2 June 2019 and caused flooding and damage in several locations around the city (Fig. 1). Over 20,000 persons have been affected, four people died, including three children, and about 30 suffered minor injuries (UNICEF 2019). It was also reported that about 4250 people had been displaced from their homes to nearby areas (UNICEF 2019). The water levels have not receded and vary between 0.5 to 2 m, depending on the area.

The government allocated LYD10 million (USD7.1 million) to the initial relief and recovery of the reported damage (Podlaha et al. 2019). There was severe damage to infrastructure, telecommunications networks, and farmland vital for livelihoods. Ghat hospital was partially flooded, and service provision was affected. The risk of running out of fuel and domestic commodities because of infrastructure damage was reported (OCHA 2019).

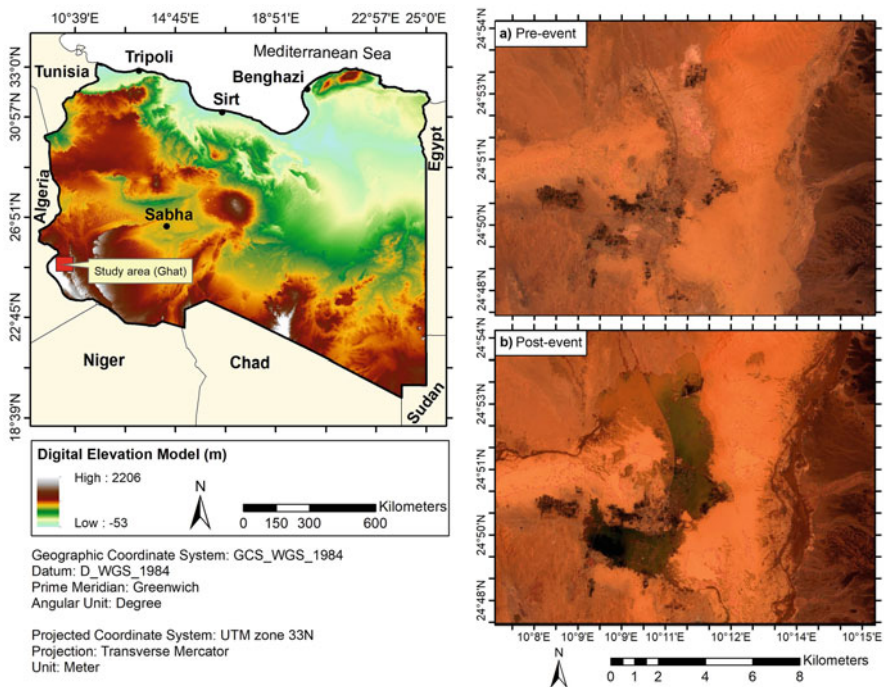


Fig. 1 Location map of the study area (i.e., Ghat) in the Fezzan region of southwestern Libya; (a) pre-event Sentinel-2 image acquired on the 23rd of May 2019, and (b) post-event Sentinel-2 image acquired on the 07th of June 2019

2.2 Climatic Characterization of the Region

The Saharan Ghat region in Africa is mediated by the tropical desert regions according to the “KOPPEN” climate classification (Markus et al. 2006), however its climate is subject to the influence of the climatic system that rules over the northern hemisphere where the temperature rises in summer (June, July, August) and decreases in winter (December, January, February) with one well-defined thermal seasonal cycle. The climate of the region is also characterized by one seasonal cycle of rainfall, if less, accompanied by three peaks, the highest in March, followed by January and October. This is due to the region’s rather strong and indirect effect on seasonal trade winds during spring and autumn, respectively, resulting from their collision with the northern foothills of the front of the Tassili mountain range, located in the middle of the Sahara Desert to the west and northwest of the Ghat region with the Algerian border. The largest part of this series is situated in the territory of the Algerian state, Where it reaches a maximum height of more than 2000 meters above sea level.

By analyzing the climatic data of the region during the period (1981–2010) available at the Libyan national meteorological center (Fig. 2), it can be noted that the climatology of annual temperature reaches (24.1 °C), which is the highest at the national level, with a desert diurnal temperature range (DTR) of up to 15.0 °C. At the season level, the hottest is summer season (32.5 °C), followed by spring season (25.3 °C), followed by autumn season (25.0 °C), then the winter (the coldest) is 13.8 °C. January (12.2 °C) is considered the coldest and the hottest month is June (32.8 °C), June and July represent the most extremes of daily maximum temperature

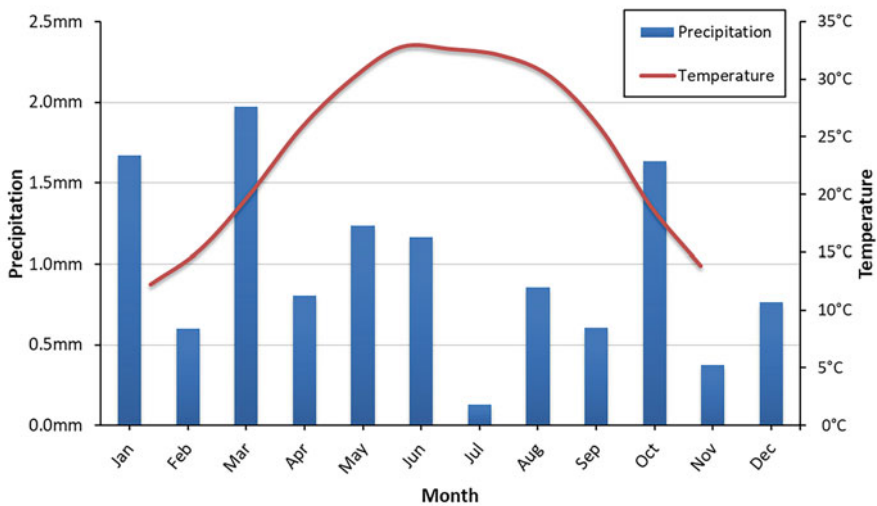


Fig. 2 Climatic profile of temperature and precipitation climatology of the region during the period (1981–2010)

that reached (45.8 °C), while January is considered is the month with the most daily minimum temperature extremes that reached (6.7 °C) below freezing (0 °C). This justifies the high annual of diurnal temperature range that prevails in this region.

The annual average of very little precipitation is about (11.5 mm) however, the spring season represents the highest percentage of this average (34%), followed by winter, autumn, and summer seasons by about 25.7%, 22.1% and 18.2% respectively. Climatically, the most frequent rainy months are March (2.0 mm), followed by January (1.7 mm) then October (1.6 mm), this explains the presence of 3 peaks during the rainfall season. On the other hand, rainfall of June (1.2 mm) contributes about 54% of the summer rainfall. The climatology of the number of rainy days ($> = 0.1$ mm) does not exceed 3 days per year, however, the year 1981 experienced the highest number of rainy days, which was 7 days. The region also experienced a relative climatic extreme of a maximum rainfall in a day, where the highest was recorded in March (1995) to reach about (20.0 mm/day), while January (2000) and October (2002) reached about (11.0 mm/day) and (10.0 mm/day) respectively. It is noteworthy that, the seasonal cycle of temperature is inversely proportional to the seasonal cycle of rainfall, this explains the significant poor health of vegetation cover in the region.

2.3 Data and Methods

This study applied three-step approaches, the first step is to extract the flood extent (10.2.2.1), the second step is to map the land cover within the study area, and third step is to assess the significant effect of the storm on the land cover during the flood period (10.2.2.2). In the first step of the analysis, pre-processed Sentinel-2 imagery available through the Google Earth Engine (GEE) platform was used to extract the flood extent using a numerical indicator derived from optical satellite imagery (i.e., spectral index) (Table 1). In the second step, the land cover classification technique was applied and evaluated using ArcGIS software (i.e., deep learning technique) and PlanetScope imagery (Table 1). The high-resolution PlanetScope imagery was also used as a reference dataset for training and validating the classification. The resulting land cover classification was used to evaluate the flood damage during the storm event.

Table 1 Data sources and descriptions

Data layer	Source	Resolution	Date
Sentinel-2 MSI: Multi-Spectral instrument, level-2A	Google Earth Engine (GEE), data provided by European Union/ESA/Copernicus	10–60 m	2019
PlanetScope imagery	Planet application program Interface: In space for life on earth. San Francisco, CA.	3 m	2019

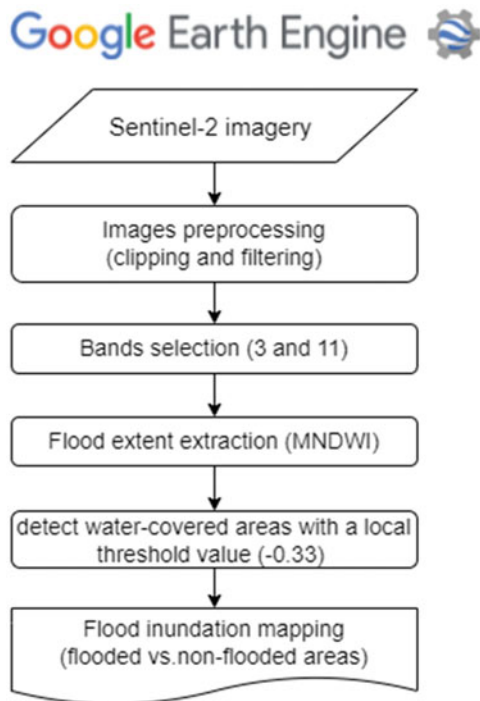
2.3.1 Flood Extent Extraction

Google Earth Engine facilitates a fast analysis platform by using Google’s computing infrastructure (Zurqani et al. 2018). In this analysis, the flood detection technique was applied by developing code in the GEE platform (<https://earthengine.google.org/>) using Sentinel-2 MSI (Multispectral Instrument) imagery. Sentinel-2 is an Earth observation mission from the Copernicus Programme that systematically acquires optical imagery at high spatial resolution (10 m to 60 m) over land and coastal waters. The flooded areas were mapped based on Sentinel-2 imagery acquired on the 7th of June 2019. In order to extract the flood extent, the modified normalized difference water index (MNDWI) was calculated using the green (band 3) at 10 m, and the shortwave infrared (SWIR1) (band 11) at 20 m through the following Eq. (1):

$$MNDWI = \frac{(Green - SWIR1)}{(Green + SWIR1)} \tag{1}$$

Then a thresholding approach (Martinis et al. 2009) was applied to the index image to detect water-covered areas. In this analysis, an optimal local threshold value (−0.33) was utilized to classify water and non-water pixels and separate the flooded from non-flooded regions (Fig. 3).

Fig. 3 Flowchart of flood extent extraction process in the GEE platform



2.3.2 Land Cover Classification Analysis

Land cover classification using remote sensing is predicated on the assumption that different land cover types have distinct reflectance properties. The unique spectral signatures (training sites) to characterize desired land cover classes were derived from the PlanetScope imagery using recent classification work from Zurqani (2021) as a reference. A total of more than 1930 polygon samples were created to represent these land cover classes throughout the study area. The identified classes were (1) tree canopy, (2) shrubs, (3) agriculture, (4) urban or built-up, (5) roads/paved surfaces, (6) barren land, and (7) sand dunes (Table 2).

Land cover classification using remote sensing data is the process of classifying pixels or objects whose spectral characteristics are similar and allocating them to the designated classes (Lee et al. 2020). Various techniques have been applied to land cover classification, including traditional statistical algorithms and recent machine learning approaches (Waske et al. 2009; Campos-Taberner et al. 2020; Zurqani et al. 2021). Deep learning is a subset of machine learning that yields high-level abstractions by compositing multiple non-linear transformations (Bengio et al. 2013). In this study, a U-Net deep learning model was used because it is effective in the task of classifying pixels (Robinson et al. 2017; Ilyas et al. 2021). The max epochs were set to 20, meaning the training data were passed through the neural network a maximum of 20 times to reduce the error rate. However, the model was set to stop training when the model was no longer improving, despite the max epoch number. The validation percentage was set to 10, so 10% of the training samples were used to validate the deep learning model (Fig. 4).

U-Net is a convolutional neural network model that was developed by Ronneberger et al. (2015) and is an improved FCN model characterized by symmetrical U-shaped architecture consisting of the symmetric contracting path and expansive path. The encoding path extracts hierarchical features/patterns given labelled input data, while the feature decoding path learns spatial information

Table 2 The description of land cover classes

No.	Land cover classes	Description
1	Tree canopy	The area is covered by trees that include forest trees and fruits trees.
2	Shrubs	It is primarily used to replace missing rainfall in periods of drought and protect plants against frost.
3	Agriculture	Annual and perennial crops.
4	Urban or built-up	This area includes residential, industrial and commercial complexes and mixed urban and built-up areas. This land cover is related to centers of population.
5	Roads	All roads, parking lots, sidewalks, and paved surfaces
6	Barren land	All land not covered by tree canopy, shrubs, agriculture, urban or built-up and sand dunes
7	Sand dunes	This area is piling up of sand grains shaped into a mound or ridge by the wind

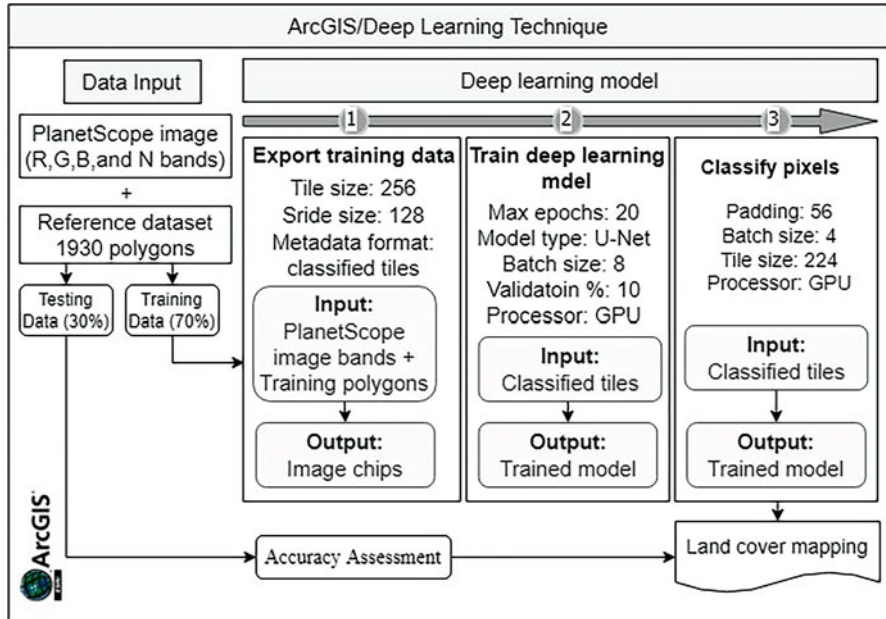


Fig. 4 Workflow of the creation of the land cover map using deep learning

required in order to reconstruct the original input (Ronneberger et al. 2015). This process enables the model to extract local features and obtain a better result. Finally, following Yang et al. 2018, a hand-editing process was applied to correct mapping errors. In some areas, hand-editing was used to correct misclassified pixels (e.g., roads reflection in some urban areas, etc.).

In general, U-Net models performed better in terms of minimizing misclassification errors (Malik et al. 2021). The accuracy assessment for land cover classification result was calculated to understand the performance of the deep learning model using the overall accuracy (Eq. 2), and Kappa Coefficient (Eq. 3) which reflect the difference between actual agreement and the agreement expected by chance. Then, F1 score (Eq. 4) is used which shows how good the performance of the deep learning algorithm is in the context of both producer’s (recall or true positive rate or sensitivity) and user’s (consumer’s accuracy or precision or positive predictive value) by weighting the average of producer’s (Eq. 5) and user’s (Eq. 6):

$$\text{Overall accuracy (OA)} = \frac{2 * TP}{2 * TP + FN + FP} \tag{2}$$

$$\text{Kappa Coefficient (KC)} = \frac{OA - \left(\frac{(TP+FP)(TP+FN)}{(TP+TN+FP+FN)^2} + \frac{(FN+TN)(FP+TN)}{(TP+TN+FP+FN)^2} \right)}{1 - \left(\frac{(TP+FP)(TP+FN)}{(TP+TN+FP+FN)^2} + \frac{(FN+TN)(FP+TN)}{(TP+TN+FP+FN)^2} \right)} \quad (3)$$

$$\text{F1 score} = \frac{2 * TP}{2 * TP + FN + FP} \quad (4)$$

$$\text{Producer's accuracy (PA)} = \frac{TP}{TP + FN} \quad (5)$$

$$\text{User's accuracy (UA)} = \frac{TP}{TP + FP} \quad (6)$$

Where:

TP is the True Positives, which means that the actual class and the predicted class are both positive. **TN** is the True Negatives, which means that the actual and predicted class are both negative. **FP** is the False Positives, which means that the actual class is negative whereas the predicted class is positive. **FN** is the False Negative, which means that the actual class is positive, but the predicted class is negative.

3 Results and Discussion

3.1 Flood Inundation Mapping

Flooding is one of the major natural disasters that can cause loss of human life, damage to property, and destruction of vegetation and animals (Zurqani et al. 2019). The results of the GEE analysis indicated that approximately 2255.67 ha of the study area were flooded during the heavy rainfall and thunderstorm event in June 2019 (Fig. 5).

The flood inundation map generated by this approach could result in time saved while planning rescue missions and could possibly reduce cost by allocating resources to places that are most in need. Earth observations using satellite remote sensing techniques provide an effective and efficient tool for detecting water body areas and the extend of flood inundation on a large area. In addition, using the modified normalized difference water index (MNDWI) has the advantage of suppressing the response of both vegetation and built-up areas leading to enhanced detection of water-covered areas (Xu 2006).

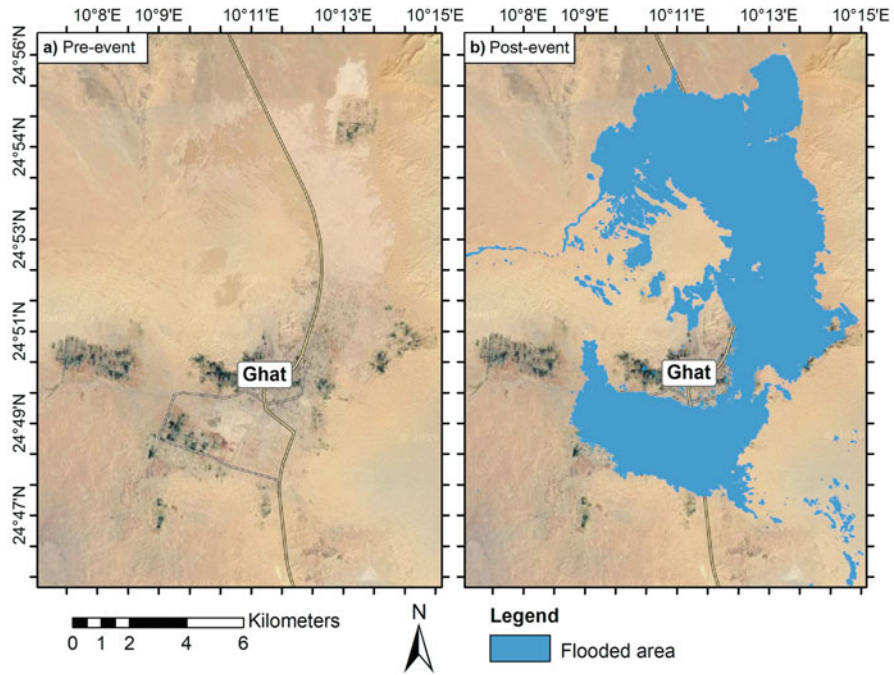


Fig. 5 Map of the spatial extent of flood inundation

3.2 Land Cover Mapping

The land cover classification map for the entire study area was produced using a U-Net deep learning model with a PlanetScope image via ArcGIS Pro 2.9 (ESRI n.d.) for the year 2019 in a total of seven common land cover categories (Fig. 6). The overall accuracy was 94.45%, while user’s accuracies of each land cover classification ranged between 62.30% (tree canopy) and 99.74% (sand dunes) (Table 3).

The distribution of individual class areas is summarized in Table 4. At a larger scale of the region, the detailed land cover features such as residential areas, local roads, and streets can clearly be identified in this high-resolution classification map. The barren land area class cover about 48.97% of the study area which is 5943.77 ha. The sand dunes class was the second-high class percentage over the study area with 42.62%. In comparison, the percentage vegetation cover was around 5% of the study area where the shrubs were 317.84 ha followed by 211.4 ha of agriculture land and 120.60 ha of tree canopy. The urban area and roads were represented by about 3% of the study area, which is 305.74 and 64.8 ha, respectively.

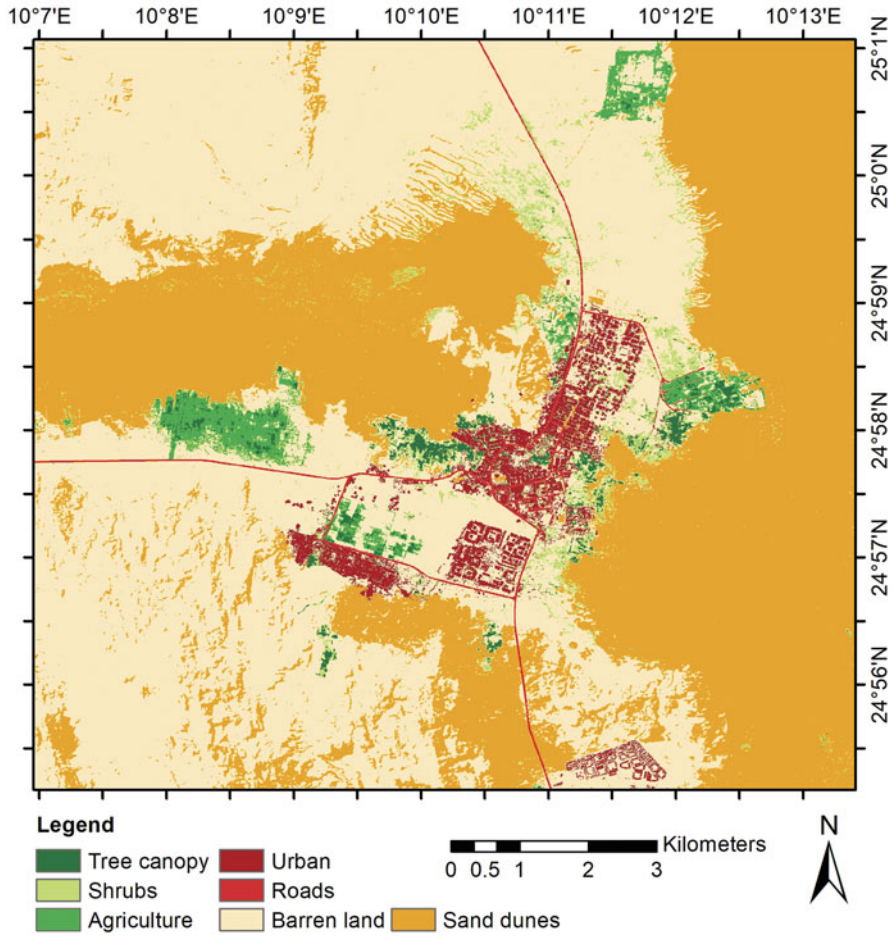


Fig. 6 Spatial extent of land cover

Table 3 The percentage of producer and user accuracy, F1 score, overall accuracy, and kappa statistic for land cover classification

No	Types	User's accuracy	Producer's accuracy	F1 Score
1	Tree canopy	62.30%	94.25%	0.75
2	Shrubs	76.85%	74.92%	0.76
3	Agriculture	98.79%	77.80%	0.87
4	Urban	99.43%	96.75%	0.98
5	Roads	99.94%	98.44%	0.99
6	Barren land	70.00%	77.96%	0.73
7	Sand dunes	99.74%	96.85%	0.98
	Overall accuracy	90.45%		
	Kappa coefficient	0.8861		

Table 4 The distribution of land cover classes based on PlanetScope image classification

No	Types	Hectares	(%)
1	Tree canopy	120.60	0.99
2	Shrubs	317.84	2.62
3	Agriculture	211.4	1.74
4	Urban	305.74	2.52
5	Roads	64.8	0.53
6	Barren land	5943.77	48.97
7	Sand dunes	5173.7	42.62
	Overall total	12137.85	100.00

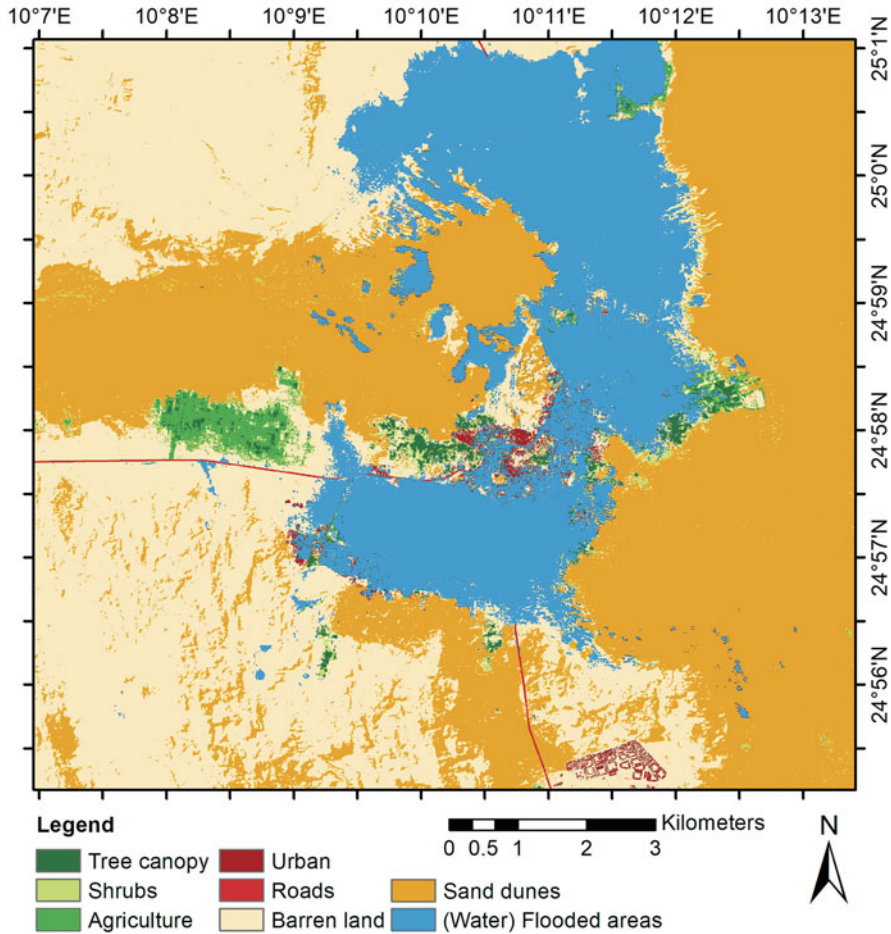


Fig. 7 Affected areas. (During the flood event, June 2019)

Table 5 The distribution of land cover classes affected areas. (During the flood event, June 2019)

No	Types	Hectares	(%)
1	Tree canopy	25.26	1.12
2	Shrubs	176.31	7.82
3	Agriculture	76.23	3.38
4	Urban	221.36	9.81
5	Roads	44.51	1.97
6	Barren land	1608.7	71.32
7	Sand dunes	103.29	4.58
	Overall total	2255.67	100.00



(a)



(b)

Fig. 8 Flood damage in the city of Ghat during the flood event, June 2019 (Photos courtesy: The Libyan Red Crescent Society, Ghat branch)

3.3 Flood Damage Assessment

The distribution of land cover classes affected areas during the flood event, June 2019 (Fig. 7 and Table 5). The barren land class was the most affected area within the city with about 71.32% (1608.7 ha). Urban and shrubs areas were the second-high percentage class inundated by flood which is approximately 9.81 and 7.82% respectively while 4.58% of Sand dunes and 3.38% of agricultural lands were flooded, representing almost 103.29 and 76.23 ha respectively. The areas least affected by the flood were roads and tree canopy that estimated less than 2% of the study area.

As shown in Fig. 8a, the flood damage in urban areas that occurred from the flash floods in the city led to high levels of water in the streets and roads. Additionally, considering the magnitude and scale of the floods, relatively a lot of livestock and farm animals died (Fig. 8b). Urban and road areas were the most fully flooded areas, where the floodwaters covered about 70% of their overall coverage in the study area. Half of the shrubs area was inundated while about 30% of agriculture, tree canopy, and barren land were flooded. The sand dunes were the least affected area (Fig. 7 and Table 5).

3.4 Effects of Frequent Flooding

Frequent floods often adversely affect economically important crops, but floods vary in natural habitats depending on the ecosystem, disruption system, and flood severity. For example, the harmful impact of flood events on plant communities is a combination of species-specific flood tolerance, changes in resource availability caused by floods and biodiversity, and changes in ecological interactions (Morris and Brewin 2014). Floods also pollute the environment and transport raw sewage, spilt toxic chemicals, and hazardous waste spills, causing pollution in the groundwater and habitats. Silts and sediments lead to the destruction of crops, and rapid water currents can uproot trees and lead the destroyed plants to die in a flood (Keller and DeVecchio 2015). Furthermore, the flood could contaminate the drinking water supply and cause gastrointestinal infections. If the flood is large enough, it can destroy wildlife habitat, lead to wildlife loss, and rarely damage endangered species. This reduces the species diversity, stability of ecosystems, habitat potential, and food levels, which can have long-term effects on wildlife survival (Langill and Abizaid 2019).

Though floods are often associated with various damages, they bring nutrients, essential ingredients, and mineral resources such as nitrogen, phosphorus, and organic matter. The flood can diffuse to the surrounding land, improving plant growth and overall ecosystem health. Over time, the nutrients and organic matter carried by the floods and deposited in the landscape can benefit. The abundance of natural fertilizer improves soil quality, positively affects plant growth and increases ecosystem productivity (Stanley and Ibrahim 1996). Besides, flood water can replenish groundwater sources; it is absorbed into the ground, infiltrates through soil and rock layers, and eventually reaches underground aquifers. These aquifers provide clean fresh water to the springs and wells in the area. Ecosystems are heavily dependent on groundwater during the dry period if groundwater may be the only source of fresh water available. A good groundwater supply positively affects soil health, leading to more productive arable land and pasture (Zhang et al. 2017).

3.5 Flood Causes and Mitigation Measures

3.5.1 Origin and Causes of Ghat Floods

The rain that falls on the Ghat region is mountainous in origin and is originally produced by the slopes of the Tassili mountain range, with an average elevation of about 1500 meters and total area of about 72,000 km². This height plays an important physical role in the formation of convection updraft air needed to form thunder clouds (orography clouds) of heavy and extreme rainfall (floods), especially during afternoon time and the early morning periods, and after this chain gained enough heat during noon times. The severity of the convection depends on the strength and coldness of the polar winds that hit the northern slopes, which are about 800 km in length. The severity also depends on the solar heating times of that chain, which are varied by the change in months and seasons.

The rainfall of Tassili with an annual climatology of about 25 mm and maximum of 150 mm in some years, contributes mainly to the flash floods that hit the entire Ghat region. The floods are launched by the force of a steep gradient, with an elevation difference of up to 800 meters across various valleys and their main streams to the east then the north. These torrents settle in the low areas of Ghat, with an elevation of about 700 m above sea level, or make its condition worse, where the level of torrential water reaches more than 1.5 m, as it happened in the worst historical climatic floods that the region experienced in June 2019 (Elfadli 2019).

The accumulated water and stagnant swamps remained for more than 2 months until they evaporated after the disaster, while the waters of the deep border valleys remain for years. Ghat floods are called cross-border flash floods. In addition, in certain climate conditions, the rainfall that originates on the Acacus mountains to the east of Ghat regions, which reach a height of 1000 meters, may have a secondary contribution to the increase in the intensity of those floods. On the other hand, Ghat’s direct rainfall, which is carried out by the western winds from the Tassili mountain range, plays a little role in those floods. In general, the terrain surrounding the region plays a major role in Ghat’s climate pattern and floods dynamic. Without this terrain, Ghat and the town of Djanet, which is adjacent to it on the Algerian side, would not have become the only flooded places in the middle of the Sahara (Saharan), despite of their rainfall scarcity.

3.5.2 Climatic History of the Ghat Floods

During the past 100 years, the region of Ghat has experienced about 14 flash floods of various classes of severity, the worst of which was the June 2019 flood (Elfadli 2019). Figure 9 shows a temporal chart of the floods that have hit Ghat over the past 100 years on a monthly basis.

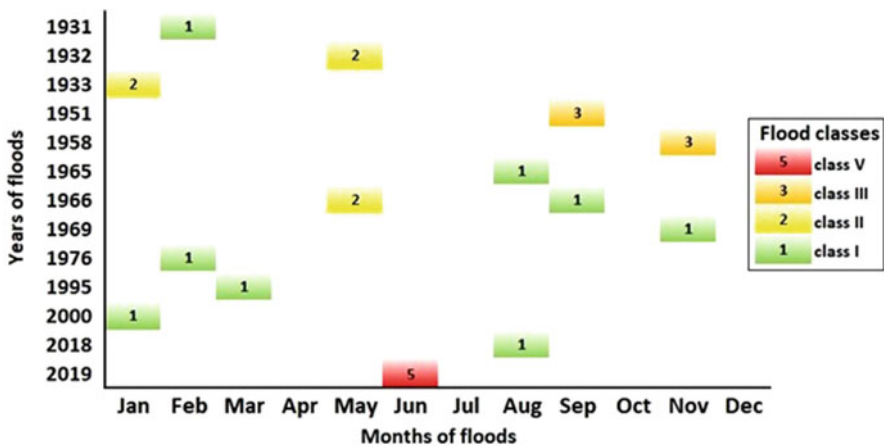


Fig. 9 Info graphic of the temporal pattern and classes of flash floods of Ghat, Libya for the past 100 years (1901–2019)

The region was hit with eight first-degree floods (the least severe), three-second class floods (the most severe), two-third class floods (the most powerful), and the one exceptional fifth-class flood (the fiercest in the history of climatic records). The region did not witness any floods of the fourth class. Floods appeared during all months except April, July, October, and December, and the year 1966 witnessed the occurrence of two floods for the only time in the history of the region, during the months May and September.

It is noted that the floods of all degrees stopped appearing for 19 years (1976–1995), while the floods of the second degree have stopped appearing since 1966 (53 years ago), and the floods of the third degree have not cleared since 1958 (61 years ago). The concept of probability theory can be used to simplify and understand the temporal distribution of floods in the study area, where the probability of the occurrence of any flood (of various degrees) reaches 12% with a flood every 20 years. In contrast, first-degree floods can appear every 15 years, and second and third-degree floods are likely to appear every 40 and 60 years, respectively.

As for the class V floods, the region experienced one for the first time from June 1st through the 6th, 2019, in terms of intensity, strength, and the time and can be considered as an exceptional flood because it is a new climatic extreme that the region has never experienced. This clearly indicates the climatic changes that began to take place in the region, as this was the first time that these floods occurred in such a month, which is considered the hottest month of the year. The excessive heating that the entire region experienced caused exceptional strength and severity of the 2019 flood. In addition, the arrival and intrusion of very cold polar air coming from the north, which is abnormal at such times, its excessive penetration and turbulence in the south, and the absence and weakness of the upper Sub Tropical Jetstream are unusual over the area at this time.

3.5.3 Possible Mitigation Measures

It is known that the great Ghat region is the most fragile and vulnerable region in Libya in the face of natural disasters and the effects of climatic change, for several reasons, including human and natural ones. In the past 100 years, the great regions of Ghat were exposed to around 14 climatic floods in most months of each year. As already mentioned, 57% of the theme includes first-class floods, which are rated as flash floods of moderate intensity and strength, and 21% of which are second degree, rated very severe, and 14% of them are third class, and are considered extreme. The flood of June 2019 was the fiercest since the end of the last century and classified as fifth degree. It caused severe economic and social damage, including the loss of property of citizens and the state and led to large-scale environmental disasters where the cost of the resulting losses is estimated at hundreds of thousands of dollars.

In order to adopt the possible measures to mitigate the negative effects of the flash flood disaster in great Ghat, it is necessary to build a general framework that enriches

the crisis management that includes short and long-term mitigation measures. Therefore, identifying the responsible parties and timetables for the infrastructure of the region are among the most effective mitigation measures. Then comes the construction of an early warning system for floods, using artificial intelligence techniques that include building and installing ground monitoring stations and sensors for rain in the valleys, installing main gathering basins, and cooperating with neighboring countries. Also, remote sensing technology serves as a powerful tool for periodic monitoring and tracking of rain and the adoption of high spatial resolution climate models helps predict diverse rainfall at different time levels (hourly, daily, monthly, seasonal).

4 Conclusion

Floods are a force of nature and one of the most frequent types of natural disasters. Accurate mapping and monitoring of flooded areas are immensely required for disaster management purposes, such as for damage assessment and mitigation. This study demonstrates a framework to identify flooded areas caused by the wave of heavy rainfall and thunderstorm that hit the southwestern Ghat region of Libya and assess the major effect of the storm on the land cover during the flood period. The results of the flood extent extraction analysis indicated that approximately 2255.67 hectares of the study area were flooded during the storm event. During this event, 70% of urban areas and roads were affected by floods, followed by half of shrubs area inundated. About 30% of agriculture, tree canopy, and barren land classes were flooded, while the sand dunes were the least affected area. Based on these results, it can be concluded that the suggested remote sensing-based approach works effectively and efficiently for flood inundation mapping, and estimates the damage and losses caused by the floods. The methodology presented in this chapter can also be utilized for sectoral planning activities, integrated planning studies, and damage assessment.

Author Contributions **Hamdi A. Zurqani**: conceptualization, methodology, supervision, software, data curation, formal analysis, validation, investigation, writing—original draft, visualization, writing—review and editing, review of analysis. **Abdulsalam Al-Bukhari**: data curation, writing—original draft, writing—review and editing. **Alsaket O. Aldaikh**: data curation, writing—original draft. **Khalid I. Elfadli**: writing—original draft. **Ali A. Bataw**: writing—original draft. All authors have read and agreed to the published version of the manuscript.

Data Availability The datasets analyzed in this study are publicly available at this GEE App (<https://hzurqan.users.earthengine.app/view/geospatial-mapping-of-the-flood-extent-in-southwest-ern-libya>). The data that support the findings of this study are available from the corresponding author upon reasonable request. Source data are provided with this chapter.

References

- Abdel-Fattah M, Kantoush S, Sumi T (2015) Integrated management of flash flood in wadi system of Egypt: disaster prevention and water harvesting. *B= Disaster Prev Res Inst Ann B 58 (B)*:485–496
- Ashour MM (2002) Flashfloods in Egypt (a case study of Drunka village–Upper Egypt). *Bull Soc Géog Égypte* 75:101–114
- Banerjee A, Bhavnani R, Burtonboy CH, Hamad O, Linares-Rivas Barandiaran A, Safaie S et al (2014) Natural disasters in the middle East and North Africa: a regional overview, vol No. 81658. The World Bank, pp 1–114
- Bengio Y, Courville A, Vincent P (2013) Representation learning: a review and new perspectives. *IEEE Trans Pattern Anal Mach Intell* 35:1798–1828
- Billa L, Mansor S, Mahmud AR, Ghazali AH (2005) AVHRR data for real-time operational flood forecasting in Malaysia. In: *Geo-information for disaster management*. Springer, Berlin/Heidelberg, pp 1357–1379
- Campos-Taberner M, García-Haro FJ, Martínez B, Izquierdo-Verdiguier E, Atzberger C, Camps-Valls G, Gilabert MA (2020) Understanding deep learning in land use classification based on Sentinel-2 time series. *Sci Rep* 10(1):1–12
- Chang H, Franczyk J, Kim C (2009) What is responsible for increasing flood risks? The case of Gangwon Province. *Korea Nat Haz* 48(3):339–354
- Colombo A, Hervás J, Vetere Arellano AL (2002) Guidelines on flash flood prevention and mitigation. European Commission Joint Research Centre (JRC)
- Dolman AJ, Gash JHC, Goutorbe JP, Kerr Y, Lebel T, Prince SD, Stricker JNM (1997) The role of the land surface in Sahelian climate: HAPEX-Sahel results and future research needs. *J Hydrol* 188:1067–1079
- Elfadli K (2019) GHAT floods; 1–6 June 2019. Government report, submitted on JUL 15, 2019
- ESRI—Environmental Systems Research Institute (n.d.) ArcGIS Pro 2.9. Available online: <https://pro.arcgis.com/en/pro-app/latest/get-started/arcgis-pro-system-requirements.htm> Accessed 13 Dec 2021
- Haq M, Akhtar M, Muhammad S, Paras S, Rahmatullah J (2012) Techniques of remote sensing and GIS for flood monitoring and damage assessment: a case study of Sindh province, Pakistan. *Egypt J Remote Sens Space Sci* 15(2):135–141
- Ilyas I, Jaelani LM, Syariz MA, Hidayat H (2021) World view-2 satellite image classification using U-net deep learning model. *J Appl Geospatial Inf* 5(2):502–509
- IRIN (2013) Preparing for floods in West Africa. Available from: <http://reliefweb.int/report/nigeria/Preparing-floods-west-africa>
- Keller E, DeVecchio D (2015) *Natural hazards: earth's processes as hazards, disasters, and catastrophes*. Pearson Higher Education, Upper Saddle River
- Korichi K, Hazzab A, Atallah M (2016) Flash floods risk analysis in ephemeral streams: a case study on Wadi Mekerra (northwestern Algeria). *Arab J Geosci* 9(11):1–11
- Langill JC, Abizaid C (2019) What is a bad flood? Local perspectives of extreme floods in the Peruvian Amazon. *Ambio*:1–14
- Lee J, Han D, Shin M, Im J, Lee J, Quackenbush LJ (2020) Different spectral domain transformation for land cover classification using convolutional neural networks with multi-temporal satellite imagery. *Remote Sens* 12(7):1097
- Lin X (1999) *Flash floods in arid and semi-arid zones*. Technical documents in hydrology. UNESCO, Paris
- Llasat MC, Llasat-Botija M, Prat MA, Porcu F, Price C, Mugnai A et al (2010) High-impact floods and flash floods in Mediterranean countries: the FLASH preliminary database. *Adv Geosci* 23: 47–55
- Malik K, Robertson C, Braun D, Greig C (2021) U-Net convolutional neural network models for detecting and quantifying placer mining disturbances at watershed scales. *International Journal of Applied Earth Observation and Geoinformation*, 104, p.102510

- Markus K, Jurgen G, Christoph B, Bruno R, Franz R (2006) World map of the Koppen- Geiger climate classification updated. *Meteorologische Zeitschrift* 15(3):259–263
- Martinis S, Twele A, Voigt S (2009) Towards operational near real-time flood detection 563 using a split-based automatic thresholding procedure on high resolution TerraSAR-X data. *Nat Hazards Earth Syst Sci* 9:303–314
- Moawad MB (2013) Analysis of the flash flood occurred on 18 January 2010 in Wadi El Arish, Egypt (a case study). *Geomat Nat Haz Risk* 4(3):254–274
- Moawad MB, Abdel Aziz AO, Mamtimin B (2016) Flash floods in the Sahara: a case study for the 28 January 2013 flood in Qena. *Egypt Geom Nat Hazards sRisk* 7(1):215–236
- Morris J, Brewin P (2014) The impact of seasonal flooding on agriculture: the spring 2012 floods in Somerset, England. *J Flood Risk Manage* 7:128–114
- OCHA (Office for the Coordination of Humanitarian Affairs) (2012) Mali complex emergency situation report no. 15. 11 September 2012. United Nations. Available from: <http://www.un.org/maintenance/>
- OCHA (Office for the Coordination of Humanitarian Affairs) (2019) LIBYA: Floods in the South – West FLASH UPDATE 2 As of 11 June 2019. United Nations
- Podlaha A, Bowen S, Darbinyan C, Lörinc M (2019) Global catastrophe recap-June 2019. Aon Benfield Analytics
- Reid I, Powell M, Laronne JB, Garcia C (1994) Flash floods in desert rivers: studying the unexpected. *EOS Trans Am Geophys Union* 75(39):452–452
- Robinson C, Hohman F, Dilkina, B (2017) A deep learning approach for population estimation from satellite imagery. In: *Proceedings of the 1st ACM SIGSPATIAL Workshop on Geospatial Humanities*, (pp 47–54)
- Ronneberger O, Fischer P, Brox T (2015) U-net: convolutional networks for biomedical image segmentation. In: *International conference on medical image computing and computer-assisted intervention*. Springer, Cham, pp 234–241
- Sene K (2012) Flash floods: forecasting and warning. Springer Science & Business Media
- Stanley M, Hirst, Abu Md. Ibrahim (1996) Effects of flood protection on soil fertility in a Riverine floodplain area in Bangladesh, *Communications in Soil Science and Plant Analysis*, 27:1–2, 119–156. <https://doi.org/10.1080/00103629609369549>
- UNICEF (2019) UNICEF Libya Humanitarian Situation Report, January – June 2019 (Issue June)
- United nation (2021) Country intervention on drought- Libya. department of economic and social affairs sustainable development: Access on 21 Dec 2021. Available at: <https://sdgs.un.org/documents/country-intervention-drought-libya-19926>
- United Nations Office for the Coordination of Humanitarian Affairs (OCHA) (2019) Floods in the South – West of Libya (As of 5 June 2019) (Issue June)
- Warner TT (2004) *Desert meteorology*. Cambridge university press, Edinburgh, p 612
- Waske B, Fauvel M, Benediktsson JA, Chanussot J (2009) Machine learning techniques in remote sensing data analysis. *Kernel methods for remote sensing data analysis*, pp 3–24
- Xu H (2006) Modification of normalised difference water index (NDWI) to enhance open water features in remotely sensed imagery. *Int J Remote Sens* 27:3025–3033
- Yang L, Jin S, Danielson P, Homer C, Gass L, Bender SM, Case A, Costello C, Dewitz J, Fry J, Funk M (2018) A new generation of the United States National Land Cover Database: requirements, research priorities, design, and implementation strategies. *ISPRS J Photogramm Remote Sens* 146:108–123
- Yousif M, Hussien HM (2020) Flash floods mitigation and assessment of groundwater possibilities using remote sensing and GIS applications: Sharm El Sheikh, South Sinai, Egypt. *Bull Natl Res Centre* 44(1):1–25
- Youssef AM, Pradhan B, Hassan AM (2011) Flash flood risk estimation along the St. Katherine road, southern Sinai, Egypt using GIS based morphometry and satellite imagery. *Environ Earth Sci* 62(3):611–623

- Youssef AM, Pradhan B, Sefry SA (2015) Remote sensing-based studies coupled with field data reveal urgent solutions to avert the risk of flash floods in the Wadi Qus (East of Jeddah) Kingdom of Saudi Arabia. *Nat Hazards* 75(2):1465–1488
- Youssef AM, Sefry SA, Pradhan B, Alfadail EA (2016) Analysis on causes of flash flood in Jeddah city (Kingdom of Saudi Arabia) of 2009 and 2011 using multi-sensor remote sensing data and GIS. *Geomat Nat Haz Risk* 7(3):1018–1042
- Zamot J, Afkareen M (2020) Geomorphological parameters by remote sensing and GIS techniques (A case study of flash flood in Mikhili Village, Al Jabal Al Akhdar, NE of Libya). In: The forth international conference for geospatial technologies – Libya GeoTec 4, Tripoli, Libya, 3–5 March 2020
- Zhang G, Feng G, Li X, Xie C, Pi X (2017) Flood effect on groundwater recharge on a typical silt loam soil. *Water*, 9(7):523
- Zurqani HA (2021) Introduction. In: Zurqani HA (ed) *The soils of Libya*, World soils book series. Springer, Cham. https://doi.org/10.1007/978-3-030-66368-1_1
- Zurqani HA, Post CJ, Mikhailova EA, Schlautman MA, Sharp JL (2018) Geospatial analysis of land use change in the Savannah River basin using Google earth engine. *Int J Appl Earth Obs Geoinf* 69:175–185
- Zurqani HA, Post CJ, Mikhailova EA, Ozalas K, Allen JS (2019) Geospatial analysis of flooding from hurricane Florence in the coastal South Carolina using Google Earth Engine. In: Graduate Research and Discovery Symposium (GRADS), p 230
- Zurqani HA, Allen JS, Post CJ, Pellett CA, Walker TC (2021) Mapping and quantifying agricultural irrigation in heterogeneous landscapes using Google earth engine. *Remote Sens Appl Soc Environ* 23:100590

Dr. Hamdi A. Zurqani is an Assistant Professor of Geospatial Science in Natural Resource Management and Conservation at the University of Arkansas Agricultural Experiment Station, Arkansas Forest Resources Center, University of Arkansas at Monticello, Monticello, AR, USA. He is also an FAA (i.e., Pt107) Certified sUAS/Drones Pilot, and has used this skill to enhance his knowledge of remote sensing and GIS. Dr. Zurqani is a recognized expert as a result of his internationally acclaimed work in the areas of environmental information science, remote sensing, geospatial analysis, land evaluation, sustainability, pedology, and soil science education. He has conducted research across the world, including the United States of America, and Africa, and has served as PI, co-PI, or co-investigator on several grants-funded research projects. Dr. Zurqani is highly collaborative as evidenced by his publications. He is the author and coauthor of many peer-reviewed publications, book chapters, and technical publications (including teaching laboratory manuals). He also edited two books with Springer Nature (i.e., “The Soils of Libya” , and “Environmental Applications of Remote Sensing and GIS in Libya”), and has published widely in many peer-review journals (e.g., *International Journal of Applied Earth Observation and Geoinformation* (Elsevier); *Remote Sensing in Earth Systems Sciences* (Springer Nature); *Scientific Reports* (Nature); *Frontiers in Environmental Science* (Frontiers); *Geoderma* (Elsevier); *Land* (MDPI); *Urban Forestry & Urban Greening* (Elsevier), and others). Dr. Zurqani is a member of the Editorial Board for *Remote Sensing* (MDPI) Journal, counseling outcome, and research evaluation. He also was appointed to serve as a Guest Editor for the Special Issue “Applications of Remote Sensing in Earth Observation and Geo-Information Science”. In addition, Dr. Zurqani conducted peer-review for many journals including *Journal of Environmental Informatics*, *Applied Sciences*, *SN Applied Sciences*, *Remote Sensing*, *Geo-spatial Information Science*, *AgriEngineering*, *Sensors*, *Heliyon*, *Geosciences*, *Land*, *Soil Systems*, *Water*, *Agronomy*, *Agriculture*, *Resources*, *Sustainability*, *Arid Land Research and Management*, *Questiones Geographicae*, *Geocarto International*, *International Journal of Environmental Research and Public Health*, *Natural Hazards*, and *Conference of the Arabian Journal of Geosciences*. Dr. Zurqani conducts cutting-edge research in the field of Environmental Information Science, Remote Sensing, Land use management/ planning, change detection of landscape degradation, and Geographic Information System

(GIS) models. He has focused his research efforts on the development of novel applications for new technologies in analyzing spatial data, remote sensing, geostatistical modeling of environmental changes such as erosion, mapping and predicting soil salinity, and land use/ land cover changes. His new publications include: "Mapping and Quantifying Agricultural Irrigation in Heterogeneous Landscapes Using Google Earth Engine" in the Journal of Remote Sensing Applications: Society and Environment; "Evaluating the integrity of forested riparian buffers over a large area using LiDAR data and Google Earth Engine" in the Journal of Scientific Reports; "Mapping Urbanization Trends in a Forested Landscape Using Google Earth Engine" in the Journal of Remote Sensing in Earth Systems Sciences; "Geospatial analysis of land use change in the Savannah River Basin using Google Earth Engine" in the International Journal of Applied Earth Observation and Geoinformation; and "Application of Non-Hydraulic Delineation Method of Flood Hazard Areas Using LiDAR-Based Data" as well as "Assessing ecosystem services of atmospheric calcium and magnesium deposition for potential soil inorganic carbon sequestration" in the Geosciences Journal.

Dr. Abdulsalam Al-bukhari is a lecture of rangeland science at the Department of Forestry and rangeland, Faculty of Natural Resources and Environmental Sciences, Omar Al-Mukhtar University, Al-Bayda, Libya. He received his MSc in environmental sciences (rangeland ecology and management) in 2010 from Omar Al-Mukhtar University, Al-Bayda, Libya. He earned his PhD (Natural Resource Management) from Cranfield University, Cranfield, UK, in 2019. He specialized in rangeland ecology and management. His main research interests focused on monitoring and assessment of rangeland degradation as well as the environmental information sciences (remote sensing and GIS). He is a member of the Editorial Board for *Al-Mukhtar Journal of Sciences*.

Mr. Alsaket O. Aldaikh is a graduate research assistant at University of Arkansas at Monticello, Monticello, AR, USA. He received his B.S. degree (Natural Resources and Environmental Science) from Omar AL-Mukhtar University, Albyda, Libya in 2016, with the main research interest in Environmental Science.

Dr. Khalid I. Elfadli is a climate expert, climate change advisor at Libyan National Meteorological Center (LNMC) since 1987, faculty member (cooperating) at technology college of Civil aviation and meteorology, a member of the national committee to combat desertification and president of the general assembly of the southern organization for sustainable development and climate change (NGO), Tripoli, Libya. In addition, he is a member of the Climate Extremes Team of the World Meteorological Organization (WMO). Dr. Elfadli received and completed his M.Sc. and Ph.D. in 2012 and 2019 respectively, in (climate change science) from Cairo University, Egypt. He specialized in climate and climate change. Most of his scientific works and research are concerned with and focused on the following topics: climate extreme, drought, and climate change; detection, trends, indices, impacts and projections, studies. He has been the head of the meteorology department at the aforementioned college and teaching courses and has supervised the graduation BA's and MA's degree students since 2012. He also contributes and participates in international scientific investigations of some climatic extremes and the annual global report of climate statement issued by WMO. He is now working as a scientific reviewer for Scientific African and, Water and climate change Journals on climate and climate change issues. He was also appointed as a focal point for Libya with the Intergovernmental Panel on Climate Change (IPCC).

Dr. Ali A. Bataw is a professor of animal ecology at the Department of Zoology, Faculty of Sciences, University of Omar Al-Mukhtar, Libya. He got his MSc (Agricultural Sciences) in 1985 from the University of Tripoli, Tripoli, Libya. He completed his PhD (behaviour ecology) in 1995 from St. Andrews University, UK. He specialized in insect ecology. His main research interests focused on wild bees' taxonomy, flowers-bees interaction, biodiversity, and insect ecology. He has been teaching courses and has supervised the graduation of master's and bachelor's degree students since 1996.

Oil Pollution Monitoring and Detection Using GIS and Remote Sensing Techniques: A Case Study from Libya



Khalifa Abdunaser

Abstract Produced water, defined as water present with oil or gas in ground formations and brought to the surface, forming a number of oil lakes of varying sizes, has been gathered and analyzed using a variety of satellite image interpretation techniques acquired between 1972 and 2018, aided by GIS techniques. This method provides a high-level overview of the characteristics and extent of produced water lakes, which can now be utilized to perform further in-depth research in the future to enhance the extent and volume of even more oil damage assessment. The main target of this project was to produce high maps of oil-contaminated surfaces as well as series time maps of events induced by oil pollution via multi-temporal satellite data and then to validate the results. The amount of produced water lakes or any oil residues are displayed as black dots spread over the studied area for the year 2018 utilizing satellite images that were identified and digitized as a polygon shape to measure the wet and polluted dry area. This study revealed that the region grew in size due to the growth in the amount of water produced and the amount of oil (volume) produced as the oil and gas fields matured. On the other hand, the amount of contaminated soil in the same areas was calculated, and it can be treated, or its constituent pollutants removed and utilized for other purposes.

Keyword Oil spill detection · Oil Lake · Landsat · Change detection · Geographic information system · Mediterranean Sea

1 Introduction

The studied area's oil lakes, which were formed as a result of petroleum activity since sixteen's of the last century, have become an undesirable part of Libya's desert, necessitating ongoing monitoring to identify the nature and degree of environmental threats. The integration of the produced water lake and other contaminated areas

K. Abdunaser (✉)
Libyan Petroleum Institute, Tarabulus, Libya
e-mail: k.abdunaser@lpilibya.com

with the environment needs constant monitoring to document the recovery of the affected land. Remote sensing can cover large areas simultaneously and periodically in a non-destructive fashion, and offers a valid alternative to traditional ground-based methods (Austin, et al. 2003; Kooistra et al. 2004; Mason et al. 2012).

As a part of remote sensing techniques, multispectral data consisting of tens of contiguous spectral bands throughout the visible-infrared and microwave spectrum could prove to be invaluable in developing environmental monitoring capabilities. Consequently, to minimize the cost and save time, remote sensing technique in addition to GIS analysis must be first utilized before any other traditional methods. Satellite imageries as a part of remote sensing has been used world widely in several projects and studies to characterize and offer invaluable information on the status of the oil lake and the oil-polluted surfaces (Al-Ajmi et al. 1994; El-Baz et al. 1994; Kwarteng and Al-Ajmi 1997; Koch and El-Baz 1998; Kwarteng and Chavez 1998. In addition to Dobson et al. (1997) who used SIR-C/X synthetic aperture radar (SAR) images to map oil lakes, surface roughness variation and vegetation distribution.

Therefore, in this study satellite image consisting of different satellite images (Landsat 4–5 MSS, Landsat 4–5 TM, Landsat 7 ETM+, Landsat 8 OLI + TIRS and Sentinel-2 L1C) acquired between 1972 and 2018 were used to map spatial and temporal changes of the oil lakes and environs and also to monitor the resilience of the affected areas. The free-flowing crude oil mixed with water which called produced water accumulated and formed a network of oil lakes. Approximately 10 oil lakes of various size were bequeathed to Al Wahat's desert environment. Some of the oil lake showed lake dried up with time to form tar mats, but the rest had become an undesirable addition to Al Wahat's environment.

In this study each field station dataset of the oilfield was processed separately as, field stations have different time of initiation, from the sixties till today, then datasets were divided into phases according to the availability of data. GIS has been the main tool used for estimating the area and extent of contamination and to monitor changes with time. To estimate total volume of contaminated water, oil and soil require knowing both the area and average contamination depth of each lake.

GIS is a powerful software technology that allows a virtually unlimited amount of information to be linked to a geographic location. Coupled with a digital map, GIS allows a user to see locations, events, features, and environmental changes with unprecedented clarity, showing layer upon layer of information such as environmental trends, soil stability, pesticide use, migration corridors, hazardous waste generators, dust source points, lake remediation efforts, and at-risk water wells. Effective environmental practice considers the whole spectrum of the environment. ArcGIS® technology offers a wide variety of analytical tools to meet the needs of many people, helping them make better decisions about the environment.

The present work is an integrated part of a series of studies carried out on soil profiles affected by oil lake in the study area in order to determine the level of contamination and depth of oil penetration within the profiles and it throws light on the physical properties of these soils, which may influence the downward migration of oil pollutants.

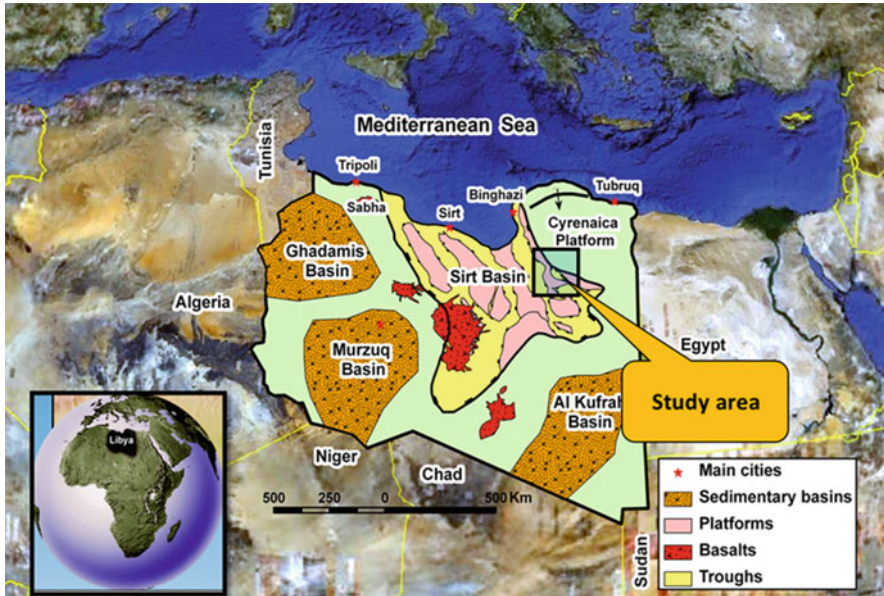


Fig. 1 Libya map shows location of the study area

General location map, (Fig. 1), was produced to show all study oilfield stations and their locations as well as separate maps for each lake details. Also, time series images were produced by interpreting different years of images that gave a clear history of the water spread through time as well as giving fast visual impression about the spread of the pollutants.

2 Geology and Hydrogeology of the Study Area

Generally, of the Post-Eocene (Mainly Miocene and Oligocene) which is of most interest in a hydrological context for the study area and known as Post-Nubian (Table 1) and (Fig. 2). The Miocene aquifer consists of a sequences of unconsolidated sand stone with intervening of clay and silt and presence of limestone in some places. Unfortunately, the Lower and middle Miocene aquifer water in Al Wahat region is deteriorating in quality, thinning and deepening, making some limitations for agricultural uses, where the water wells crossing this aquifer at Al Wahat region ranges in depths between 50 and 200 m and has poorer water quality ranges from 1500 to 5000 mg/l.

North of latitude 28° 00' N the Post-Middle Miocene deposits are composed of limestones and shales to the north and northeast with increasing proportion of sandy carbonates and sandstones to the south and southwest. The Post-Middle Miocene aquifer shows an increase in thickness on the eastern side of the study Area, where

Table 1 Description of the Post-Eocene deposits in the Sirt Basin including Al Wahat area

Age	Formation Name	Lithology and palaeo-environment	Thickness (m)
Holocene/ Pleistocene		Surface sands, gravels and calcretes	0–30
Post-Middle Miocene (PMM)	Calanscio Formation	Medium- to coarse-grained sands, grading to calcareous sandstones, with thin clay interbeds	0–210
Lower and Middle Miocene (LMM)	Maradah Formation	In the north marine carbonates and clays with evaporites; in the north-west: interbedded clays and marine carbonates; to south-east fluviatile sands and sandstone	121–697
Oligocene		- Marine facies: glauconitic calcareous sandstones, limestones, dolomites and clays with some evaporites - Non-marine facies: coarse-grained sand and sandstones with interbedded clay	242–730

Modified after Alfarrah et al. (2016)

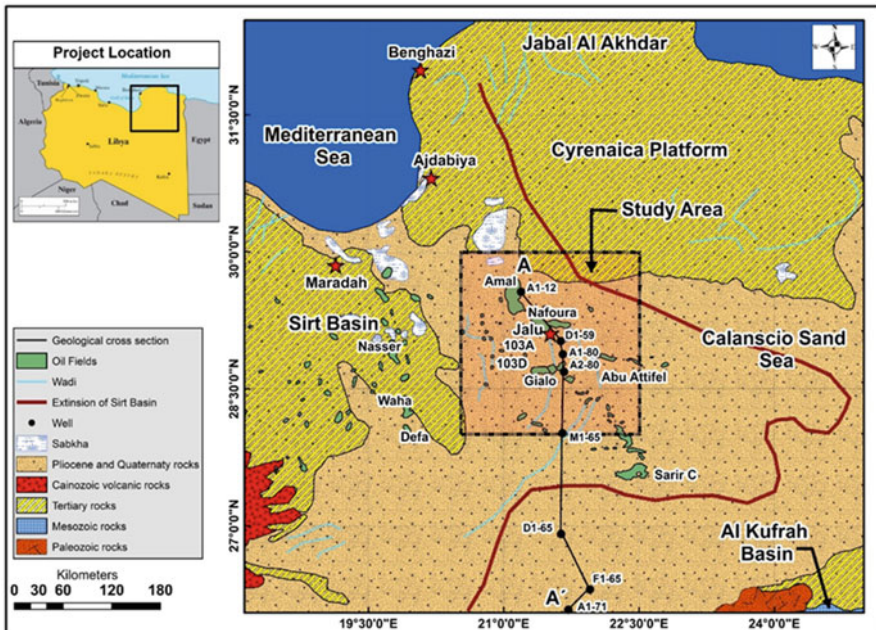


Fig. 2 Surface geology of the area of eastern Sirt Basin and Cyrenaica Platform, Libya. (Modified after Wright et al. 1982)

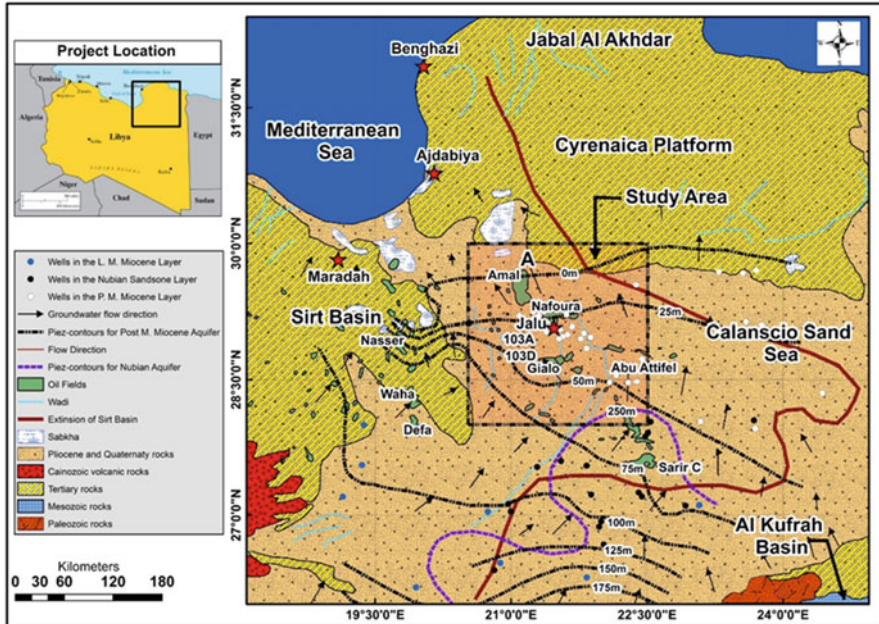


Fig. 3 Regional piezometric map for NE Libya including Al Wahat. (Modified after Alfarrah et al. 2016)

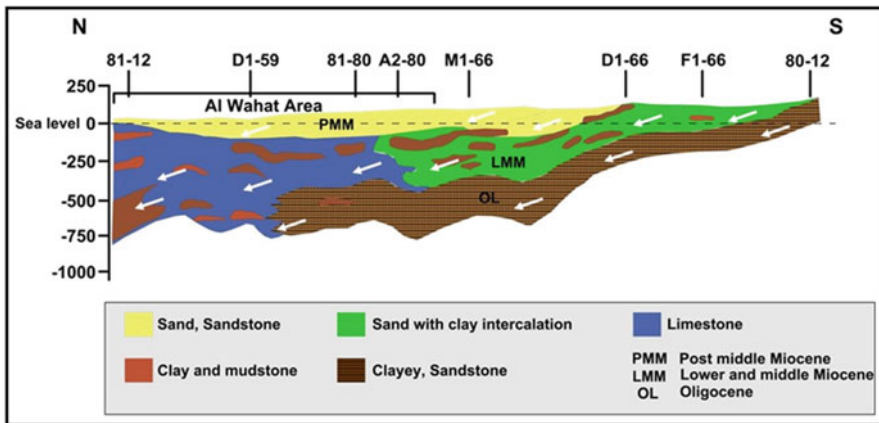


Fig. 4 Water-bearing formations and Water flow direction in the study area

the maximum saturated thickness exceeds 180 m. The mean saturated thickness ranges from 80 to 120 m. Due to the northerly dip of the piezometric surface (Figs. 3 and 4) the aquifer occurs primarily within the upper unit (Calanscio Formation) to the south of latitude 29 00 00' N and within the lower unit (Aklash Formation) to the north of this latitude.

The Oligocene aquifer consist of a sequences of marl and carbonate rocks with intervening of clay and silt and presence of gypsum in some places, the aquifer is extended from north to south up to Zallah. The Oligocene aquifer in Al Wahat region appears in the shallowest sand strata, pinch out towards the south of the area, and has limited use for agriculture because of the poor water quality. The local hydrogeology of Al Wahat region is that of the continental siliceous, sand, silt and clay sands of various textures. The shallowest groundwater was observed to occur within the sandy clay near the ground surface, the deeper groundwater is sandwiched between successive aquitards of clayey to sandy clay partially sealing layers.

3 Data Sets

All these data together were used for estimating the area and extent of contamination and to monitor changes with time. To estimate total volume of contaminated Water, oil and soil require knowing both the area and average contamination depth of each lake. The interpretation of the space born data of the studied oil field showed how helpful the satellite images in studying such rural areas as well as detecting the changes in those produced water lakes through time.

The interpretation and results will be illustrated field station by station starting with the largest. Some parts of the oil lakes were concealed by a veneer of sand and could not be observed from the surface. The need to continuously monitor the status of the oil lakes and polluted surfaces is obvious, as they might be an unwelcome addition to the study area environment for a long time to come.

4 Data Interpretation of Oil Fields

4.1 *Satellite Imageries*

The studied lakes are formed and visible in the images as black pools due to the absorption of the water by infrared wavelengths. Satellite imagery helped reduce the costs of mapping these pools and quantify the level of lake expansion. The sand and gravel on the land's surface combined with oil and soot to form a layer of hardened "tar Crete" over the lakes boundary of the area. The interpretation of the space born data of the studied fields showed how helpful the satellite images in studying such rural areas as well as detecting the changes in those lakes through time. The interpretation and results will be illustrated field by field according to the sequence of the stations' numbers:

4.1.1 Nafoora Oil Field

The Nafoora Oil Field which belongs to the Arabian Gulf Oil Company consists of about 9 stations distributed on a geographical area covering the concession 51. These stations contain produced water lakes with different sizes and areas depending on the amount of production per station and the efficiency of the separation devices. Each station has its own lake except stations (1 and 2) and (4 and 7) which each one has one lake.

4.1.2 Nafoora Oil Field (CPS 1 and 2)

The station (CPS 1 and 2), which is located near most of the infrastructure of the field as shown in Figs. 5 and 6 has the largest of produced water lakes compared with the rest of the stations. Production commenced in this field in 1960 and after nearly 50 years of continuous production of oil, huge amount of produced water was accumulated.

This study was showed that satellite images aid in showing what cannot be measured or seen by other traditional techniques where the change of the lake areas was interpreted and measured on a series of images dated from 1972, 1984, 2000, and 2018. Those satellite images registered to the projection and datum of WGS 84, Zone 34° N. The following satellite images show that the lakes have been subjected to many changes from point of size and volume:

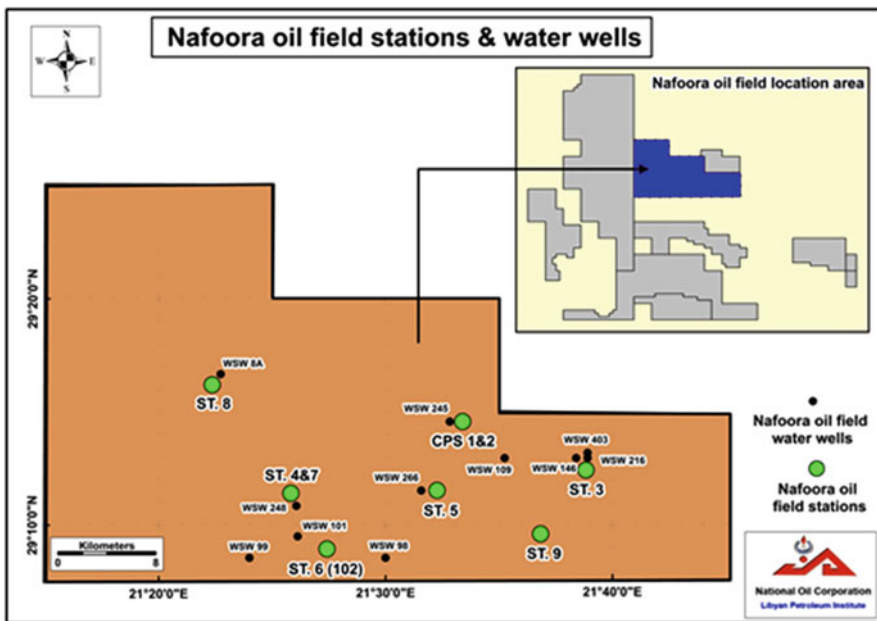


Fig. 5 Location of Nafoora Oil Field produced water pits according to the field location

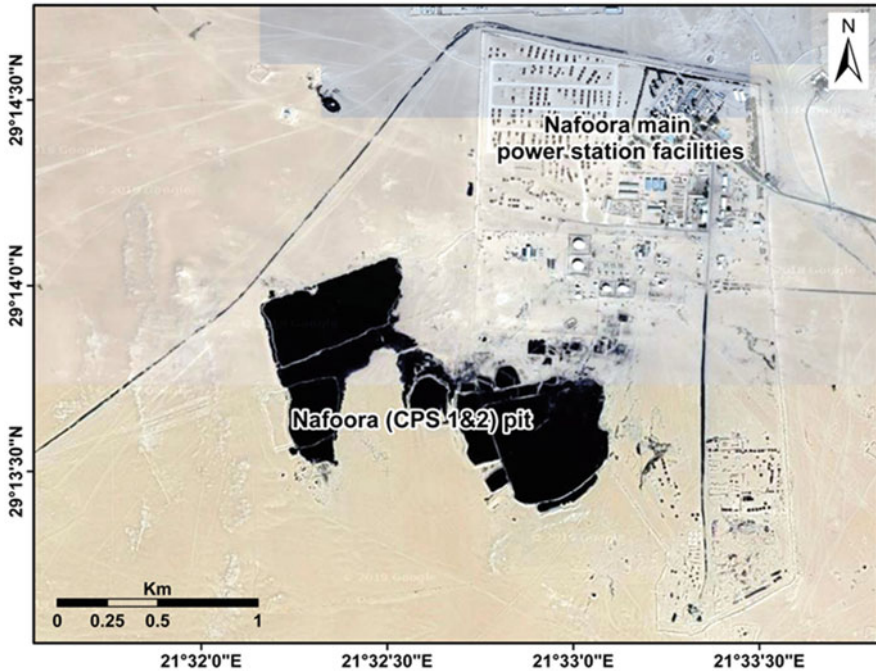


Fig. 6 Satellite image (Google Earth) shows Nafoora oil field facilities and the main pit of the main station (CPS 1 and 2)

Landsat 4 (1972)

Figure 7 is made from a sub scene of Landsat MSS acquired on 1972. The colors correspond closely to those one which could be observed from an aircraft.

The first data set is the Landsat 4 MSS of the year 1972, with spatial resolution of (72 m) and represented in band combinations of 432 RGB, it showed the lake as appearing as 2 separated black area on land represented oil lake, tarmats and soot. The dark color to a black body related to the water ability to absorb all wavelengths and reflect nothing. The sand and gravel on the land's surface combined with oil and soot to form a layer of hardened "tar Crete" over the boundary of the area. The size of CPS 1 and 2 lake in 1972 when measured from satellite image was about total lake area 439,454.1 m² (Fig. 7).

Landsat 5 (1984)

The image of Landsat 5, TM 1984, and band combination of 742 RGB confirmed the black reflection of the water area of Nafoora Oil Field CPS 1 and 2 lake (Fig. 8). It showed the development of the lake to 4 separated black areas on land represented oil lake, tarmats and soot. It was notice from this image that the lake under study

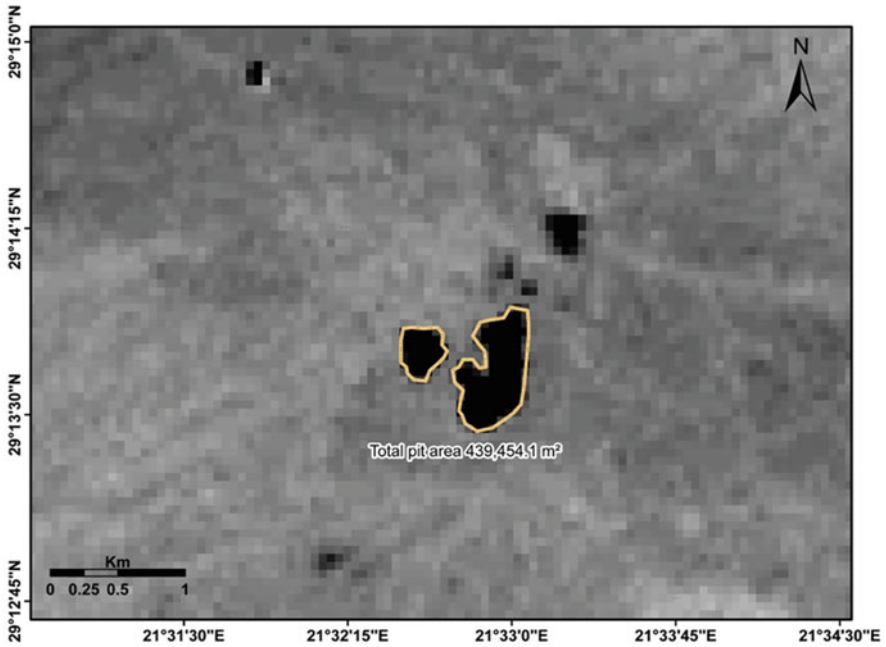


Fig. 7 Landsat 4 image (Band 5) of 1972 shows Nafoora Oil Field CPS 1 and 2 pit

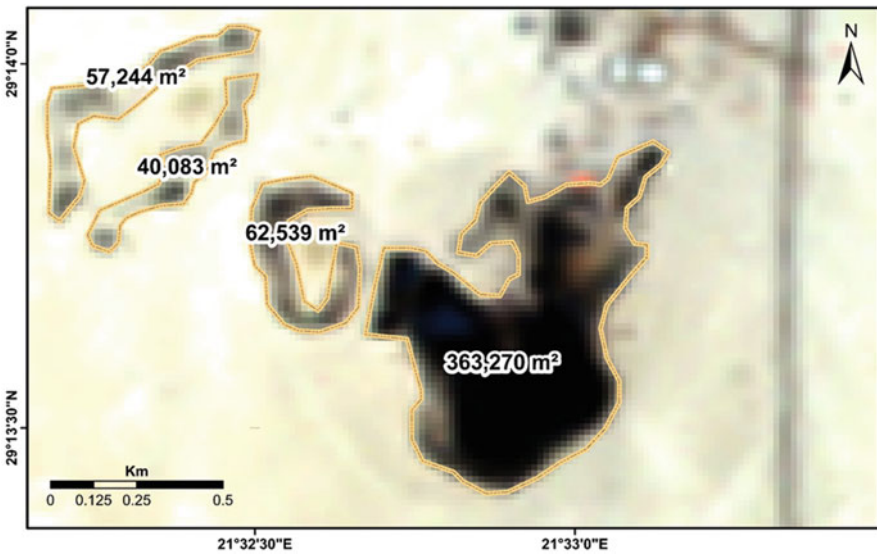


Fig. 8 Landsat 4 image of 1984 shows Nafoora Oil Field CPS 1 and 2 pit area (size) about 523,136 m²

were expanded to the southwest and produced another lake separated by a barrier. The size of CPS 1 and 2 lake in 1984 has expanded when measured from satellite image was about 523,136 m², (Fig. 8).

Landsat 7 ETM (2000)

In 2000 the study area has been imaged by Landsat 7 ETM satellite image which provides better spatial resolution (Fig. 9), the sensor had big enhancement according to the usage of the panchromatic band (15 m) resolution. Therefore, the lake was easily recognized and mapped, where the main lake under the study became as one lake and the barrier has reduced and submerged as a result of the water pumping. The lake area also expanded and measured 630,268 m². As shown in the image, (Fig. 9), the lake kept its extension towards the NE-SW direction following the low topography of the area.

Landsat 8 Operational Land Imager (OLI) (2018)

Figure 10, Landsat 8 acquired in 2018 by the Operational Land Imager (OLI) sensor, with spatial resolution for Band 8 (panchromatic) is 15 m and 742 RGB band combinations (Fig. 10). In this image the lake was still easily recognized and mapped, where the main lake under the study divided into a group of fenced lakes

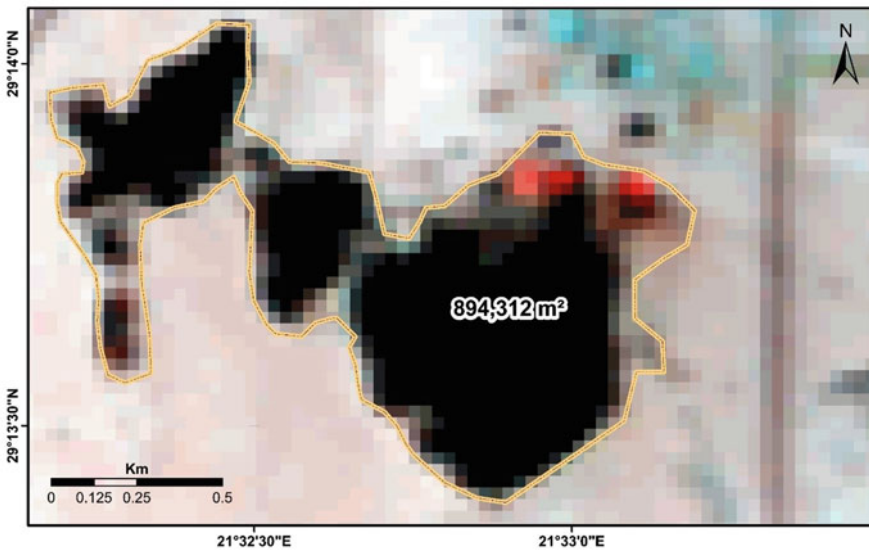


Fig. 9 Landsat 7 ETM image of 2000 shows Nafoora Oil Field CPS 1 and 2 pit shows the change in pit extension and the pit area size come to be about 894,312 m²



Fig. 10 Landsat 8 acquired in 2018 shows Nafoora Oil Field CPS 1 and 2 pit which shows the change in the pit size and volume which come to be about 790,158 m²

by means of soil barriers, but as a result of the increase in the amount of produced water it became as one lake and the barrier has reduced and submerged as a result of the water pumping. The red pixels which shown in the image represent the surface flare which burning the produced gas.

As shown in the image, (Fig. 10), the lake kept its extension towards the NW-SW direction following the low topography of the area also shows the change in the lake size and volume which come to be about 790,158 m².

It is very clear from these images that the lake is expanded mostly into north-west to south-east and the biggest change was between 2013 and 2018 which the lake increased dramatically from about 596,000 to 790,158 m² which may as a result of peak of field production during that period and the subsequent return to more favorable pumping conditions. Furthermore, the deformation in the lake shapes which reflect clear disturbance by the company to force the water follow certain direction and that could be seen clearly by following the manmade borders around the lake, as showing in satellite images (Figs. 7, 8, 9, and 10).

The volume of the lake can be measured in a certain time by multiplying the area with the average depth at that time. At 2018 the volume of the lake was as follows:

- Volume = Area \times estimated Depth which assumed as 0.5 m, then lake water quantity = 0.5 m (Water column) \times 790,158 m² (Area) = 395,079 m³
- The volume of an oil slick: The result of a calculation using parameters recorded during the detection (remote sensing instruments) and observation (visual) of related circumstances and conditions is only an estimation; for the existing quantity.

The oil appearance as black tends to follow a pattern as shown in satellite images (Figs. 7, 8, 9, and 10). The thinner oils, will normally be at the edges of the thicker oils, discontinuous true color. It would be unusual to observe thick oil without the associated thinner oils; however, this can occur if the oil has aged and /or weathered.

It should be remembering that because of the resolution of the image (generally 15 m) small areas of less than 15 m is not covered with oil but within the overall area would not show on the image. However, oil patches of less than 15 m will show up as patches of 15 m. The overall area calculations should be 'adjusted' to take into account the 'holes' (areas) of clear water within the main body of the slick.

Crude oil varies in their optical density; black oils block shows all the wavelengths to the same degree but even then there are different 'kinds of black', residual fuels can block all light passing through, even in thin layers. So most of the lake is covered by oil slick with varied thickness and estimated in this study as only 2 cm. The lake areas were measured by drawing a polygon by multiplying it with the estimated oil slick thickness in this study as only 2 cm during 2018 (Fig. 11a, b).

The most probable oil volume during year 2018 detected by satellite imagery equal to 790,158 m² multiplied by the estimated oil column (thickness) of 2 cm to get an estimated volume of 15,803 m³ multiplied by 1000 to convert to liters and divided by average of 159 to convert to barrels.

Then the probable total volume of accumulated crude oil is:

$$(15803 \text{ m}^3 \times 0.02) \times 1000/159 = \text{approximately } 96,103 \text{ barrel of oil in this lake}$$

However, we should keep in mind that these quantities of oil often do not remain on the surface of the lake, but moving and accumulate on the shores (margins) of the lake (Fig. 12) as a result of wind forces and this was ascertained by taking many samples along the shores of the lake as well as several meters away and show the soil around the lakes (about 20 m from the lakes edge) is definitely impacted, due to produced water depositing.

The impact has been recognized and ensured by both, visual observations and the results of the analyses obtained for produced water and soil nearby lakes. Therefore, we do not expect to get the full amounts mentioned in case we decided to retrieve it as crude oil.

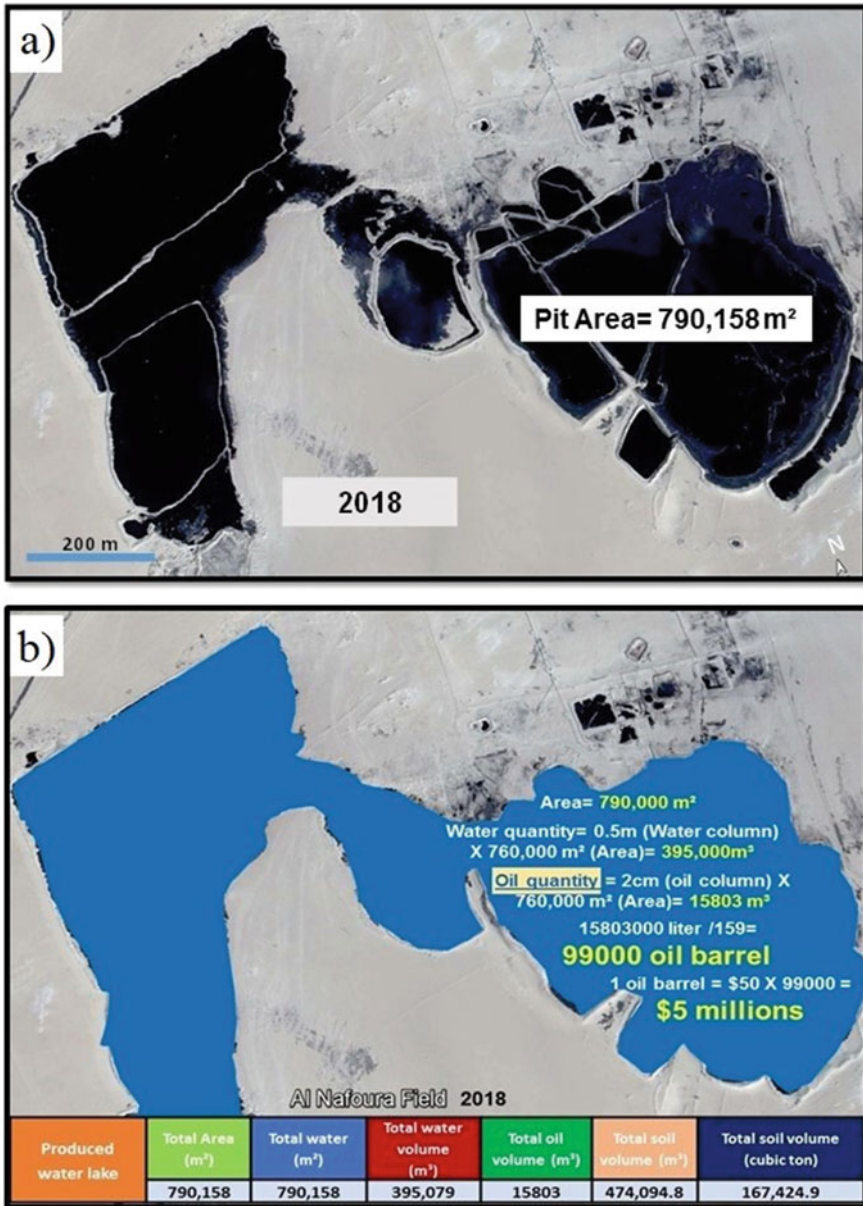


Fig. 11 (a) Produced water pit status for more details (2002–2018); and (b) Digitized map of image 2018 pit area was measured by drawing a polygon around the produced water pit and the detected oil slick where the overall length and width have been measured and estimated visually



Fig. 12 Shows how the oil often does not remain on the surface of the pit, but moving and accumulate on the shores (margins) of the pit

5 Quantities Calculation

In case the company plans or wants to implement a program for the treatment or removal of contaminants resulting from the release of produced water and some other oil residues in and around the entire station, it is very useful to use the attached (Fig. 13) which shows the status of the corresponding produced water lakes or any oil residues are shown in the form of black spots spread inside the field for the year 2018 that contains the size of areas affected by various oil contaminants and quantities of water that can be treated and used for other purposes as well as the amount of contaminated soil that can be removed or treated and the removal of pollutants.

6 Terrain and Its Landscape

The study area is located in the middle of a flat plateau, surrounded from the east by the so-called Great Sand Sea with high sand dunes, which takes longitudinal forms. The general direction of the decline of the land in area from the south to the north, it rises from the level of the sea by nearly 40 m. The topography of the study area varies in elevation between 16 and 70 m above the sea level (Fig. 13). The

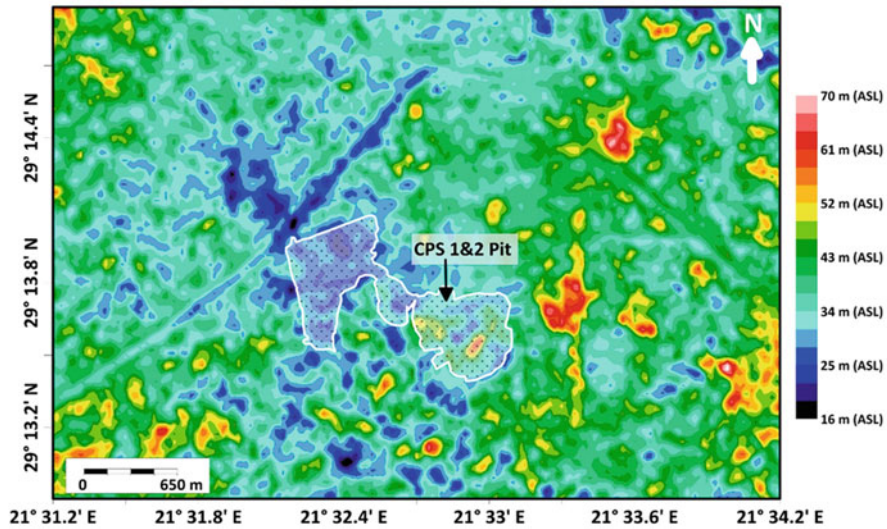


Fig. 13 Topographical map of the Nafoora oil field (CPS 1&2 pit) and the surrounding areas

topographical map of the site and the surrounding area shows that the lake is bounded by two relatively high areas in the southeast (52–61 m above the sea level) and in the southwest with the same elevation (Fig. 13). Into the north western side of the lake is relatively lower areas (25 m above the sea level) which means the topographical relief of the area suggests that the proper future extension of the lake will be mainly into north-west rather than to southeast.

7 Conclusions

Most of the used satellite images showed clear deformation in the lake shapes which reflect clear disturbance by the companies to force the water follow certain direction and that could be seen clearly by the manmade borders forms around the lakes even though a clear produced water spread out of the manmade borders have shown due to increase of water production. Most of the lakes run towards low topographic as the natural slope direction is blocked by hills. The shrinking and hiding of certain oil lakes is linked to the drying out of shallow lakes over time, which might be due to a change in production rate, the disappearance of most of the soot/black dirt, which was hidden behind a layer of sand, and a high evaporation rate.

The quantity of produced water lakes or any oil residues are exhibited in the form of black spots dispersed over all Nafoora oil field stations for the year 2018 were delimited and digitized as a polygon shape measuring about 790,158 m² of wet and polluted dry region using satellite photos. The amount of water determined by

multiplying the whole area of the lake by the maximum depth was estimated to be half a meter at the most and was approximately 395,079 m³. In addition, the amount of oil (volume) in the examined lakes was calculated by multiplying the total area of the lakes by the maximum depth, which was determined to be 2 cm and was 15,803 m³. In this instance, we estimate that there will be around 96,103 barrels of crude oil in the lake.

Furthermore, the amount of contaminated soil was calculated by multiplying the identical areas for the contaminated regions by the depth, which was estimated by fieldwork to be 60 cm and was calculated to be 474,094.8 m³ (167,424.9 cubic tons), with each m³ corresponding to 0.35 ton and those quantities can have treated and used for other. It is demonstrated that the oil, which has been mixed with soil and deposited as sludge, is driven to the lake's edges by the wind and appears in a variety of colors, ranging from black to brownish.

Acknowledgments The author would like to thank the Management of LPI for their unlimited support, encouragement, conducting and bringing this task to an end. The author expresses his sincere gratitude to Dr. Salem El Jawashi and Muftah Treban who contributed to the chemical and geotechnical test and the staff at Environment Department of LPI for maintaining and preparing test equipment for this study.

Author Contributions **Khalifa Abdunaser:** Conceptualization, methodology, formal analysis, writing-original draft, visualization, Data Interpretation, review and editing. The author has read and agreed to the published version of the manuscript.

References

- Al-Ajmi D, Misak F, Khalaf FI, Al-Sudairawi M, Al-Dousari AM (1994) Damage assessment of the desert and coastal environment of Kuwait by remote sensing. Kuwait Institute for Scientific Research, Report KISR 4405, Kuwait
- Alfarrah N, Hweesh A, Van Camp M, Walraevens K (2016) Groundwater flow and chemistry of the oases of Al Wahat, NE Libya. *Environ Earth Sci* 75:985. <https://doi.org/10.1007/s12665-016-5796-x>. Amsterdam, VII, 2757–2779
- Austin JM, Mackey BG, Van Niel KP (2003) Estimating forest biomass using satellite radar: an exploratory study in a temperate Australian Eucalyptus forest. *Forest Ecol Manag* 176:575–583
- Dobson MC, Kwarteng AY, Ulaby FT (1997) Use of SIR-C/XSAR to monitor environmental damages of the 1991 Gulf War in Kuwait. In: Proceedings of the 1st Saudi-Japanese symposium on remote sensing application, Riyadh, Saudi Arabia, 19–21 October, pp 105–117
- El-Baz F, Abuelgasim A, Koch M, Pax-Lenney M, Lambin E, Al-Doasari A, Marr P, Ryherd S, Morency R (1994) Detection by satellite images of environmental change due to the Gulf War. In: El-Baz F, Makharita RM (eds) *The Gulf War and the environment*. Gordon and Breach Sci Publishers, Lausanne, pp 1–24
- Koch M, El-Baz F (1998) Identifying the effects of the Gulf War on the geomorphic features of Kuwait by remote sensing and GIS. *PE&RS* 64(7):739–747
- Kooistra L, Salas EAL, Clevers JGPW, Wehrens R, Leuven RSEW (2004) Exploring field vegetation reflectance as an indicator of soil contamination in river floodplains. *Environ Pollut* 127:281–290

- Kwarteng AY, Al-Ajmi D (1997) Satellite remote sensing applications in the state of Kuwait. Kuwait Institute for Scientific Research, Kuwait
- Kwarteng AY, Chavez PS Jr (1998) Change detection study of Kuwait City and environs using multi-temporal Landsat Thematic Mapper data. *IJRS* 19(9):1651–1662
- Mason DC, Davenport IJ, Neal JC, Schumann GJP, Bates PD (2012) Near real-time flood detection in urban and rural areas using high-resolution synthetic aperture radar images. *IEEE Trans Geosci Remote Sens* 50:3041–3052
- Wright EP, Benfield AC, Edmunds WM, Kitching R (1982) Hydrogeology of the Kufra and Sirte Basins, eastern Libya. *Q J Eng Geol* 15:83–103

Dr. Khalifa Abdunaser is an exploration manager at Libyan Petroleum Institute, Tripoli, Libya. He received his B.S.C in Geology from Tripoli University, Tripoli- Libya in spring 1985; Master's degree in remote sensing in Geology from Dundee University, Scotland-UK in 1992; and Doctor of Philosophy (PhD) in Structural geology and remote sensing from Durham University, UK in 2012. Dr. Abdunaser has 36 years' experience worked as a leader of many working group in exploration department.

Conclusions and Recommendations for Environmental Applications of Remote Sensing and GIS in Libya



Hamdi A. Zurqani 

Abstract This chapter highlights the most important conclusions and recommendations from all chapters to provide perspective and guidance for students, teachers, researchers, decision-makers, etc. It includes summarized information on the latest research studies that used remote sensing (RS) and geographical information systems (GIS) techniques for environmental applications in Libya. Conclusions of different Libyan case studies related to the use of remote sensing and GIS tools have been described and several modeling approaches have been introduced. The current chapter also includes set recommendations that illustrate the relationships between remote sensing, field observations, laboratory analysis, and GIS for an integrated analysis of managing Earth's natural resources more sustainably and addressing many of the environmental problems humans face today.

Keywords North Arica · Environmental disturbance · Sustainability · Modeling · Geospatial analysis · Geographic Information System (GIS) · Google Earth Engine (GEE)

1 Introduction

The applications of remote sensing and GIS technologies have proved to be effective in addressing natural resources and environmental concerns at national and global scales (Zurqani et al. 2018a, b, 2020; Wulder et al. 2019; Bolick et al. 2021; Tarazona et al. 2021). Remote sensing data has the advantage in monitoring detection on the surface of the Earth because of its large spatial coverage, high time resolution, and wide availability. The availability of the historical record of remotely sensed data and the modern geospatial technology, such as the Google Earth Engine (GEE), has enabled the scientific community to investigate and identify

H. A. Zurqani (✉)

University of Arkansas Agricultural Experiment Station, Arkansas Forest Resources Center, College of Forestry, Agriculture and Natural Resources, University of Arkansas at Monticello, Monticello, AR, USA

e-mail: Zurqani@uamont.edu; Hzurqani@uark.edu

environmental disturbances to study the relationship between the human influence on Earth's surface and its consequences on the environment over time (Zurqani et al. 2018a, b). In Libya, the environmental disturbance can be visualized and documented using freely available geospatial technology (i.e., GEE) to monitor the extent of environmental disturbance (e.g. desertification, salinization, deforestation, land use changes, etc.) and may provide management strategies to mitigate the environmental consequences of these disturbances (Zurqani et al. 2019).

2 Conclusions

The use of remote sensing data and GIS capabilities in developing countries have become important tools for detecting, mapping, and monitoring degradation problems including their spatial variability and impact over time. Recent advancements in the fields of remote sensing (RS), geographic information systems (GIS) and global positioning system (GPS), and a higher level of computation will help in providing and handling a range of data simultaneously in a time- and cost-efficient manner. The book illustrates detailed methodological research approaches of using RS and GIS technologies in Libya for environmental assessment and natural resource management purposes. The technologies presented in this book include monitoring and mapping soil salinity and prediction of soil properties, monitoring and mapping of land degradation, spatiotemporal land use/cover, agricultural drought monitoring, and hydrological applications such as spatial rainfall distribution, surface runoff, geo-morphometric analysis, flood hazard assessment and mapping, hydrologic and hydraulic modeling, pollution hazard assessment, and climate-related geophysical processes.

As Libya strives to achieve its sustainable development goals (SDGs), the multifaceted and specialized capabilities offered by geospatial technologies will play a defining role for information management in the future with applications in many different fields at the national, and local levels as discussed in the previous chapters.

The remote sensing technique has an advantage over traditional/conventional techniques in terms of spatial, spectral, radiometric, and temporal data availability. It offers the acquisition of real- or near-real-time data also from inaccessible or remote areas within a very short span of time. At the regional scale, Landsat satellite imagery data were suitable and effective in characterizing land cover types and identifying the spatial and temporal changes of land cover that occurred as a consequence of land use change driven by both human and natural forces in the area. Likewise, the Moderate Resolution Imaging Spectroradiometer (MODIS) data products provide a good opportunity for more accurate and higher resolution monitoring of drought.

Also, web-based GIS platforms, such as Google Earth Engine and ArcGIS online, gives users easy-to-use tools to access, edit, and analyze GIS data. They also provide excellent performance in terms of enabling access to remote sensing products through the cloud platform and providing pre-processing to archived data from the US Geological Survey (USGS) collection. These types of tools allow high-speed analysis using advanced processing tools for large regions and large datasets, without the need to search and download remote sensing data for desktop processing, which in turn leads to more action research in solving environmental problems in the region and facilitates the achievement of SDGs in the country.

3 Recommendations

Recommendations are presented for Environmental Applications of Remote Sensing and GIS in Libya. These recommendations emerged from all the chapters of this book.

1. Google Earth Engine (GEE) platform represents a significant improvement for monitoring and evaluating land cover over large areas and in long-term monitoring of changes in land cover and land use over a large-scale area. It also supports the use of algorithms that pool data from multiple years, sensors, and models.
2. Recent advances in remote sensing and GIS have led to a revolution in the field of geomorphological mapping and have placed remotely sensed data as a core geomorphological data source.
3. As a tool in management and decision making, remote sensing and GIS could effectively be used to develop a variety of maps such as land cover, vegetation, soil, and geology maps.
4. GIS helps in the creation of a database for the catchment which is very useful for carrying out spatial analysis thereby helping the decision-makers in framing appropriate measures for critically affected areas.
5. The use of deep learning (DL) and machine learning (ML) approaches demonstrated promising results for land cover classification using remote sensing data at multiple scales.
6. Monitoring urban expansion and detecting land use change is one of the most important and successful applications of remote sensing and GIS techniques. As urban areas are expanding rapidly, routine surveying is not accurate, time and labor-consuming, and expensive and tedious.
7. The integration of remote sensing and GIS techniques, and field measurements are shown to be effective and promising methods for accurately predicting soil properties at unsampled locations, estimating soil loss, and identifying salt-affected soils, especially those with high salinity.
8. The integrated application of remote sensing and GIS techniques is also convenient for water resource evaluation and extraction of hydrological parameters of

any terrain (i.e., morphometric analysis) as satellite images provide a synoptic view of a large area.

9. Employing remote sensing and GIS techniques is an efficient tool for mapping flood extent and assessing flood impacts on inundated areas.
10. The use of remote sensing and GIS technologies has also proven to be an excellent management tool to develop approaches to oil spill hazard monitoring and assessment, especially in places with broad geographical areas.
11. Future research in environmental applications of remote Sensing and GIS in Libya should continue to explore the application of integrated technologies to assess the environmental conditions and the integration of scientific results into a decision analysis framework.
12. The primary spatial datasets can be made readily available to decision-makers, and landscape assessment tools could be developed to assist in the interpretation of results within a natural resource and future planning process to pursue the Sustainable Development Goals (SDGs) in the country.

Author Contributions Hamdi A. Zurqani: conceptualization, methodology, supervision, software, data curation, formal analysis, validation, investigation, writing—original draft, visualization, writing—review and editing, review of analysis. The author has read and agreed to the published version of the manuscript.

References

- Bolick MM, Post CJ, Mikhailova EA, Zurqani HA, Grunwald AP, Saldo EA (2021) Evaluation of riparian tree cover and shading in the Chauga River watershed using LiDAR and deep learning land cover classification. *Remote Sens* 13(20):4172
- Tarazona Y, Zabala A, Pons X, Broquetas A, Nowosad J, Zurqani HA (2021) Fusing Landsat and SAR data for mapping tropical deforestation through machine learning classification and the PVts- β non-seasonal detection approach. *Can J Remote Sens* 47(5):677–696
- Wulder MA, Loveland TR, Roy DP, Crawford CJ, Masek JG, Woodcock CE, Allen RG, Anderson MC, Belward AS, Cohen WB et al (2019) Current status of Landsat program, science, and applications. *Remote Sens Environ* 225:127–147
- Zurqani H, Mikhailova E, Post C, Schlautman M, Sharp J (2018a) Predicting the classes and distribution of salt-affected soils in Northwest Libya. *Commun Soil Sci Plant Anal* 49(6): 689–700
- Zurqani HA, Post CJ, Mikhailova EA, Schlautman MA, Sharp JL (2018b) Geospatial analysis of land use change in the Savannah River Basin using Google Earth Engine. *Int J Appl Earth Obs Geoinf* 69:175–185
- Zurqani HA, Mikhailova EA, Post CJ, Schlautman MA, Elhawej AR (2019) A review of Libyan soil databases for use within an ecosystem services framework. *Land* 8(5):82
- Zurqani HA, Post CJ, Mikhailova EA, Cope MP, Allen JS, Lytle BA (2020) Evaluating the integrity of forested riparian buffers over a large area using LiDAR data and Google Earth Engine. *Sci Rep* 10(1):1–16

Dr. Hamdi A. Zurqani is an Assistant Professor of Geospatial Science in Natural Resource Management and Conservation at the University of Arkansas Agricultural Experiment Station, Arkansas Forest Resources Center, University of Arkansas at Monticello, Monticello, AR, USA. He is also an FAA (i.e., Pt107) Certified sUAS/Drones Pilot, and has used this skill to enhance his knowledge of remote sensing and GIS. Dr. Zurqani is a recognized expert as a result of his internationally acclaimed work in the areas of environmental information science, remote sensing, geospatial analysis, land evaluation, sustainability, pedology, and soil science education. He has conducted research across the world, including the United States of America, and Africa, and has served as PI, co-PI, or co-investigator on several grants-funded research projects. Dr. Zurqani is highly collaborative as evidenced by his publications. He is the author and co-author of many peer-reviewed publications, book chapters, and technical publications (including teaching laboratory manuals). He also edited two books with Springer Nature (i.e., “The Soils of Libya”, and “Environmental Applications of Remote Sensing and GIS in Libya”), and has published widely in many peer-review journals (e.g., *International Journal of Applied Earth Observation and Geoinformation* (Elsevier); *Remote Sensing in Earth Systems Sciences* (Springer Nature); *Scientific Reports* (Nature); *Frontiers in Environmental Science* (Frontiers); *Geoderma* (Elsevier); *Land* (MDPI); *Urban Forestry & Urban Greening* (Elsevier), and others). Dr. Zurqani is a member of the Editorial Board for *Remote Sensing* (MDPI) Journal, counseling outcome, and research evaluation. He also was appointed to serve as a Guest Editor for the Special Issue “Applications of Remote Sensing in Earth Observation and Geo-Information Science”. In addition, Dr. Zurqani conducted peer-review for many journals including *Journal of Environmental Informatics*, *Applied Sciences*, *SN Applied Sciences*, *Remote Sensing*, *Geo-spatial Information Science*, *AgriEngineering*, *Sensors*, *Heliyon*, *Geosciences*, *Land*, *Soil Systems*, *Water*, *Agronomy*, *Agriculture*, *Resources*, *Sustainability*, *Arid Land Research and Management*, *Quaestiones Geographicae*, *Geocarto International*, *International Journal of Environmental Research and Public Health*, *Natural Hazards*, and *Conference of the Arabian Journal of Geosciences*. Dr. Zurqani conducts cutting-edge research in the field of Environmental Information Science, Remote Sensing, Land use management/ planning, change detection of landscape degradation, and Geographic Information System (GIS) models. He has focused his research efforts on the development of novel applications for new technologies in analyzing spatial data, remote sensing, geostatistical modeling of environmental changes such as erosion, mapping and predicting soil salinity, and land use/ land cover changes. His new publications include: “Mapping and Quantifying Agricultural Irrigation in Heterogeneous Landscapes Using Google Earth Engine” in the *Journal of Remote Sensing Applications: Society and Environment*; “Evaluating the integrity of forested riparian buffers over a large area using LiDAR data and Google Earth Engine” in the *Journal of Scientific Reports*; “Mapping Urbanization Trends in a Forested Landscape Using Google Earth Engine” in the *Journal of Remote Sensing in Earth Systems Sciences*; “Geospatial analysis of land use change in the Savannah River Basin using Google Earth Engine” in the *International Journal of Applied Earth Observation and Geoinformation*; and “Application of Non-Hydraulic Delineation Method of Flood Hazard Areas Using LiDAR-Based Data” as well as “Assessing ecosystem services of atmospheric calcium and magnesium deposition for potential soil inorganic carbon sequestration” in the *Geosciences Journal*.